The Micromechanisms of Fracture in Metal Matrix Composites

Paul Malcolm Mummery
Wolfson College, Oxford

A thesis submitted for the degree of Doctor of Philosophy
Hilary Term, 1991

Micromechanisms of Fracture in Metal Matrix Composites.

Paul Malcolm Mummery
Wolfson College, Oxford
A thesis submitted for the degree of Doctor of Philosophy
in the University of Oxford, Hilary Term, 1991

Abstract

The effects of systematic variations in the size and volume fraction of reinforcing phase on the mechanical properties of and fracture processes in silicon carbide particle-reinforced aluminium matrix composites have been studied.

Tensile tests to failure have been performed to determine the mechanical properties of the composites. A simple model has been proposed for this behaviour.

The micromechanisms of fracture have been investigated by a combination of fractographic and dynamic techniques. Matched fracture halves have been obtained from the composites and the fracture processes elucidated. Fracture proceeded by a ductile void nucleation, growth and coalescence mechanism. Void nucleation occurred at the reinforcing phase, with a change in nucleation mechanism on varying the micrstructural parameters. A simple critical stress criterion has been proposed for the nucleation process. Support for this proposal has been obtained by the study of sections through the failed tensile specimens.

In situ scanning electron microscopy fracture studies have been performed. These revealed void nucleation before the onset of macroscopic cracking. Crack propagation has been shown to occur by the concurrent formation of microcracks ahead of the crack tip and failure of the joining matrix ligaments. The magnitude of matrix deformation has been shown to determine the extent of microcracking.

Acoustic emissions have been monitored during tensile straining. Void nucleation events have been recorded from the onset of plastic deformation and continuing throughout the plastic régime until final failure. The suppression of void coalescence by the constaint imposed on matrix flow by rigidly-bonded interfaces has been proposed to account for the extended void growth in materials containing fractured particles. The importance of the local values of the microstructural parameters on the far-field strain at nucleation has been shown.

To my Mother
who almost saw it completed

Preface

This thesis describes research carried out by the author in the Department of Materials, University of Oxford, between October 1987 and March 1991 under the supervision of Dr. Brian Derby, and is original unless otherwise stated. Some of the results have been presented at the EMRS Spring Meeting (1990) and at the TMS Fall Meeting (1989).

I would like to thank the following, who have been a great help to me:

Professor Sir Peter Hirsch, FRS, for providing the laboratory facilities.

Brian, my supervisor, for being interested, available, patient and human.

The team at the Advanced Engineering Materials Group, AEA Technology, Harwell for fabricating the material and valuable discussions. I would like to mention in particular Ian Pearson, for explaining the ins-and-outs of hot pressing, and James Tweed, for bearing with me and explaining ductile rupture processes.

The demons in the workshop, Bill Bryant, David Pinfold and John Short, who have performed miracles with bent pieces of extruded, impossible-to-machine material, and taught me all I know about cycle maintainence.

The other members of "Derbysmen", a truly good group of people despite what people say. In particular Richard and Charles, who have helped me through the last three months and produced the excellent figures enclosed. The acoustic microscopy reported in this thesis is also the work of Charles Lawrence.

The group at the National NDT Centre, AEA Technology, Harwell for the use of their excellent facilities and expertise. Particular thanks to Kevin Stacey, who extracted the results from an unwilling computer, and David Buttle and Chris Scruby, who both tried their best to explain acoustics to me and for the use of figures 5.21 and 5.22.

The photographers, Mohammed Taheri and Andrew McKnight, who have produced wonders from poor negatives.

My Father, for who he is.

Finally, especial thanks must go to my wife, Ann, who has suffered far more than she has deserved. She has been a constant support and source of joy, without whom the past years would have been unendurable.

CONTENTS

Chapter 1: Introduction and Review of Previous Work

1.1 What is a Metal Matrix Composite?

A composite consists of two or more distinct phases combined to give a novel material. Reinforced composites can be generally classified into three types, characterised by the aspect ratio, that is the ratio of length to width, of the reinforcing phase: i) long, continuous or unbroken fibres of effectively infinite aspect ratio; ii) chopped or short fibres and whiskers, which are substantially defect-free single crystal short fibres, having a finite aspect ratio; and iii) particles, which are approximately equiaxed. The last two are known as discontinuously reinforced while the former is continuously reinforced. A Metal Matrix Composite (MMC) is a metal which has been reinforced by such a second discrete phase, normally a ceramic. The goal is to produce a material combining the attractive characteristics of both constituents, namely the stiffness and theoretical strength of the ceramic with the toughness and ductility of the metal. As this rather general definition could as well be applied to, for example, dispersion-strengthened alloys, the term MMC in this thesis shall refer only to those materials where the second phase has been deliberately added and not formed *in situ*.

MMCs have attracted great scientific and industrial interest recently due to the potential improvements in both mechanical and physical properties which they may show over monolithic metals and polymer-based composites. Cheaper sources of the ceramic reinforcements have become available, making such composites more commercially attractive. MMCs of a low density matrix metal, such as aluminium, and reinforcing ceramic, such as silicon carbide, show promise for stiff and high-strength, low-weight applications such as replacements for conventional alloys used in the aerospace industry [1,2]. The durability of MMCs also makes them potential replacements for carbon-fibre-reinforced plastics, especially in hostile environments such as space where polymeric materials are susceptible to low temperature, high UV radiation levels and erosion from atomic oxygen. Another advantage of MMCs is the higher working temperature range, which can be extended up to 400°C and cannot currently be matched by any polymer-based alternatives. Other specialised properties such as good wear resistance and high thermal conductivity add to the advantages of MMCs over their competitors.

Continuously reinforced MMCs have the potential for exceptional unidirectional properties. This, however, comes at a price both financially, with the high cost of the fibres and processing, and, in some instances, in the mechanical properties due to their large degree of anisotropy.

Discontinuous reinforcements can improve the performance of the metal substantially for a reasonable price, although they cannot be aligned to the same extent as continuous fibres and give such exceptional properties. Thus, the physical properties of discontinuously reinforced MMCs are essentially isotropic. Commercial interest in whisker reinforcements has diminished because of the possible hazard to health they present. This increases handling and processing costs substantially for little improvement in composite performance over the last class. The least expensive MMCs are those reinforced with particles. Currently used in large quantities as commercial abrasives, reinforcements such as silicon carbide and alumina are readily available in a variety of grades and sizes. The major benefit of incorporating the reinforcing phase has been to increase the modulus, typically from 70GPa to 100GPa for the addition of 20% silicon carbide particles in aluminium, with smaller increases in strength, particularly for high-strength matrix alloys. The improvements in mechanical properties of particle-reinforced MMCs (PRMMCs) have, however, been mirrored by a degradation of the fracture-related properties such as toughness and tensile ductility. It is the low values of these properties which is currently restricting widespread application of MMCs. Aluminium PRMMCs, however, have potential for immediate commercial exploitation, because of their relative ease of fabrication and secondary processing. They form the subject of this thesis.

The basic technologies of the four principal fabrication routes for PRMMCs have already been developed as they are adaptations of processes currently used for monolithic alloys. There are three casting routes: stir cast, where the reinforcement is stirred into a melt of matrix; squeeze cast, where the reinforcement is held in a "pre-form" within a die and molten matrix forced into it; and spray forming, where the molten alloy is atomised into a spray into which the reinforcement is introduced. The fourth is a standard powder metallurgical process where the powdered alloy and reinforcing phase are mixed and pressed, either hot or cold. These are discussed in more detail in Chapter 2. Typical particle sizes used range from 3μm to 20μm and volume fractions from 10% to 30% with an upper limit of about 50% volume fraction, above which it is impractical to achieve discrete ceramic reinforcement. This choice of parameters is found to give significant improvements in stiffness and strength, but may also be forced by the fabrication route. For example, it is at present difficult to introduce more than 20% volume fraction of reinforcement by the stir cast route and less than 20% by the squeeze cast route. Silicon carbide and alumina are the most popular reinforcements as they are stiff and relatively cheap. Titanium diboride, while having excellent properties, is used far less frequently because it is much more expensive. The raw ingots normally then undergo secondary processing such as extrusion or forging. Research into processing techniques and the effects of processing parameters on the subsequent properties of PRMMCs is currently very active.

1.2 Microstructure

The microstructure of a PRMMC is potentially complex with contributions from the alloy material, the reinforcing phase, and any interfacial reactions which may occur between the two. This last point is a problem in cast material in particular. The basic features of the microstructure are the matrix grain size, the reinforcing particles and their distribution, matrix precipitates and dislocation sub-structure. The incorporation of significant quantities of ceramic particles into an alloy, combined with the mechanical processing, tend to produce a matrix of fine grain size, roughly the same size as the spacing of the reinforcing phase, with the majority of the reinforcing particles found at the grain boundaries [3]. Powder route processing produces oxide particles within the matrix in addition to any age-hardening precipitates. The dislocation structure may arise from the processing or from differential thermal contraction of matrix and reinforcement, where, in the case of aluminium and silicon carbide, the matrix material has an expansion coefficient some six times greater than the ceramic. On cooling, dislocations are generated to maintain the displacement compatibility across the interface [4-7]. The addition of a second phase into a metal, as opposed to the formation of one *in situ*, may produce a non-equilibrium thermodynamic state encouraging an interfacial reaction [8-12], which in turn may deplete the matrix of elements controlling its microstructural development [13-20].

The interface controls the load transfer between the metal and ceramic and, therefore, the successful operation of modern composites or tribological systems. This interfacial strength is significantly affected by alloy chemistry and reinforcement type. There have been no attempts to measure directly the interfacial bond strength of PRMMCs, only to infer them from a general understanding of the ductile fracture mechanism [21]. This technique, where the stress levels at voids is determined by sectioning tensile specimens, has been applied successfully to determine the interfacial bond strength in spheroidised 1045 steel, Cu-0.6%Cr alloy and maraging steel containing Fe_3C, Cu-Cr and TiC particles [22-25]. Direct measurements of the interfacial shear strength in a number of continuously-reinforced MMC systems has been made using flat plate and fibre pull-out tests [26]. These studies have, in general, shown that there is a very good interfacial bond between aluminium alloys and silicon carbide, being of the order of 1-2GPa [21].

A major influence on the microstructure and, therefore, the properties of PRMMCs is choice of fabrication process. The development of MMCs has, in general, been controlled by advances in processing. Nominally the same material fabricated by different routes has different properties, even material manufactured by the same route may be variable, as can be seen from several review papers [27-30]. This variability in mechanical and fracture properties has made the development and interpretation of

models of PRMMC behaviour difficult since there can be no guarantee that the intrinsic properties of the composite have been studied rather than the imperfections in the processing.

A number of changes to the composite microstructure may occur on altering the fabrication route. The matrix microstructure itself may be changed, having a different grain size or residual dislocation density, although this can normally be removed by subsequent thermomechanical processing. An interfacial reaction product may be formed as outlined earlier [8-12,31-36], or the spatial distribution of second phase may be altered, which has been shown to affect mechanical properties significantly. Secondary mechanical processing, such as extrusion, hot- or cold-rolling and forging, has been shown to improve the mechanical properties of PRMMCs [37-42]. This has been associated with an homogenisation in the spatial distribution of the reinforcement, although at present this link can only be made qualitatively. Attempts to describe quantitatively the distribution of a second phase within a parent material has been the subject of a number of studies in many branches of the physical and biological sciences [43-49] and attempts have been made to apply these results to the study of PRMMCs [50-54].

There is an extensive literature on the mechanical and fracture properties of continuously and discontinuously reinforced MMCs of many composite systems. Studies of light alloy matrices such as aluminium [1-20,55-64] and continuously-reinforced titanium [65,66] constitute the bulk of this although there is a growing literature on MMCs of intermetallic matrices [67-69] and even of uranium [70]. This review will concentrate on the particle-reinforced aluminium composites as they form the subject of the thesis.

1.3 Mechanical Properties

The mechanical properties of a PRMMC are strong functions of the microstructural parameters outlined above. Despite the extensive literature and current interest in PRMMCs there are relatively few papers which study the influence of these parameters independently on the mechanical and fracture behaviour, most reported work varying several parameters at the same time or none at all. These in turn show the influence of one parameter in isolation which, combined with the great sensitivity of material behaviour on fabrication route and subsequent thermomechanical treatment, makes extrapolation to other composite systems suspect. In addition to those listed below, there are other papers which report the properties of single composite systems and, therefore, do not show the general effect of the microstructural parameters at all [71-80]. These must be used in conjunction with other work to show the trends in behaviour and are useful from that standpoint. An overview of the general patterns of

behaviour can be obtained by reference to several compilations of data [27-30].

1.3.1 Elastic Properties

The increase in stiffness of a PRMMC over the unreinforced alloy is monotonic with volume fraction over the range used in practice [27-30,81-87], is weakly dependent on matrix alloy and particle aspect ratio, with whisker-reinforced composites stiffer than particle-reinforced, but is independent of particle size [27-30].

1.3.2 Strength

The dominant parameter controlling the strength of a PRMMC is the choice of matrix material, where, in general, a high yield strength matrix alloy gives a high yield strength composite [27-30,81,88,89]. The increase in strength of the composite over the unreinforced alloy is more pronounced in the low strength alloy matrices where the introduction of the reinforcing phase produces significant strengthening [84-86,90-92]. However, for high-strength alloy matrices, such as the 2XXX and 7XXX series, the strengthening is far less marked [72,81,83,93] and in some studies a lowering of proportional limit is found [27,81]. Increased strength is observed on increasing volume fraction [27,81-87,90,93,94-96], reducing particle size [84-87,93,94,97,98] and on quenching [84-87,90,95].

1.3.3 Work-Hardening Rate

The work-hardening rate of PRMMCs at low strains is much greater than the unreinforced alloy [81,84]. Thus, while the proportional limit is sometimes reduced in the high-strength alloy matrix PRMMCs, the ultimate strength is increased [27,81], although there is one study where both the composite yield and ultimate strengths are lower than the unreinforced alloy [99]. The often quoted 0.2% proof stress is, thus, strongly affected by the work-hardening rate. The work-hardening rate is increased on increasing volume fraction [81,83] and quench temperature [83,95].

1.4 Interpreting Mechanical Properties

Attempts to interpret and model the mechanical properties of PRMMCs have ranged from those based on purely continuum analyses and finite element techniques to strict dislocation mechanics via hybrids of the two. The continuum models assume that there is some load redistribution between the two phases, lowering the effective stress in the matrix. Yield is said to occur when the effective matrix stress satisfies a prescribed stress criterion, such as the von Mises criterion. Inherent in the models is that the

matrix is plastically homogeneous and can, therefore, be adequately described by global parameters. However, for these continuum models to work well, the mechanical properties of both matrix and reinforcement need to be accurately known and specified, and it is not certain that the bulk properties of these will represent their behaviour in a composite. The dislocation micromechanics approach is based on a knowledge of the deformation processes at an atomic level with load transfer from the matrix to the particles occurring via unrelaxed Orowan loops [100]. These models assume that there is enhanced dislocation storage at the reinforcing phase, producing a plastically inhomogeneous matrix.

1.4.1 Elastic Properties

The elastic moduli of PRMMCs can be predicted by existing continuum models with good agreement between theory and experiment. The original shear lag model of Cox [101] has been modified to account approximately for the finite aspect ratio of the particles and enhanced load transfer at the particle ends [102]. Models based upon the equivalent inclusion technique of Eshelby [103,104] have also been developed more successfully [105-109].

1.4.2 Strength

There has been some success in modelling the bulk mechanical behaviour of PRMMCs of the higher strength aluminium alloy matrices using finite element methods [110-115], methods based on extensions of Eshelby's [103,104] equivalent inclusion technique [116-118], and the modified shear lag analysis [119,120]. The continuum models work for these materials because the matrix dislocation motion is dominated by the matrix precipitates themselves, as shown by the importance of matrix strength in determining composite properties, and, therefore, the unreinforced alloy is a good representation of the matrix of composite.

The continuum models do not, however, predict one of the consistent results of the mechanical behaviour, namely the yield strength dependence on absolute particle size, as outlined above. These models are, however, sensitive to changes in shape of the reinforcement with the predicted yield strength dependent upon particle aspect ratio. Recently, attempts have been made to reconcile the observed behaviour with the models [121,122]. The continuum mechanics models, however, also fail when modelling the behaviour of composites of low-strength alloys [84,90,123]. The mechanical properties of these alloys are dominated by secondary strengthening processes such as residual dislocation density and grain size, since they are not dispersion strengthened. Thus, in general, quoted values for properties of the unreinforced alloys give poor representations of the matrix of the composite as the matrix microstructure is strongly

influenced by the processing and reinforcing phase.

The models based on dislocation micromechanics have had greater success in modelling the properties of these low-strength matrix alloy composites [84-86]. In these models yield occurs when the applied stress is sufficient to move dislocations through the bulk of the material. This stress is, therefore, governed by the barriers to dislocation motion, as outlined by Humphreys [84], which have been characterised over many years of study of two phase alloys. Confirmation of this approach is provided by Arsenault *et al.* [94]. They observed the same yield stress from a composite and an unreinforced, commercially pure aluminium alloy which had been thermomechanically processed to the same residual dislocation density, implying low load-bearing by the reinforcements with most of the strengthening coming from the matrix alone. The behaviour of a material at the atomic level is, however, poorly understood for all but the simplest of situations. Models for the behaviour of complex metallurgical systems such as PRMMCs based upon such an understanding are necessarily great approximations. They do, however, have the advantage of a true physical representation where the approximations can be assessed readily. The models do require, therefore, detailed knowledge of the matrix microstructure.

1.5 Fracture and Fracture-Related Properties

The same fracture mechanism is observed in all aluminium matrix PRMMCs. The microstructural parameters, however, alter the mode of failure within this same, broad mechanism. The fracture-related properties, such as ductility and toughness, are strong functions of the microstructural parameters and failure mode.

1.5.1 Fracture

Although PRMMCs show limited ductility on a macroscopic scale, SEM fractography has shown that fracture has occurred by a ductile rupture mechanism, characterised by fine dimples on the fracture surface [124-126]. The dimple distribution is often bimodal, with one set of dimples associated with the reinforcing phase, and the other, much smaller, associated with ductile failure of the matrix [73,87,91]. For the higher volume fraction materials, the dimples are very similar in size to the reinforcing phase, indicating limited void growth. There is usually no macroscopic necking of the specimen, particularly for PRMMCs of high strength matrices, with the fracture process zone localised to very near the crack surface, although stable voids have been observed on the surface of tensile specimens and on sectioning through the fracture surface [87,127]. The influence of the reinforcing phase on the crack path is a matter of debate. Some studies have indicated that the fracture path is attracted to the particles [51,91], while others have the crack avoiding the particles [54] or taking a random path through

the matrix [71,79,83]. The spatial distribution of the reinforcing phase is found to be important, with evidence of early nucleation in regions of locally high volume fraction [51,52,54,71,73,83,91].

The ductile rupture mechanism involves the sequence of a) nucleating a void by particle cracking or by decohesion at or near the particle/matrix interface, b) growth of these voids, and c) their coalescence to give total failure of the specimen. Although voids may be nucleated within the matrix independently of second phase particles [128,129], in the vast majority of cases nucleation is associated with the presence of a second phase where inhomogeneous deformation occurs. Models of the ductile rupture mechanism generally propose that nucleation occurs at a fixed, critical strain. The voids then grow under the applied stress and strain fields until either the plastic constraint between voids is overcome, when the void height is equal to the intervoid spacing and coalescence occurs by simple shearing of the joining matrix ligaments, or secondary nucleation mechanisms are activated.

In PRMMCs there is evidence of clean decohesion at the particle/matrix interface [73,87,98,99,130,131], propagation through the matrix near the interface [9,78,132] and particle fracture [71,79,83,133]. Transitions between these different failure modes may occur on changing particle size [87,134] for a given matrix alloy and heat treatment, interfacial bond strength [98,130,131] and matrix microstructure [52,54,76,99]. Thus, the experimental observations are, in general, specific to the composite system under study, although the influence of the microstructural parameters on the fracture micromechanisms can be readily interpreted.

1.5.2 Ductility

It is well known that the addition of the reinforcing phase severely reduces the elongation to failure of a monolithic alloy [135]. Similarly, for a given matrix alloy, elongation to failure is reduced on increasing the volume fraction [27,83-87] and particle size [75,87,97,98,136]. Composites of high-strength alloy matrices have lower ductility than those of low-strength alloy matrices [27-29,88], with decreasing ductility on ageing to peak strength [27,52,54,81,83]. The ductility is also found to be affected significantly by the spatial distribution of the reinforcing phase, with highly inhomogeneous distributions giving lower ductility. Studies have shown that secondary working of the material, such as rolling or extrusion, can increase the ductility [37-42]. This has been associated with an improved homogeneity in the distribution of reinforcing phase.

1.5.3 Toughness

The toughness of the unreinforced alloy is similarly lowered by the addition of the

second phase. For a given matrix alloy, toughness, as measured by a number of parameters, is reduced on increasing volume fraction [75,91-93,137-139] but on decreasing particle size [75,93,98]. Flom and Arsenault [92] have only found this trend, however, for particles above a critical size.

1.6 Discussion of Fracture Studies

The experimental observations have been interpreted in two ways, both of which can account for the fractography and low ductility by appealing to previous work on ductile rupture in dispersion-strengthened alloys.

1.6.1 Fracture Mode

The interpretations of the experimental results differ only in the sequence of processes which constitute fracture and not in the processes themselves. Most authors [for example 28,40,73,91] have fracture in PRMMCs following the same sequence as in dispersion-strengthened alloys, namely nucleation at the second phase followed by failure in the matrix by void coalescence. You *et al.* [71], with experimental support from Roebuck [79], argue that a different sequence of events may occur. They suppose that the increased levels of stress and high levels of plastic constraint imposed by the second phase particles on the matrix lead to void nucleation in the matrix as the initiation step, with the final stage of fracture being the decohesion or cracking of the particles. Isolation of the nucleation process would distinguish between the two mechanisms.

Simple void growth models [139] developed for dispersion-strengthened alloys indicate that as the volume fraction of second phase, and therefore potential void nucleation sites, reaches 15% to 20%, the nucleation strain becomes the dominant factor controlling ductility. In these high volume fraction regimes, the interparticle spacing decreases and, hence, so does the growth strain, becoming zero at a volume fraction of about 16% [140] where a nucleated void is already as large as the intervoid spacing. In real materials with random particle distributions, areas of local volume fraction greater than the mean will be found, suggesting that this critical condition could be reached locally with lower mean values than 16%. It would seem likely that in materials such as PRMMCs, with large volume fractions of secondary phase, factors controlling void nucleation will be critical aspects of material design and, indeed, many of the experimental observations can be rationalised by invoking this type of arguement.

The various void nucleation models and criteria have been reviewed [141]. It is generally agreed that two criteria must be satisfied for a void to nucleate at a second phase particle. First, the elastic energy released on nucleation must be greater than the

increase in surface energy on forming the void. Second, the local stress must be greater than the particle or interfacial bond strength. The first criterion is considered to be necessary but not sufficient for particles greater than 25nm for it has been shown to be always satisfied on satisfying the second criterion [142].

Consider a simple critical stress criterion for void nucleation. Let nucleation occur when the local stress reaches either the particle fracture stress or interfacial bond strength. A change in failure mode may be expected, therefore, as the relative values of these parameters is varied. As the reinforcing phase is a brittle ceramic, a decrease in particle fracture stress may be expected on increasing particle size due to the increased probability of finding a critically sized flaw. The interfacial bond strength is independent of particle size and, therefore, a transition in failure mode from cracking to decohesion may be observed on decreasing reinforcement size [87,134].

The influence of bond strength on failure mode has been studied. On changing the reinforcement from silicon carbide to boron carbide, Stephens *et al.* [98] observed a change in failure mode from particle fracture to interfacial decohesion. Another method has also been examined. To simulate events which may occur during processing, composites were fabricated with oxidised and as-received reinforcements [130,131]. The oxidation of the silicon carbide led to the formation of a spinel phase ($MgAl_2O_4$) at the interface which, although giving depletion of magnesium in the matrix, did not hinder the formation of matrix precipitates. This was accompanied by a reduction in mechanical strength and increase in ductility over the material without oxidised particles. There was also a change in failure mode from particle cracking to failure at the spinel/reinforcement interface.

As outlined earlier, the addition of the reinforcing phase may affect the microstructural development of the matrix [13-20] and, indeed, changes in failure mode on overageing has been caused by this effect [52,54]. Microstructural evaluation of the material in those studies by Strangwood *et al.* [143] showed interfacial segregation of the matrix alloying elements. This was accompanied by a vacancy loss to the interface, which gave a nucleation-depleted precipitate-free zone (PFZ) and a changed solute concentration near the interface, thus weakening the PFZ. The presence of the weakened PFZ between the reinforcement and matrix concentrated the strain in the PFZ which then failed by shear. This was mirrored by a loss of toughness and a change in failure mode.

Thus, a simple critical stress criterion seems sufficient to account for the changes in failure mode.

1.6.2 Ductility

Ductility is reduced on increasing volume fraction and matrix strength. On straining, dislocations are generated at the particle/matrix interface to maintain the displacement compatability across the interface, as described by Ashby [144]. Plastic relaxation, by this generation of secondary dislocations, becomes increasingly difficult on continued straining as the dislocation motion away from the interface is hindered by the presence of the dislocations formed at lower strains. This impingement of one plastic zone on another occurs at lower strain on increasing volume fraction. Any other barriers to dislocation motion, such as matrix precipitates, will, therefore, also increase the local stress for a given far-field strain and reduce the ductility. This may be thought of as a rapid exhaustion of work-hardening capacity.

The importance of the particle spatial distribution can now be appreciated and is discussed in detail by Hunt *et al.* [51]. Indeed, Thomson and Hancock [146], in their study of Swedish iron containing only 1% by volume of iron oxide particles, showed that an important factor determining the nucleation strain was the tendency for clustering of the particles. In these regions of high volume fraction, the stress relaxation processes are severely restricted. This is combined with increased local plastic constraint, raising the hydrostatic stresses, and high quenched dislocation density. Embury suggests [145] that nucleation first occurs in regions of lowest interparticle spacing proceeded by percolation of damage through the clustered regions.

The increased ductility on decreasing particle size is presumably due to a higher critical nucleation stress. However, this is in competition with the processes exhausting the work-hardening capacity and increasing the local flow stress.

1.6.3 Toughness

The large energy-absorbing process in the fracture of PRMMCs is the ductile failure of the matrix ligaments. Thus, increased toughness is accompanied by the increased interparticle spacing resulting from lowering the volume fraction for a given particle size and from increasing particle size for a given volume fraction [75,91-93,137-139].

The fracture behaviour of PRMMCs is, therefore, phenomenologically similar to that of a high volume fraction dispersion-strengthened alloy of high work-hardening rate and low work-hardening ability.

1.7 Summary

The current state of understanding of the mechanical and fracture behaviour of PRMMCs could well be likened to "looking through a glass darkly"; much is assumed or inferred, fairly disparate pieces of the jigsaw are assembled, but how they go together to form a whole is another matter entirely. In the main, improvements in material performance have come about through purely empirical, sledgehammer-and-nut approaches. Thus, there is a large body of information and results on many different composite systems, but most of it is specific to single combinations of matrix, reinforcement and processing. Extrapolation between these results to infer the performance of untried composite systems has proved to be difficult. This is in part due to the complex nature of the beast, with many related influences, but also there have been no attempts to do a study of the effects of a systematic variation in the major microstructural parameters, such as volume fraction and size of reinforcing phase, on the mechanical and fracture behaviour in well-characterised composites fabricated by the same route. In addition, many properties of the composites have been compared with unreinforced alloys fabricated by different routes [4,5,6,27,71,117]. As a result, many of the basic questions relating to PRMMC performance remain unanswered. The aim of this thesis is to address one or two of the questions which relate to fracture by undertaking such a systematic study. These are:

i) what parameters determine the mode of fracture in PRMMCs?

ii) does the mode of fracture influence the ductility?

iii) what is the relative importance of each stage in the ductile rupture process?

iv) what are the local and far-field conditions at fracture nucleation?

v) how are these conditions affected by the microstructural parameters?

vi) can a simple model for fracture be developed based upon models developed for monolithic alloys?

In addition, the effect of the microstructural parameters on the mechanical properties will be found and a simple extension of current models proposed. The limitations of this model are fully appreciated and it is only to be seen as an example of a method suitable for use in the analysis of PRMMCs.

Chapter 2: Material Fabrication and Characterisation

2.1 Fabrication Routes

PRMMCs can be fabricated by a number of routes including compocasting [36,147], spray forming [148,149], melt infiltration [150,151,152] and powder processing [153,154,155].

Compocasting, or stir-casting, involves the addition of the reinforcing particles into a stirred melt of matrix material. The melt may then be poured into a mould or undergo secondary processing as a wrought billet. The method facilitates large volume production of composite material but has considerable technical difficulties. These include control of the particle spatial distribution and wetting of the particle-matrix interface to produce a good bond. The choice of potential matrix alloys is limited by the need to prevent reactions between the reinforcement and molten matrix which are in contact at high temperatures for long periods.

Melt infiltration, or squeeze-casting, is performed by pouring molten matrix alloy into a die cavity containing a preform of reinforcing phase, usually held together by an organic binder which is burnt off, and applying a pressure, normally by a hydraulic ram. The applied pressure and ram displacement can be monitored easily, and operation in a controlled atmosphere is possible. This method has the potential for near finished-shape fabrication, thus reducing any secondary processing.

In spray forming, the ceramic reinforcements are introduced into a spray of molten matrix material and deposited onto a target. This technique is still in the early stages of development and has similar advantages and disadvantages to compocasting. An additional problem is the control of volume fraction of reinforcing phase in the final billet. However, the material spends a much shorter time at high temperatures allowing a greater variety of combinations of matrix and reinforcement.

Many powder processing techniques have been tried. In essence these involve premixing powdered matrix alloy with the reinforcing phase, either wet or dry, followed by hot- or cold-pressing to a billet and secondary consolidation processing, such as extrusion, rolling or die-casting. The technique allows very close control over the final microstructure and a completely free hand on choice of matrix alloy as the processing usually takes place in the solid state where reactions are much slower. The initial pressing is sometimes performed at a temperature just above the solidus in a semi-solid state. This achieves higher densities at this stage in shorter times [153]. It is not, however, suited to high capacity production and will probably be restricted to instances where novel matrix alloys are needed. By requiring a powder production step before

consolidation, this process will always be a more expensive fabrication route than the previous methods.

The choice of fabrication route affects the microstructure of nominally similar composites [27-30,150]. In order to obtain the full strengthening effect of the second phase, a good interfacial bond must be formed to ensure efficient load transfer from the matrix. However, deleterious chemical reactions should be avoided. Fabrication routes involving molten matrix material are prone to these interfacial reactions if there is prolonged exposure of the ceramic to the molten metal [156-160]. Similarly, interfacial oxide layers are often formed during powder processing routes [150] which inhibit bonding between matrix and reinforcement. This problem may be overcome by the introduction of plastic shear deformation during consolidation which disperses the oxide layer. This has been shown to improve both mechanical and fracture properties [150,161].

For this study, powder formed material was used exclusively because of the better microstructural control that could be achieved in the available equipment.

2.2 Material Selection and Fabrication

The experimental material was manufactured by using the standard powder metallurgical processes of vacuum hot-pressing and extrusion by the author at the Advanced Engineering Materials Department, AEA Industrial Technology, Harwell Laboratory. This route was chosen because it allowed close control of the microstructure with the possible use of novel alloy matrices. The aim was to perform a systematic set of tests on well characterised material. A series of matrix alloys was chosen progressing from the simplest, commercially pure aluminium, through a solid solution strengthened, aluminium-1% magnesium to the most complex, a precipitation-hardened matrix containing the same magnesium concentration, namely Al-6061. Thus, the influence of matrix and interfacial bond strength could be studied. The pure aluminium matrix allowed the mechanical effects of the reinforcing phase on matrix dislocations to be studied without any complicating second phase or chemical interactions. Unfortunately, lack of time prevented the study of the Al-6061 matrix composites in this thesis. The study of these more complex alloy systems is an area of continuing work in Oxford.

The two matrix materials were an argon gas-atomised, commercially pure aluminium powder, designation Al-1070, of 7μm mean particle size, and a gas-atomised aluminium-1%magnesium alloy, designation Al-5050, with particle size less than 45μm. The powders were supplied by Alpoco. These powders were blended dry with three commercially available grades of C6 quality silicon carbide grit of nominal sizes 3, 10 and 30μm supplied by Sohio Electro Minerals Co. (U.K) Ltd.. The grit containing the largest particles was sieved at 28μm and 40μm to narrow the spread in its size

distribution. Composites of 5, 10 and 20% volume fractions were manufactured. This choice of particle sizes and volume fractions included those of commercial interest, but also gave the oppurtunity to study the differing effects of the microstructural parameters.

The powder blend was tumbled for 24 hours before hot-pressing, to aid homogeneity of the reinforcement distribution, and loaded into a cylindrical graphite die of 75mm internal diameter. The die was placed in a single acting GCA vacuum hot press of 300kN capacity. The die was induction heated with the temperature controlled via thermocouples in the die walls and shown schematically in Figure 2.1. Any chemical species evolved during the degassing and pressing cycle are recorded by a Leybold Quadrex 100 (Faraday cup) mass spectrometer. The pressing system is instrumented to record ram load and displacement, load transmitted through the powder compact, and die temperatures.

A typical pressing cycle has three stages. The first is a degassing for two hours at the pressing temperature with no applied load. This allows the temperature to equilibriate throughout the powder mix. The pressing temperature, chosen to be just below the solidus, was 650°C for the Al-1070 matrix composites and 630°C for the Al-5050 matrix composites. The load is then applied for two hours after major ram displacement has ceased. The pressing load was controlled at 11.7MPa. This gave loads in the range 5MPa to 9MPa transmitted through the powder blend, the remaining pressing load lost to the die walls by friction between ram and die. The final stage is cooling to room temperature under load in an argon atmosphere.

The rough edges of the hot-pressed billets are machined to give a reasonable shape for extrusion. Approximate density measurements were made at this stage, with an average density of 95% after hot pressing. Extrusion was performed on a Fielding vertical extrusion press of 500 ton capacity at an extrusion ratio of 50:1. This large ratio was used to improve the homogeneity of the particle spatial distribution and disperse any aluminium oxide films formed during the initial hot-pressing operation. The machined billets were heated to 420°C. A heated nose of unreinforced aluminium was placed on the billet before extruding through 90° shear dies made of tool steel. The press is instrumented for load and displacement as a function of time.

A convention for labelling the different composite systems will now be introduced. Each system will be given a label of the form: volume fraction/particle size/(heat treatment)/matrix alloy. Thus, 10/3/Qu/5050 corresponds to an aluminium-1% magnesium matrix containing 10% by volume of 3μm particles which has been quenched.

2.3 Material Characterisation

A number of microscopy techniques have been used to characterise the material. There are several microstructural features of interest:

i) the morphology and distribution of the reinforcing phase,

ii) the extent of damage in the reinforcing phase introduced during fabrication, and

iii) the distribution of the chemical species.

2.3.1 Optical Microscopy

Transverse and longitudinal sections were cut from the extruded bars using a diamond saw and then mounted in bakelite. After initial grinding on silicon carbide papers, the sections were polished on short-nap cloths with successively finer grades of diamond paste, down to a 1μm finish. A final short polish by hand in Syton W30 on a longer nap cloth removed the last remnants of damage from the matrix surface. This, however, left a small amount of relief between the matrix and silicon carbide surfaces which was estimated to be approximately 0.5μm by focussing on the top of the reinforcing phase and then on the matrix.

Typical micrographs of the composite of the Al-1070 matrix containing 30μm are shown in Figures 2.2 a-f. These show sections both longitudinal and transverse to the extrusion direction. Figures 2.2 a and 2.2b show longitudinal sections of the 5/30/1070 composite at different magnifications, showing that while the spatial distribution of particles appears homogeneous at low magnifications, it is in reality quite clumped. This is again shown in Figures 2.2c and 2.2d of the 20/30/1070 material. By comparing Figures 2.2c&d with 2.2e&f, of transverse sections in the 20/30/1070 material, one can see that a certain amount of alignment of the particles has occurred on extrusion.

Micrographs of the polished sections were converted into computer-recognisable, electronic form by scanning on an Apple Macintosh scanner. The subsequent electronic images were examined in an "Ultimage" image processing system. This allowed the basic morphology of the silicon carbide particles to be determined and also to show the effect of extrusion on their spatial distribution. The aspect ratio distributions of the reinforcing phase are shown in Figures 2.3a-e for both orientations. These results show the particles to be "blocky" rather than platelet or cubic and confirm the alignment during extrusion. The increase in aspect ratio with particle size should also be noted as this will be of importance when discussing the mechanical properties. Simple statistical tests on the particle spatial distributions have been performed by S. Petts [162]. These show the spatial distributions in the composites are not significantly different from random distributions generated by Monte Carlo simulations. Thus, models based on

mean-field approximations are likely to be valid on a macroscopic scale.

2.3.2 Scanning Acoustic Microscopy (SAM)

The principle objective of this thesis is to characterise the micromechanisms of fracture in PRMMCs. It is, therefore, necessary to assess the extent of any damage which may have been introduced during fabrication. It would not be surprising, for example, to find cracked silicon carbide particles on the fracture surface if they had been broken during extrusion. Indeed, the presence of particles damaged prematurely during fabrication has been cited as the cause of the disappointingly low values of toughness and ductility in PRMMCs [28,40].

An inherent problem in assessing damage levels in PRMMCs is the large residual compressive stress in the particles. This stress is generated on cooling from the fabrication or heat treatment temperatures by the large difference in thermal expansion coefficients of the two phases. Any cracked particles would, therefore, be held together, making their observation in the optical or scanning electron microscope difficult. The scanning acoustic microscope (SAM) was used to overcome this problem. As is shown in Figures 2.4a-b, cracks are visible in SAM which are not revealed by optical microscopy.

Specimens were prepared as for optical microscopy and examined in the SAM. Particular care was taken to ensure that the surface relief between the two phases was kept to a minimum. In the SAM an image of the sample is produced by mechanically scanning an acoustic lens in a raster pattern parallel to the specimen surface. Water is used to couple the longitudinal acoustic waves generated by the lens into the specimen. By displaying the signal reflected from the surface as a function of lens position, an "impedance" image of the specimen is produced. Additionally, on defocussing the microscope, by decreasing the lens-specimen separation to below the focal length, Rayleigh waves can be excited in the specimen surface [163]. These waves can interact with cracks normally incident at the surface, giving rise to characteristic fringe patterns which clearly delineate the cracks. Potentially, surface incident cracks of 9nm width can be detected in a SAM operating at 2GHz [164]. The instrument used in the present study was an E. Leitz SAM operating at an imaging frequency of 2GHz, giving a spatial resolution of 0.7μm.

SAM showed that extrusion caused insignificant damage in any of the composite systems, with less than 5% of the particles fractured. Extrusion ratios of 50:1, therefore, can be used without fear of breaking the reinforcing phase. There was, however, an increase in damage on increasing volume fraction, particle size and aspect ratio. The majority of the damage was in the form of surface spalling. An example of this can be seen in Figure 2.5. This mode of failure was seen frequently during further fracture

experiments as will be described in later chapters.

2.3.3 Electron Microprobe Analysis

Magnesium is a common alloying element for aluminium. It is used in the majority of alloy systems, either on its own, in the 5XXX series, or more commonly with silicon and copper. There have been several reports in the literature, however, of magnesium segregation to the particle/matrix interface in PRMMCs of these magnesium-containing aluminium alloys [143,156,159]. This segregataion has, in general, been accompanied by a degredation in the mechanical properties, in particular the ductility, of the composite.

The variation in magnesium concentration on crossing the particle/matrix interface was investigated by electron microprobe analysis. The wavelength dispersive spectrum of the magnesium K_α peak was used. Lapped and polished samples of the Al-5050 matrix composites were examined in a Cameca SU-30. Figure 2.6 shows the marked increase in magnesium concentration at the interface. This layer was, however, too thin for quantitative analysis making its complete identification by this technique impossible.

2.3.4 Transmission Electron Microscopy (TEM)

Preliminary TEM studies on the composites have been undertaken by Mr. C-F Man and are reported here briefly for completeness.

Specimens have been prepared by two techniques. The first has been developed to study the interface between the particle and matrix. Here, spark-eroded discs of the composite were mechanically dimpled to 100μm and then ion-beam thinned at a voltage of 4kV, at an angle of 20° until perforation. The ion milling was performed on a liquid nitrogen cooled stage to reduce damage to the specimen. The second preparation route, of electropolishing, allowed the matrix microstructure to be investigated without the possiblity of spurious mechanical damage being introduced.

The particle/matrix interface in specimens of the as-fabricated Al-5050 and Al-1070 matrix composites were examined. The abrupt, planar interface in the Al-1070 matrix material is shown in Figure 2.7, indicating no interfacial reaction. This should be contrasted with the interface in the Al-5050 matrix material shown in Figure 2.8. An interfacial product is clearly visible. This has been definitely identified as magnesium oxide in the high volume fraction composites, with the possibility of a spinel phase in the low volume fraction composites [165].

The effect of the heat treatment on the grain size was investigated in the electropolished specimens. This revealed that for the higher volume fraction composites, the grain size is approximately equal to the interparticle spacing. The particles were found at grain boundaries, in common with previous work [3]. The grain size of the low volume fraction composites was significantly smaller than the interparticle spacing [166].

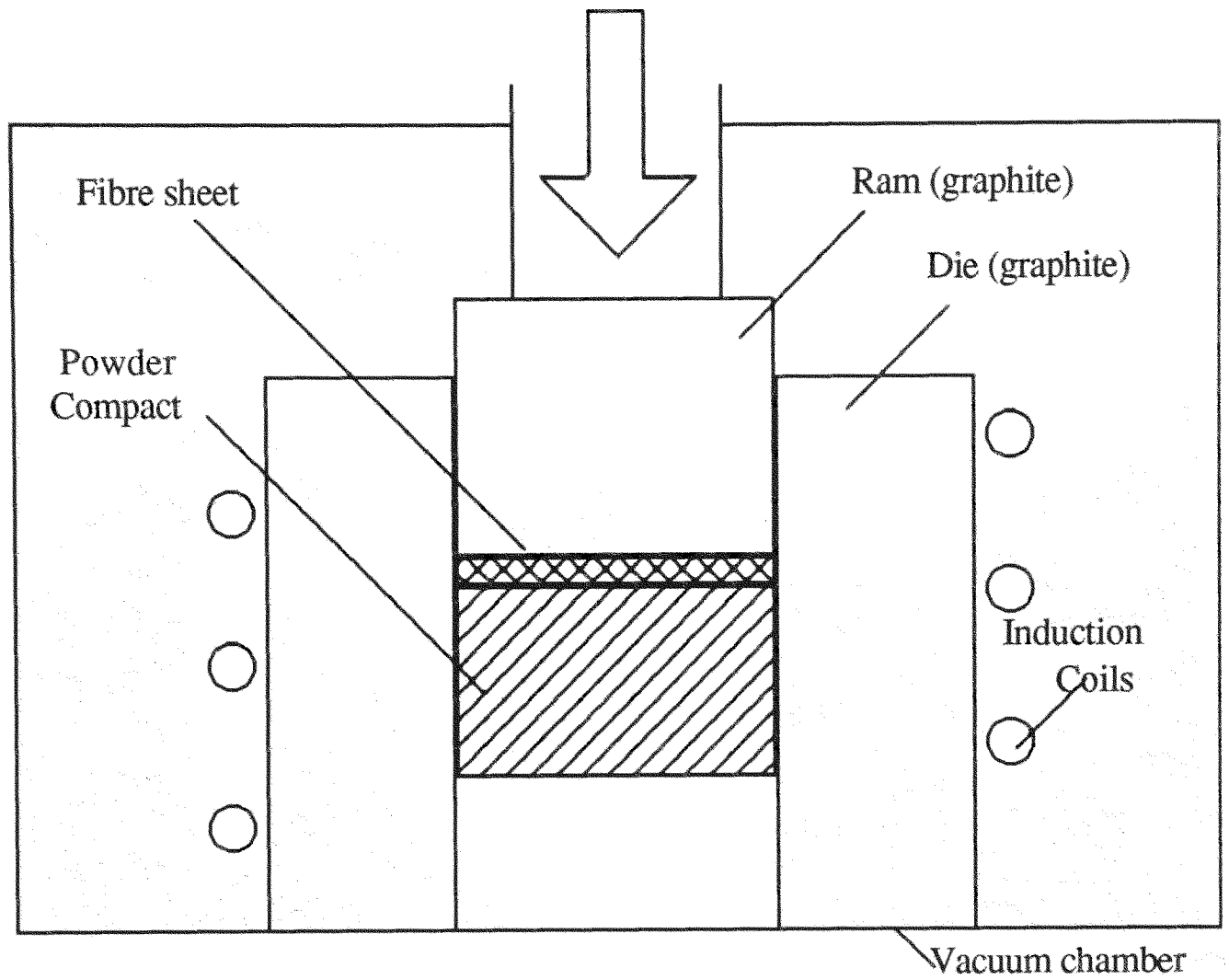

Figure 2.1: Schematic section of vacuum hot press

(a)

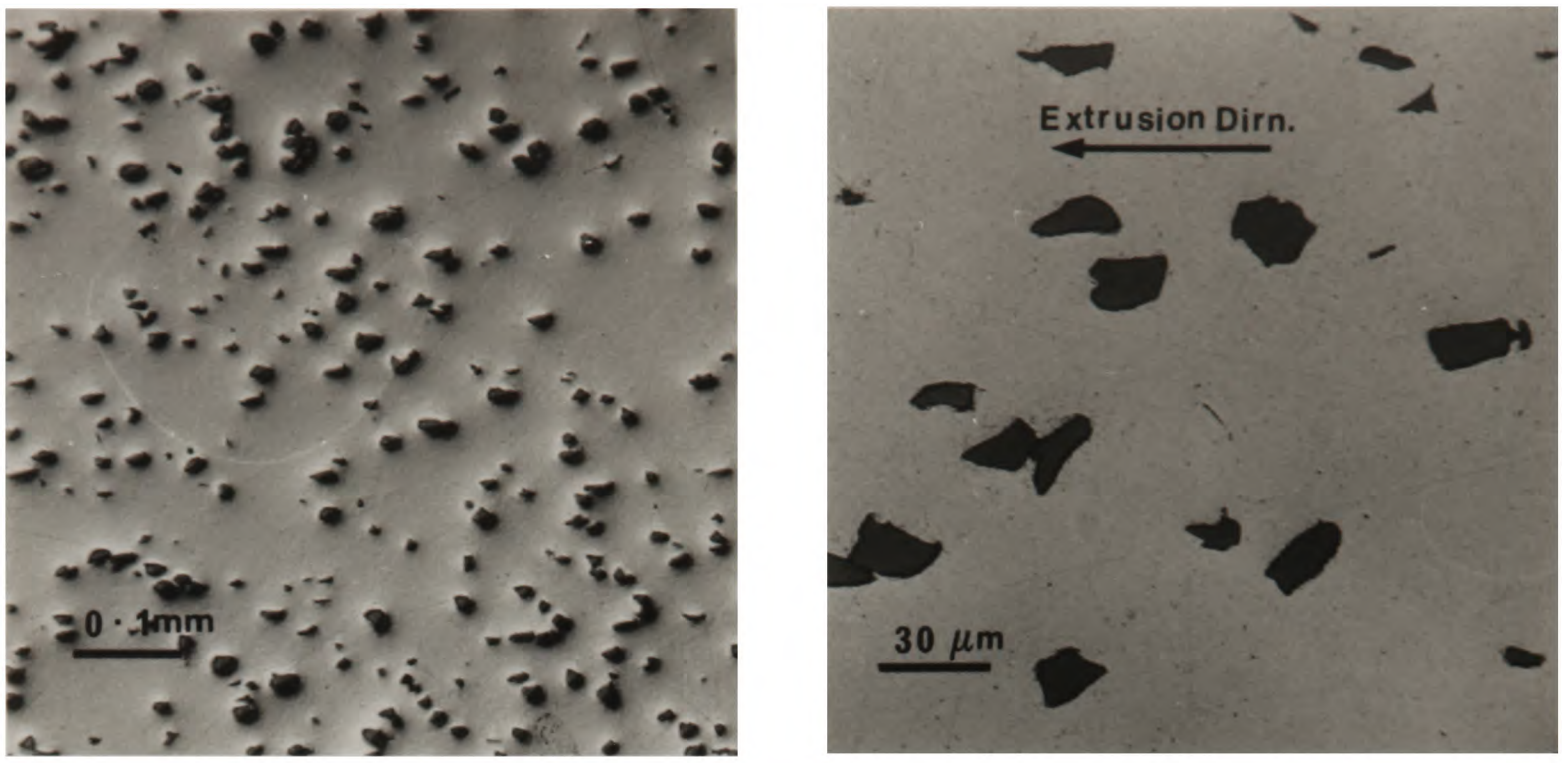

Figures 2.2 a+b: Longitudinal sections of 5/30/1070.

(c)

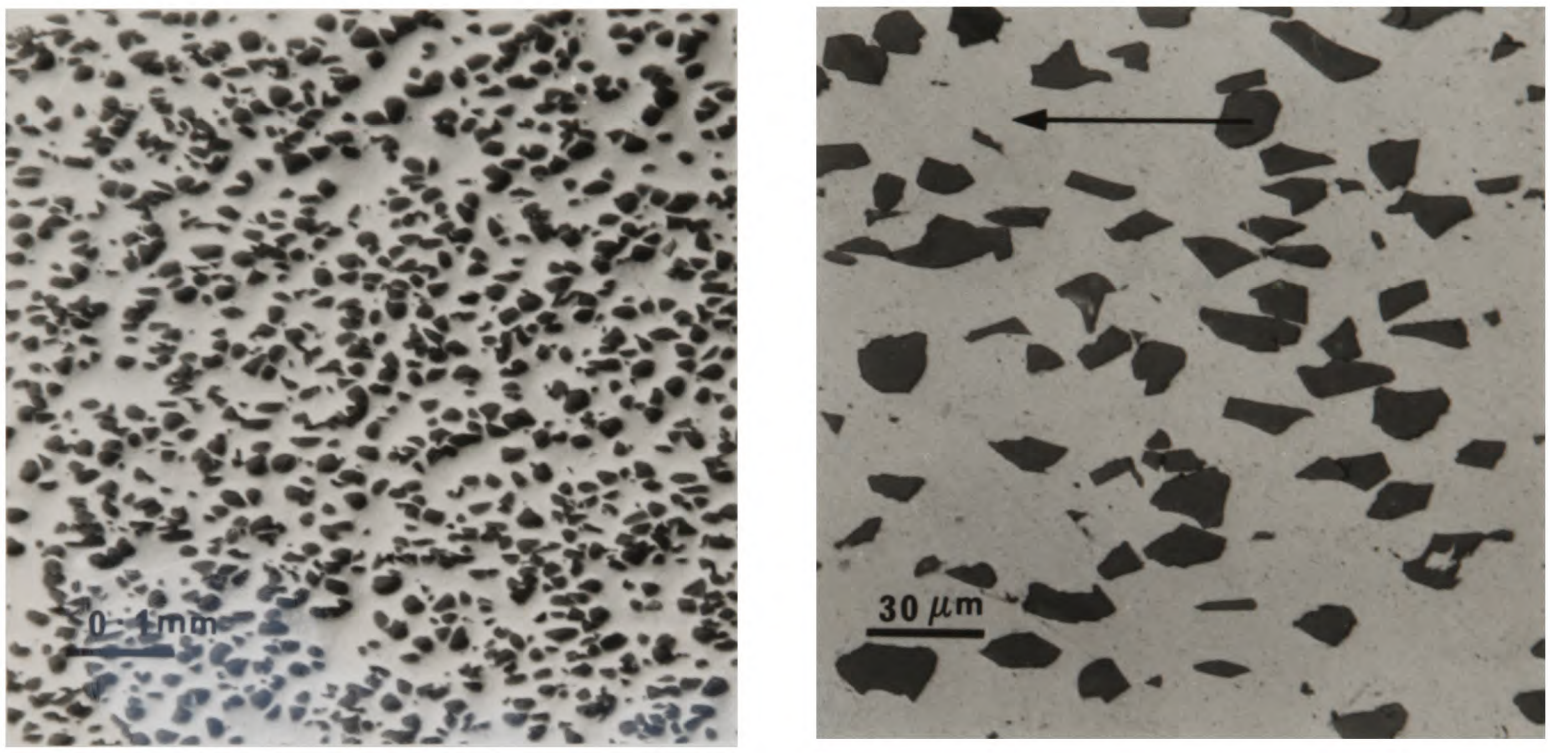

Figures 2.2 c+d: Longitudinal sections of 20/30/1070.

(e)

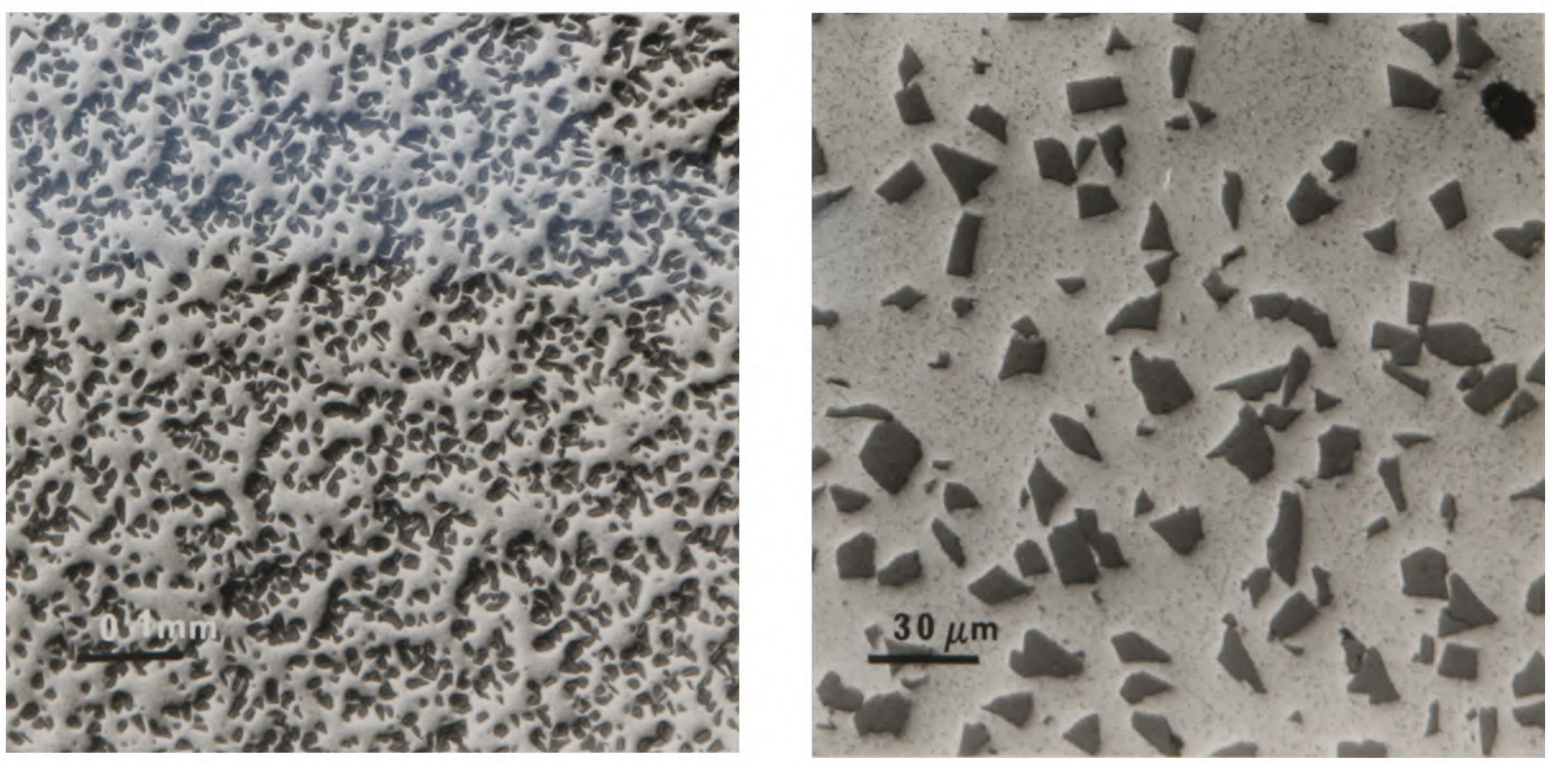

Figures 2.2 e+f: Transverse sections of 20/30/1070.

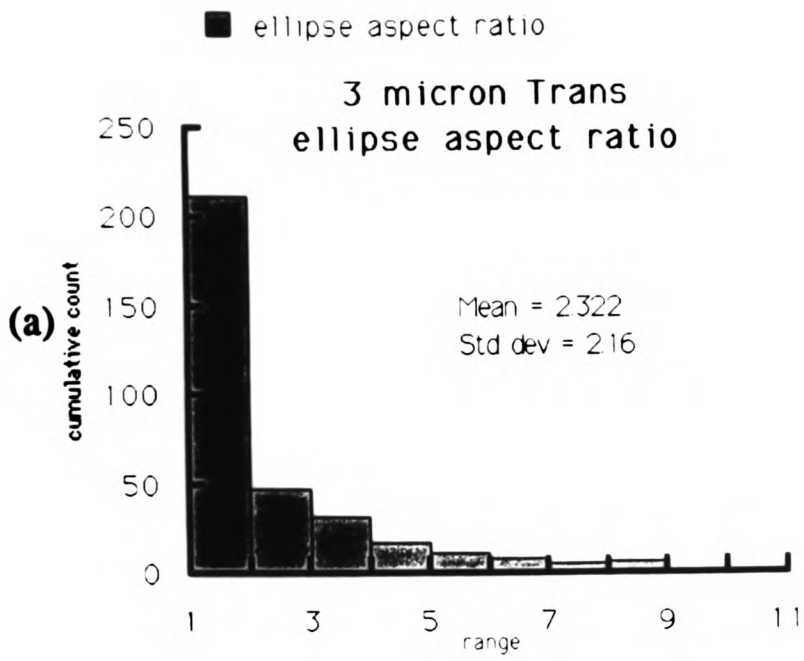

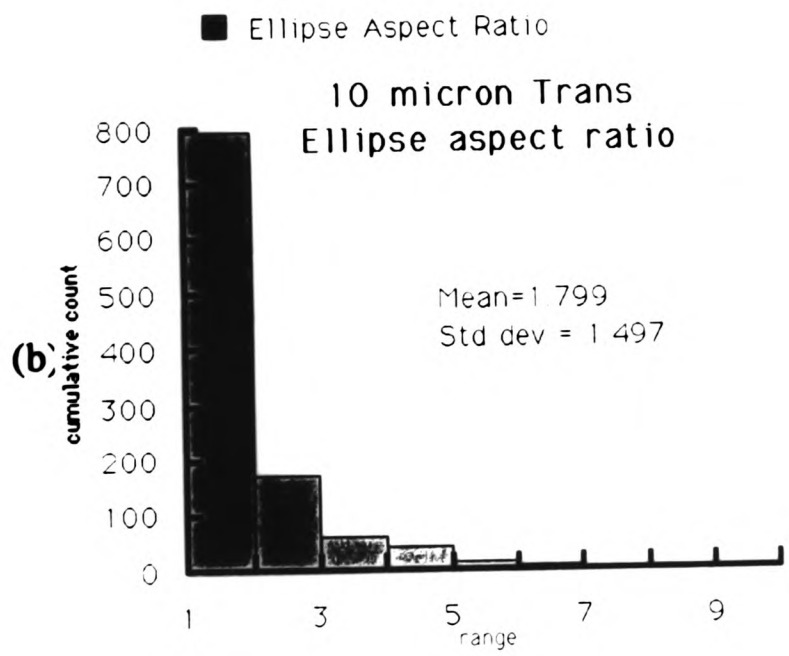

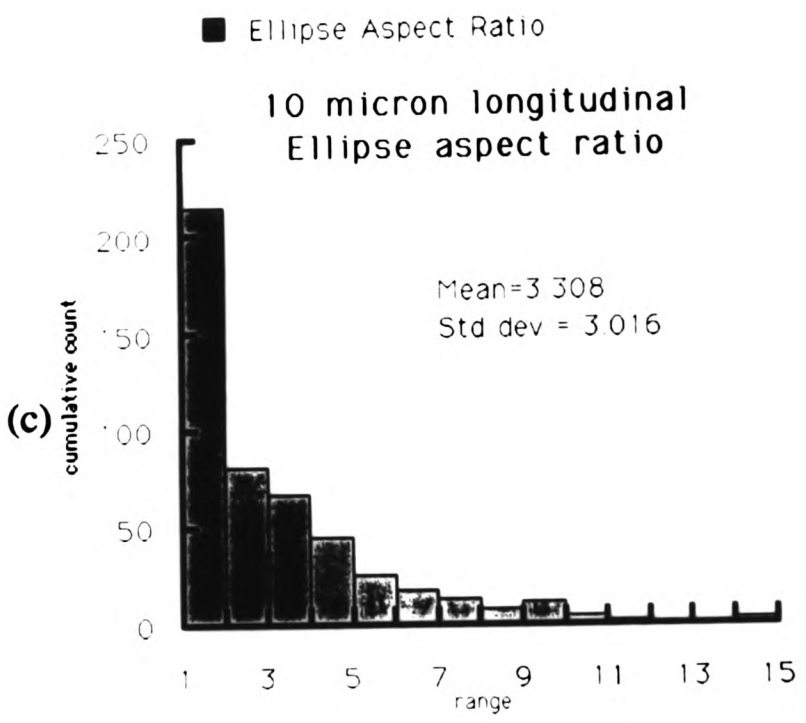

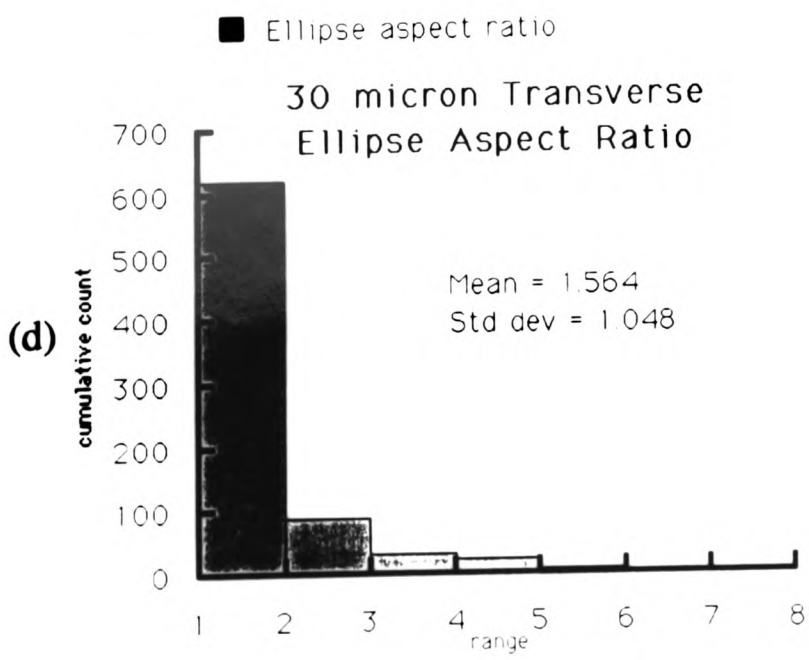

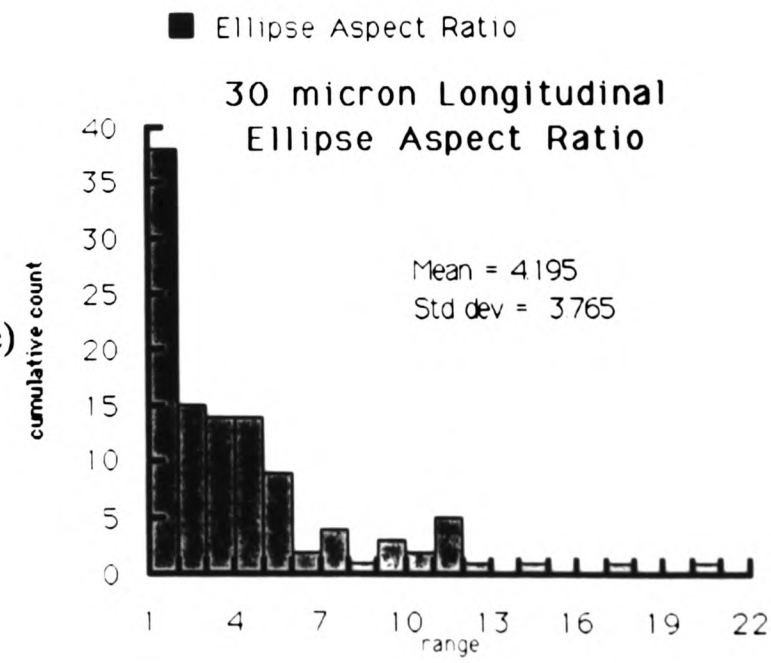

Figures 2.3 a-e: Aspect ratio distributions of the three particle sizes transverse and longitudinal to the extrusion direction.

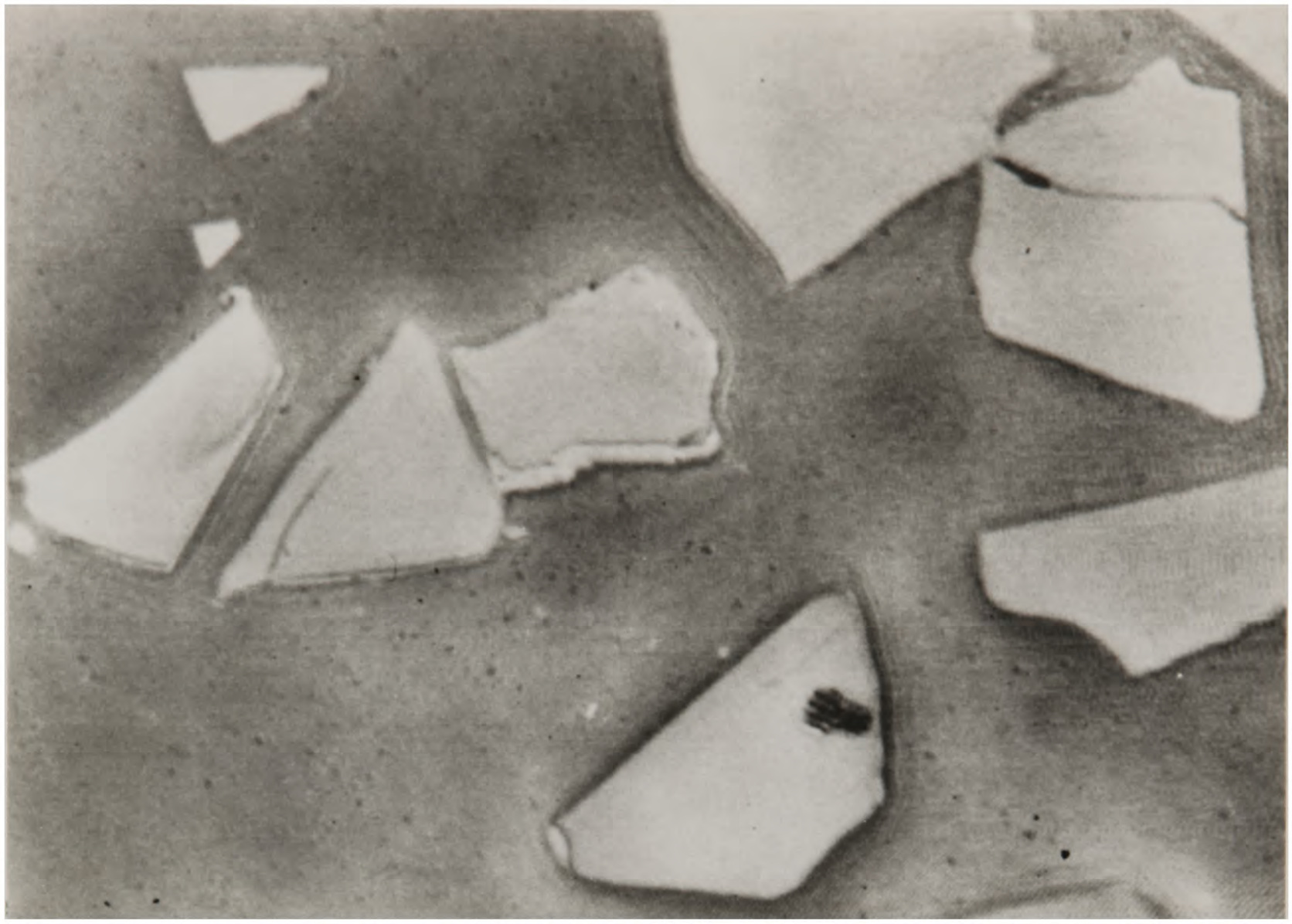

(a)

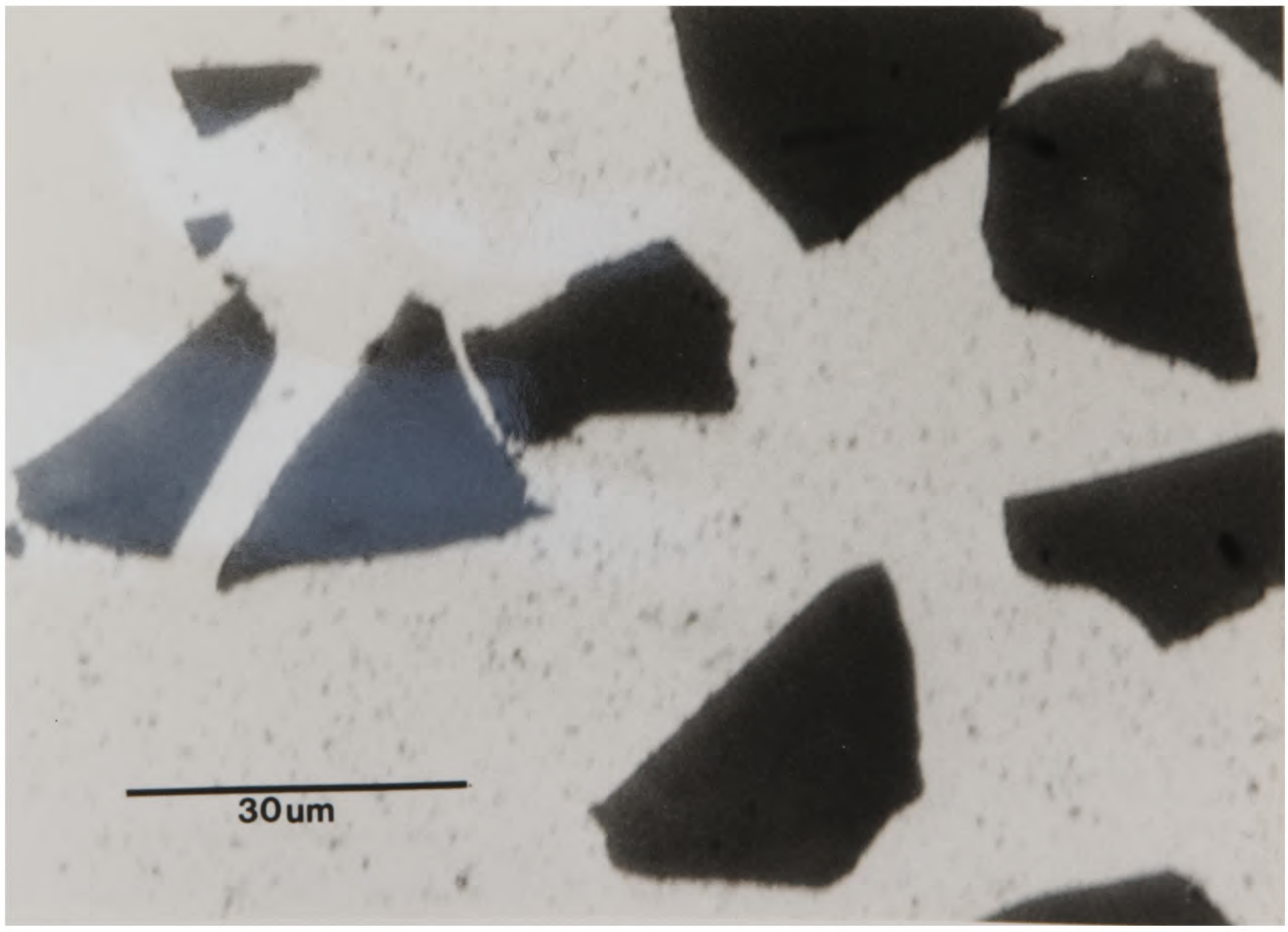

(b)

Figures 2.4 a+b: Comparison of acoustic (a) and optical (b) micrographs of 20/30/1070.

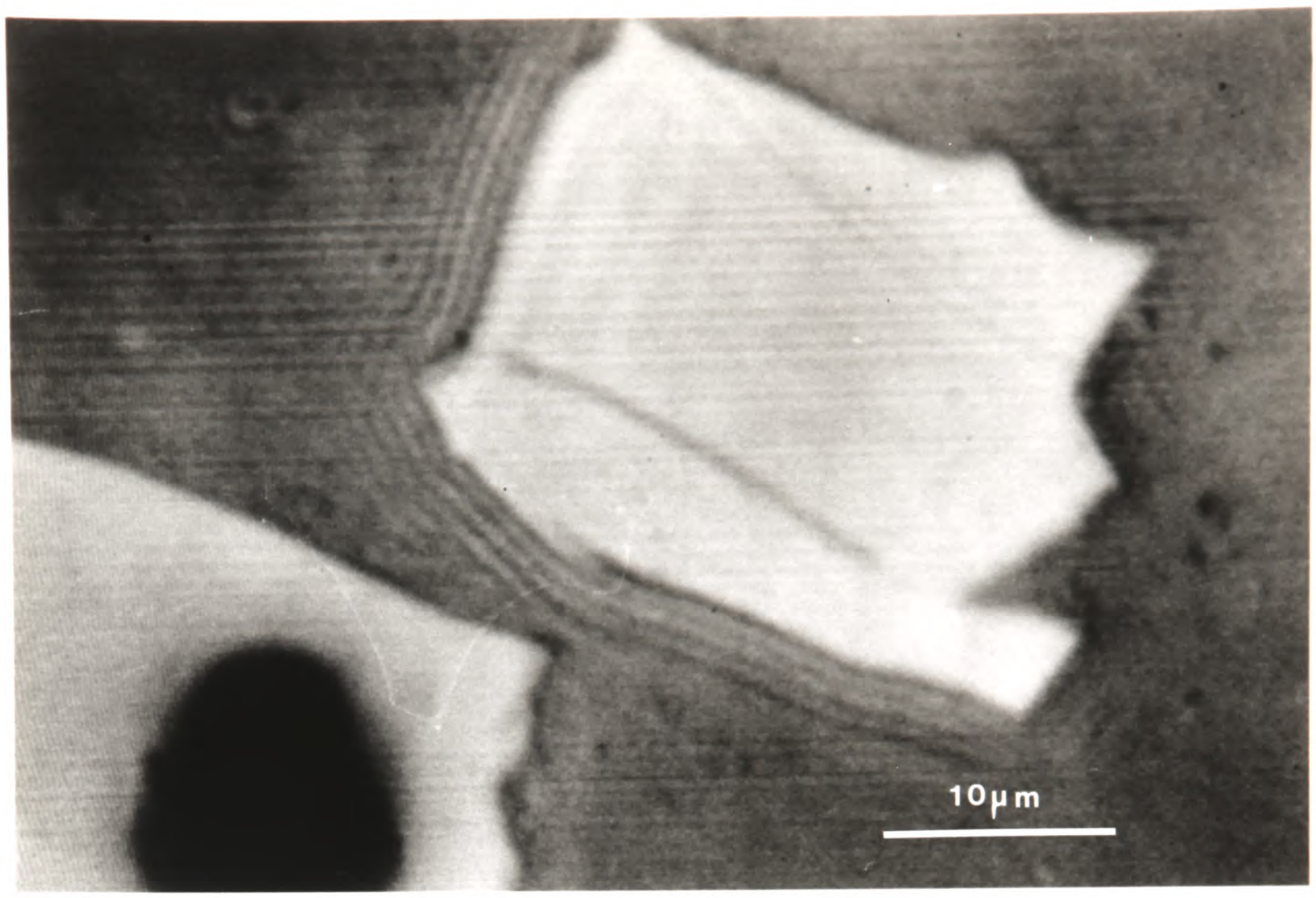

Figure 2.5: Acoustic micrograph of 5/30/1070 showing spall failure.

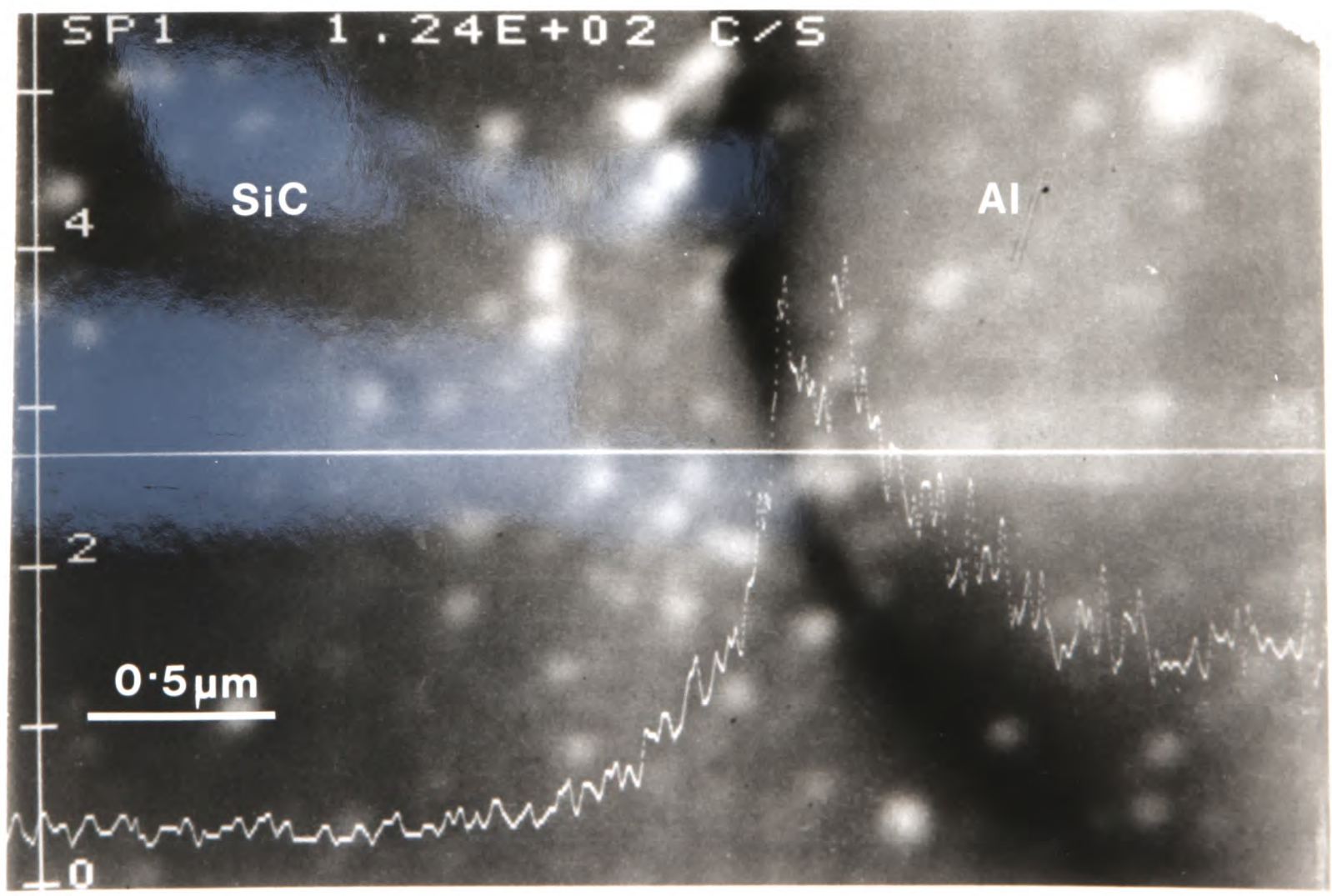

Figure 2.6: Variation in Magnesium concentration on traversing interface in 5/30/5050.

Figure 2.7: Bright field image of interface in 20/3/Qu/1070. Taken at 200 kV on Philips CM-20.

Figure 2.8: Bright field image of interface in 20/30/Qu/5050. Taken at 200 kV on Philips CM-20.

Chapter 3: Mechanical Properties

3.1 Introduction

The mechanical properties of PRMMCs are controlled by the complex interaction of matrix and reinforcement. The addition of a second phase of different elastic properties induces inhomogeneous deformation and, therefore, strain concentrations. In order to maintain the displacement compatibility across the interface on the application of a far-field strain, dislocations are generated at the particle-matrix interface. Also, the difference in thermal expansion coefficients between the two phases necessitates the generation of dislocations to accommodate thermal strain on changing temperature. The interaction of matrix dislocations with these dislocations, with matrix precipitates and with the reinforcing phase determines the mechanical behaviour of the material, as outlined in Chapter 1. Simple matrix alloy composites allow the influence of the reinforcement on dislocation motion to be studied directly without the complicating effects of matrix precipitates. The response of the material to applied strains can be studied macroscopically and locally by a combination of techniques.

The aim of this Chapter is to study the effect of systematic variations in reinforcement volume fraction, particle size and heat treatment on the mechanical behaviour of composites of two simple alloy matrices. The results will be compared with the predictions of current continuum and micromechanical models of PRMMCs.

3.2 Experimental Procedure

Tensile tests to failure were performed on the composites in two heat treated conditions; an annealed and a quenched state. The specimen geometries and heating cycles are shown in Figures 3.1 and 3.2. The heat treatment was performed after machining to remove any residual stresses that may have been introduced. The inability to cut threads in the Al-5050 matrix material, due to shear failure during machining, necessitated the change in specimen geometry. The specimen gauge lengths were polished to a 1μm finish to show the extent and nature of surface deformation away from the fracture surface.

The tests were carried out on an Instron 1122 at a strain rate of $3{\cdot}2\times10^{-5}$ s^{-1}. Two strain gauges per specimen were used, each forming part of a three wire, quarter bridge amplifier circuit, with data from each recorded separately. The inactive gauge in each amplifier circuit was attached to a piece of composite and placed near the test specimen to reduce thermal and electrical variations. The analogue strain and load data were converted to digital data and recorded serially on an Opus-III PC microcomputer. This was driving a CIL-Microsystems data acquisition package. The data were

subsequently analysed using a Borland "Quattro-Pro" spreadsheet program. The load-displacement data were also recorded on the Instron chart paper allowing the elongation to failure and ultimate stresses to be evaluated.

The modulus was measured during unloading and reloading from within the plastic regime to remove any effects of microyielding. Microyielding occurs when the values of stress are sufficient to cause local yielding of the matrix. This has been reported to have a significant influence on measured values of the modulus [105,167,168]. For some specimens the modulus measurement was repeated at larger strains.

3.3 Results

The results were analysed to show the effect of the microstructural parameters on the following for each matrix alloy:

i) Modulus;

ii) 0.05% and 0.2% proof stresses;

iii) Initial and secondary work-hardening rates.

The effect on elongation to failure was also investigated and the results will be discussed later in the light of the fractographic results.

The results are given in Tables B.1 to B.11 in Appendix B and presented here graphically in Figures 3.3 to 3.14 which show more clearly the effects of the parameters.

All the stress/strain curves show a near parabolic form for the nominally elastic region, consequently making the determination of the onset of deviation from linearity very difficult. This has also been observed by other workers in many different composite systems [27,81,105,133]. It is assumed that this is caused by microyielding on a widespread scale. The observed stress/strain behaviour is the result of the competitive effects of local stress concentrations and local plastic constraint. Stress concentrations occur near the reinforcing phase which may cause local microyielding, lowering the proportional limit, while at the same time the presence of the reinforcing phase restrains the matrix from plastic flow, increasing the proportional limit. Indeed, the observed lowering of proportional limit for some high-strength aluminium alloys is due to this effect. The values quoted in the text are, therefore, for defined 0.05% and 0.2% proof stresses. The 0.2% proof stress is now a strong function of the work-hardening rate.

The experimentally determined values of modulus for the Al-Mg matrix composites are higher than those of the corresponding pure aluminium matrix composites. The modulus is found to be independent of particle size but increases monotonically with volume fraction for both matrices. Although quenching increases the

modulus of the Al-1070 matrix composites slightly, no consistent trend was found in the Al-5050 matrix composites. The modulus, however, decreases on increasing strain for very low increments of plastic strain. This has also been observed recently in Al-6061 composites [83] and a "model" PRMMC system of silicon particles precipitated from an Al-Si-Mg alloy [121].

The defined proof stresses are, in general, increased on increasing volume fraction for a given reinforcement size, and on decreasing reinforcement size for a given volume fraction. This trend is more apparent in the composites of the Al-1070 matrix than in those of the Al-5050 matrix. This has also been observed in previous studies [81-87,93-98] on a number of matrix alloys. The higher strength of the unreinforced Al-5050 matrix is translated into higher composite strengths. Quenching in turn further increases these yield stresses for composites of both matrices, again a common result on a range of matrices [84-87,90,95]. Quenching appears to have a greater influence on the lower volume fraction composites, with increased strengthening over the unreinforced alloy matrices.

The work-hardening behaviour of the composites was examined by assuming a simple power law hardening expression of the form

$$\sigma = k\epsilon^n$$

The behaviour is described by the coefficient, n, and the pre-exponential factor, k, which is an effective plastic modulus and defines the rate of work hardening. The rates, k, and exponents, n, were evaluated at two strains for each composite. One at the onset of the plastic region and the other at a much higher strain, corresponding to two regions where different models of work-hardening behaviour are appropriate. The first applies before the relaxation of dislocation loops, and the second during secondary dislocation generation.

The values of n during primary work hardening, measured at the onset of deviation from linearity, show no clear trends, taking values close to one. The coefficients are, however, greater for the Al-5050 matrix composites than for the Al-1070 matrix composites and are increased on quenching. The coefficients are also greater for the composites than for the unreinforced matrices. The primary rates, k, show well-defined trends, increasing with volume fraction and on quenching. The values of n and k during primary work hardening are strongly dependent on the choice of strain at which they are measured, with increasing values on decreasing strain. Whilst every effort was made to be consistent, the difficulty in determining the onset of yield, and thus the strain at which n was evaluated, may have led to the true behaviour being obscured.

The values of n and k are much smaller during secondary work hardening than during primary work hardening. The rates show well-defined trends similar to those of the yield stress. There is increased rate on decreasing particle size for a given volume fraction and on increasing volume fraction for a given particle size.

3.4 Current Interpretations of Mechanical Properties

The two broad approaches to modelling the mechanical behaviour of PRMMCs were outlined in Chapter 1 and will be discussed in more detail here. The case for a description combining both approaches is made along with a tentative suggestion for such a very simple hybrid model.

3.4.1 Continuum Models

Before discussing the various models, it is pertinent to ask whether the continuum approximation can be justified. The basic criterion which must be satisfied for the approximation to be valid is that the matrix should be homogeneous; that is have the same properties at every position. For this to be true, there must be no enhanced dislocation storage at the reinforcing particles or, put another way, the scale at which deformation occurs is much finer than the scale of the reinforcing particles. Goods and Brown [141], in their review of void nucleation, determine a critical particle size above which continuum models are valid. This can be expressed as follows:-

$$r_c = \frac{\alpha^2 \mu^2 b}{\sigma_y} \left(\frac{d\sigma}{d\epsilon}\right)^{-1}$$

where r_c = critical particle size,
α = constant,
μ = shear modulus of matrix,
b = magnitude of Burger's vector,
σ_y= yield stress of matrix.

Using $\frac{d\sigma}{d\epsilon}=\frac{\mu}{300}$ and $\sigma_y=\frac{\mu}{750}$, the critical size is of the order of 1-2μm, implying that the application of continuum models to PRMMCs is valid. It should be made clear that the criterion is only just satisfied and that for the smaller reinforcements it may, therefore, be an oversimplification. This result may be expected intuitively as the particle size is much greater than the dislocation spacing.

The myriad of continuum models fall into three basic categories. The first are based on simple assumptions of the load partitioning between the two phases, the second are finite element techniques, and the third are those based on Eshelby's equivalent inclusion technique. The latter two will be discussed briefly as the detailed

predictions of these models are not available without computation. The first category gives simple analytical solutions which can be compared directly with experiment.

3.4.1.1 Load Sharing Models

The original shear lag model of Cox [101], developed to model the strength of paper by considering the long cellulose fibres, has been discussed in detail [169] and used to predict many mechanical properties of fibre-reinforced materials [169-172]. In the original formulation of the model, load is transferred from the matrix to the fibres by shear forces at the interface, partitioning and, thereby, reducing the effective stress in the matrix. The tensile transfer of load at the fibre ends is ignored. For fibres of finite and, in the case of particles, unity aspect ratio, the tensile transfer at the fibre ends cannot be ignored since it makes a significant contribution to load partitioning. Nardone and Prewo have developed a simplified model based upon this modification to the shear lag analysis [102]. By assuming a platelet geometry for the particulate reinforcements, they predict the composite yield stress to be given by

$$\sigma_{cy} = \sigma_{my}\left(\frac{V_f\,(S+4)}{4} + (1\text{-}V_f)\right)$$

where σ_{my} = matrix yield stress,
S = aspect ratio of reinforcement,
V_f = volume fraction of reinforcement.

Good agreement is claimed for the yield stress of whisker-reinforced Al-6061 [102] and similar models have also been developed which claim good agreement with experiment [119,120]. Taya and Arsenault [123] show, however, that this model consistently underpredicts the experimental results for particle-reinforced composites. Substitution of reasonable values for the above variables for a PRMMC shows that an increase in yield stress of only a few per cent is predicted. Note also the dependence on aspect ratio of reinforcement, not absolute size. The mechanism of load transfer from matrix to reinforcement may be radically altered on extrapolation from long fibres to equiaxed particles, thereby undermining a basic component of the model.

Continuum models based on the rule of mixtures have been developed for the load partition in two-phase materials of differing elastic properties [173-175]. For an aggregate or alloy consisting of two phases, α and β, deformed in simple tension, the modified rule of mixtures for stress and strain is given by the following equations:

$$\sigma_c = \sigma_\alpha V_\alpha + \sigma_\beta V_\beta$$
$$\epsilon_c = \epsilon_\alpha V_\alpha + \epsilon_\beta V_\beta$$

where V is the volume fraction, σ and ϵ are the average values, respectively, of the

directional components of stress and strain in the direction of the applied load, and the subscripts refer to the composite alloy, c, and the two phases, α and β, respectively. The qualifying term, "modified", is used to indicate that the average values of the stresses and strains in the two phases are *in situ* values and not the bulk properties as would be the case for the classical rule of mixtures. These *in situ* values are difficult to determine experimentally.

Originally developed for systems such as dual-phase steels and α/β brasses, these models have been adapted to consider metal composites [176]. The models predict the overall stress/strain behaviour of the material and not the local values of the fields. The plastic deformation of such systems can be modelled by combining the rule of mixtures with dislocation-continuum hardening behaviour [177,178].

3.4.1.2 Finite Element Modelling

Finite element models have two basic components: a constitutive equation detailing the local material behaviour, and a network or cell structure dividing the entire body. The solutions of the constitutive equation are forced to obey specified boundary conditions at the cell boundaries. This broad framework allows great flexibility in formulating problems. The solutions to the constitutive equations are, in general, only tractable numerically and, even in the simplest geometrical arrangements, limited by the available computing power. Thus, solutions are at the moment generally restricted to two-dimensional problems or to conditions of plane stress or strain. An attraction of these models is the prediction of local values of the stress and strain fields. This should enable composite properties governed by these local stresses, such as fracture, to be modelled, giving increased understanding of material behaviour. The entire stress/strain characteristic can be predicted, although a criterion for failure must be formulated or the model will continue to predict performance to infinite strain!

The properties of PRMMCs have been modelled by such finite element techniques with some success [110-115]. These models do not, however, predict the observed particle size dependence on yield stress. Also, the models are necessarily highly sensitive to the form of the constitutive equation and to the cell structure, giving concern over the stability of predictions.

3.4.1.3 Eshelby's Equivalent Inclusion

Eshelby showed that an analytical solution can be obtained for the stress field in and around an elastic inhomogeneity embedded within an infinite matrix under an applied far-field strain, provided the inhomogeneity has an ellipsoidal shape [103]. The stress field is disturbed by the presence of the inhomogeneity which is constrained by

the surrounding material. By a series of cutting and welding exercises, Eshelby shows that the inhomogeneity can be replaced by an equivalent inclusion of the same elastic constants as the surrounding matrix which has undergone a stress-free strain chosen such that it has the same final constrained shape as the inhomogeneity. Thus, the inhomogeneity and equivalent inclusion can be interchanged without disturbing the matrix. The solution to the similar elastically homogeneous problem is also due to Eshelby. Therefore, by calculating the equivalent stress-free strain required to imitate the inhomogeneity, the solution to the inhomogeneous problem is also solved. The stress-free strain, $\boldsymbol{\epsilon}^t$, and the constrained strain, $\boldsymbol{\epsilon}^c$, are simply linked by Eshelby's accommodation tensor, $\mathbb{S}$, which is solely dependent upon the inclusion geometry and Poisson's ratio of the medium, as follows:

$$\boldsymbol{\epsilon}^c = \mathbb{S}\boldsymbol{\epsilon}^t$$

The model has been extended to non-dilute composites containing significant volume fractions of dispersed inclusions by adopting mean-field approximations. Initially the mean-field models were formulated in two non-equivalent ways [179,180]. Later work on elastically homogeneous composites clarified the models and the relationships between them [181,182]. These approaches were finally unified by assuming that the inclusions sample the mean matrix stress [183].

It is an attractive model as it can be easily extended to model all the elastic properties of the composite, such as modulus and thermal expansion coefficient, as well as the response to an applied stress or strain by a simple superposition of the stresses. The plastic behaviour can similarly be predicted, given a yield criterion and an expression for the *in situ* work-hardening response of the matrix.

The model predicts the effects of the microstructural parameters on the material response. The disturbance in the homogeneous stress field due to the presence of the dispersion of inclusions and, thus, the mean matrix stress is determined by $\boldsymbol{\epsilon}^t$ and $\mathbb{S}$. $\mathbb{S}$ is a function of the inclusion geometry and elastic constants, with the geometrical dependence primarily on aspect ratio, not on absolute size. There is increased load transfer on increasing inclusion aspect ratio.

The mean-field approximation has the same form as a simple rule of mixtures, namely

$$V_f\langle\sigma\rangle_i + (1\text{-}V_f)\langle\sigma\rangle_m = 0$$

where V_f = inclusion volume fraction,
$\langle\sigma\rangle_i$ = mean inclusion stress,
$\langle\sigma\rangle_m$ = mean matrix stress.

A reduction in mean matrix stress is therefore expected on increased inclusion aspect ratio and volume fraction, which is shown as increased composite yield stress and stiffness. These trends are confirmed by experiment, with an increase in yield stress on moving from particulate to whisker reinforcements [27,106,]. Note once again, however, that the mean stresses are independent of absolute particle size. The predicted values of the elastic properties are in good agreement with experiment [105,106,109] for all but the composites of low-strength matrix alloys [108,109]. The predicted yield points and plastic response are not in such good agreement [106,109], with the discrepancies accentuated by the low-strength alloy matrices. However, Bauschinger effects are predicted well [106], implying that the load transfer from matrix to reinforcement is correctly modelled but the criterion for yield is poor. To model the plastic properties requires accurate values of the *in situ* constrained matrix properties which are often not well represented by the unreinforced matrix. The adoption of a mean-field approximation, necessary to predict the behaviour of all but very dilute dispersions, imposes a restriction on the model, namely that the model can no longer predict the local values of the fields.

3.4.1.4 Comments on Continuum Models

The validity of applying continuum models to these composite systems has been asserted and justified earlier. This, however, only implies that the continuum approximation is valid and the models, therefore, describe the mechanics of material behaviour well. The models do not describe, nor do they attempt to describe, the physics of material behaviour and are, therefore, dependent solely upon representations of the material. It is in these representations that the continuum models are lacking.

In the specific case of PRMMCs, the *in situ*, constrained flow properties of the matrix are unknown and must be approximated or assumed from the unreinforced matrices. The representations of the elastic properties of materials are, in general, good, leading to the close agreement of theory and experiment. This also confirms the validity of the continuum approximation as the load transfer and partitioning are correctly assigned. However, the representations of plastic behaviour are poor with even the onset of plasticity predicted unreliably, as was shown earlier. If a true representation could be made or input variables known accurately, then the models would necessarily predict the material behaviour correctly.

Improved representations will be the product of a deeper understanding of the physics of composite behaviour at an atomic, or at least dislocation, level. The understanding of monolithic alloys at this level, although still fairly limited, is far more complete, with well established models and results. A first step to an improved representation of a composite is to establish whether these models can be successfully or

even meaningfully applied to a PRMMC.

3.4.2 Dislocation Mechanics Models

The only thorough attempts to test the fundamental applicability of dislocation models to PRMMCs are due to Humphreys and his co-workers [84-86], although there has been some work by other groups [4,5,7]. The barriers to dislocation motion are delineated, based on the known results of studies on dispersion-strengthened alloys, and a scheme for adding these separate effects together is formed. Yield in this model is defined as the onset of dislocation motion through the bulk of the matrix; that is when sufficient stress is applied to overcome the barriers to dislocation motion.

The barriers to dislocation motion are: grain and sub-grain boundaries, reinforcement particles, matrix precipitates and solutes, residual stresses, and residual dislocations [84,85]. A detailed description of the discrete contributions of each to composite strengthening has been given by Humphreys [84] and only the two dominant terms for low-strength alloys, without matrix precipitates, shall be considered here. This description closely follows the arguments presented there.

3.4.2.1 Grain and Sub-grain Boundaries

The contribution of grain size, D, to the strengthening, σ_{gb}, is given by the well-known Hall-Petch relation:

$$\sigma_{gb} = \frac{K_y}{\sqrt{D}}$$

The constant K_y is typically $0.1 MNm^{-3/2}$ [184] and for fine grained material can have a higher value of $0.15 MNm^{-3/2}$ [185]. The thermomechanical processing of PRMMCs tends to produce a fine grained structure [3], of the order of a few microns, and this term is likely to make a significant contribution to the strengthening. For the low strength alloy matrices this may be the dominant term. However, if grain growth occurs, this term will be greatly reduced.

If one assumes that each reinforcing particle, of diameter d, nucleates a single spherical grain, an estimate of the grain size can be made as a function of particle size and volume fraction, V_f, as follows:

$$D = d\left(\frac{(1-V_f)}{V_f}\right)^{1/3}$$

This result has been verified by Miller and Humphreys [85] for the recrystallised matrix of a composite. Note that an increased composite yield stress on increasing volume fraction and decreasing particle size is predicted, in accord with experimental results.

The grain sub-structure formed on working the material also has a strengthening effect which has the same form as for grain boundary strengthening, but with the constant K_y now taking a lower value.

3.4.2.2 Residual Dislocation Density

As outlined in Chapter 1, the large difference in the thermal expansion coefficients of aluminium and silicon carbide causes dislocations to be generated on cooling to maintain the displacement compatibility across the interface. Some of this dislocation density will be relieved by plastic relaxation of the matrix and by diffusion processes. There will, however, be a retained dislocation density. There is also an additional elastic stress surrounding the particles due to the inability to relieve all the strain mismatch.

The quenched dislocation density may be estimated by assuming the Brooks criterion, namely that dislocations are generated to relieve the misfit when this misfit is larger than the Burgers vector [84]. Humphreys considers a dispersion of cubic particles of side d and volume fraction V_f with the linear strain across the particles given by the product of the temperature difference, δT, and difference in thermal expansion coefficients, δC. If all the strain is relieved by punching square prismatic loops on the cube faces, the dislocation density, ρ, may be expressed by:

$$\rho = 12 \frac{V_f \, \delta C \, \delta T}{b \, d}$$

Taya and Mori [186] have carried out a similar calculation based upon Eshelby's equivalent inclusion technique [103] and used it to calculate the dislocation punching distance. If a uniform distribution is assumed, the strengthening effect of this dislocation density, σ_d, through some forest-hardening mechanism, is given by:

$$\sigma_d = \alpha G b \sqrt{\rho}$$

where α is typically between 0.5 and 1.0, and G is the matrix shear modulus.

Once again, the model predicts increased composite yield stress on increasing volume fraction of reinforcement and decreasing particle size, as observed experimentally. This mechanism of strengthening has been proposed by a number of authors to contribute to and account for the observed increase in yield stress [4,5,90,95,109,117,186,187]. Derby and Walker [90], by measuring the Vickers hardness of specimens quenched from different temperatures, found an approximately linear relationship between hardness increment and volume fraction, and hardness increment and quench temperature. Arsenault and his co-workers have also modelled this

contribution to strengthening and measured the residual dislocation density in "thick" TEM specimens in a high voltage electron microscope [7]. They find the measured densities are lower than predicted, but still significant with the dislocations arranged in a cell structure.

3.4.2.3 Addition of Strengthening Terms

Having delineated the strengthening contributions, a second problem is how to add them together to find a yield stress for the composite. The contributions are not necessarily simply additive because a dislocation samples these stresses and obstacles in different ways [188,189]. The effect of strong obstacles, such as dislocations and particles, is best represented by the square root of the sum of the squares of the strengthening effects [190]. The hardening from weak obstacles, such as solutes, and the internal stresses can be added linearly. This is acknowledged to be an oversimplification [84].

In the full description [84], including all the strengthening terms, the yield stress of the composite is

$$\sigma_{cy} = \sqrt{(\sigma_d{}^2 + \sigma_p{}^2 + \sigma_r{}^2)} + \sigma_{gb} + \sigma_i + \sigma_s$$

where σ_d = residual dislocation strengthening,
σ_p = matrix precipitate strengthening,
σ_r = particle strengthening,
σ_{gb}= grain boundary strengthening,
σ_i = internal stresses,
σ_s = solute strengthening.

There is now a yield stress dependence on the absolute particle size as well as on the volume fraction.

3.4.2.4 Work Hardening

The dislocation mechanics approach also allows the effect of the microstructural parameters on work hardening to be discussed. The continuum models require a representation of the plastic behaviour and, therefore, form no basis for a discussion of the fundamental processes that occur. There are models to describe two regions of work-hardening behaviour. The first, just at the onset of plastic deformation, is assumed to occur by load transfer from the matrix to the particles by means of Orowan loops.

Brown and Stobbs [180] give the mean stress in the matrix due to unrelaxed dislocation loops as

$$\tau = G\,\Gamma\,V_f\,\epsilon$$

where ϵ = unrelaxed strain,
G = shear modulus,
V_f= Volume fraction of second phase,
Γ = Eshelby's accommodation factor;

with the work-hardening rate, therefore, as

$$\frac{d\tau}{d\epsilon} = G\,\Gamma\,V_f$$

This initial rate is modelled as linear and directly proportional to volume fraction. In PRMMCs, however, it is doubtful whether complete Orowan loops will form around the reinforcing particles. In material processed by powder routes in particular, the particles tend to be found at grain boundaries, as in the current study, and not within grains. If loops did form, they would be large and unstable. When these factors are taken together, a non-linear rate may be expected, corresponding to a work-hardening coefficient slightly less than unity.

After small strains the dislocation loops are relaxed, due to the generation of large stresses at the interface, and a second region of work-hardening behaviour is entered. At these higher strains, dislocations necessary to maintain compatibility across the interface are generated. These geometrically necessary dislocations [144] interact with the gliding matrix dislocations, thereby work hardening the matrix. An estimate of the work hardening due to these is given by Ashby [144]

$$\frac{d\tau}{d\epsilon^{1/2}} = \alpha\,G\left(2V_f\frac{b}{d}\right)^{1/2}$$

This secondary rate is, therefore, proportional to $(V_f/d)^{1/2}$ and much lower than the primary rate.

2.4.2.5 Comments on the Dislocation Mechanics Model

The model is based on the deformation processes at a fundamental level with every term that is incorporated having a physical meaning which can be readily interpreted and justified. This, however, means that its full and complete solution is intractable as the understanding of these processes is incomplete. In particular, the problem of the interaction of the various strengthening terms is daunting. It correctly predicts material behaviour which is not predicted by any of the continuum models,

namely the absolute-particle size dependence of the yield stress through grain boundary strengthening and quenched dislocation generation.

The model assumes that yield of the composite occurs on reaching the yield stress of the matrix, with the reinforcing phase deforming purely elastically. The effect of the reinforcing phase on the yield strength of the matrix is then predicted, and this is equated to the composite yield stress. The model does not, however, consider load partitioning between the phases. The result of this, therefore (if one ignores the direct effects of the reinforcing phase on dislocation motion such as the internal stress and Orowan bypassing of the particles), is to equate the composite to a monolithic alloy of the same grain size and residual dislocation density. This approach models, in effect, the *in situ* matrix yield stress.

Where a detailed knowledge of the microstructure is available, the model achieves good agreement with experiment. The model has been applied successfully to the low-strength alloy matrices which are poorly modelled by continuum approaches [84-86]. This good agreement gives confidence in applying these models developed for monolithic alloys to the deformation processes in PRMMCs. In addition, the plastic behaviour of PRMMCs can be modelled.

3.5 Hybrid Model

The strict continuum models lack a physical description of material behaviour whilst the dislocation model ignores the effects of load transfer and partitioning. Both models achieve good agreement with experiment in certain well-defined situations, and are thus equally important components in describing the behaviour of PRMMCs. It would, therefore, be expected that hybrids of the two approaches will give improved agreement between experiment and theory.

The combination of dislocation mechanisms with continuum mechanics has been tried for all the continuum models outlined earlier with quite some success. Indeed, most models of the behaviour of any material include aspects of both approaches. The mean stress, given by a continuum model, is considered to trigger some dislocation mechanism, the effect of which is in turn fed back into the calculation of the mean stress. The dislocation density generated on quenching has been modelled by the Eshelby technique [95,109,117,186,187] and used to model the increased strengthening. Plastic relaxation at the interface by the generation of secondary dislocations has also been included [95]. This secondary dislocation generation, modelled by Ashby [144], has been used in combination with finite element techniques to model the plastic response and onset of fracture [23,25]. Even the simple rule of mixtures has been successfully adapted to predict the plastic behaviour of two-phase materials [177,178].

As outlined in the previous section, the dislocation model predicts the effect of the reinforcing phase on the *in situ* matrix properties. It is the representation of these properties which limits the continuum models. Thus, an attempt to model PRMMC deformation by combining aspects of both approaches seems appropriate.

3.5.1 Simple Model

A simplified dislocation micromechanical model for the increased strengthening of the matrix, which considers the grain boundary and quench effects only, wiill be used in conjunction with the modified shear lag model which partitions the load between the two phases. This is probably the simplest, and worst, hybrid model that could be imagined and is used here purely for illustrative purposes. The shear-lag model of the load partitioning between the phases is the least mechanical and the detailed microstructural information is unknown. Improvements would include substituting the model of the matrix, furnished by dislocation mechanics and complete with the correct values of grain size, into the Eshelby model for load partitioning.

The modified shear lag analysis gives the expected composite yield stress as:

$$\sigma_{cy} = \sigma_{my}\left(\frac{V_f\,(S+4)}{4} + (1\text{-}V_f)\right)$$

with the terms as defined earlier.

A simplified version of the dislocation model, suggested by Miller and Humphreys [85] and now taken to represent the matrix yield stress for the reasons outlined in the previous section, is given below:

$$\sigma_{my} = \sigma_{Al} + \sigma_{gb} + \sigma_{d}$$

σ_{Al} represents the contributions from the other strengthening terms described by the model which are not introduced directly by the reinforcing phase, such as the internal stresses from unrelaxed dislocations and strengthening by the particles themselves, acting as impassable barriers to dislocation motion. This is taken to be the yield stress of the unreinforced matrices in the annealed condition. The other terms are as defined earlier.

By using this simple combination, the load partition and the *in situ* matrix properties may be modelled both physically and mechanically.

3.6 Discussion

Figure 3.15 shows the predicted and experimental 0.05% proof stresses for the 3μm and 10μm particles in the annealed condition for the Al-5050 matrix. Note that the model consistently underpredicts the experimental results, but with improved agreement on increasing volume fraction. This behaviour is observed in the majority of the composite systems studied here with the exception of the 5,10,20/3/Qu/5050 materials where the predicted results are higher than those obtained experimentally. In addition, the variation of proof stress with volume fraction is, in general, more linear than that predicted by the model.

The discrepancies between experiment and model are due to a number of factors. First, the modified shear-lag model would incorrectly partition the loads between the two phases. It is based upon fairly crude corrections to a model developed for physically very different systems, as described earlier in this chapter. This is shown by Table 3.1 which contains the corrections in yield stress from unreinforced alloy to composite. The details of particle aspect ratios were obtained experimentally and the values for the longitudinal direction were taken as this was the direction of loading in the tensile test. Note the very low multiplying factors in all but the composites containing 20% volume fraction of reinforcing phase. It should also be remembered that the aspect ratio of the particles increases with particle size, as reported in Chapter 2, which should be associated with increased proof stresses. The composite behaviour would probably be predicted with increased accuracy with a better description of the load redistribution than that given by the modified shear-lag, such as those based upon the equivalent inclusion technique of Eshelby or finite element methods.

Second, the improved agreement between experiment and the model on increasing volume fraction implies that the microstructure of the matrix is better described by the model at higher volume fractions. The assumption that each particle will stimulate the nucleation of one matrix grain is incorrect at low volume fractions unless particular care is taken over the thermomechanical processing of the composite. The TEM investigations have shown that there are many matrix grains between the particles at low volume fractions of reinforcement [166]. The almost linear variation in composite properties with volume fraction obtained experimentally is in greater accord with a constant matrix grain size for each composite system. This could be the original matrix powder size used in fabrication. This supports the original tenet of the dislocation model, namely that the composite properties are dominated by those of the matrix and that the reinforcing phase supports low loads during the elastic region [94]. These results show the need to characterise the microstructure of the matrix carefully before applying the dislocation mechanics models.

The work-hardening behaviour was also predicted by the dislocation mechanics model for two regions of the stress/strain curve; at the onset of plastic deformation, called primary here, and after further straining, called secondary.

The primary rate is predicted to be linear and independent of particle size and directly proportional to volume fraction. The values of the work-hardening coefficients, n, take values close to unity and increase with both volume fraction and decreasing particle size. This implies that the mean matrix stress due to unrelaxed dislocation loops is lower than predicted, but approaches the theoretical value on decreasing particle size. This is associated with an increased stability of Orowan loops on reducing loop size. The rate is increased on quenching because of higher residual dislocation densities.

The secondary behaviour is modelled on the generation of dislocations which maintain the displacement compatibility across the particle/matrix interface. This model, due to Ashby [144], predicts increased rate with decreasing particle size and increased volume fraction, as observed experimentally.

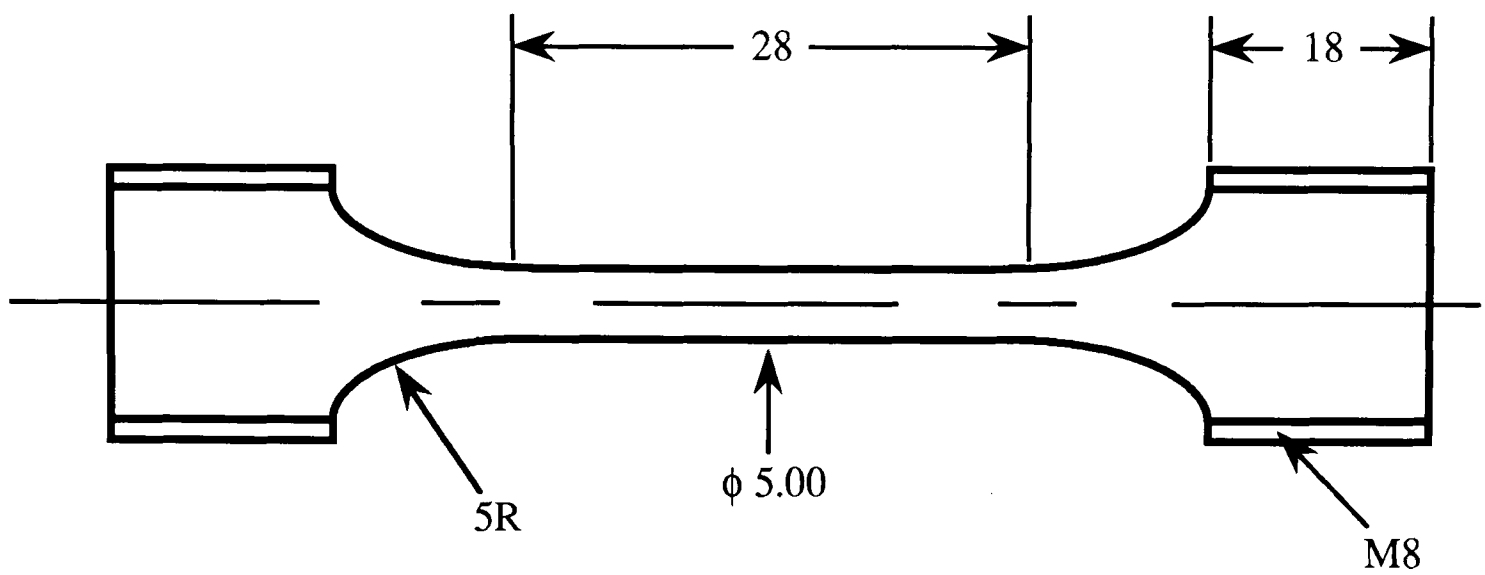

(a)

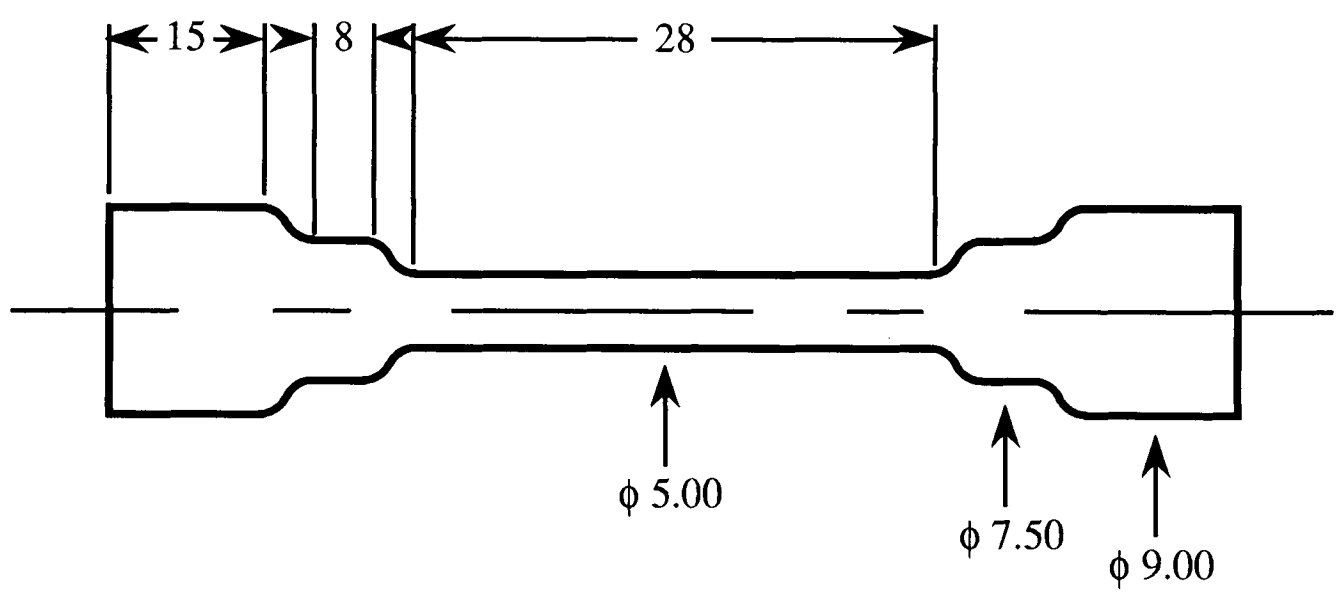

(b)

Figure 3.1: Tensile Specimen Geometries

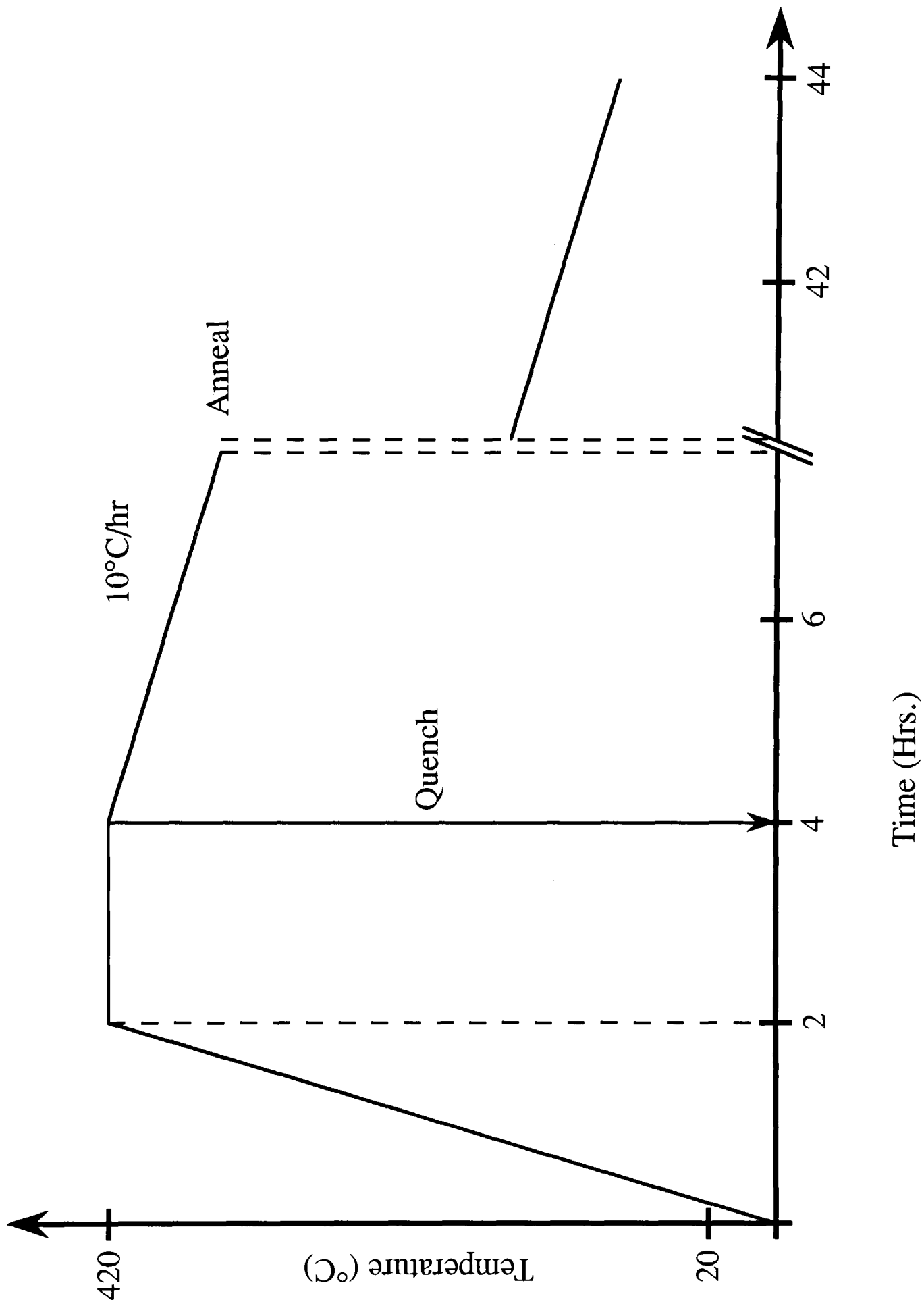

Fig. 3.2: Heating Cycles

Figure 3.3: Secondary Pre-exponential Factors, k, for Al-5050

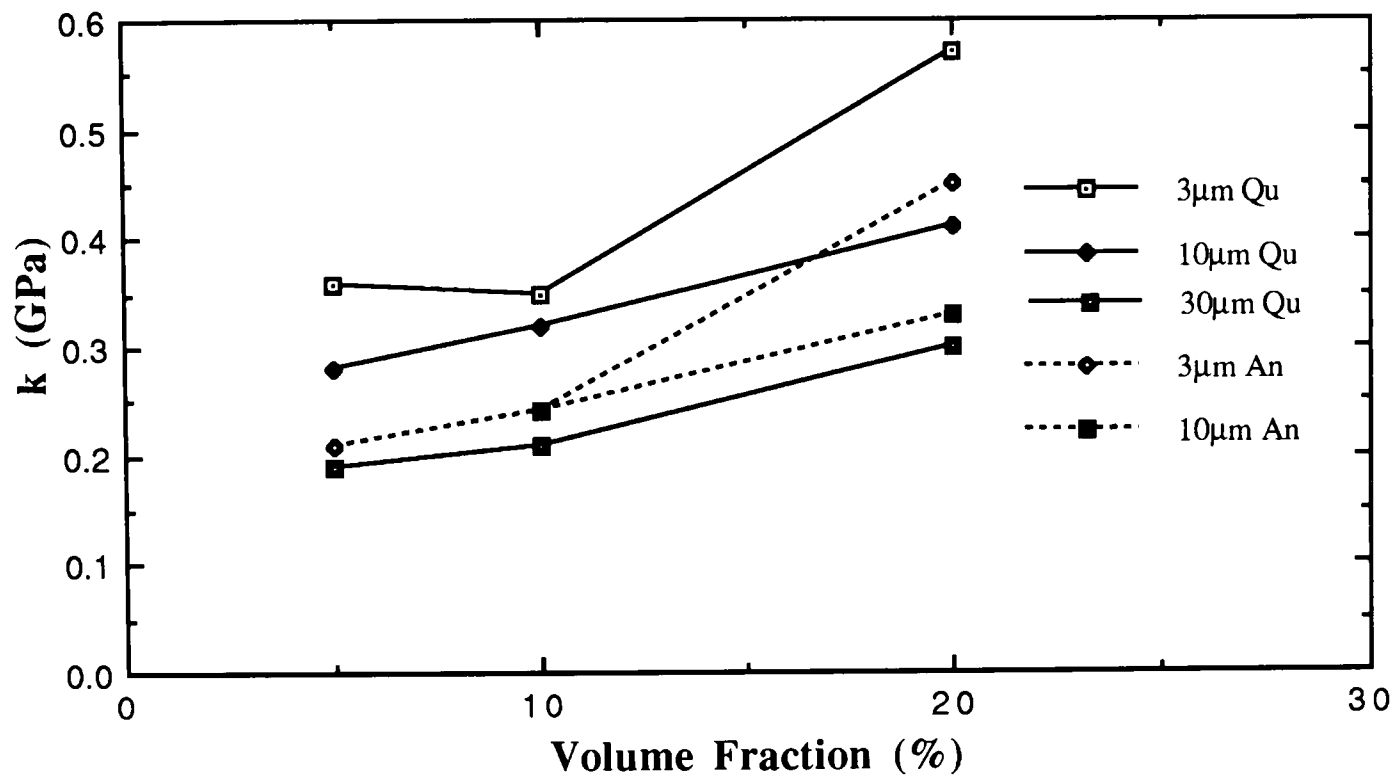

Figure 3.4: Secondary Pre-exponential Factors, k, for Al-1070

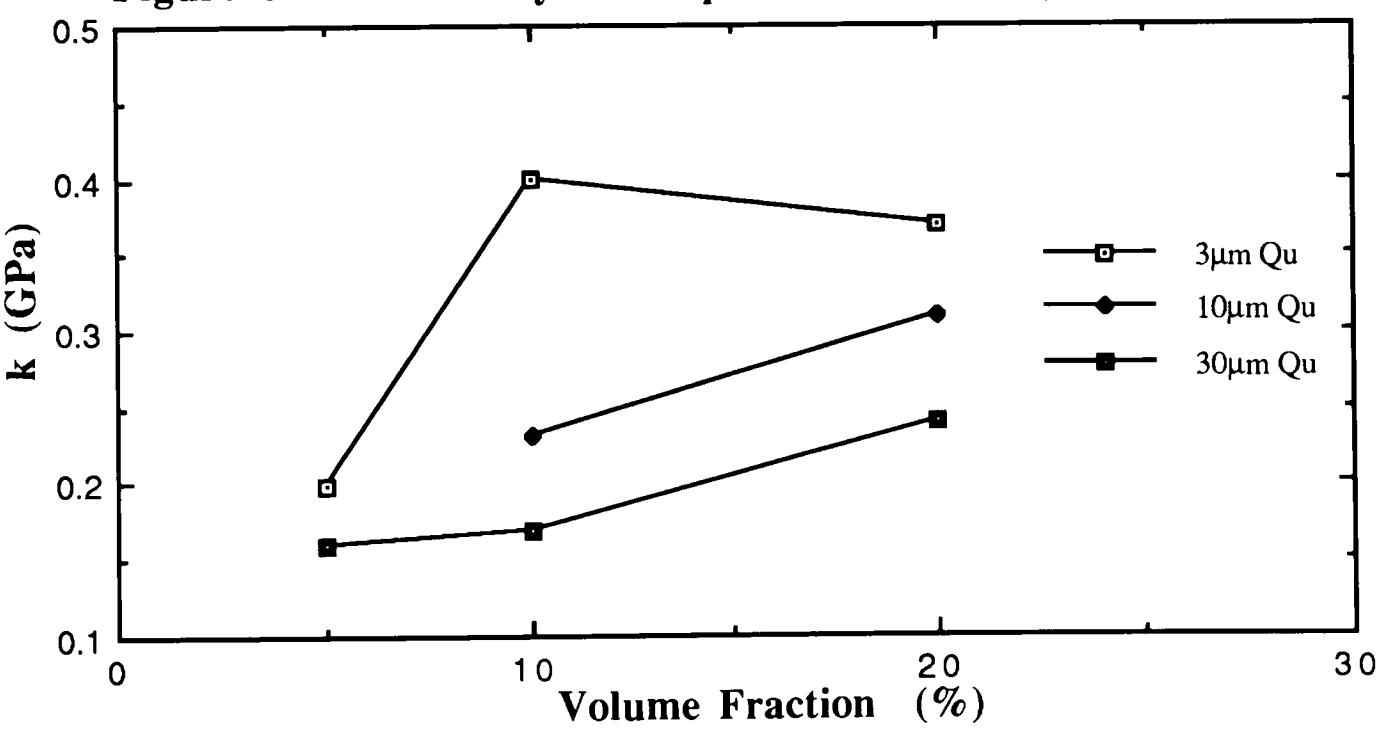

Figure 3.5: Secondary Work-hardening Coefficients, n, for Al-1070

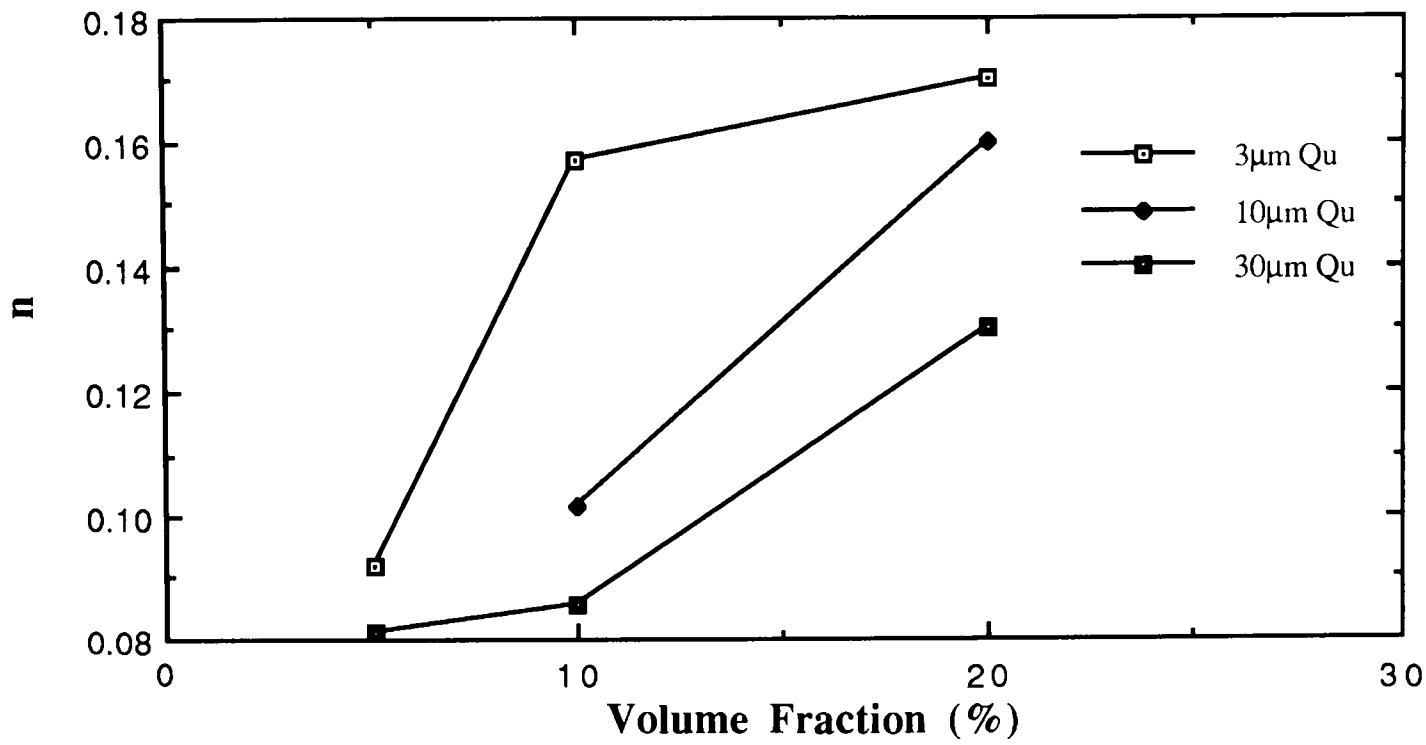

Figure 3.6: Secondary Work-hardening Coefficients, n, for Al-5050

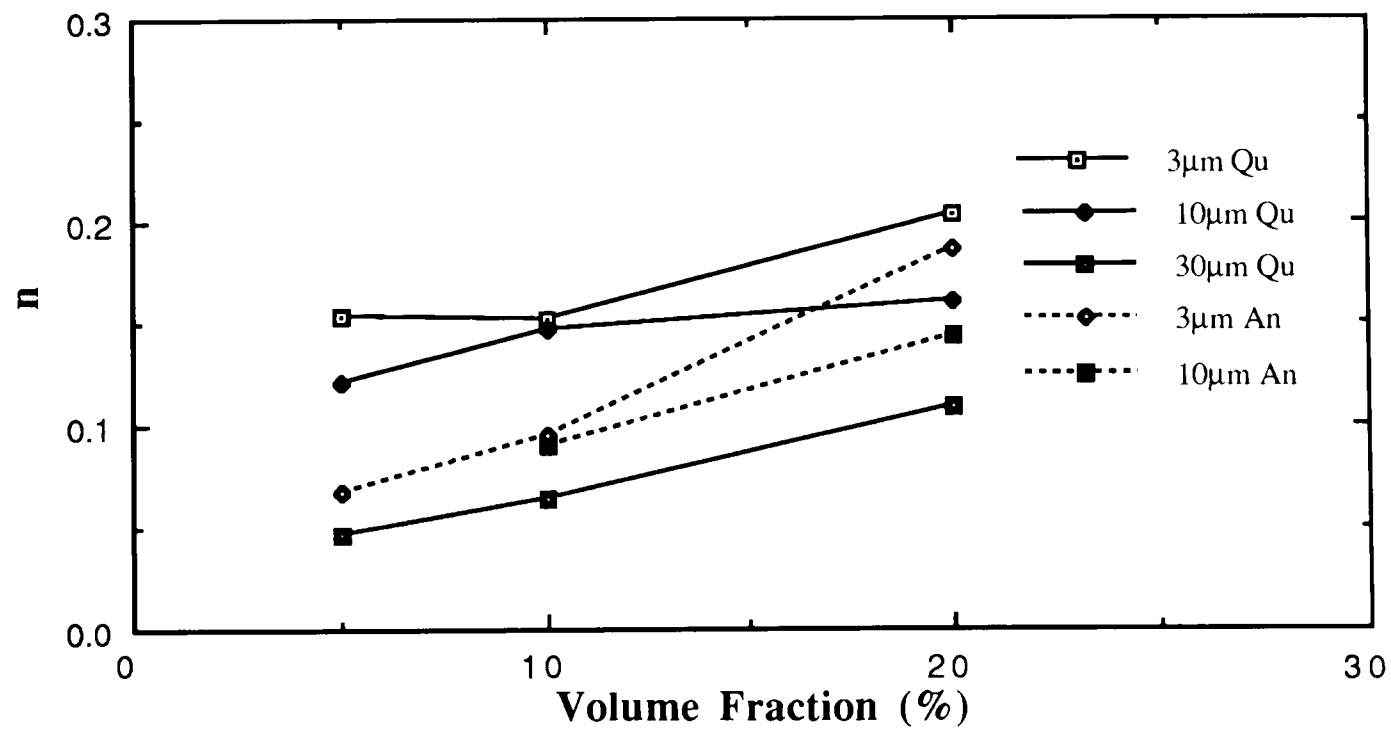

Figure 3.7: Modulus of annealed Al-5050 composites as a function of strain.

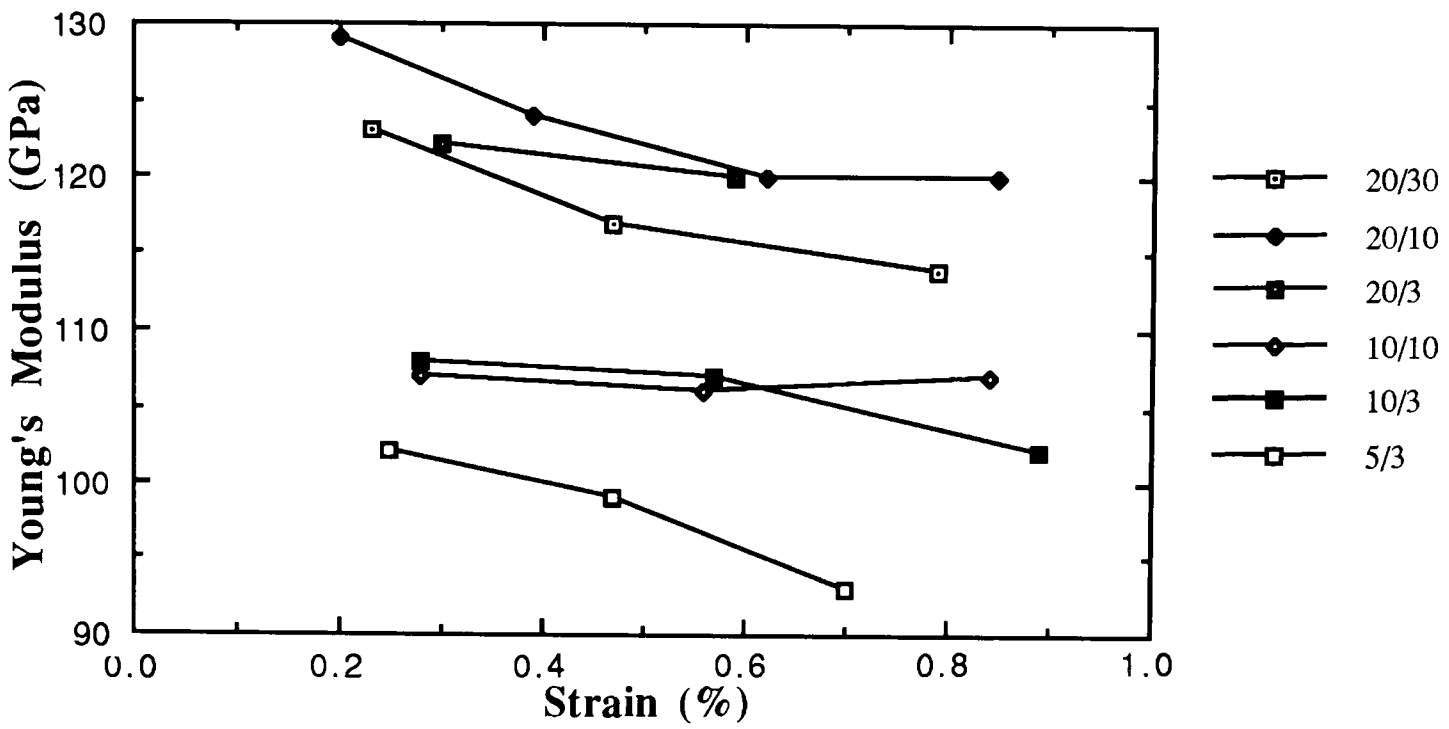

Figure 3.8: Modulus of quenched Al-5050 composite as a function of particle size and volume fraction.

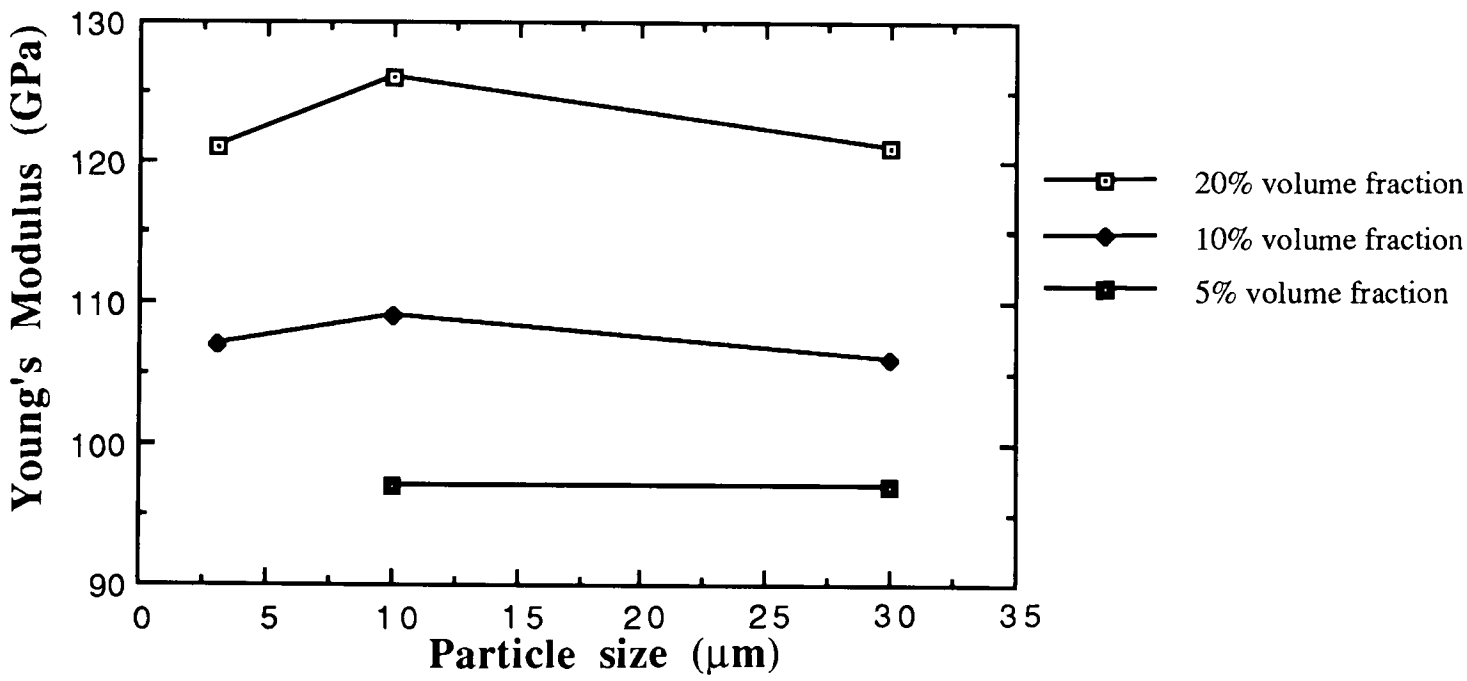

Figure 3.9: Proof stress of annealed Al-1070 composite as a function of particle size and volume fraction.

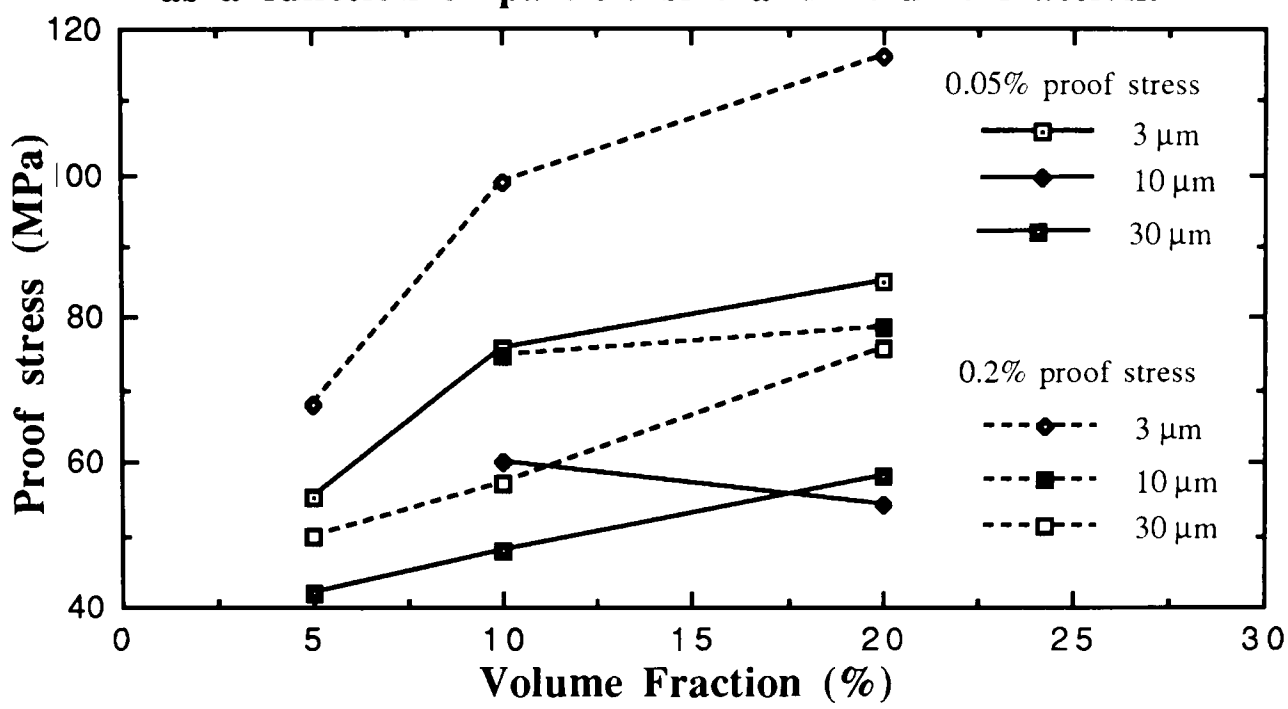

Figure 3.10: Proof stress of quenched Al-1070 composite as a function of particle size and volume fraction.

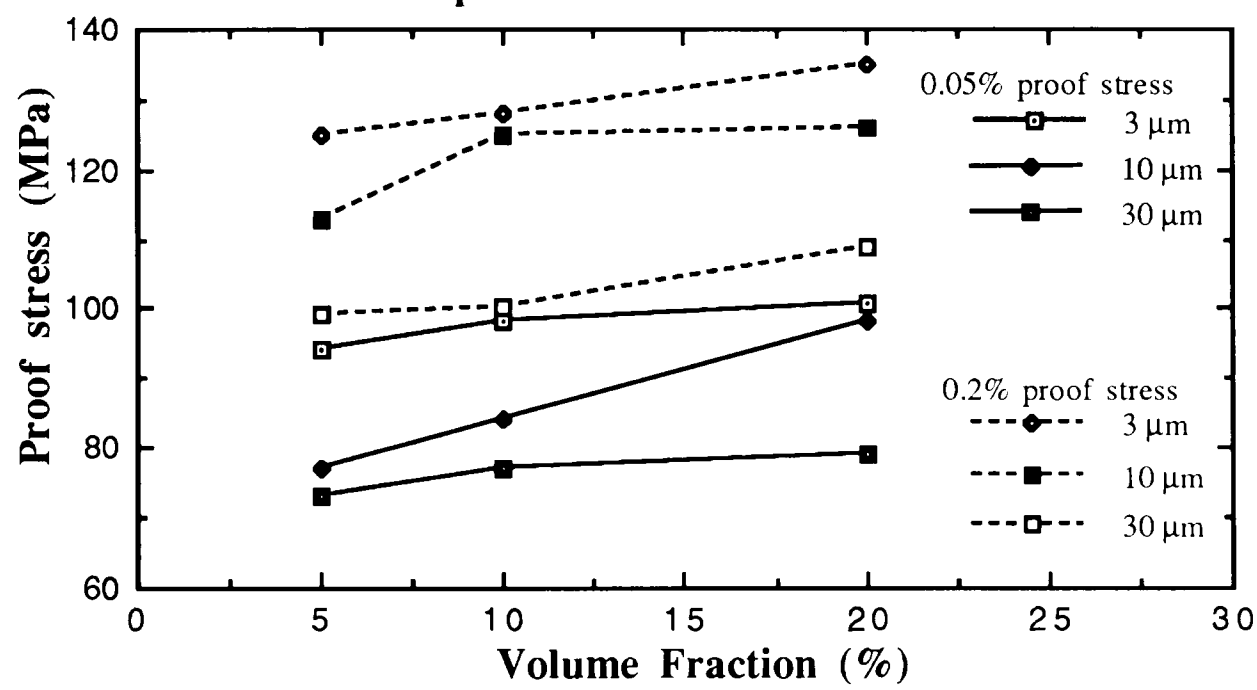

Figure 3.11: Proof stress of annealed Al-5050 composite as a function of particles size and volume fraction.

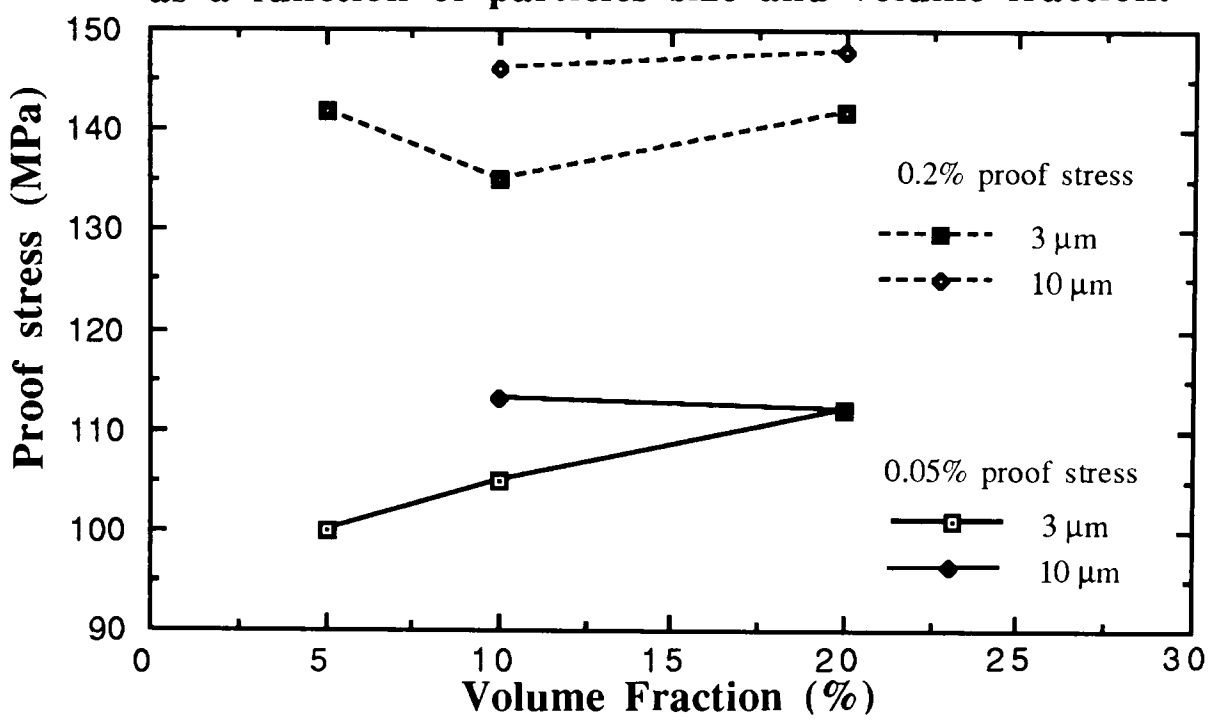

Figure 3.12: Proof stress of quenched Al-5050 composite as a function of particle size and volume fraction.

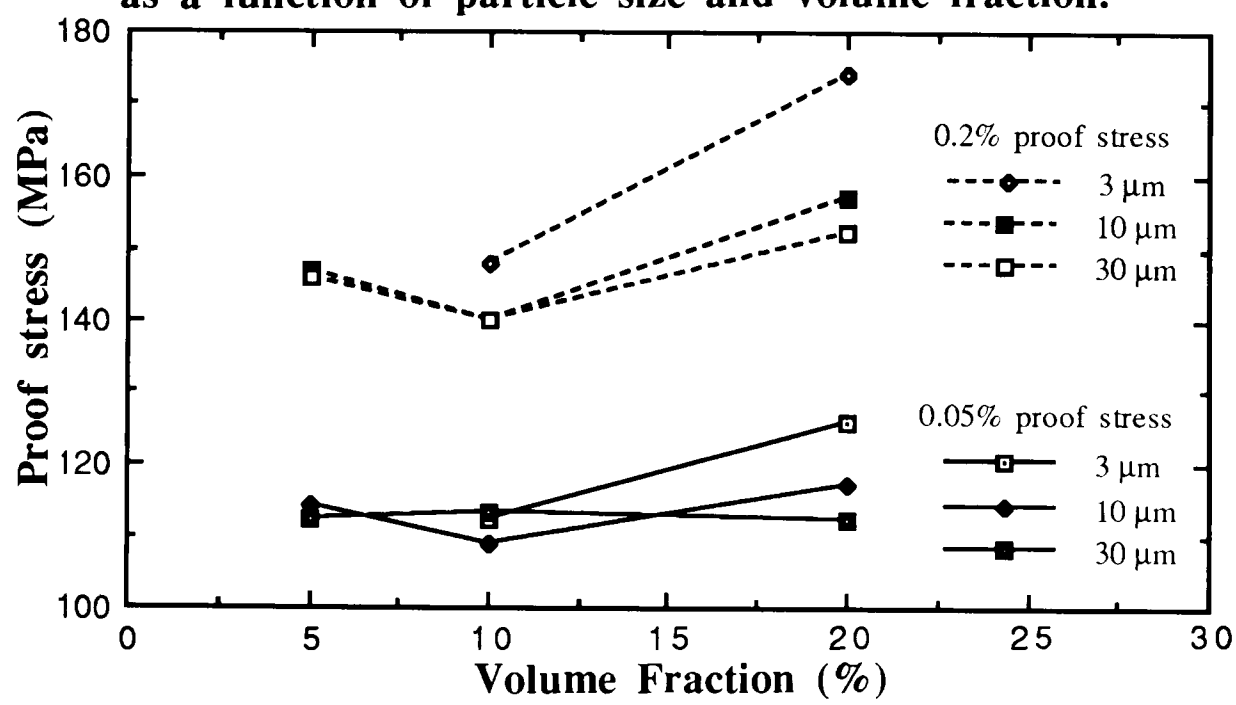

Figure 3.13: Elongation to Failure (%) versus Volume Fraction of Particles for Al-1070 Matrix Composites.

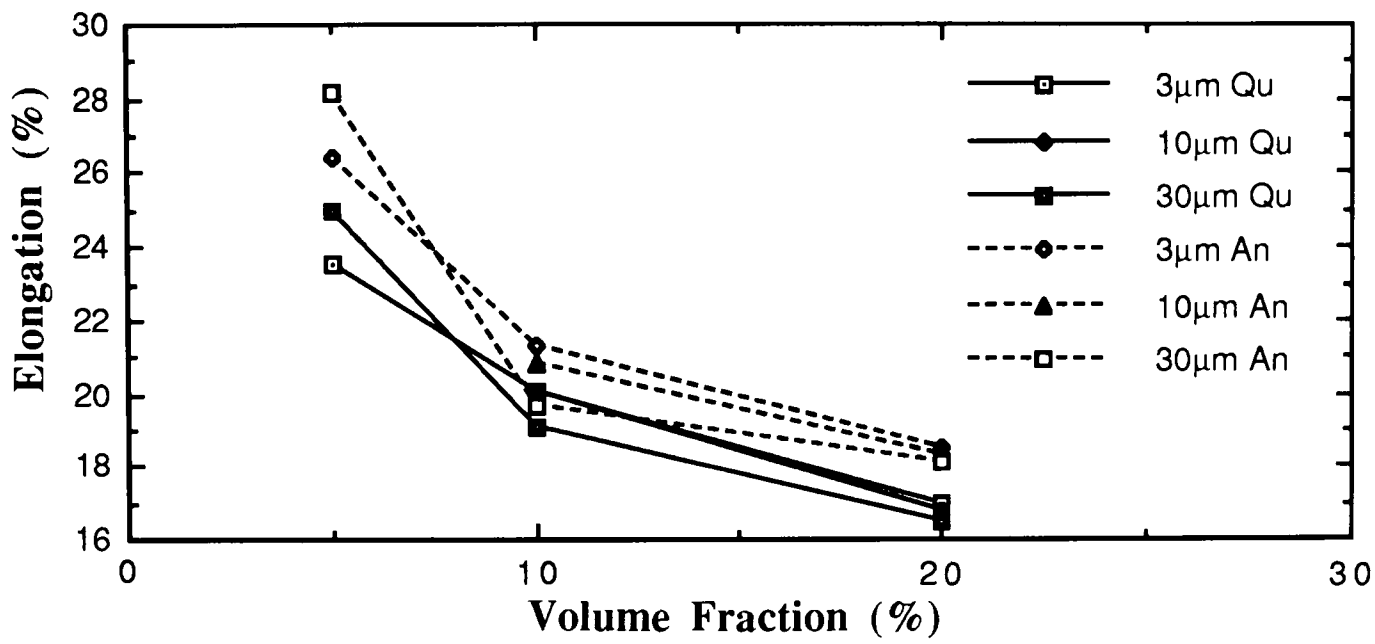

Figure 3.14: Elongation to Failure (%) versus Volume Fraction of Particles for Al-5050 matrix composites.

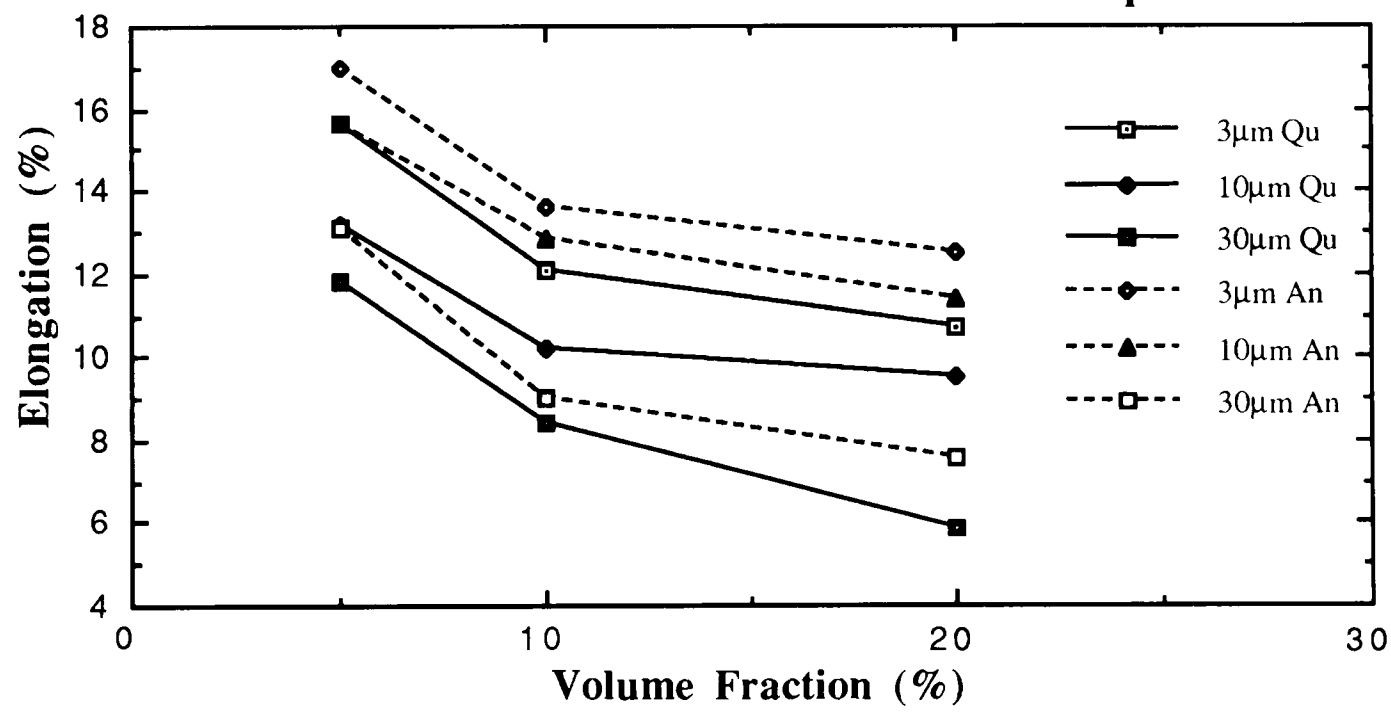

Figure 3.15: Comparison of experimental 0.05% Proof stresses with simple hybrid model.

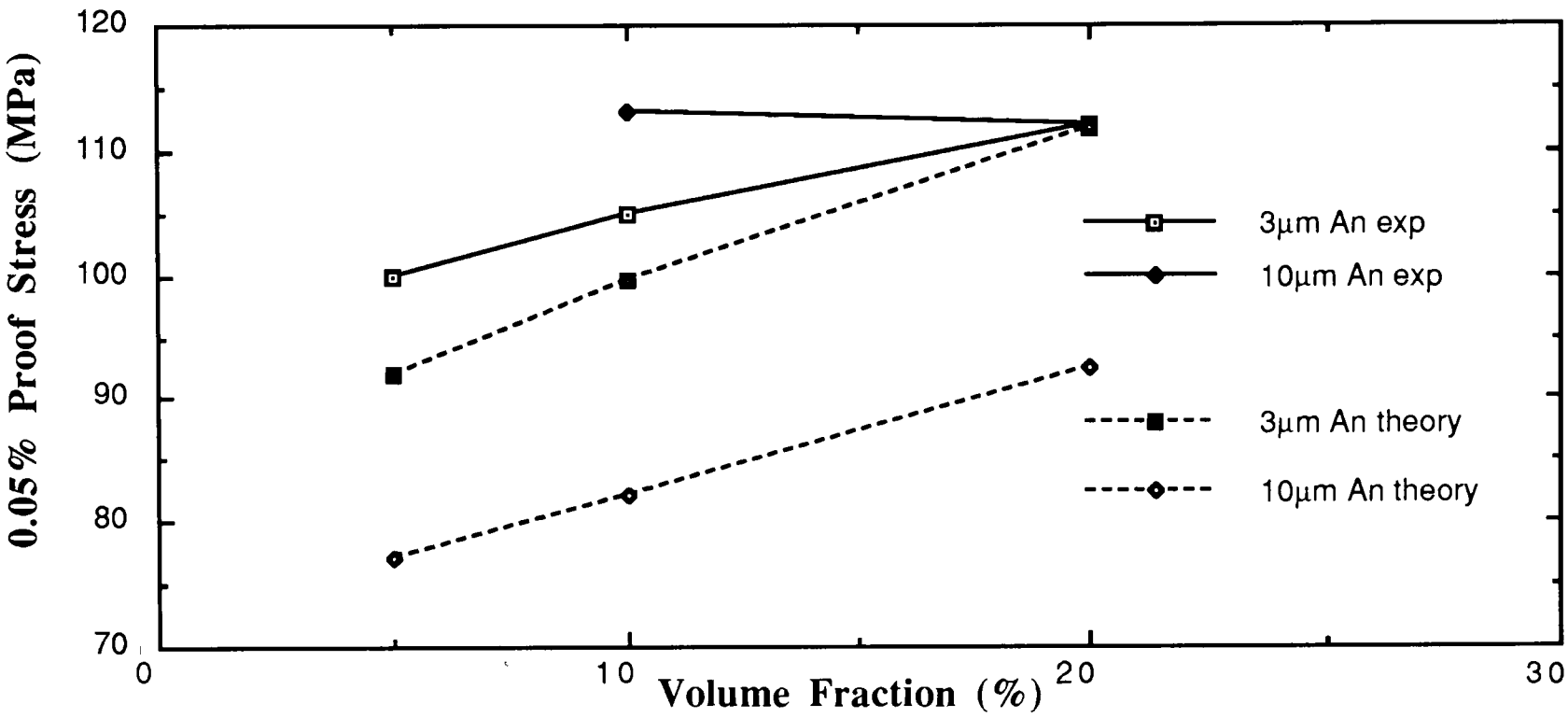

		Volume Fraction(%)		
		5	10	20
Particle	3	1.03	1.06	1.12
Size	10	1.04	1.08	1.17
(μm)	30	1.05	1.11	1.21

Table 3.1: Modified Shear-Lag Strengthening Factors

Chapter 4: Fractography

4.1 Introduction

The term fractography is generally taken to mean the study of fracture surfaces. In addition, other static, post fracture studies will be considered here. This is to make the distinction with dynamic fracture experiments which form the subject of Chapter 5. Basic fractographic studies reveal the micromechanisms of fracture and are fundamental, therefore, to any description of failure.

Careful study of fracture surfaces, whilst delineating unambiguously the fracture processes, gives neither an indication of the order in which these processes have occurred nor their relative influence on the fracture-related properties. There are also a number of unanswered questions, as outlined in Chapter 1, which will not be addressed by a study of the fracture surfaces alone. The effect of systematic variations in volume fraction, particle size and matrix alloy on the fracture processes, coupled with the local and far-field conditions leading to fracture, have not been reported. Criteria for the important void nucleation process have not been developed. The constraining influence of the well-bonded particle/matrix interfaces on void growth and coalescence has been inferred but not studied directly [83]. These important details governing the ultimate ductility are unclear.

Additional static and dynamic studies are required to furnish these pieces of information. Common static techniques include sectioning through stable halted cracks and sectioning along the tensile axis of failed tensile specimens to reveal information from the microstructure just below the fracture surface.

4.2 Fracture Surfaces

There have been many previous fractographic examinations of PRMMCs, for example [40,71-73,79,83,124-126]. As outlined in Chapter 1, fracture occurs by a matrix ductile, void nucleation and growth mechanism. Particle fracture [71,79,83,133], decohesion at the particle/matrix interface [73,87,98,99,130,131] and failure in the matrix away from the interface [9,78,132] have all been reported, the mechanism strongly affected by the choice of matrix alloy and heat treatment, and reinforcement type and size. However, the majority of these studies have examined only one of the two fracture surfaces produced on failure and, as Roebuck states [79], cannot, therefore, uniquely define the fracture processes. Study of matched fracture halves, which show the corresponding areas on both fracture surfaces, is the only way to determine these processes unequivocally.

4.2.1 Experimental

Fracture halves were obtained from bulk specimens loaded in a constant displacement, double cantilever arrangement. Here, a wedge of constant angle was driven into a spark-eroded notch in the specimen until total failure occurred. Spark erosion introduced insignificant damage, eliminating a possible source of artefacts in the microstructure. This technique was chosen for two reasons. First, the position of the crack was known in advance. Secondly, specimens are produced with flat surfaces which can be put back-to-back, greatly facilitating matching. Similar specimens could be produced by loading a notched bar of square cross section in four-point bending. The fracture surfaces were observed immediately after failure in an Hitachi S-530 SEM. Areas far from the edge of the specimen were matched to ensure that approximately plane strain conditions were satisfied. The material was examined in the same two heat-treated conditions as detailed earlier for the mechanical tests.

4.2.2 Results and Discussion

Fractography revealed that although the composites showed limited ductility on a macroscopic scale, fracture occurred by a matrix ductile rupture mechanism for all composite systems studied, in common with previous work on the fracture of PRMMCs. While the basic failure mechanism was the same for all PRMMCs examined, the mode of fracture was highly sensitive to variations in the microstructural parameters. Different fracture modes were observed on changing the matrix alloy composition as well as the size and volume fraction of reinforcing phase.

In the ductile rupture process, fracture proceeds by the nucleation, growth and coalescence of voids, and has been the subject of extensive research in monolithic alloys [135,191-195]. In the vast majority of these cases, void nucleation occurs at a second-phase particle by either the cracking of the particle or decohesion at the particle/matrix interface [141]. The voids then grow under the applied loads and influence of local plastic constraint until a coalescence mechanism is activated, followed shortly by the total failure of the specimen. This leads to the classic dimpled, after the English translation of "cupule" [196], cup-and-cone appearance of the fracture surfaces. The morphology of the PRMMC fracture surfaces was found to be similar to that of monolithic alloys, consisting of dimples, where extreme local deformation has occurred, and exposed second-phase particles. This basic appearance was affected by the choice of matrix alloy.

For composites of the Al-1070 matrix, the dimple size scaled with the interparticle spacing, indicative of void coalesence by a simple shear linkage mechanism, as shown in Figures 4.1 a-f. Here, the voids grow in the direction of the applied load until the plastic

constraint between neighbouring voids is overcome when the voids coalesce through shear failure of the joining matrix ligaments, as shown schematically in Figures 4.2 a-c for the two-dimensional case. This forms the basis of the simple model for the ductile rupture mechanism due to Brown and Embury [139]. There was also some evidence of a bimodal dimple distribution as shown in Figure 4.3. The larger dimples were associated with the reinforcing phase and the smaller dimples with ductile failure in the matrix, probably due to the presence of impurities such as aluminium oxide from the processing, and iron from the original matrix powder. This bimodal distribution has been reported by other workers in several different composite systems [40,91]. Figure 4.4 shows serpentine glide, characterised by the wavy lines on the inside of voids. These occur when matrix slip lines intersect the growing void and are indicative of shear linkage between voids [197].

The fracture surfaces of the Al-5050 matrix composites did not have such a simple appearance. The relationship between dimple size and interparticle spacing was no longer found to hold. Here, there were many more large dimples associated with the failure of the matrix alone. These matrix dimples were often elongated in the extrusion direction, as can be seen in Figure 4.5a and at higher magnification in Figure 4.5b. This is probably due to the large Al-5050 powder particles being drawn out during extrusion, giving an asymmetric grain structure. This implies that other coalescence mechanisms may be operating in addition to shear linkage. The increased stress leads to secondary nucleation of matrix voids which themselves grow. The large size of these matrix voids implies that this failure is due to some intergranular process, possibly as a result of magnesium segregation to the grain boundaries. The presence of the additional voids removes some local plastic constraint thereby reducing the growth strain before coalescence can occur, leading to lower extensions to failure. This secondary nucleation in the matrix, rather than an increased matrix yield strength, is a major cause of the lower ductility in PRMMCs of particle-strengthened alloys.

The size and volume fraction of reinforcing phase were also found to have a significant influence on the fracture processes. A change in failure mode from cracking of the particles themselves to decohesion at the particle/matrix interface on decreasing the particle size to 3μm was observed in composites of both matrix alloys as can be seen in Figures 4.6a to 4.8b for the composites of Al-5050 matrices. This dependence of failure mode on particle size has been observed in other studies [87,91,92]. In addition, a similar transition from particle cracking to interfacial decohesion was found on decreasing the volume fraction from 20% to 5% in composites of the Al-5050 matrix containing 30μm and 10μm particles as shown in figures 4.9a to 4.10b. This is associated with failure through the interfacial magnesium oxide layer which inhibits good bonding between the matrix and reinforcement, as has been reported in another study [156]. Secondary cracking of the 10μm and 30μm particles in the base of voids was observed.

This occurred with lower frequency on decreasing the volume fraction for the 10μm particles, probably due to a reduction in local plastic constraint.

The large decohered particles in the composites of the Al-5050 matrix provided evidence of an interfacial reaction, as seen in Figures 4.11a-b. Many of the cracked particles in the pure aluminium matrix still have matrix material bonded to them, indicating the high strength of this interfacial bond. The bond between aluminium and silicon carbide is recognised to be strong. Previous work, using scanning Auger microscopy on a specimen fractured *in situ*, has reported that even where interfacial decohesion was thought to have occurred, a thin residual layer of aluminium was left on the particles, implying that failure was through the matrix just away from the interface [9]. As discussed in Chapter 1, the microscopic properties of the interfacial bond are critical in determining the subsequent macroscopic behaviour of the composite.

It is generally thought that the nucleation of voids at a second phase requires the attainment of a critical normal stress at the particle/matrix interface [25]. This is a local condition and difficult to model as it depends on the size, shape and location of the particles and their mutual interaction [198]. However, one may adopt a simple critical stress criterion to determine whether particle fracture or decohesion will occur. Suppose that nucleation occurs, by the appropriate mechanism, when the local stress at the particle, σ_l, reaches either the interfacial bond strength, σ_i, or the fracture stress of the particle, σ_f. Then the nucleation mode or mechanism would be determined solely by the relative values of σ_i and σ_f. Indeed, Flom and Arsenault [21] have attempted to measure the interfacial bond strength *in situ* by applying this criterion. The observed particle size dependence on failure mode could be interpreted in terms of this criterion. If one assumes that the interfacial bond strength is independent of particle size, then a reduction in particle fracture stress on increasing particle size is required to mirror the experimental results. As the reinforcements are brittle ceramics containing a distribution of flaw sizes, then a purely statistical arguement would expect a reduction in mean fracture stress on increasing particle size. The apparent inconsistency in the fractographic observations of previous workers studying different composite systems is due to the changes in the relative values of σ_i and σ_f. The extrapolation of results between PRMMC systems is, therefore, not simple. However, this arguement would not predict the observed volume fraction dependence of failure mode. As this result was only seen in the Al-5050 matrix material, it may be assumed to be caused by an extended interfacial reaction, lowering σ_i, and not by the need to satisfy another fracture criterion.

A summary of the fractographic results is shown in Table 4.1.

4.3 Sections through Cracks

Information on crack propagation can be provided by sectioning halted cracks. These studies of a crack under plane strain conditions also provide a very important, and rarely performed, check on the results of *in situ* observations of crack growth where the crack observed at the surface is necessarily under plane stress conditions.

4.3.1 Experimental

Stable cracks were introduced into the material by the same constant displacement, double cantilever arrangement described in Chapter 3. The cracks were then electrodelessly nickel plated to provide support for the crack edges during polishing, and sectioned by spark erosion. The sections were mounted in bakelite and polished for optical microscopy using a similar technique to that outlined in Chapter 2. Care was taken to ensure that the voids were not polished out by the use of hard plastic, PAD-K, discs down to a 1μm finish instead of the short-nap cloths. Preparation ended with a short polish by hand with OPS. The material was studied in the quenched condition only.

4.3.2 Results and Discussion

The sections showed the crack propagation sequence, provided some evidence for the nucleation mechanism and confirmed the fractographic results. They share some common features which are generic to the propagation process, and some features which differ for reasons similar to those put forward for the fractographic results.

Figures 4.12 a-d show a series of micrographs of the crack in the 20/30/Qu/5050 material. This choice of composite has been made solely for illustration purposes and any differences between materials will be shown in later micrographs. Figures 4.12c and 4.12d show the crack passing through the silicon carbide particles with some nucleation events ahead of the crack tip. At a lower magnification in Figure 4.11a one can see several regions of fairly extensive void growth linked by failure through the joining matrix ligaments. The crack path is not tortuous but follows the damage region ahead of the crack tip. There is little evidence for the crack branching which has been observed during *in situ* experiments [87,132].

Crack propagation may, therefore, be due to fracture nucleation events in the stress field ahead of the crack tip, by either particle fracture or decohesion, followed by void growth and linkage of these regions with the growing crack. The damage region ahead of the crack tip is fairly limited, perhaps extending over one interparticle spacing. This is in accord with the models of Kamat *et al.* [75] and Crowe *et al.* [73]. These

models, based upon one developed by Rice and Johnson [199], estimate the extent of the region of intense straining ahead of the crack tip from a knowledge of K_{Ic} and yield stress. They concluded that the extent of the region is comparable to the spacing between the reinforcements in their composites which exhibited stable crack growth. Results of *in situ* crack growth monitoring experiments do not provide such support, reporting a far larger damage region of the order of tens of interparticle spacings [87,130-132]. If the crack approaches a region of high local volume fraction then many nucleation events may occur locally, resulting in areas of substantial voiding, as reported in the following chapter. The isolated voids ahead of the crack tip suggest that nucleation occurs by failure at the reinforcing phase, rather than in the matrix near the particles. However, neither the local conditions leading to this nucleation nor the far-field strain at which it occurs are revealed by this experiment.

Variation of the microstructural parameters leads to changes in secondary features such as the extent of lateral damage. In the composites containing 30μm particles, there is some evidence of nucleation events to the side of the main crack. Lateral cracking is not observed for any other particle sizes due to the localisation of damage, as can be seen in Figures 4.13a and 4.13b of material containing 10μm particles. The propagation of a crack loaded in the constant displacement, double cantilever arrangement localises intense deformation to the region ahead of the crack tip. This reduces the likelihood of damage away from the crack tip.

4.4 Sections through Tensile Specimens

Sections through failed tensile specimens parallel to the tensile axis show the extent of damage away from the fracture surface. Because of the non-uniformity of the deformation, distances from the fracture surface correspond to a distinct strain state. This localised deformation can be seen clearly in Figures 4.14a to 4.15b. These show sections through the tensile specimens of 5% and 20% volume fraction of 30μm particles in both the Al-1070 and Al-5050 matrices. The increased ductility of composites of lower volume fraction and pure aluminium matrix is evident. The micrographs, therefore, show the strain history of the specimen to the failure strain, furnishing information similar to sections through a series of interrupted tests. Thus, the relative importance of the differing stages of strain in the ductile rupture process can be assessed. The shapes and distributions of the voids are also directly related to the local stress and strain states. The mechanism by which the particles are loaded and the constraint imposed on the matrix flow by the particles are, thus, also revealed.

4.4.1 Experimental

One half of each broken tensile specimen was nickel plated electrolessly and

sectioned parallel to the tensile axis by spark erosion. The sections were mounted in bakelite and mechanically polished as described in section 4.3.1. Investigations by optical microscopy were undertaken.

4.4.2 Results and Discussion

The objective of these experiments was to shed some light on the far-field and local conditions leading to failure. Additionally, information on the relative importance of void nucleation and growth processes was obtained.

Figure 4.16 shows a region near the fracture surface of the 20% volume fraction, 30μm particles in an Al-1070 matrix. Note that most of the particles are cracked through their centre with the plane of the crack normal to the applied stress. This tends to support a model of particle fracture based upon a fibre loading, shear lag mechanism rather than a blocked slip or dislocation pile-up mechanism. A pile-up mechanism would predict a random distribution of cracks with respect to position along particle length. Fibre loading assumes that the tangential forces exerted on the particle surface by the yielding matrix are balanced by a tension in the elastically-deforming particle [169]. The total force exerted on the particle increases with distance from the particle end and so the maximum stress within the particle is found at the centre. This gives some confidence in applying the results of shear lag analysis to the study of PRMMCs, at least for large reinforcements. The figure also shows the limited, but not negligible, void growth in high volume fraction composites.

Figure 4.17 shows a similar region near the fracture surface of the composite of 30μm particles but only 5% volume fraction. Extensive void growth can be seen in the tensile direction but no lateral growth, indicating the great constraining effect of the still well-bonded interfaces. Indeed, linkage between two voids is rarely seen. It is only observed where fractured particles are side by side, as seen in Figures 4.18a-b. By comparing Figure 4.16 with 4.17, one can see that increasing the volume fraction of reinforcing phase greatly reduces the growth strain before total failure, in agreement with models of the ductile rupture process [22,200,201].

Figures 4.19a-b show two damaged regions in the same 20% volume fraction, 30μm particle composite. One is at the fracture surface and the other at a lower far-field strain, as determined by the reduction in area of the cross section. The figures show the reduced damage levels at lower far-field strains. By comparison with Figures 4.20a-b, which show regions at similar strains but in composites containing 10μm particles, it can be seen that the damage is reduced yet further. Thus, the level of microstructural damage at a given far-field strain is a function of reinforcing particle size. This is in agreement with the results of Gurland [202] who determined the effect of stress state on

particle fracture in carbon steel. In addition to finding that cracking occurred preferentially in the centre of particles on planes normal to the maximum principle stress direction, in accord with the fibre loading model, he also observed a particle size dependence, with larger particles fracturing at lower strains. This was attributed to either the decreasing ability of plastic relaxation to relieve large stress or strain concentrations at the particle interface, or to the sensitivity of the particle fracture stress to surface and volume flaws. As the particles considered here are much larger than those in Gurland's study, making the relaxation processes inefficient, the second explanation is more likely.

If Figures 4.19a-b are compared with Figures 4.21a-b, which show the 30μm particles at similar far-field strains but now in a composite of 5% volume fraction, one can see that the extent of damage is again reduced. This implies that nucleation is determined by the local stress rather than strain. As discussed in Chapter 1, the composites of higher volume reinforcing phase have difficulty in relieving the stress concentrations at the interface by the generation of secondary dislocations due to the interaction of the plastic zones of surrounding particles. Thus, the local stress at the particles is increased on increasing volume fraction for a given far-field strain. This is confirmed by comparison of the composites of Al-1070 matrices with those of Al-5050 as shown in Figures 4.22a-b. More extensive microstructural damage can be seen at lower strains for the higher strength matrix, implying the dependence on local values of stress.

Figures 4.23a-b are sections through the 5/30/Qu/5050 material. The lower magnification of Figure 4.23a shows voids nucleated by decohesion at the particle ends. Similar observations have been made during *in situ* TEM studies of whisker-reinforced composites [59,78]. This has been associated with stress concentrations at the corners of the reinforcing phase. The 30μm particles studied here have an aspect ratio equivalent to that of many whisker reinforcements. Of additional interest in Figure 4.23a is the small amount of growth seen with these voids below the fracture surface when compared with the similar voids in the Al-1070 matrix shown in Figures 4.21a-b. This is due principally to the reduced elongation to failure of the Al-5050 composites which is, in turn, affected by the secondary nucleation of matrix voids and the reduced plastic constraint of decohered voids, allowing easier void coalescence. Figure 4.23b shows the coalescence of two neighbouring voids.

The tensile specimens were polished to a 1μm finish prior to testing. The surfaces of the gauge lengths were examined after failure to further assess the extent of damage. Figures 4.24a-b, of Al-1070 matrix composites containing 5% and 20% volume fraction of 30μm particles, show stable voids similar to those found below the fracture surface with the same characteristics of shear loading described earlier. Note also the change in the surface displacement from the intense, wavy patterns of upheaval in the 5% volume

fraction material to the planar appearance of the composite of 20% volume fraction. This surface deformation and particle cracking extends much further from the fracture plane than the internal damage revealed by sectioning.

Thus, the criterion for nucleation appears to be a function of the particle size, local volume fraction and matrix yield stress, with the far-field strain to nucleation reduced on increasing all of these parameters. Where there is a clustered region of high local volume fraction, nucleation is found to occur at lower far-field strains. This has been observed in other studies [51,52,54,71,73,83,91]. The observed reduction in modulus on increasing strain, reported in Chapter 3 and confirmed by recent other work [83,121], is an expression of this nucleation behaviour and will be discussed further in Chapter 5. If one assumes that the composites contain a random spatial and size distribution, then regions of sufficiently high volume fraction to cause nucleation at very low levels of far-field strain may exist. These cracked particles reduce the load-bearing capacity of the reinforcing phase, thereby lowering the modulus. There is a greater reduction in modulus on increasing the number of cracked particles. The modulus reduction experiments also showed the particle size dependence on nucleation, with greater loss of stiffness for a given strain on increasing particle size and volume fraction. A major aim of the dynamic fracture studies described in Chapter 5 is to determine at what stage during straining fracture nucleation events occur.

The sections also show the relative importance of the nucleation and growth processes. As described earlier, nucleation may occur locally at low levels of plastic strain. The presence of many stable voids in cracked particles below the fracture surface shows this to be true. The restriction on void coalesence by the plastic constraint of the still well-bonded interfaces ensures that void growth occurs even for the high volume fraction composites. The simple model of the ductile rupture process due to Brown and Embury [139] described earlier would predict zero growth strain for such a high volume fraction of second phase particles. Thus, although there is nucleation very early in the straining process, total failure does not occur until further strain has been applied. Indeed, recent work by Lloyd has shown that much of this early damage is recoverable [83]. Here, specimens of an Al-6061 matrix reinforced with silicon carbide were strained to varying degrees and unloaded. The material was then resolutionised to recover the matrix defect damage, such as dislocations. This did not recover particle fracture or cavitation. The specimens were then reloaded and the strain and yield stress to failure recorded. It was found that the strain to failure of the uninterrupted test, some 7-8%, was maintained for prestrain levels up to 5.5%. Thus, the solution treatment had recovered the damage produced by the prestrain. While the ductility was recovered, the yield stress consistently fell below that of the uninterrupted test.

The ductility measured during the tensile tests should be discussed in the light of

the fractographic results. A simple critical stress criterion is assumed, consistent with the above results, whereby voids nucleate if either the local stress exceeds the interfacial bond strength, when decohesion occurs, or the fracture stress of the particle, when particle cracking occurs. In the pure aluminium matrix composites, the interfacial bond strength is independent of particle size and it may be assumed that nucleation by particle cracking occurs at a lower local stress for the 30μm particles than for the 3μm particles. On applying Ashby's model for the deformation of plastically non-homogeneous materials [203], one finds that the stress at the particle is directly proportional to the far-field strain which implies that nucleation occurs at a lower strain for the larger particles. Thus, in composites where the same nucleation mechanism occurs, an increase in strain to failure would be expected on decreasing particle size, as has been reported by other workers [75,97,98,136]. For the high volume fraction composites, void growth is limited and a reduction in strain to nucleation should be mirrored by a corresponding reduction in strain to total failure, which is consistent with the results of this study for both matrix alloys. However, in the low volume fraction materials there is substantial void growth before coalescence. In the Al-1070 matrix composites containing 5% of reinforcement, a reduction in strain to failure is observed on decreasing particle size, contrary to the results of the composites with a high volume fraction of reinforcement. In the same 5% volume fraction composites of the Al-5050 matrix, where the same nucleation mechanism is found for all particle sizes, this trend is not observed. In these systems it is postulated that the void produced by particle fracture is heavily constrained by the still rigidly bonded interface, making void coalescence difficult and giving increased additional growth strain over the void produced by decohesion. This is contrary to the model for void growth due to Evensen and Verk [204]. Here, a reduction in strain to failure is predicted for two-phase systems where the second phase fails by cracking. They propose that the increased stress concentration at the crack tip leads to enhanced void growth.

Quenching was found to reduce the strain to failure of all composite systems studied. Large dislocation densities are produced on quenching because of the mismatch in thermal expansion coefficients of the two phases. These dislocations are believed to impede the stress relaxation processes by the generation of secondary dislocations at the particle/matrix interface and thereby increase the local stress there. Thus, a higher local stress is maintained at the interface for a given far-field strain, increasing the likelihood of particle fracture and decohesion. This is translated into a reduced strain to failure.

The ductility of all the Al-5050 matrix composites was lower than the corresponding composite with an Al-1070 matrix. The solution strengthening of the unreinforced Al-5050 matrix inhibits stress relaxation processes at the particle/matrix interface in a similar manner to the quenched dislocations. This increases the local stress for a given far-field strain and manifests itself in a reduced elongation to failure.

In addition, fractography revealed dimples associated with failure in the matrix by secondary void nucleation processes. These remove some of the local plastic constraint, leading to void coalescence at lower growth strains, again reducing the elongation to failure.

4.5 Summary

The fractographic studies have shown the micromechanisms of failure and also the effect of various microstructural parameters on the fracture processes. They can be summarised as follows:

a) Fracture proceeds by a ductile, void nucleation and growth mechanism.

b) The nucleation process is a strong function of the microstructural parameters and is governed by the relative strengths of the interfacial bond and particle. The presence of an oxide layer or reaction product appears to have lowered this bond strength in the composites of the Al-5050 matrices which has resulted in a change in fracture mode and reduced ductility.

c) Nucleation may be described by a simple critical stress criterion. The macroscopic far-field strain at which it is satisfied is dependent upon the local values of particle size, volume fraction and matrix yield strength. The particle spatial distribution is seen to play an important part.

d) From c), nucleation may occur locally at low levels of plastic strain. The objective of the following chapter is to investigate this.

e) The void growth strain, while being limited in composites of high volume fraction, is not negligible because of the constraint on the plastic flow and, therefore, coalescence imposed by the particles. This is seen directly in the composites of small volume fraction of reinforcing phase where there is additional growth strain before failure.

f) Crack propagation is by the nucleation of voids in regions ahead of the advancing crack tip. These regions are linked to the main crack by failure through the joining matrix ligaments.

(a)

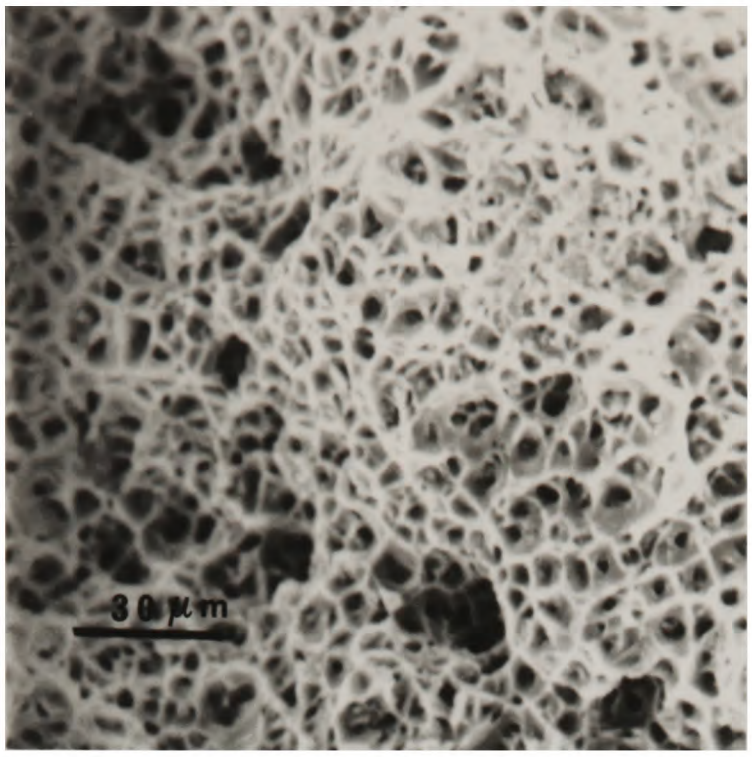

(b)

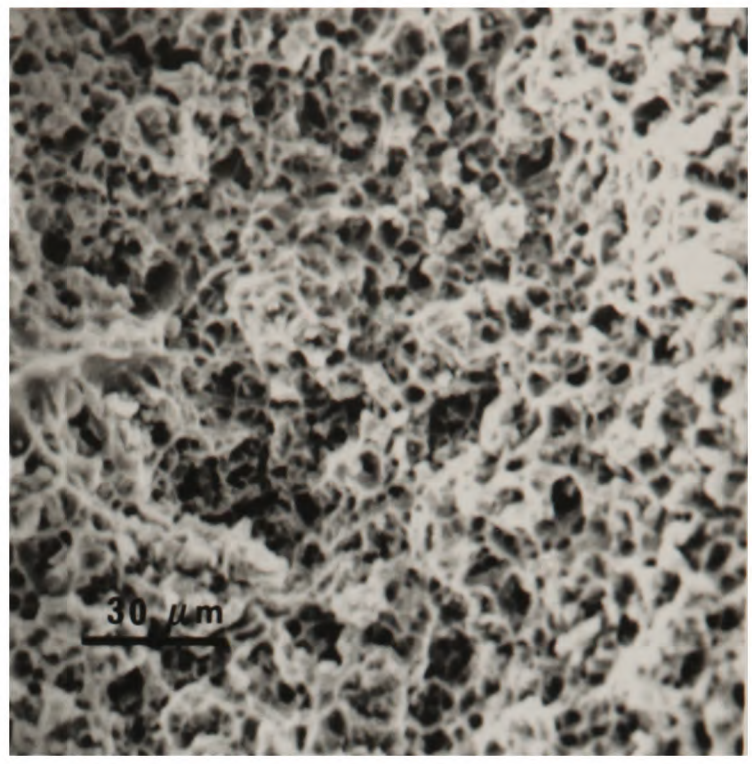

Figures 4.1 a+b: Fracture surfaces of (a) 5/3/1070 and (b) 20/3/Qu/1070.

(c)

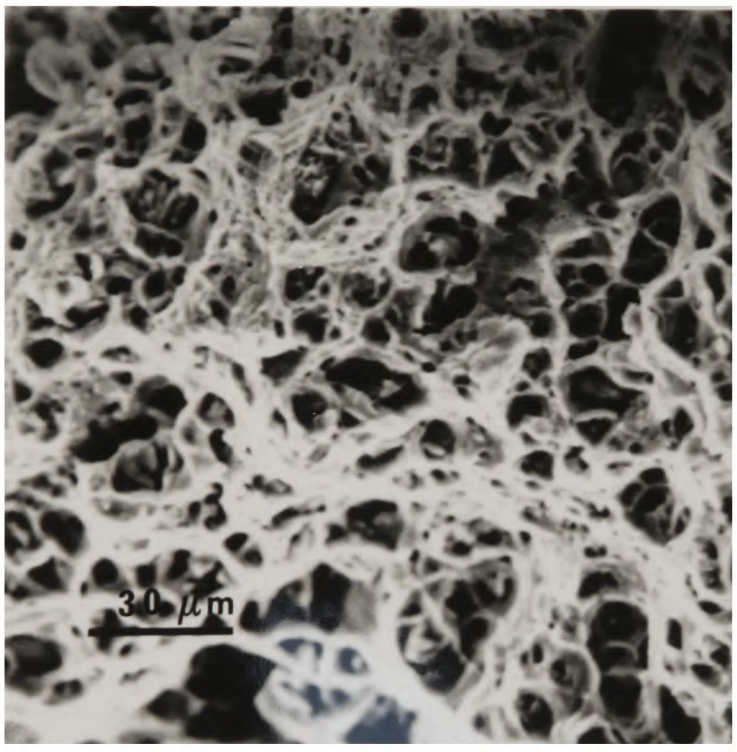

(d)

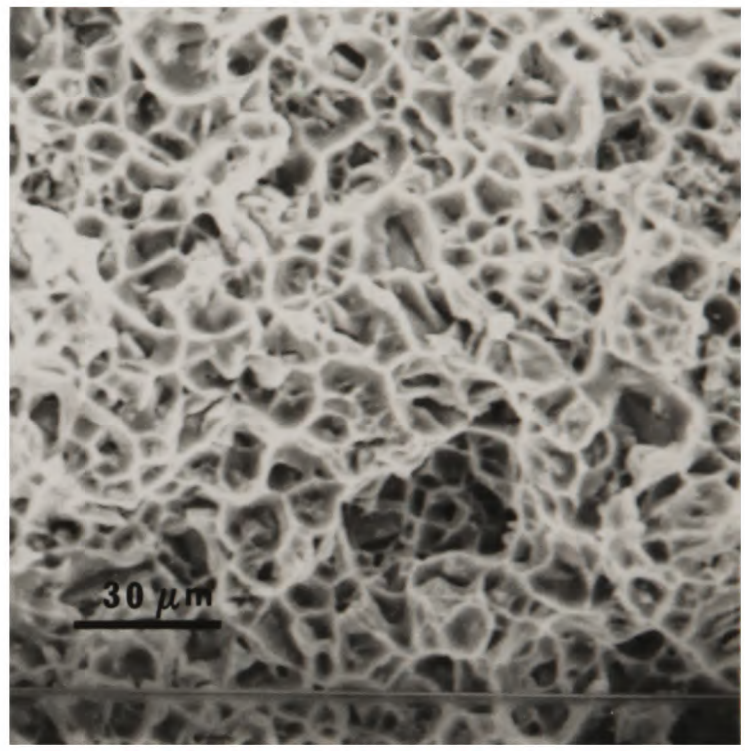

Figures 4.1 c+d: Fracture surfaces of (c) 5/10/Qu/1070 and (d) 20/10/Qu/1070.

(e)

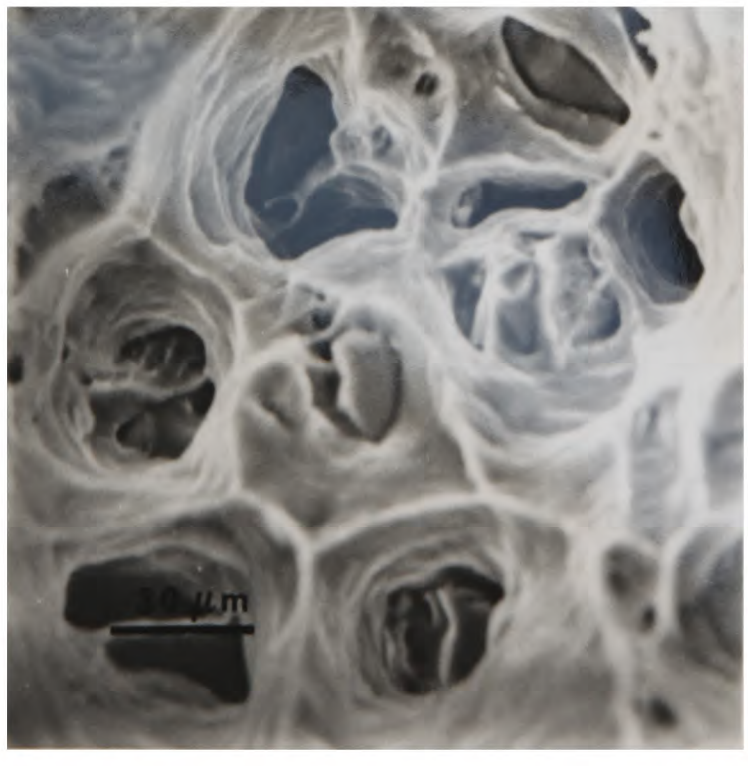

(f)

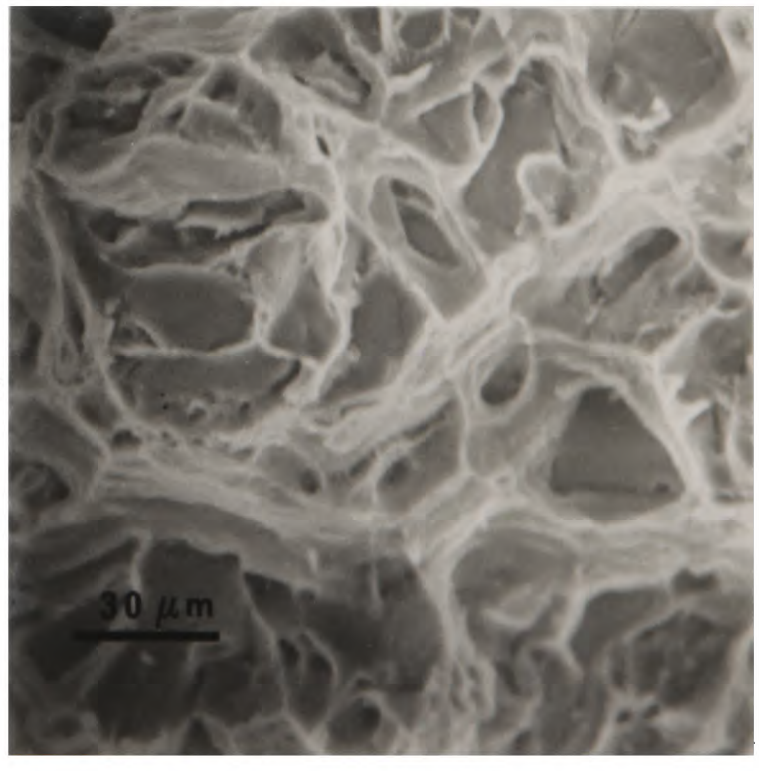

Figures 4.1 e+f: Fracture surfaces of (e) 5/30/Qu/1070 and (f) 20/30/Qu/1070.

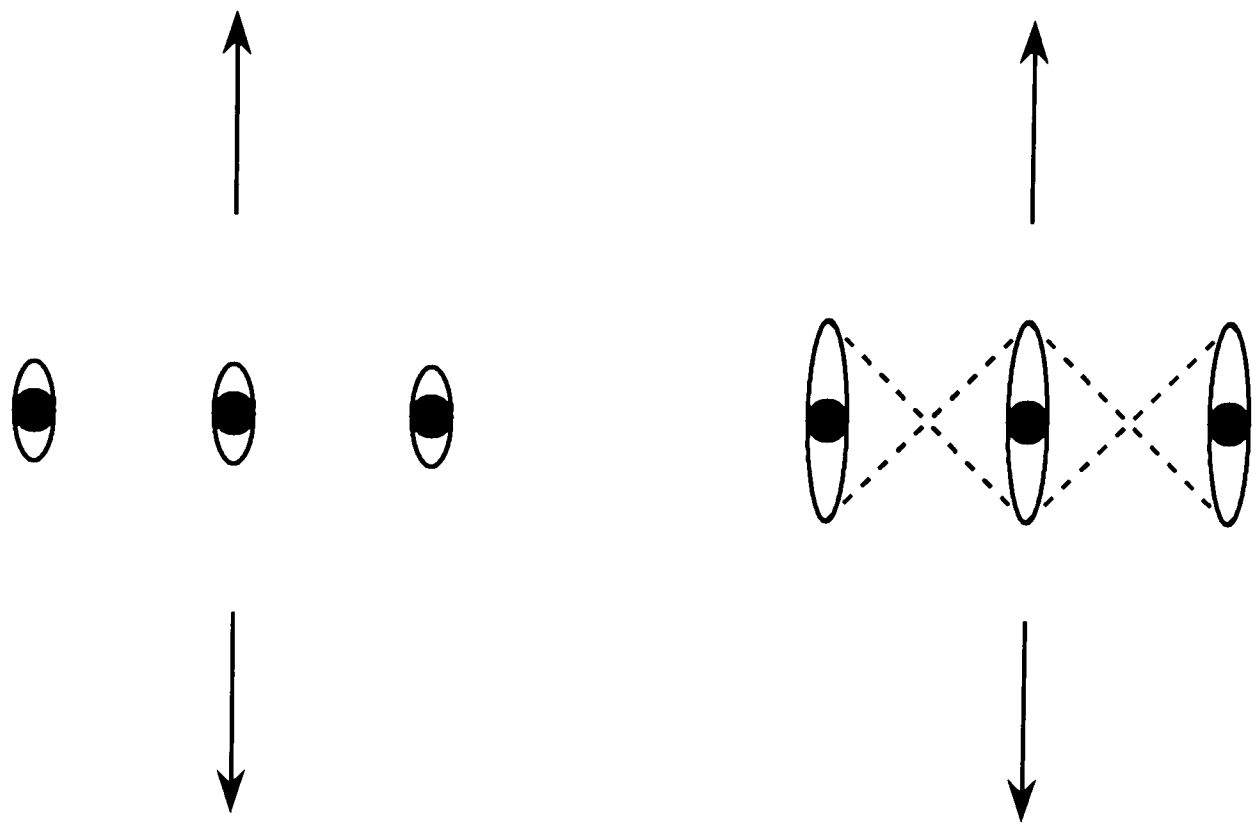

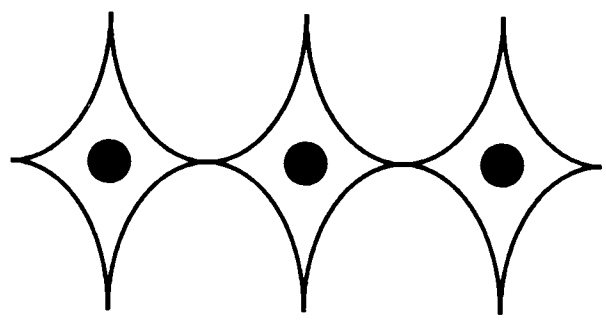

(c)

Figure 4.2: Void Coalescence by Simple Shear on Removing Plastic Constraint.

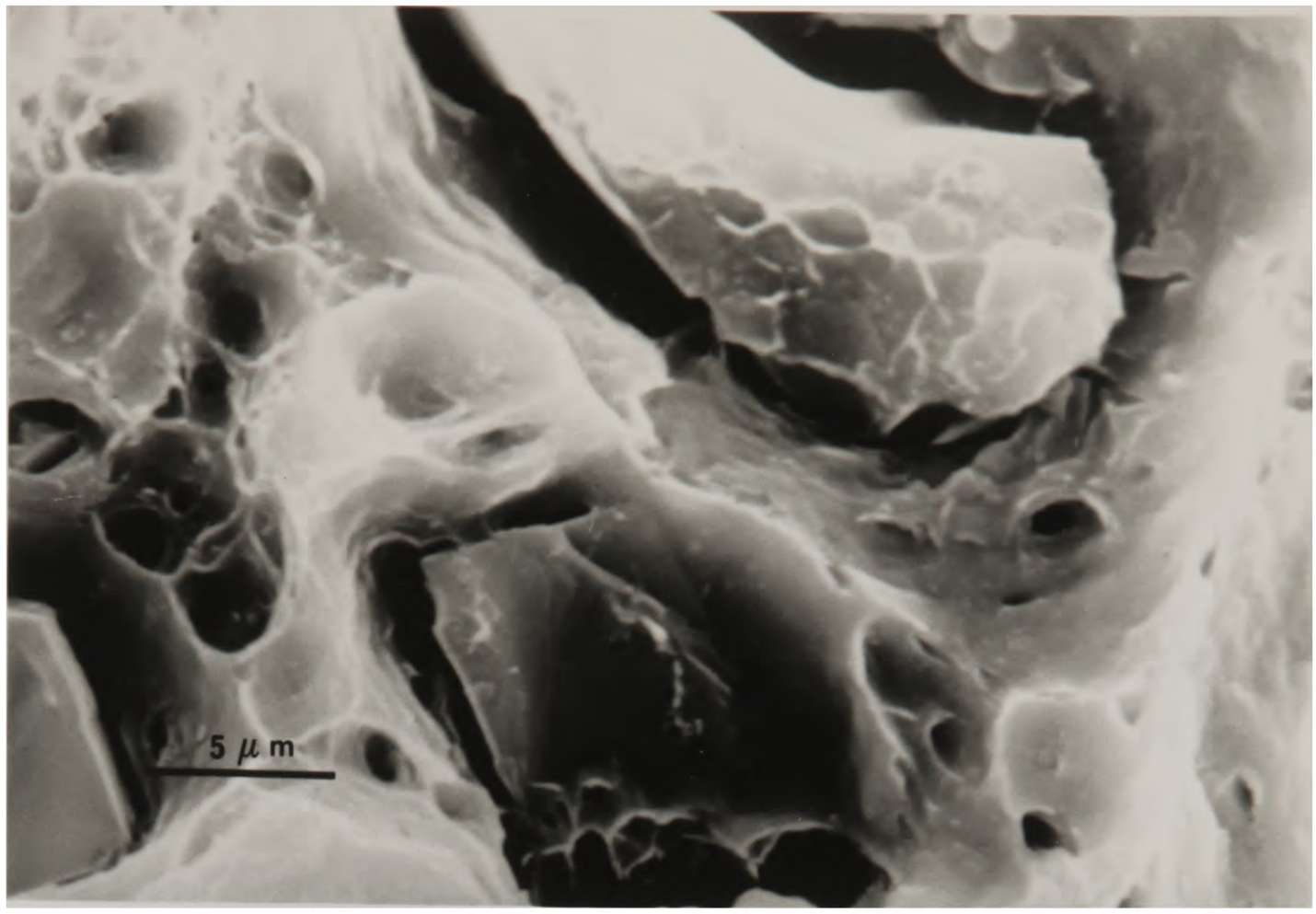

Figure 4.3: Bimodal void distribution in 20/10/Qu/1070.

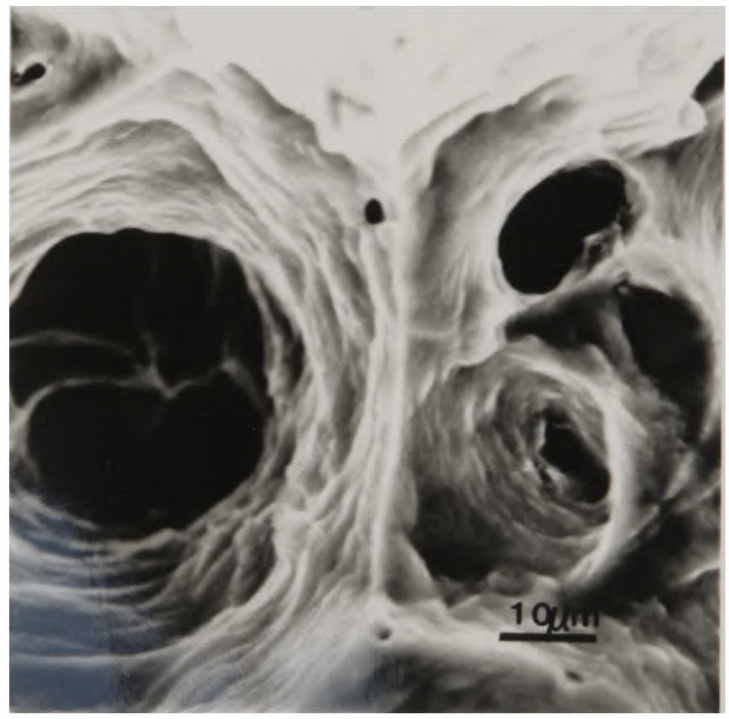

Figure 4.4: Serpentine glide in 5/30/Qu/1070.

(a)

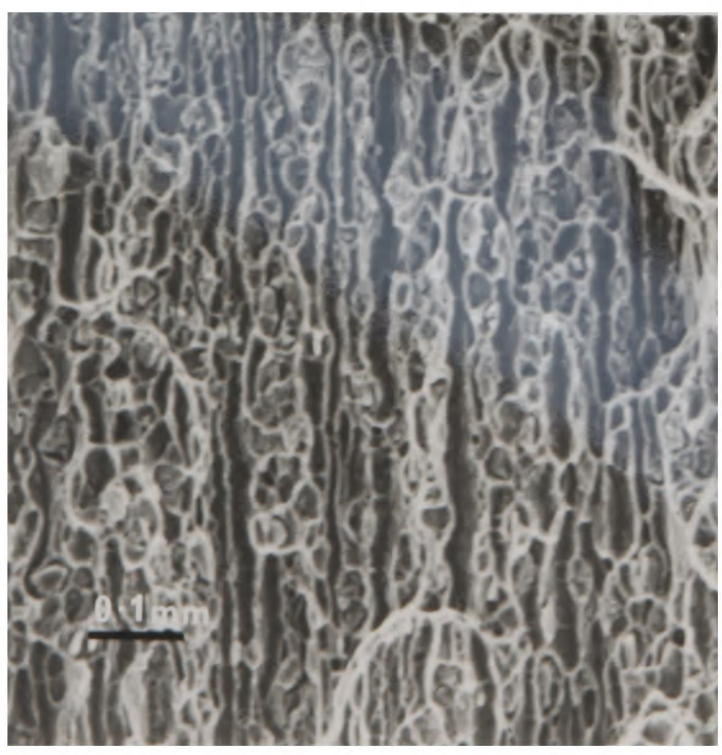

(b)

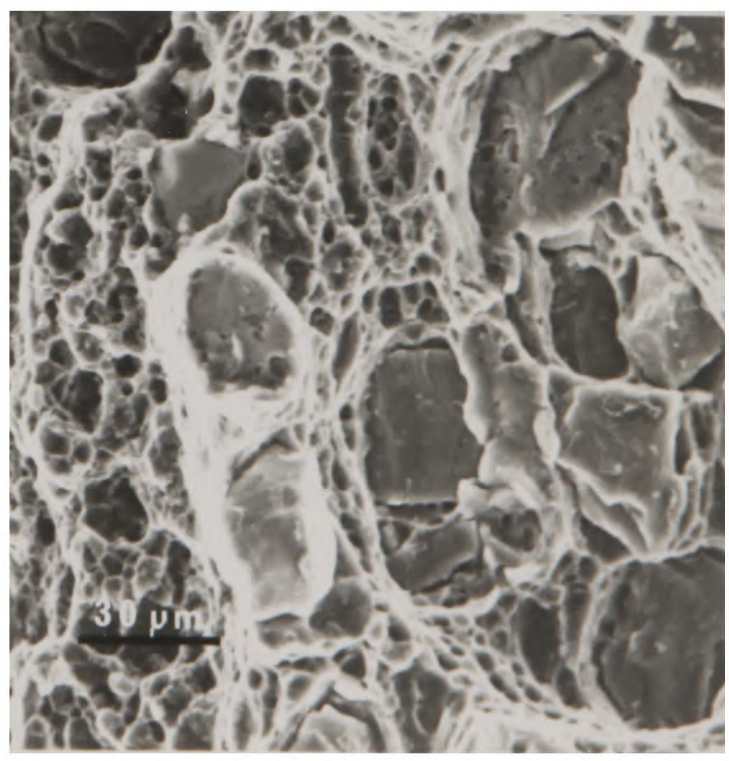

Figure 4.5 a+b: Different fracture surface morphology of Al-5050 composites shown in 5/30/Qu/5050.

(a)

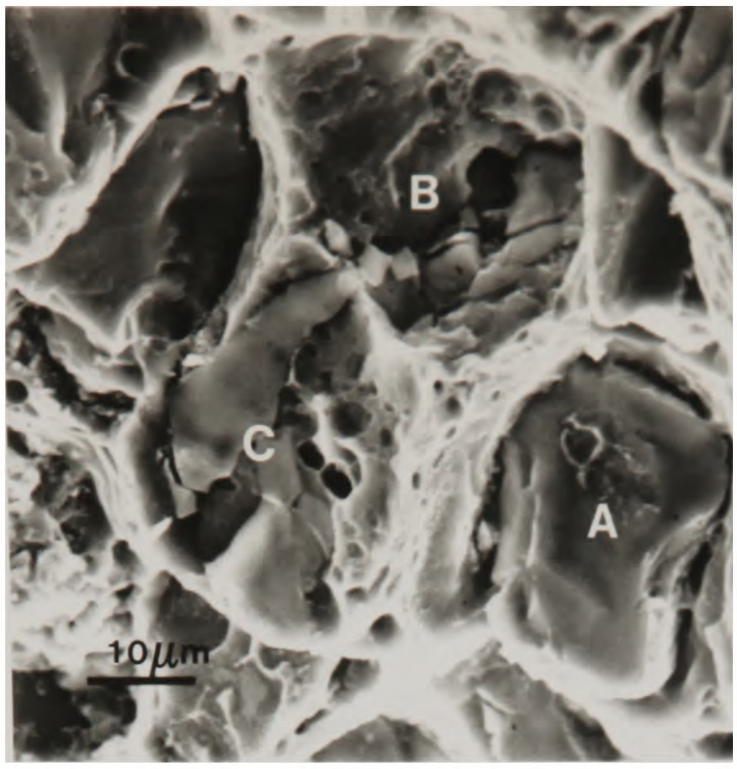

(b)

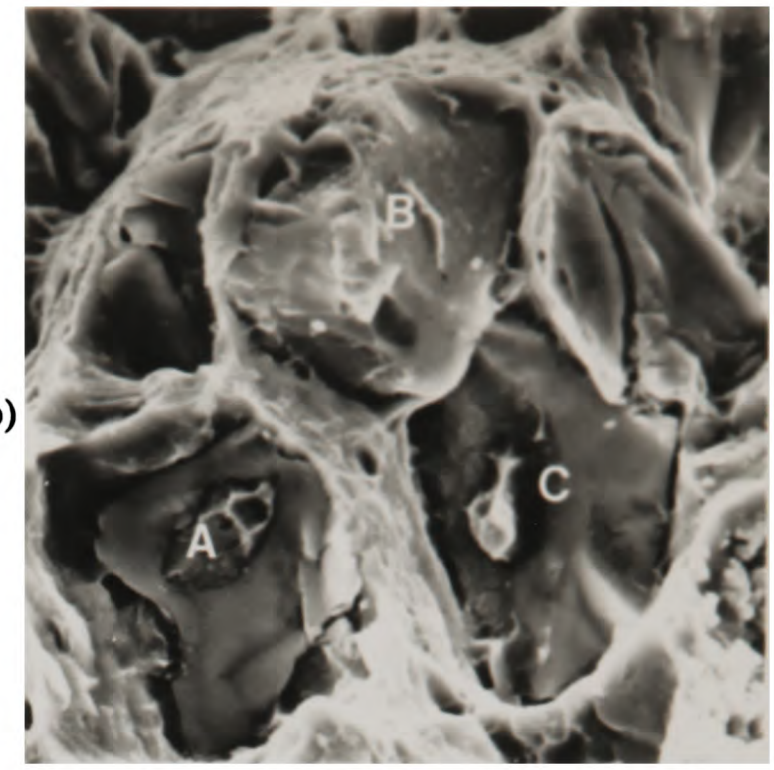

Figures 4.6 a+b: Matched fracture halves of 20/30/Qu/5050 showing particle fracture.

(a)

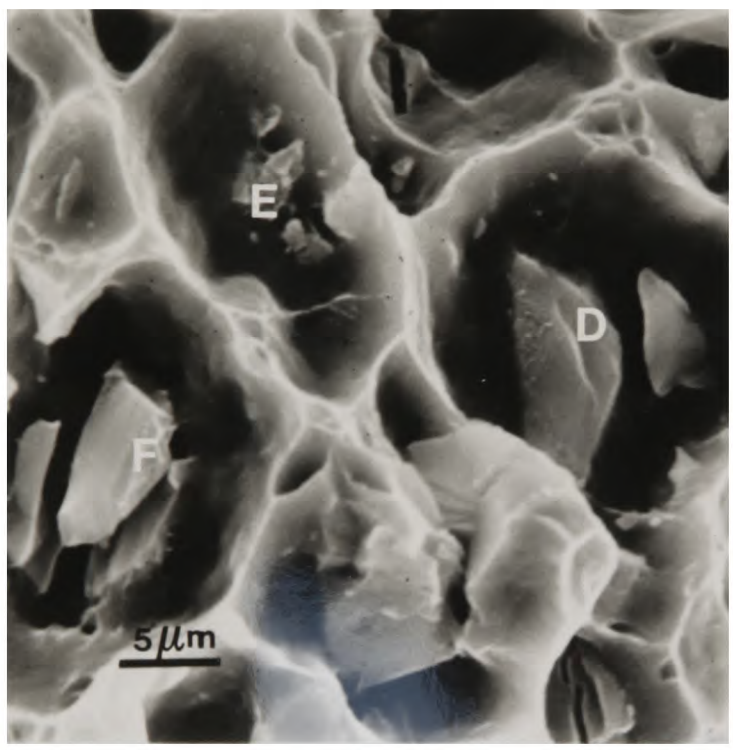

(b)

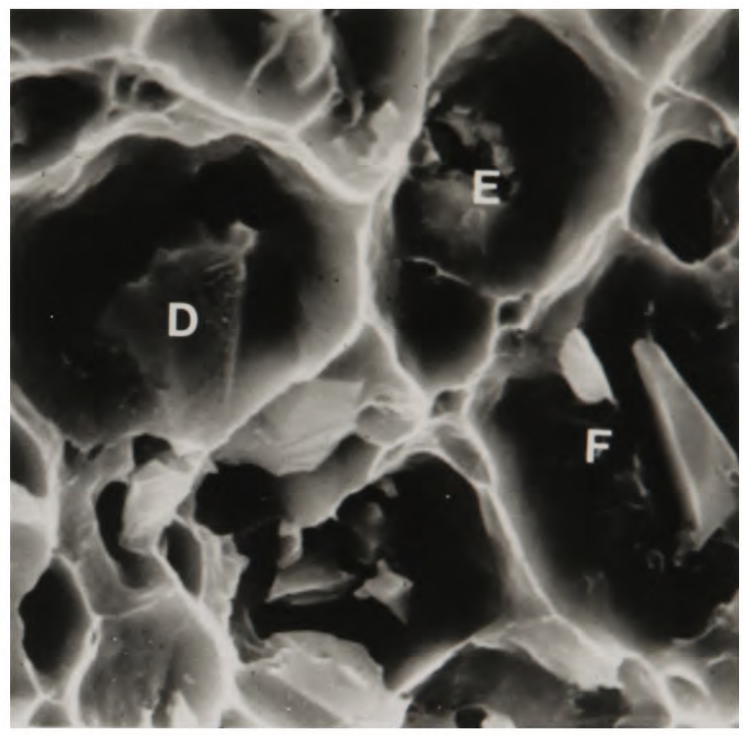

Figures 4.7 a+b: Matched fracture halves of 20/10/Qu/5050 showing particle fracture.

(a)

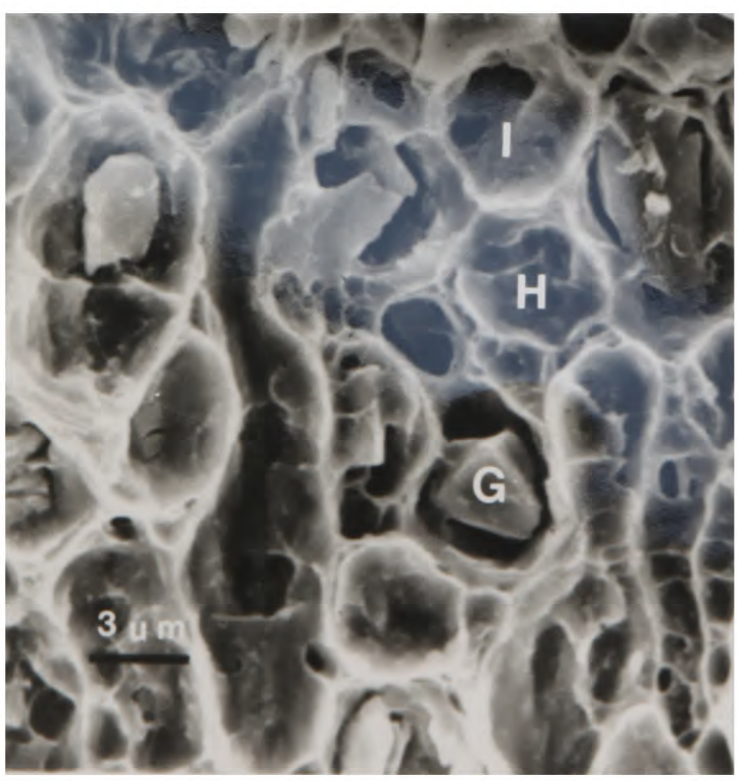

(b)

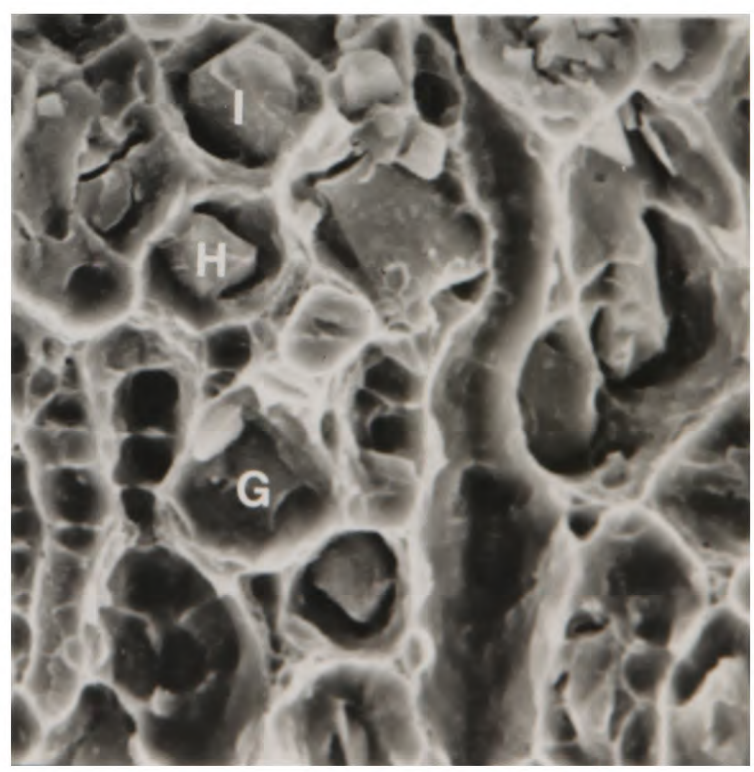

Figures 4.8 a+b: Matched fracture halves of 20/3/Qu/5050 showing interfacial decohesion.

(a)

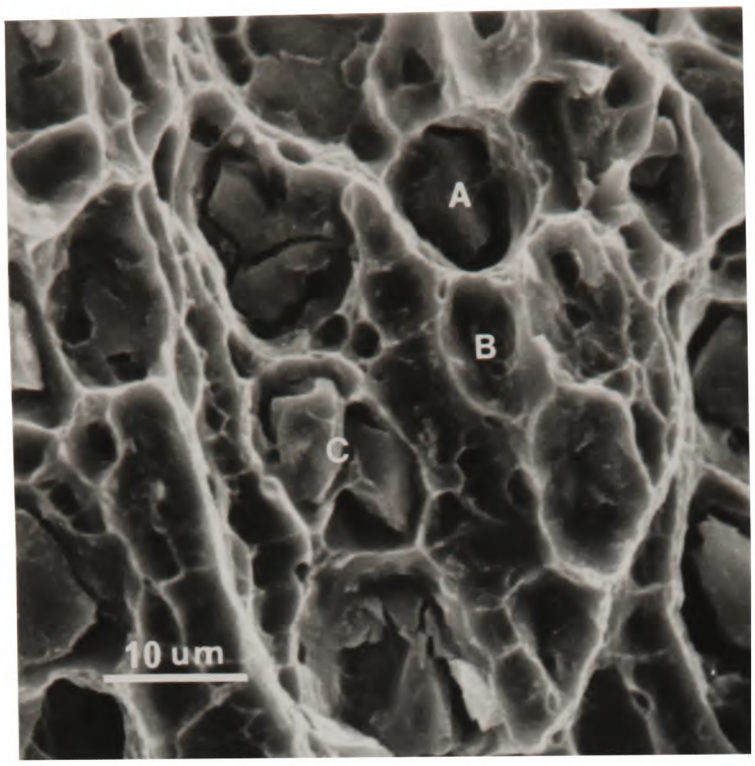

(b)

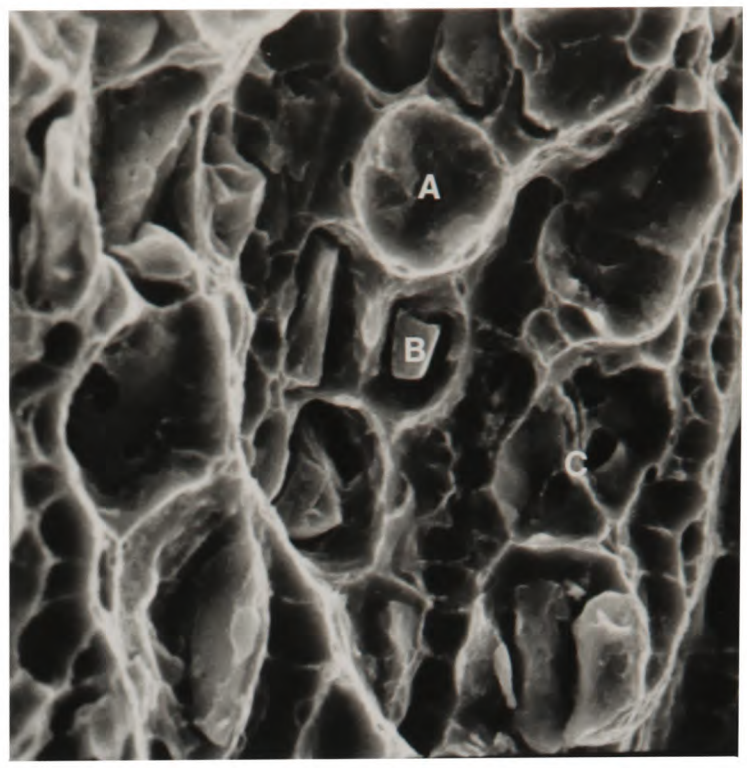

Figures 4.9 a+b: Matched fracture halves of 5/10/Qu/5050 showing interfacial decohesion.

(a)

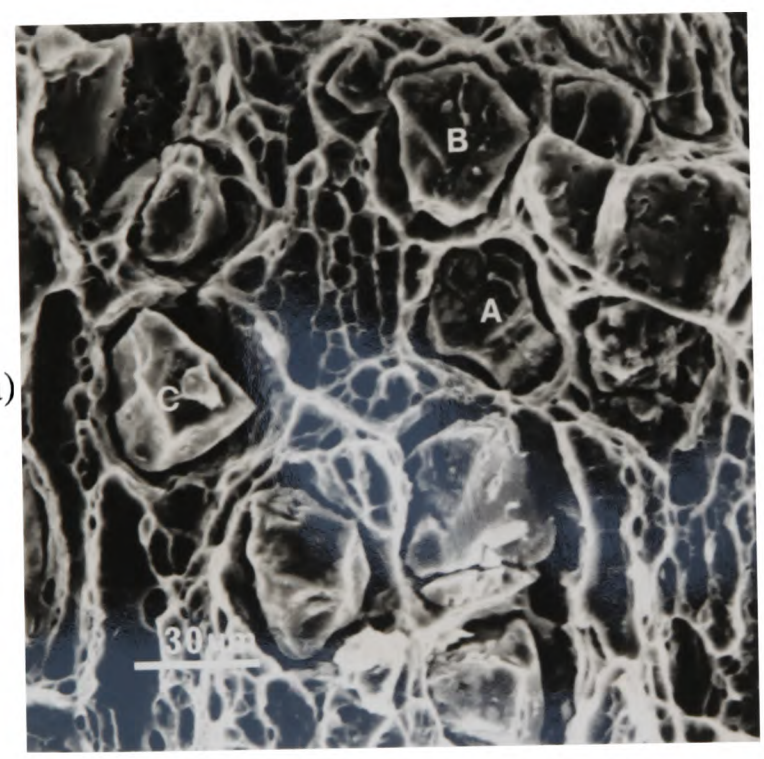

(b)

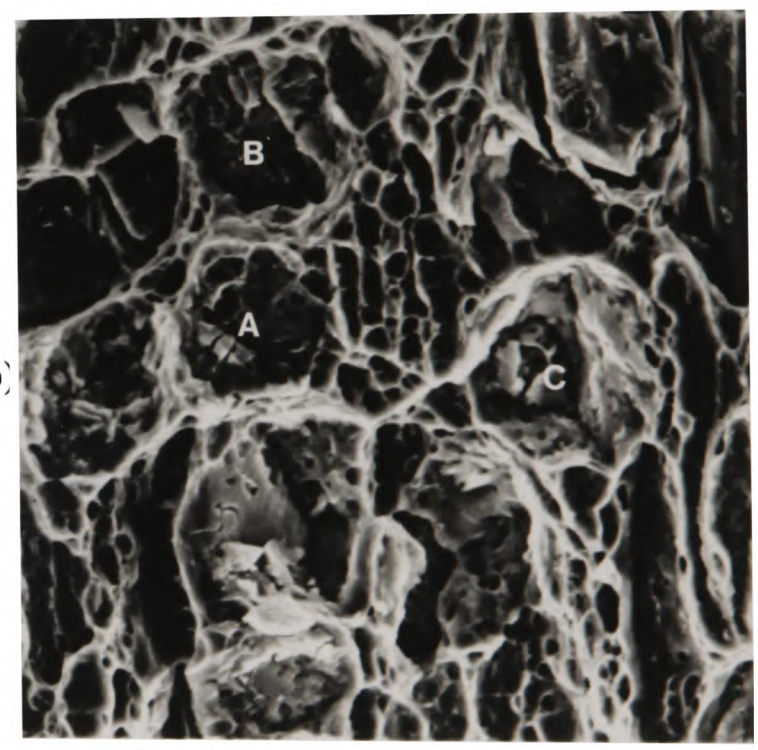

Figures 4.10 a+b: Matched fracture halves of 5/30/Qu/5050 showing interfacial decohesion.

(a)

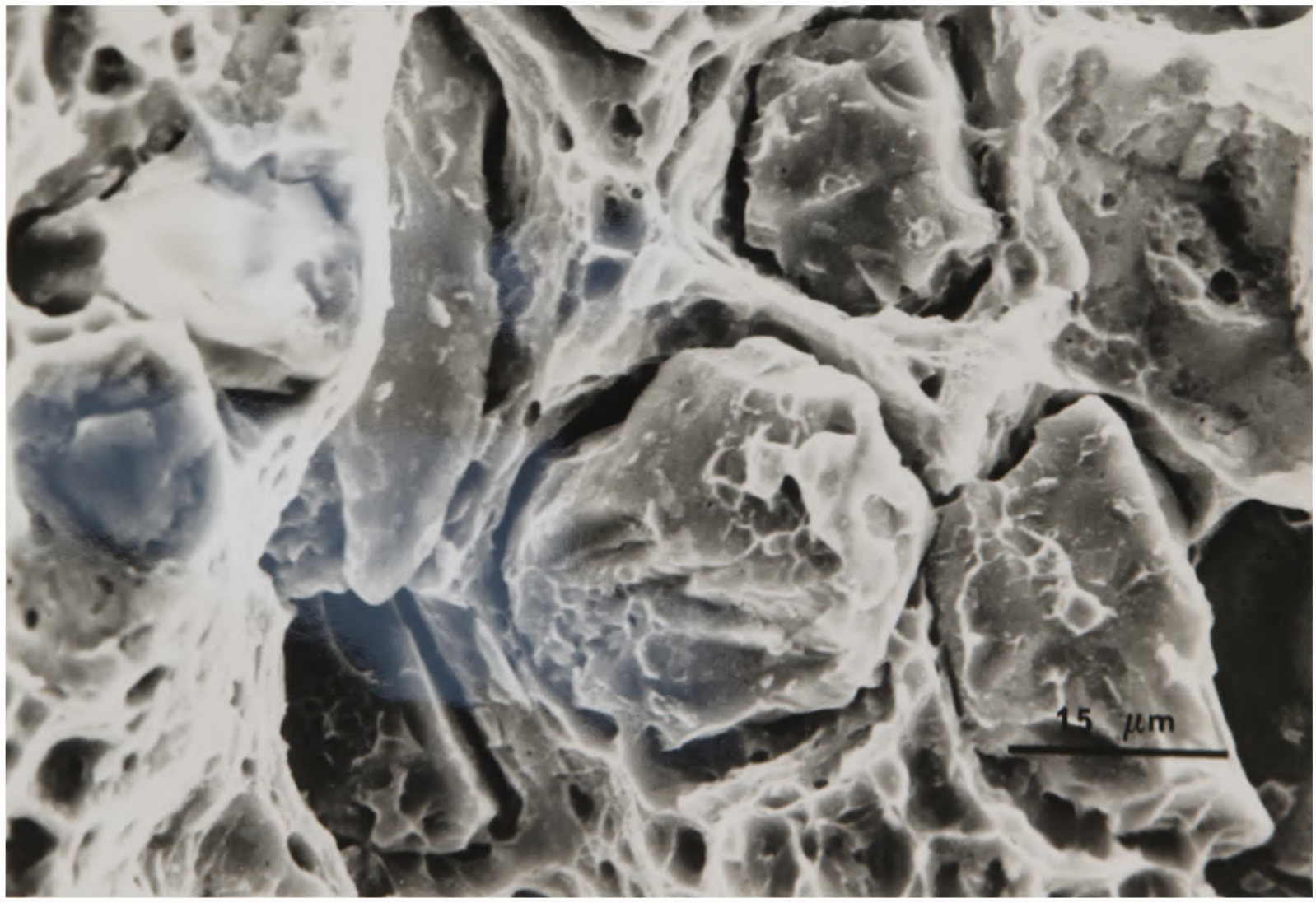

(b)

Figures 4.11 a+b: Debris on surface of 20/30/Qu/5050 indicative of interfacial reaction.

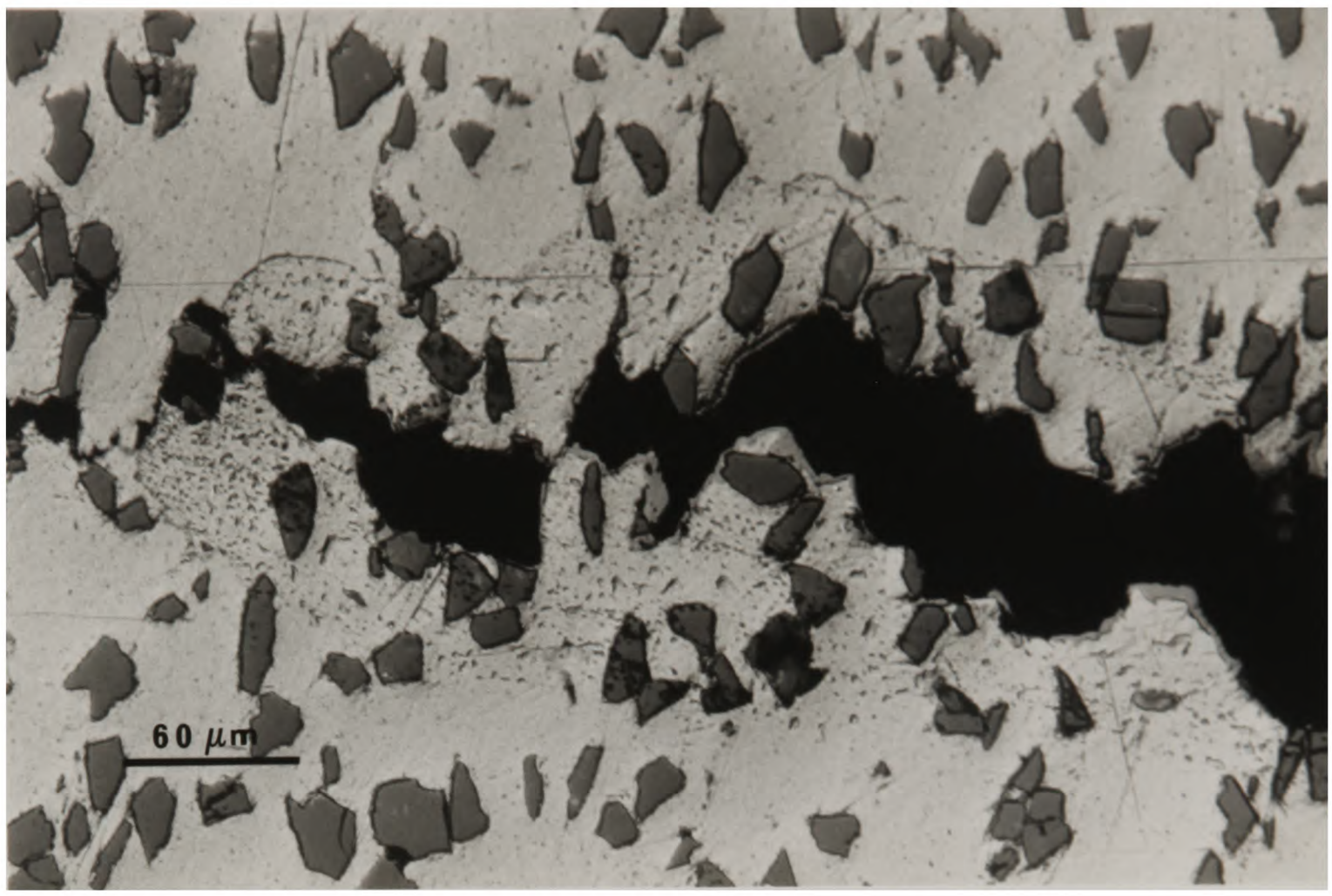

(a)

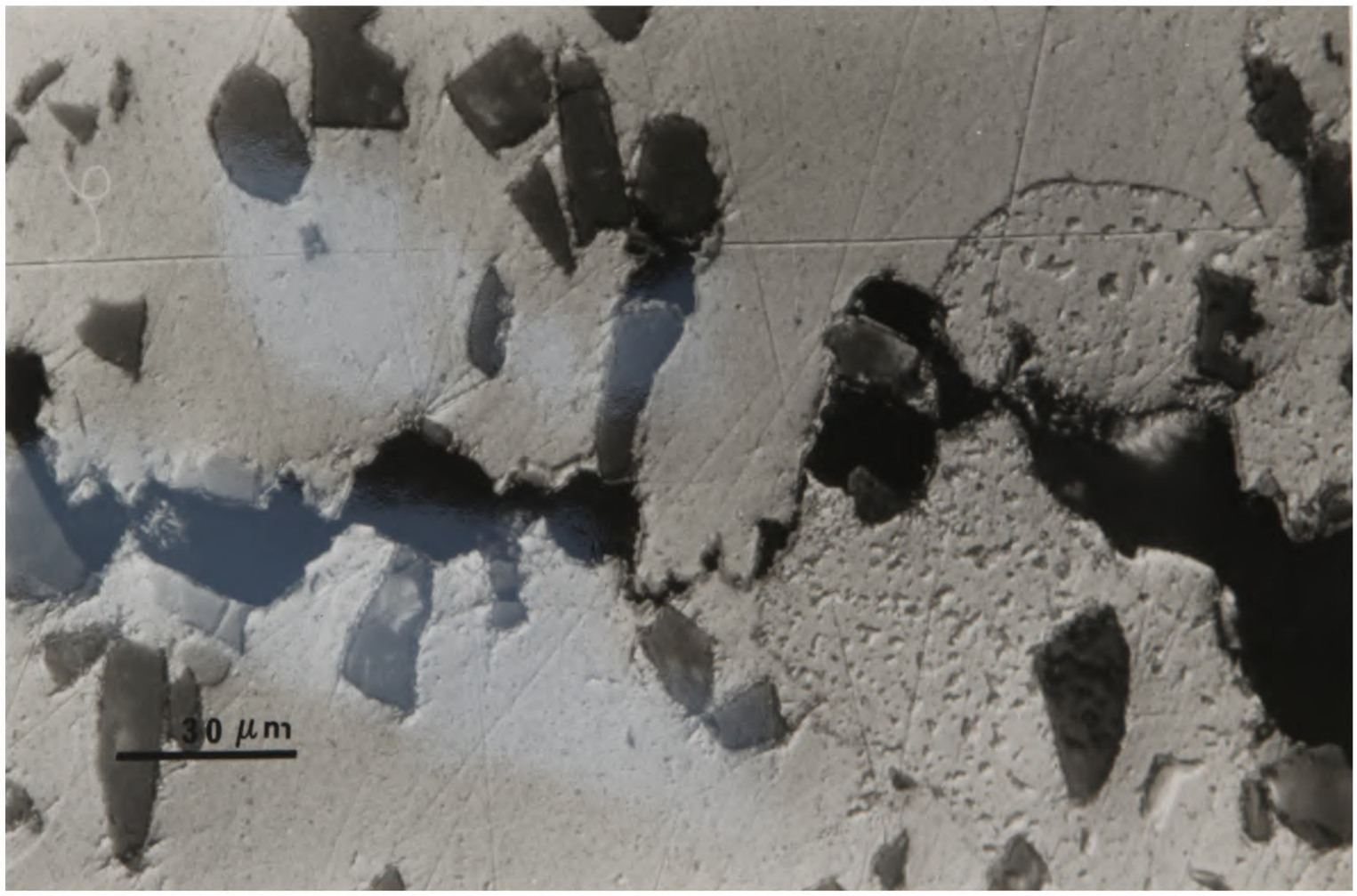

(b)

Figures 4.12 a+b: Section through stable crack in 20/30/Qu/5050 showing propagation sequence

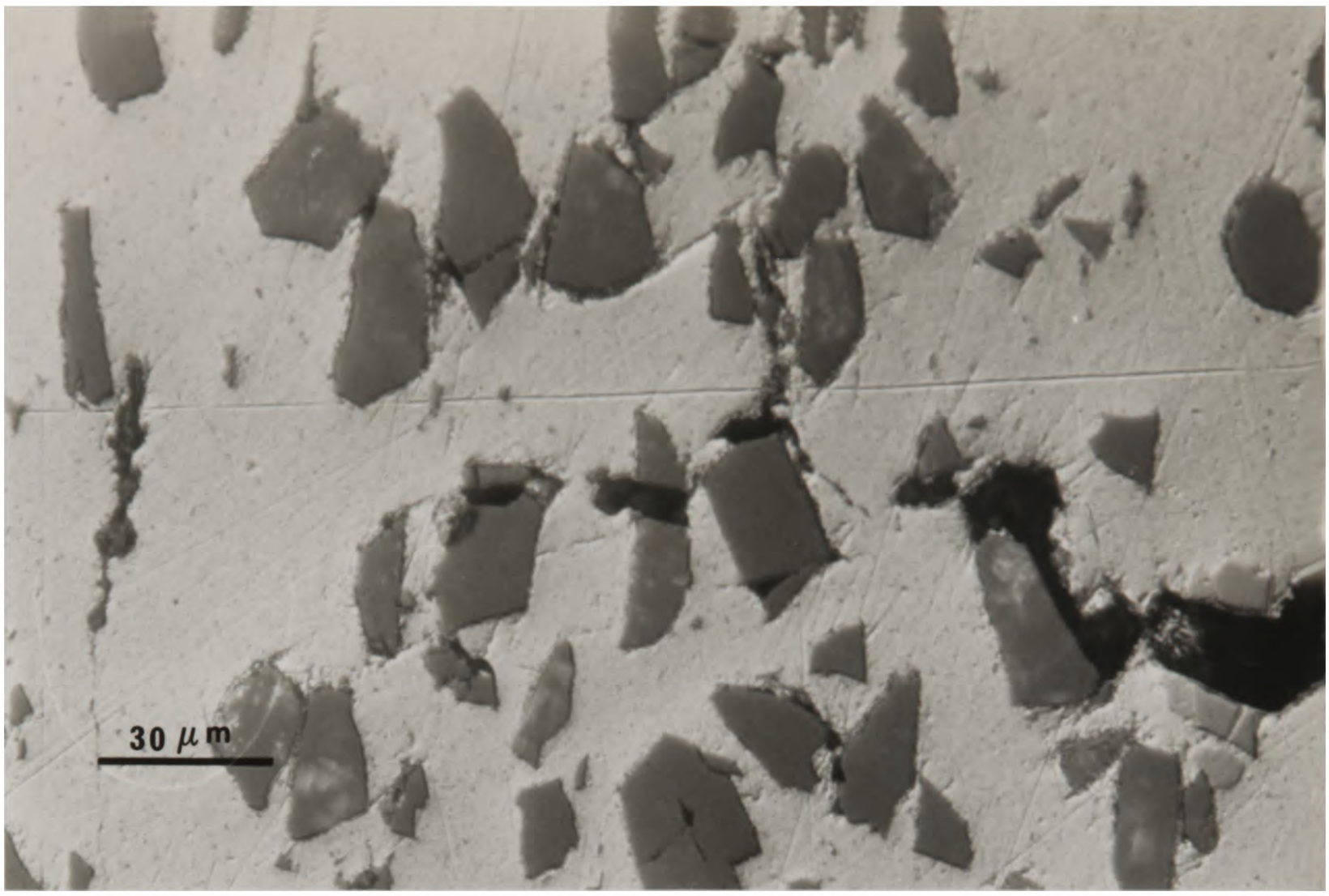

Figure 4.12c: Crack passing through SiC particles.

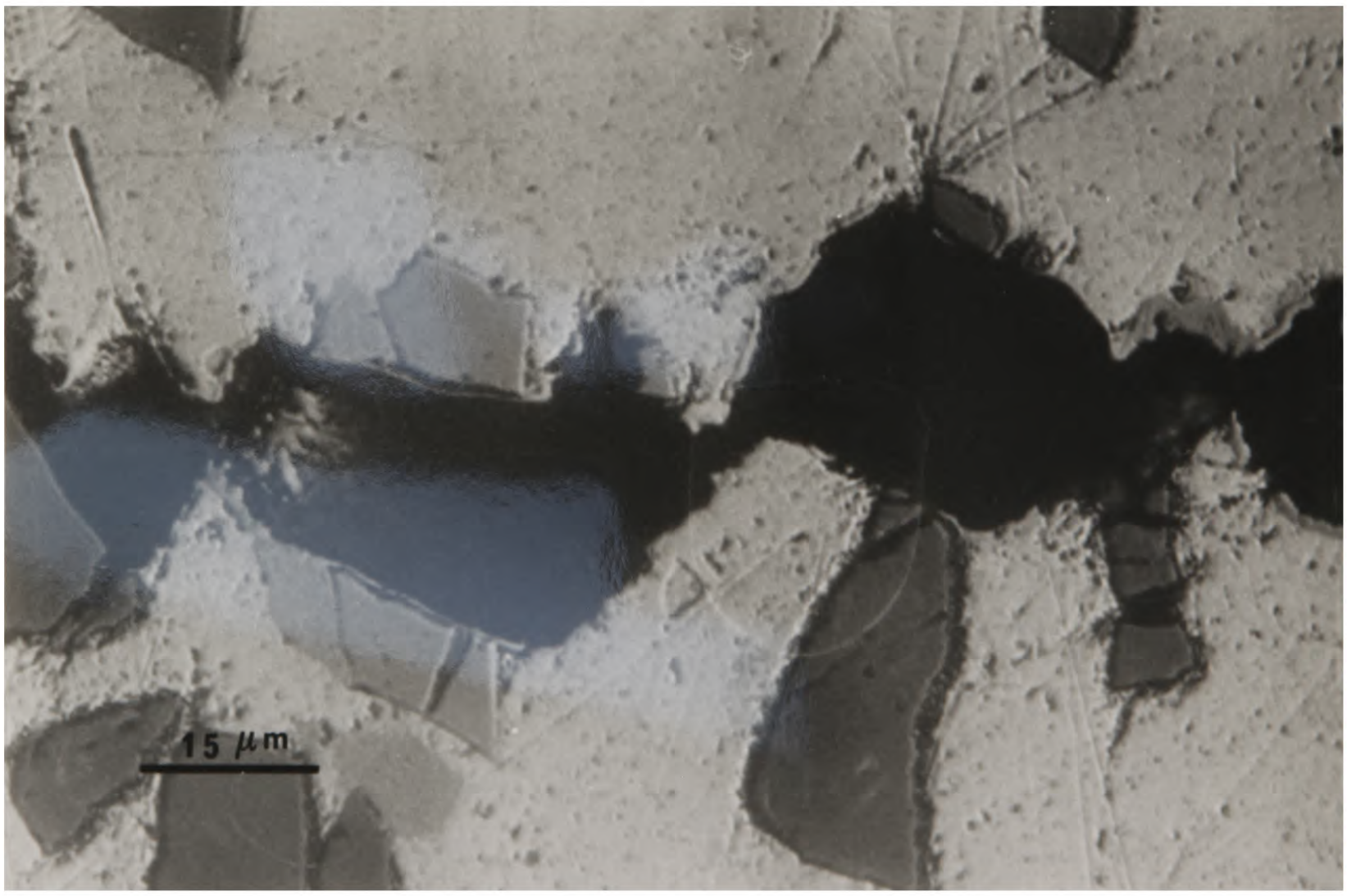

Figure 4.12d: Nucleation events ahead of crack tip.

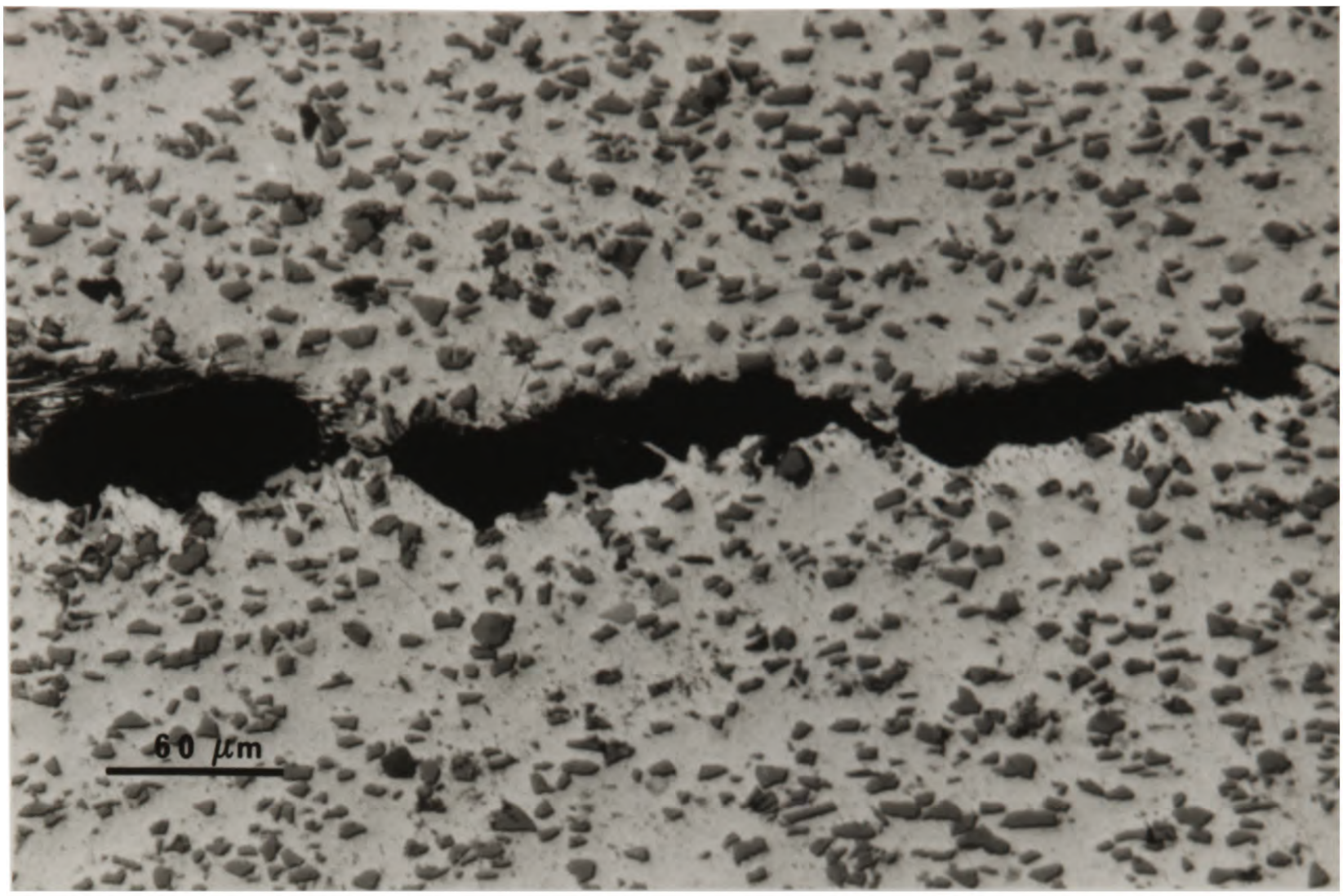

Figure 4.13a: Crack propagation in 20/10/Qu/5050.

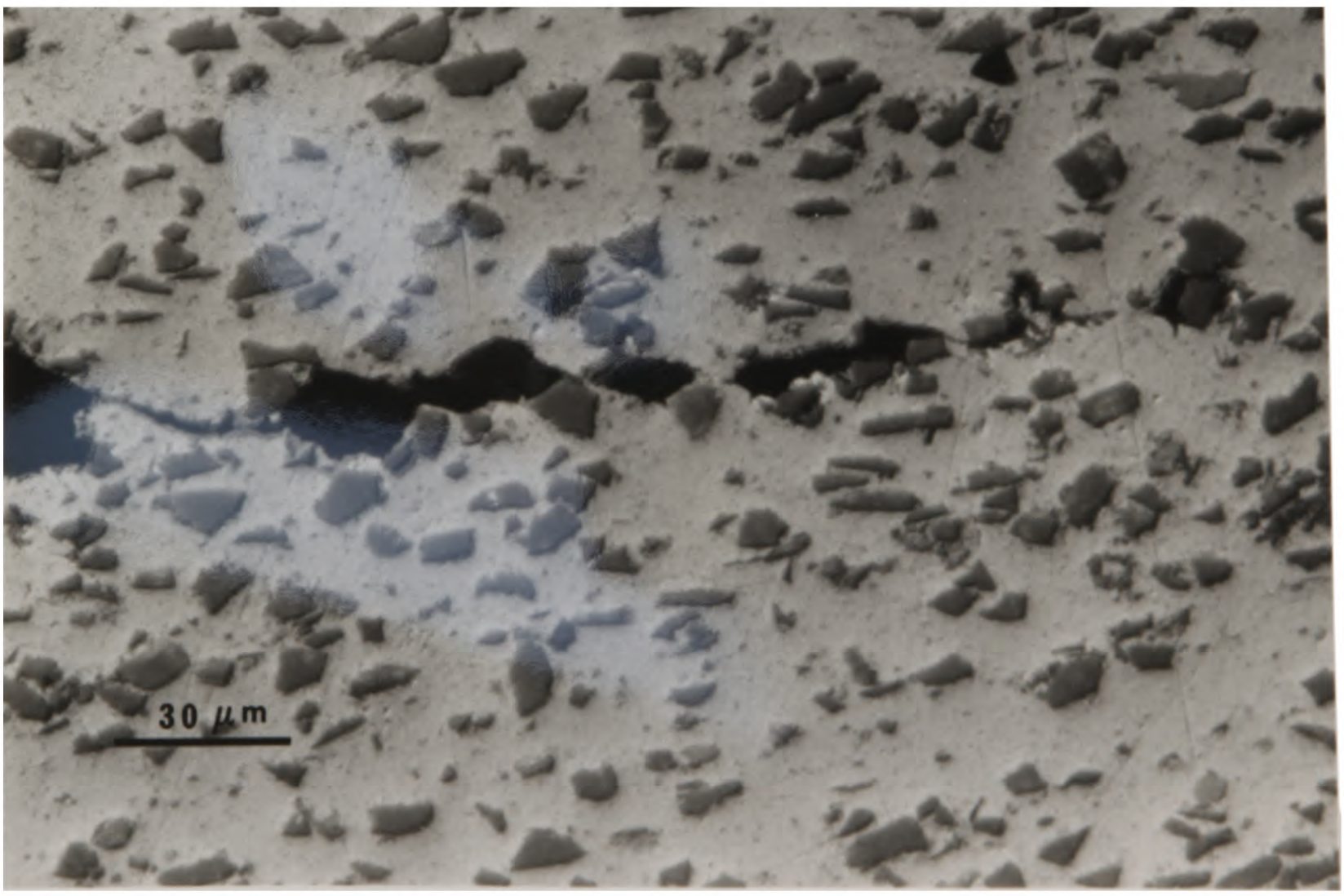

Figure 4.13b: No nucleation events away from plane of crack in 20/10/Qu/5050.

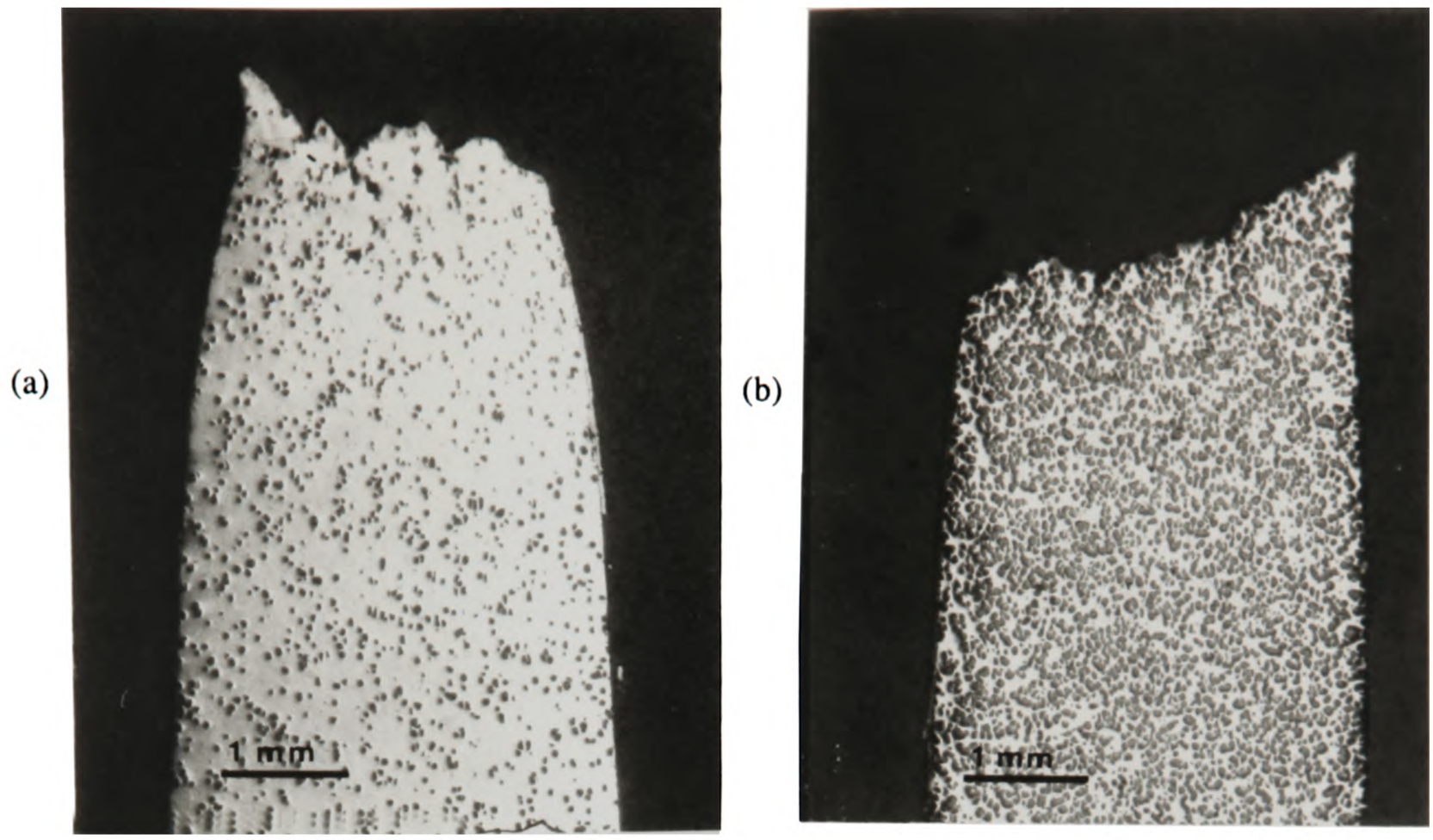

Figures 4.14 a+b: Low magnification sections through failed tensile specimens of (a) 5/30/Qu/1070 and (b) 20/30/Qu/1070.

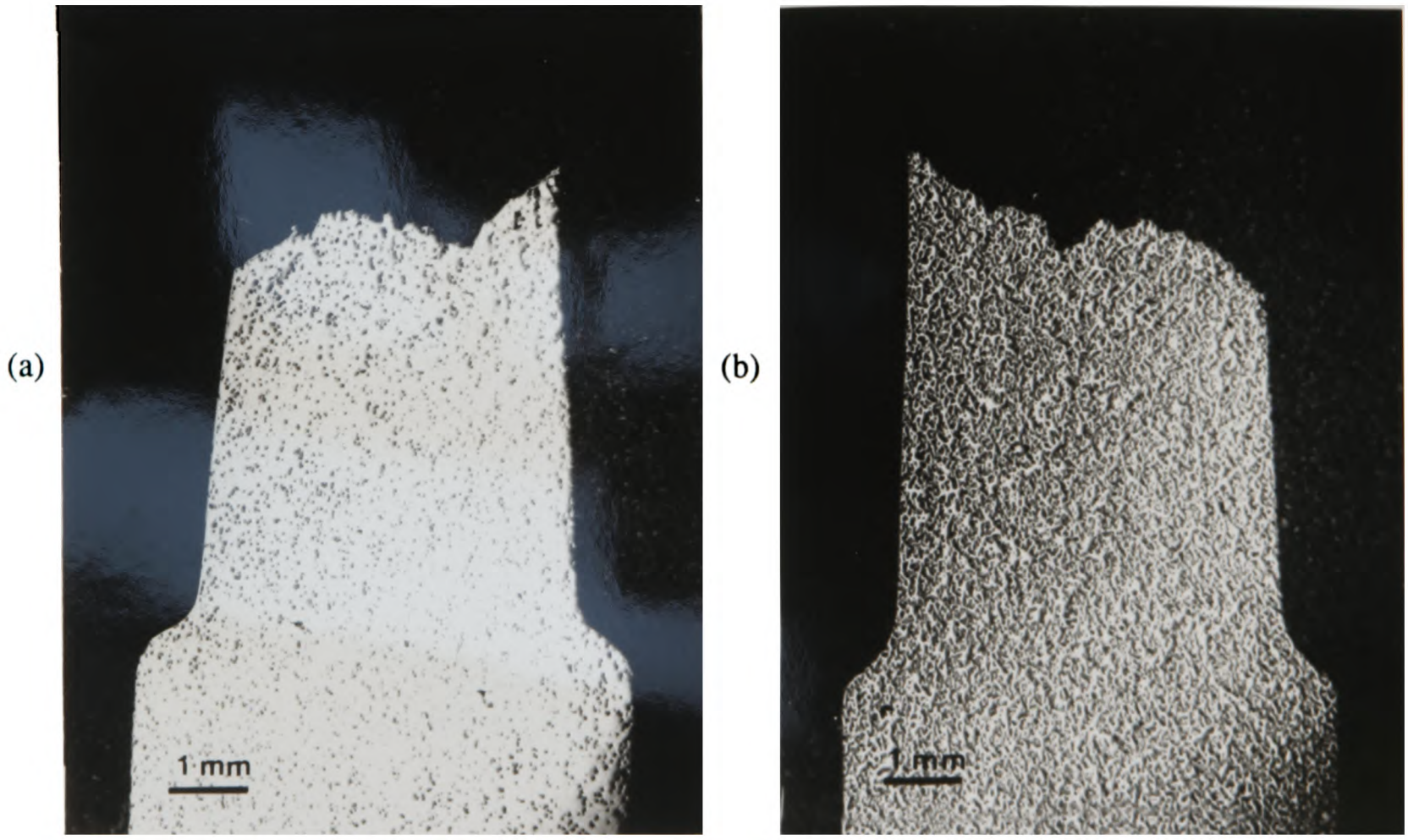

Figures 4.15 a+b: Low magnification sections through failed tensile specimens of (a) 5/30/Qu/5050 and (b) 20/30/Qu/5050.

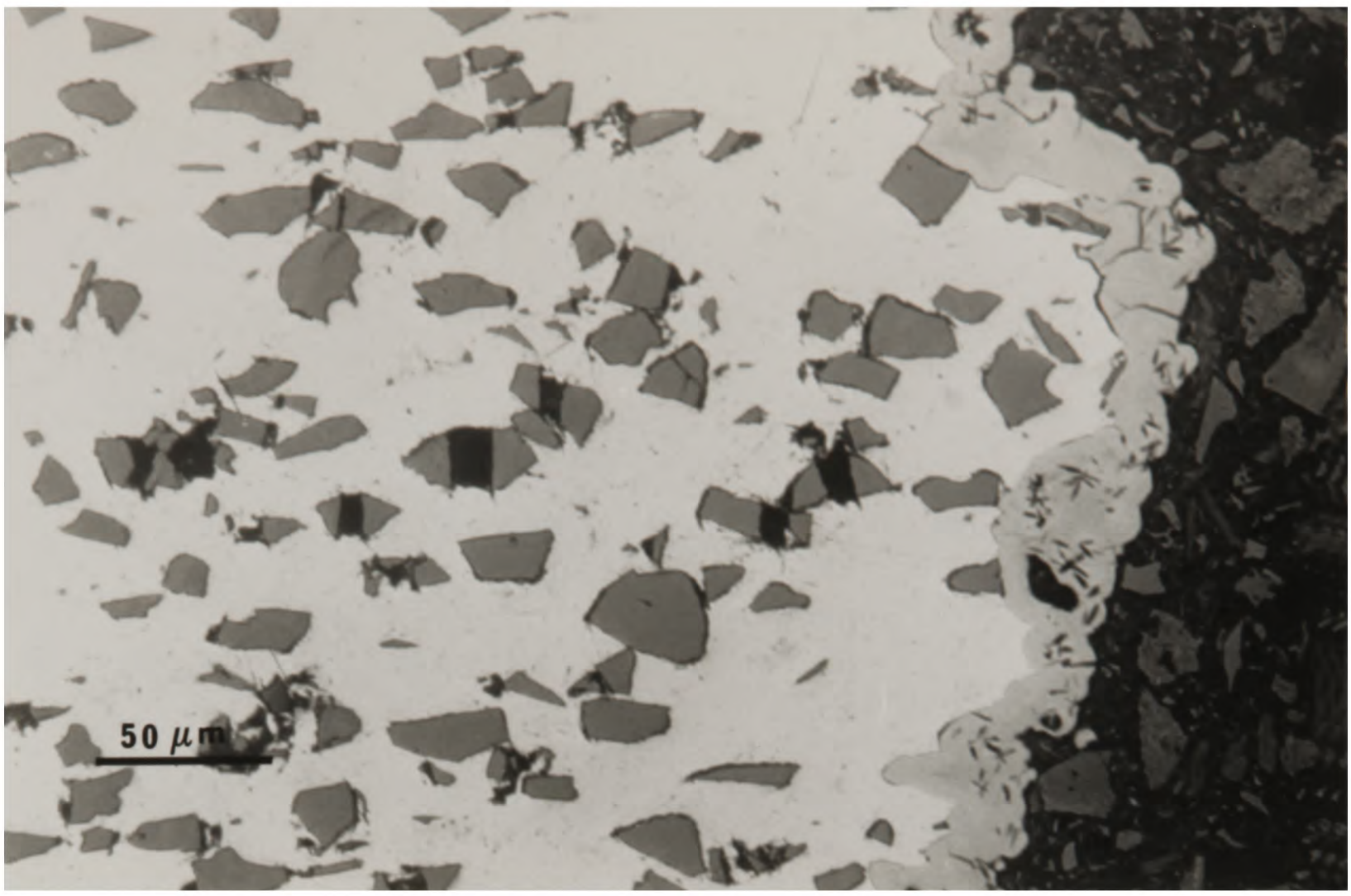

Figure 4.16: Section near fracture surface of 20/30/Qu/1070.

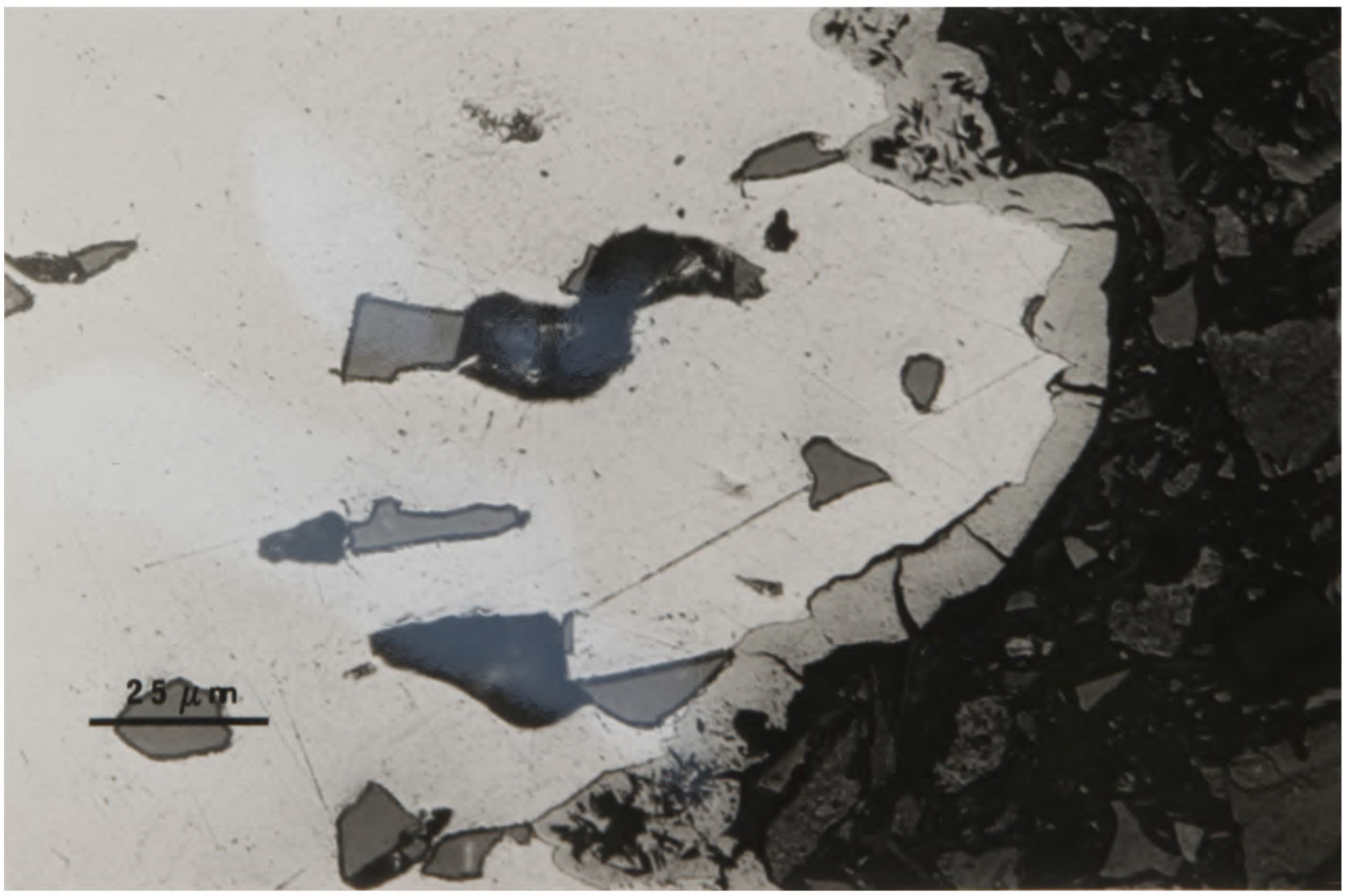

Figure 4.17: Section near fracture surface of 5/30/Qu/1070.

(a)

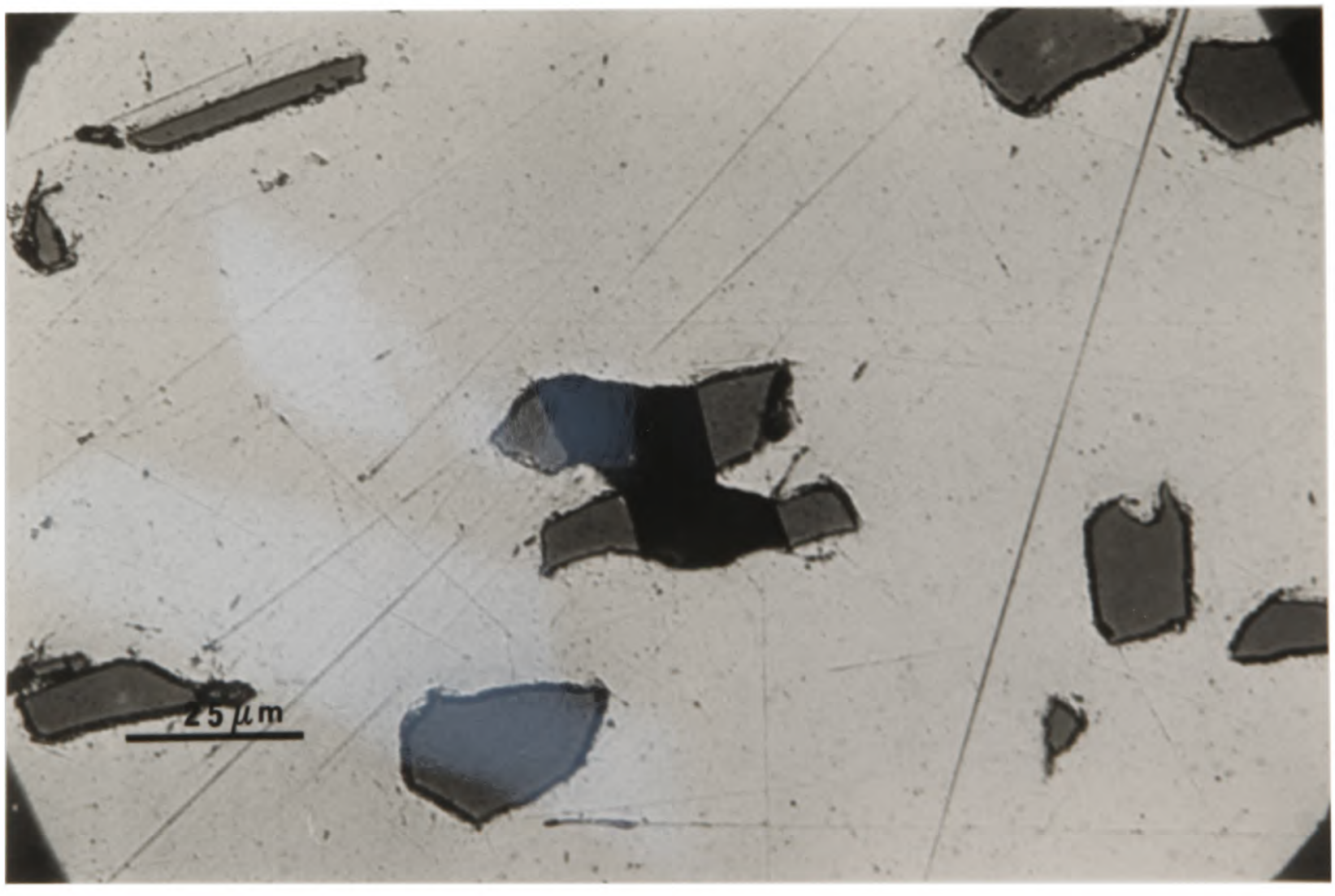

(b)

Figures 4.18 a+b: Void coalescence between neighbouring particles in 5/30/An/1070.

(a)

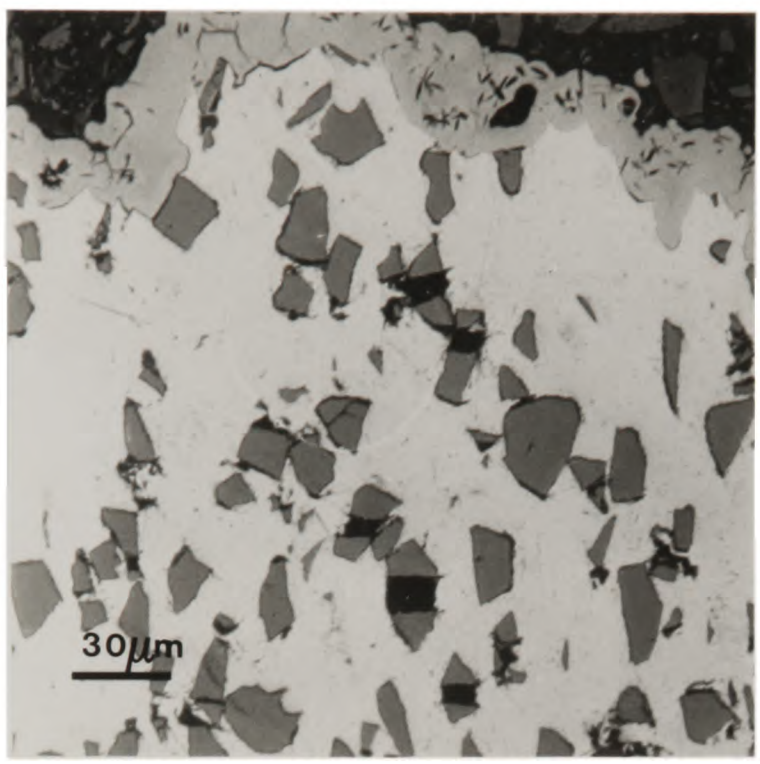

(b)

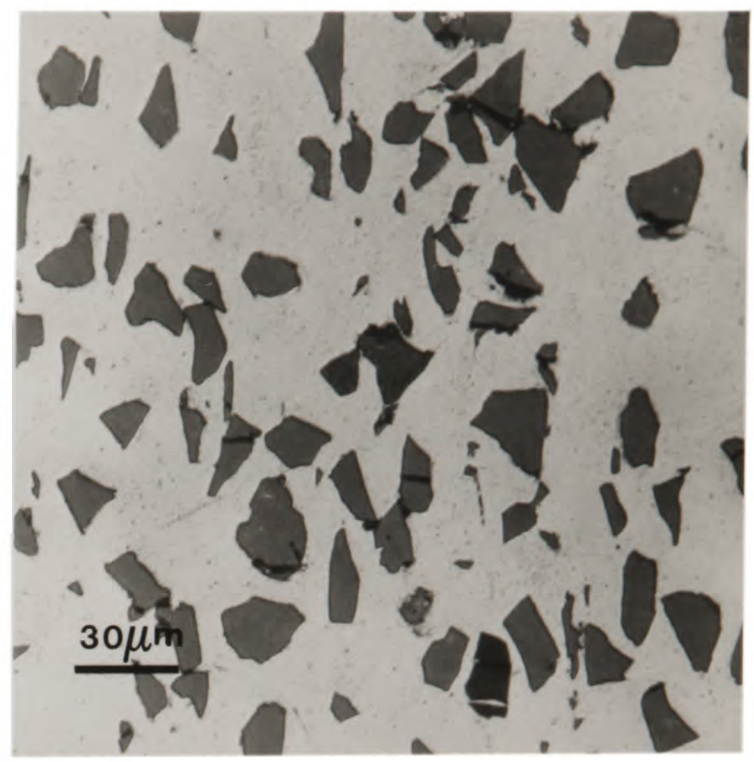

Figures 4.19 a+b: Sections through tensile specimen of 20/30/Qu/1070 at (a) the fracture surface and at (b) a strain of 4%.

(a)

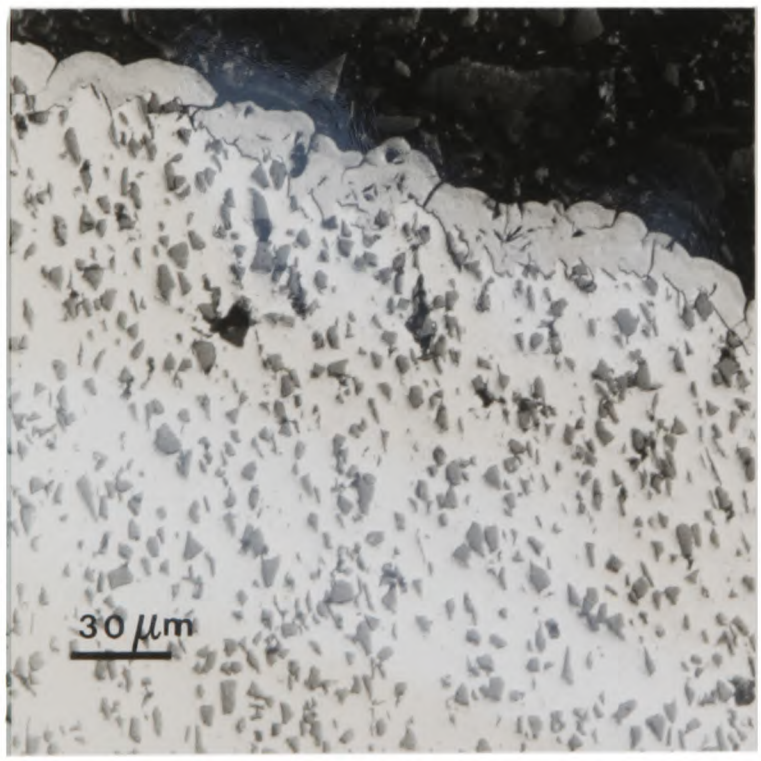

(b)

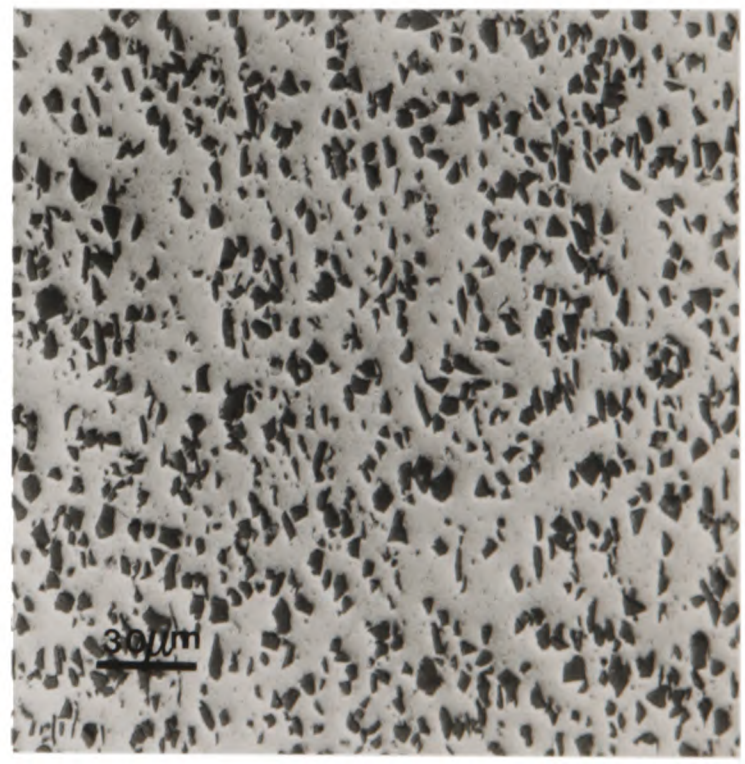

Figures 4.20 a+b: Sections through tensile specimen of 20/10/Qu/1070 at (a) the fracture surface and at (b) a strain of 4%.

(a)

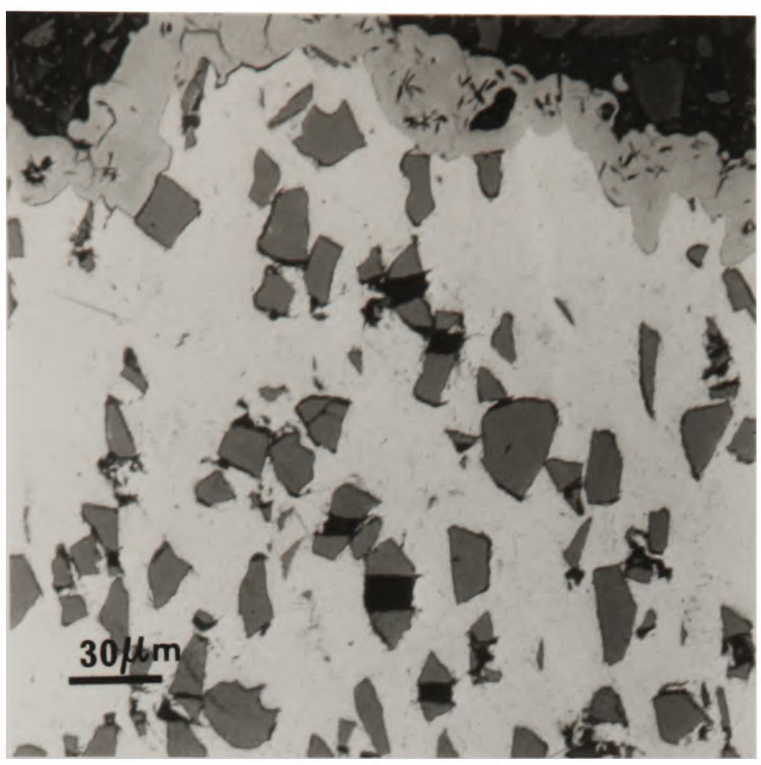

(b)

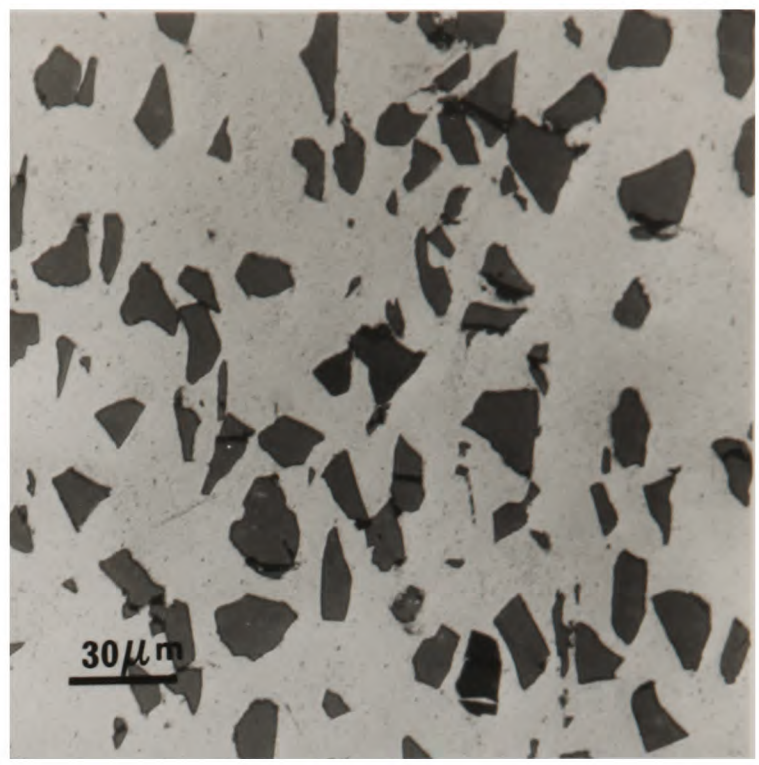

Figures 4.19 a+b: Sections through tensile specimen of 20/30/Qu/1070 at (a) the fracture surface and at (b) a strain of 4%.

(a)

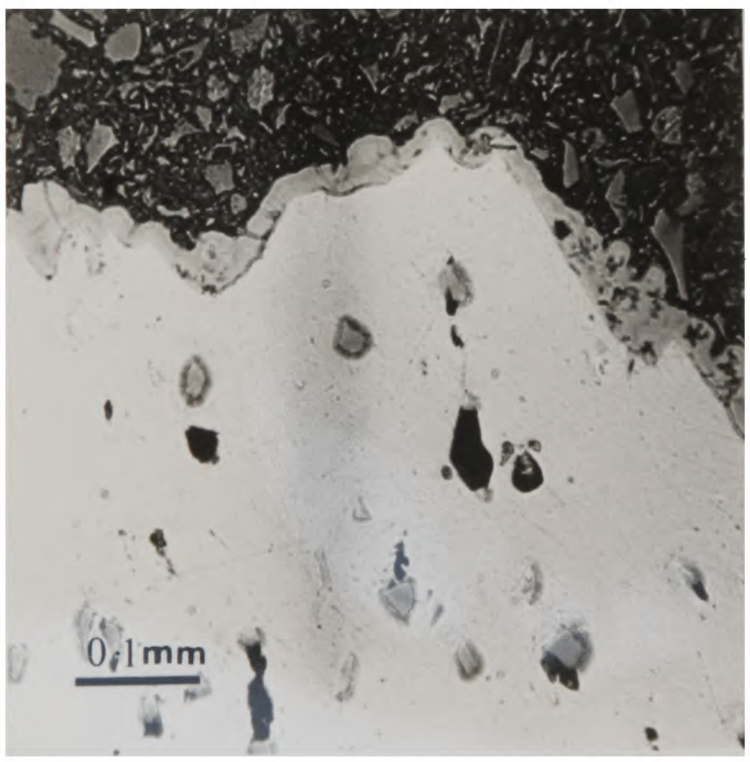

(b)

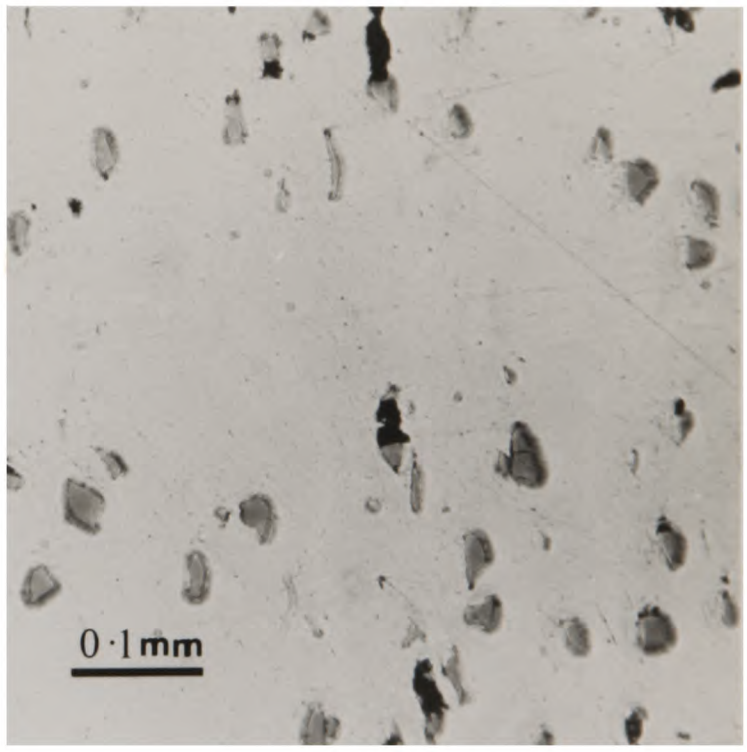

Figures 4.21 a+b: Section through tensile specimen of 5/30/Qu/1070 at (a) the fracture surface and at (b) a strain of 4%.

(a)

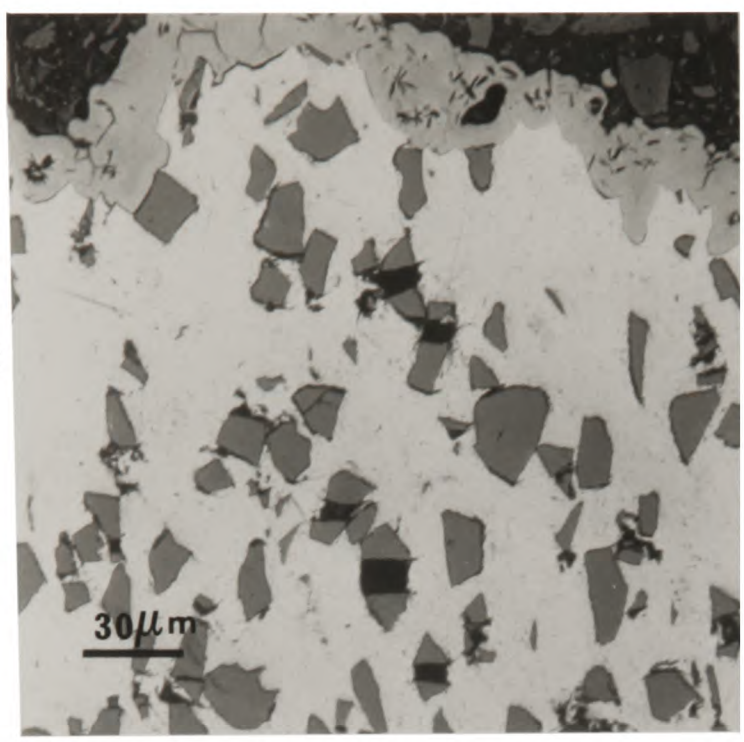

(b)

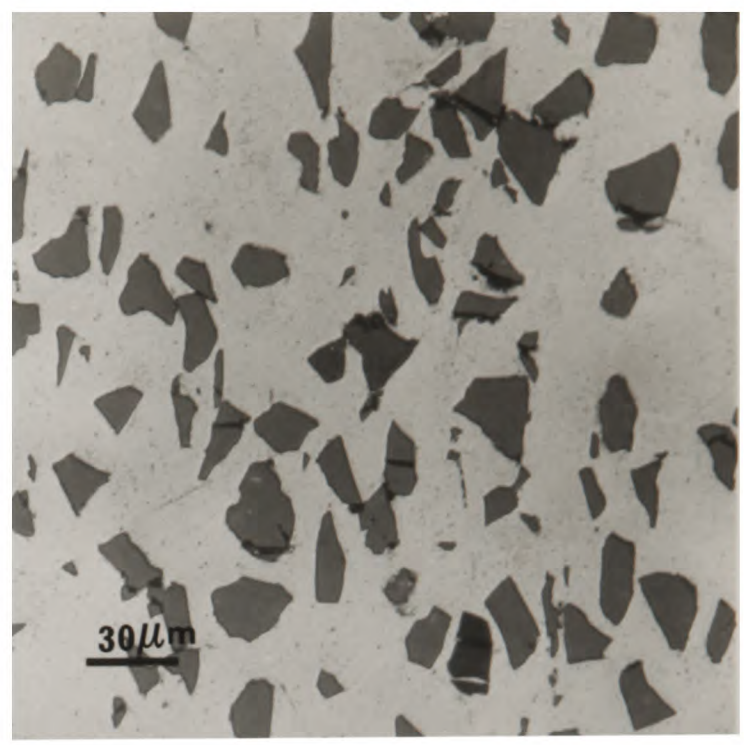

Figures 4.19 a+b: Sections through tensile specimen of 20/30/Qu/1070 at (a) the fracture surface and at (b) a strain of 4%.

(a)

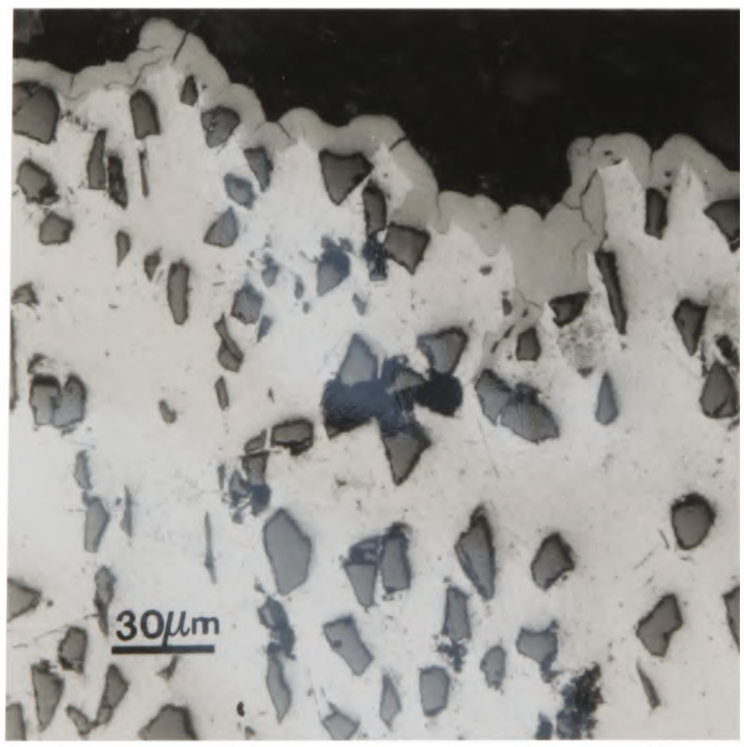

(b)

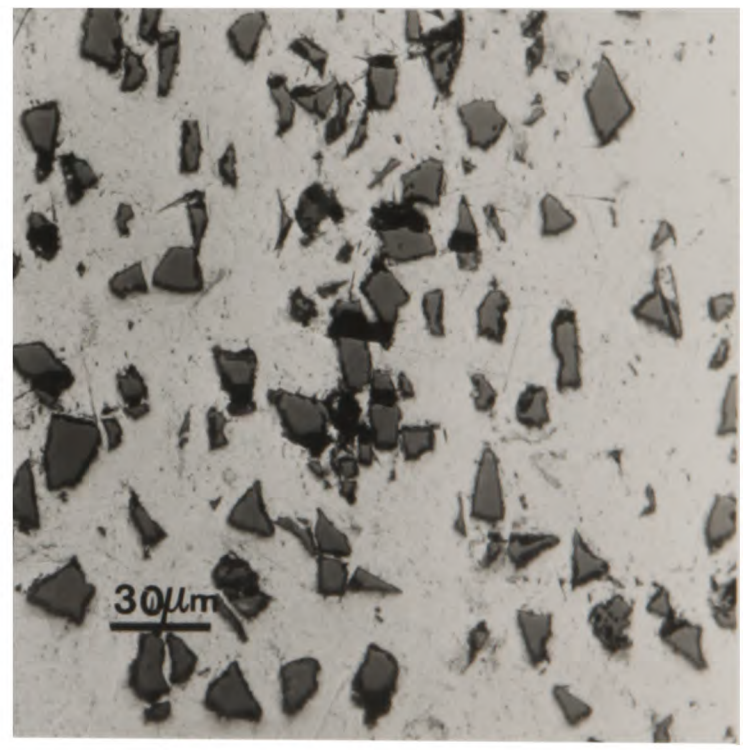

Figures 4.22 a+b: Sections through tensile specimen of 20/30/Qu/5050 at (a) the fracture surface and at (b) a strain of 1%.

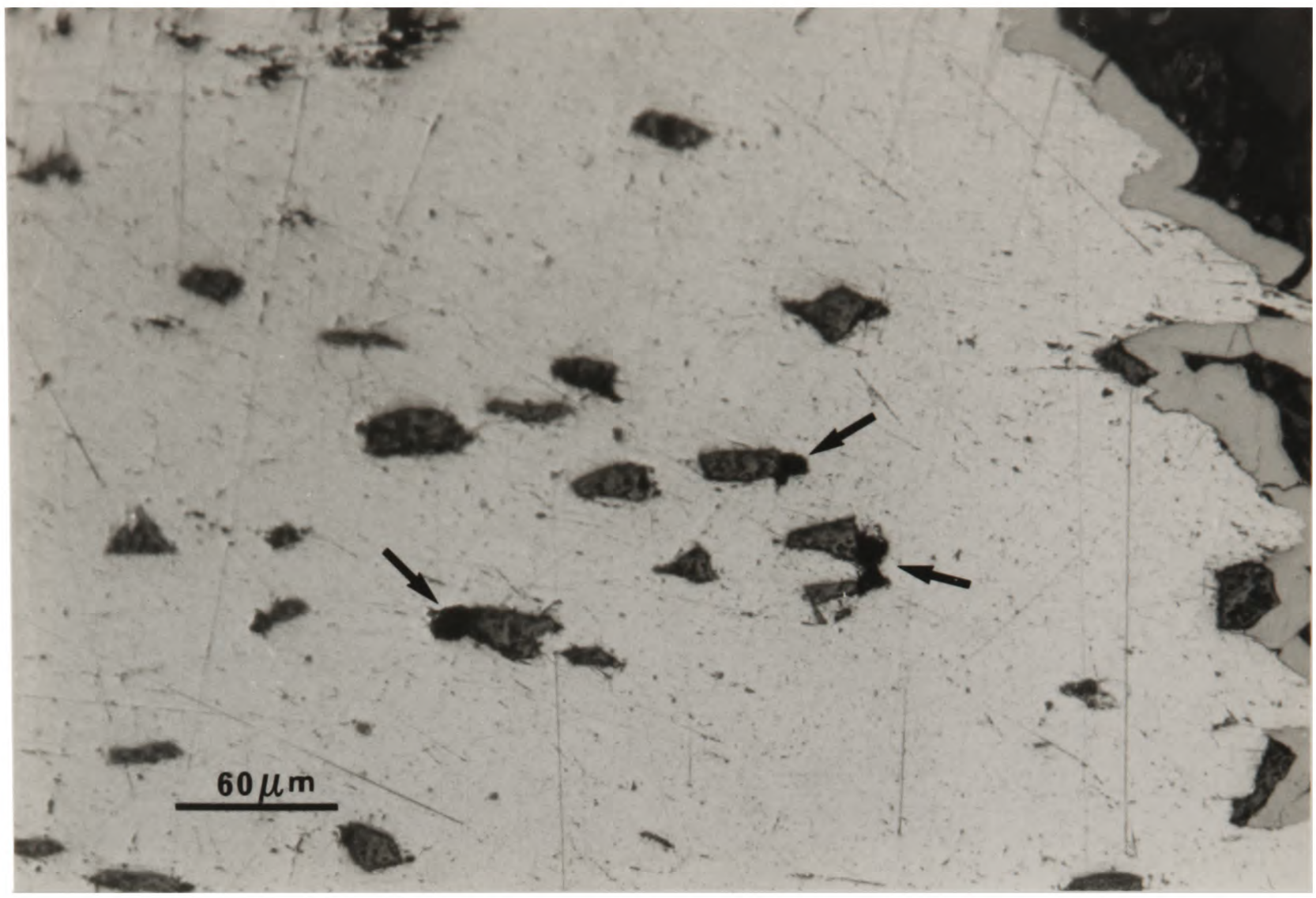

Figure 4.23a: Voids nucleated by decohesion at particle ends in 5/30/Qu/5050 material.

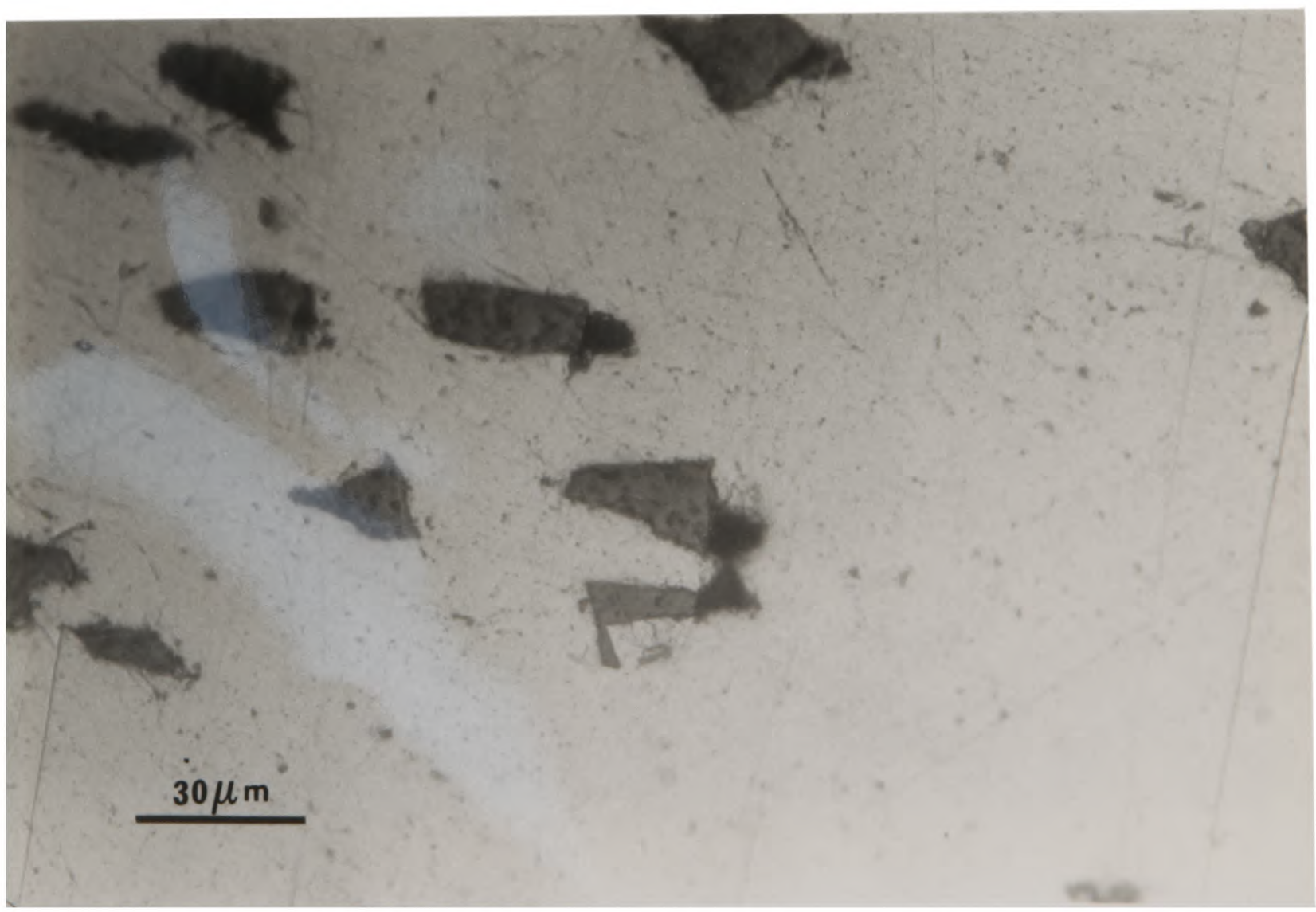

Figure 4.23b: Void coalescence in the same material.

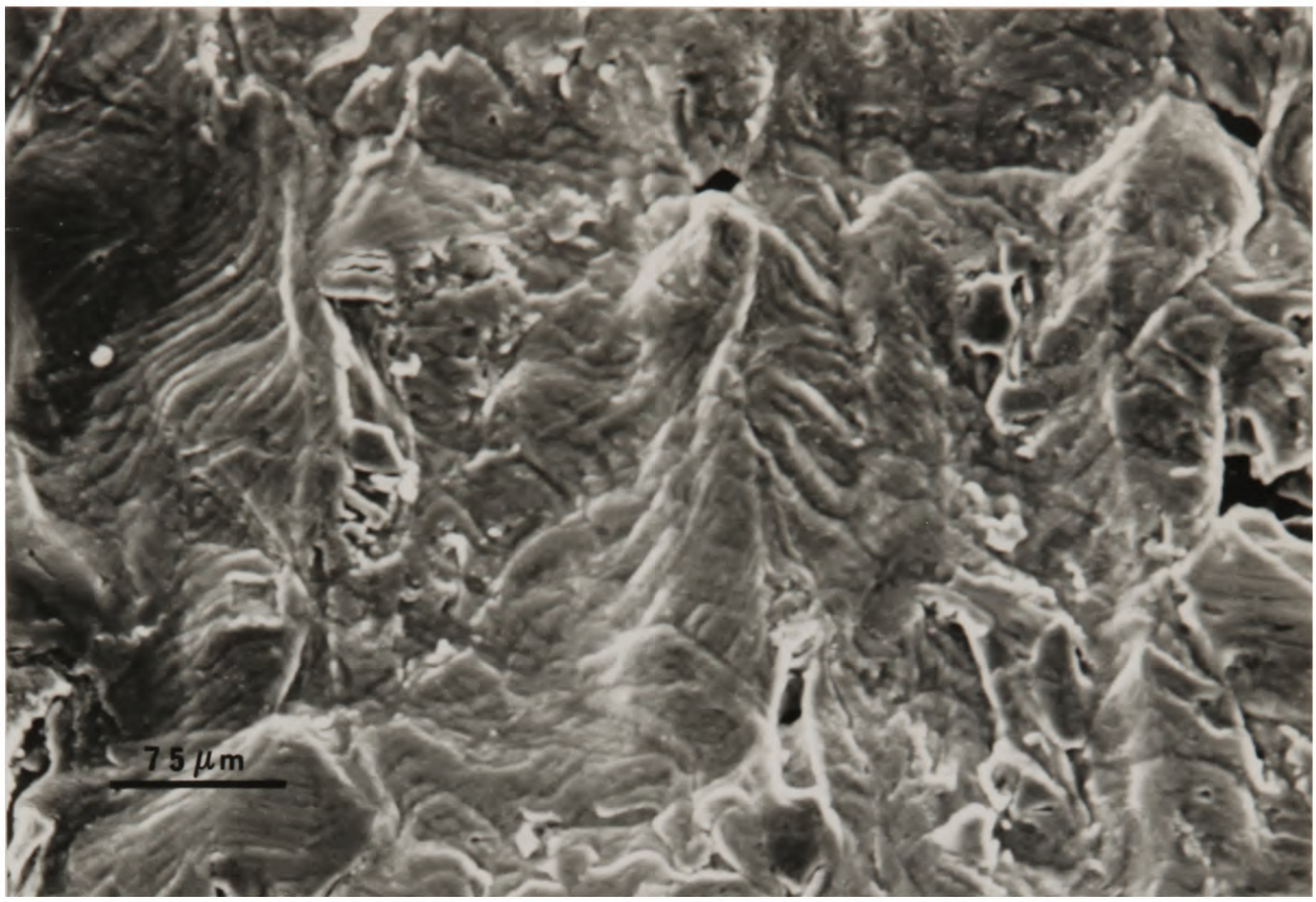

Figure 4.24a: Gauge length of 5/30/An/1070 showing extensive surface deformation.

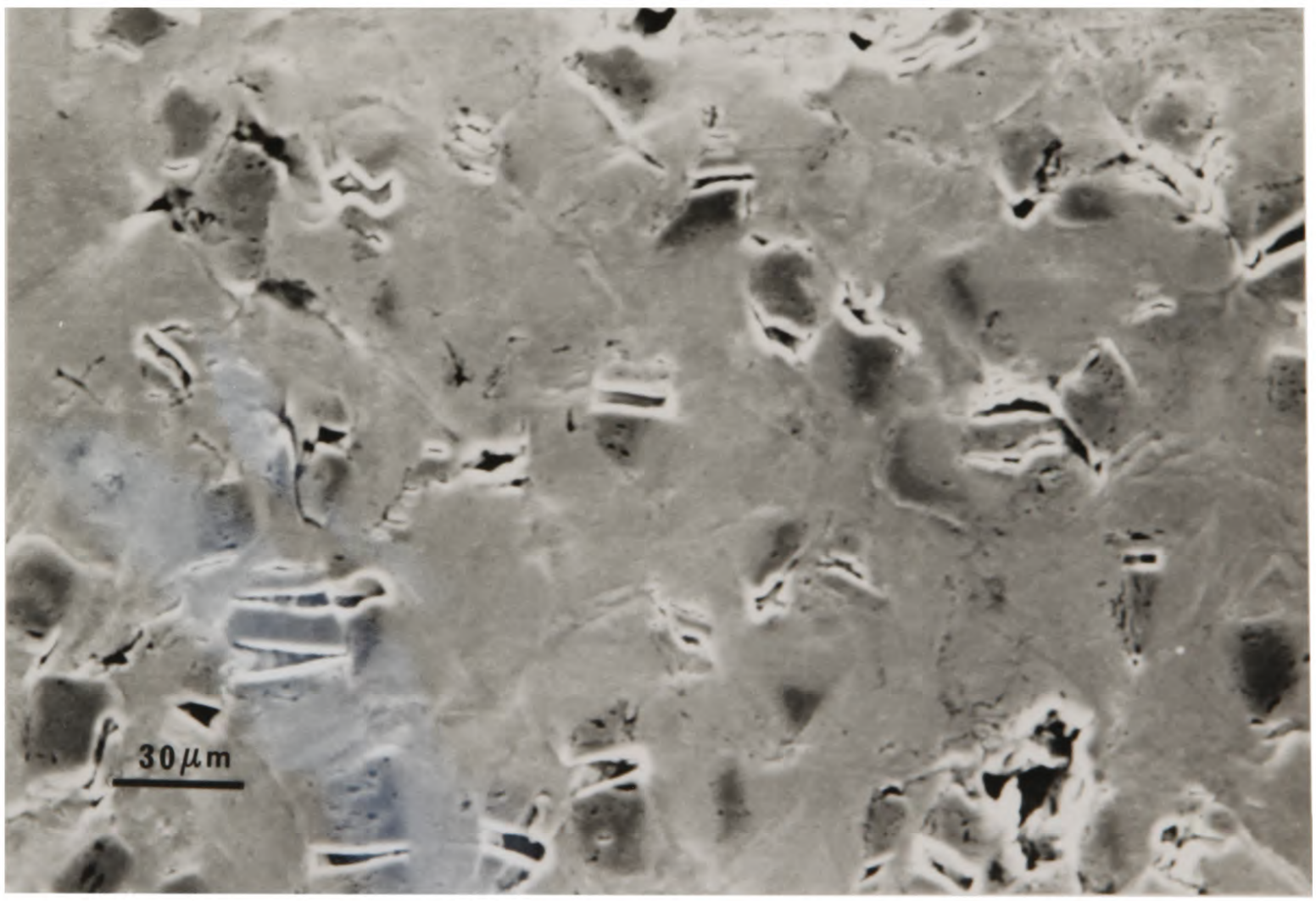

Figure 4.24b: Gauge length of 20/30/An/1070 showing fractured particles far from the fracture surface.

Al-1070		Volume Fraction (%)		
		5	10	20
Particle	3	Decohesion	Decohesion	Decohesion
Size	10	Fracture	Fracture	Fracture
(μm)	30	Fracture	Fracture	Fracture

Al-5050		Volume Fraction (%)		
		5	10	20
Particle	3	Decohesion	Decohesion	Decohesion
Size	10	Decohesion	Fracture	Fracture
(μm)	30	Decohesion	Fracture	Fracture

Table 4.1: Summary of Fractographic Results

Chapter 5: Dynamic Fracture Studies

5.1 Introduction

Although fractography can identify the basic micromechanisms of fracture, it cannot identify the order in which the events occur. Additional dynamic studies must be undertaken to provide a more complete picture of the fracture process. The term "dynamic" is taken here to mean "in real time" and not to imply fracture studies at high strain rates as it has been used elsewhere. The aim of this chapter is to investigate by direct observation *in situ* the predictions that can be made from the post fracture experiments. These are that nucleation can occur at very low plastic strains; that void coalescence is severely restricted by the presence of the silicon carbide, leading to greater strain to failure than predicted by simple void growth models [139]; and to provide further evidence of the crack propagation sequence. Additional insights into all the stages of fracture may also be obtained.

It is proposed to do this by two methods; *in situ* SEM fracture studies and monitoring of acoustic emission during tensile straining.

5.2 *In situ* SEM Fracture Studies

Studying a crack as it grows can give many insights into the fracture mechanisms of materials and has been recognised as a valuable aid to understanding such processes. In view of this, surprisingly few *in situ* fracture studies on PRMMCs have been reported by other workers [76,130-132]. All of these studies have concentrated on the crack propagation stage and cover a range of both high- and low-strength aluminium alloy matrices reinforced with silicon carbide and alumina particles. The results from all of these systems were consistent, with fracture proceeding by the failure of matrix ligaments between microcracked regions ahead of the crack tip and the crack tip itself. These studies also emphasise the large extent of these microcracked regions which was of the order of tens of interparticle spacings.

Wu and Arsenault loaded in tension specimens of differing SiC particle sizes in an Al-1050 matrix [132] . These had been pre-cracked in fatigue prior to straining and, therefore, no information on the evolution of damage prior to nucleation or the nucleation stage itself could be obtained. Using the results of this study in isolation, they postulated that fracture occurred by the failure of matrix ligaments between particles which were already cracked during fabrication. There was no evidence of particle cracking or decohesion during crack extension and so, they reasoned, it never happened, contrary to substantial fractographic evidence from other studies e.g. [71,73,79,83,87].

Manoharan and Lewandowski [76] did not study the early stages of deformation either. Specimens of alumina particles in Al-6061 were loaded in tension and the load/displacement characteristic determined. After the initiation of a crack, the crack tip region was monitored. The crack was now in an unstable configuration, limiting the range of observations available.

The researchers at the Université Paris-Nord have published two papers covering a wide range of silicon carbide reinforced aluminium alloy matrices [130,131]. The experiments performed were truly dynamic in that they were continuous with the real time image quality improved by image processing techniques. This does, however, run the risk of missing certain events. The first paper is in a similar vein to those described above, having no information on the early stages of the fracture process. The second paper considers this problem. The crack was, however, still studied in an unstable configuration.

Other observations of a growing crack have been made on fatigue cracks [205-207] and by *in situ* TEM [78]. The work of Shang and Ritchie on fatigue crack growth has produced similar results to the *in situ* SEM studies. Here cracked particles are seen ahead of the advancing crack tip. They model the toughness of PRMMCs by considering the local reduction in crack driving force at the crack tip by these bridging ligaments. *In situ* TEM necessarily examines very thin specimens and this behaviour may not be representative of the bulk composite.

The experiments described in this thesis were designed to allow all three stages of the ductile rupture process, the nucleation, growth and coalesence of voids, to be studied. In addition, the microstructural damage prior to nucleation and the subsequent growth of the crack in a stable configuration could also be investigated. To do this, the specimens were loaded in a constant displacement, double cantilever (CDDC) arrangement described earlier in Chapter 4 and in more detail in Lawn and Wilshaw [208]. This is a standard configuration for measuring the toughness of ceramics and it was hoped that the toughness of the PRMMCs could be measured similarly by noting the crack tip advance for a given wedge increment.

5.2.1 Experimental

The experiments were undertaken in a JEOL 35-X SEM which has a commercial manually operated straining stage as shown in Figure 5.1. The stage was modified to perform the CDDC tests and a close up of the wedge and specimen arrangement is shown in Figure 5.2. The wedge is on the end of a long, hand driven thread which allows the displacement of the wedge to be measured to 2μm. Specimens were made to

the geometry shown in Figures 5.3a-b. Slices parallel to the longitudinal direction were taken from the extruded bar by spark erosion. The central reduced section and notch were also spark eroded, which ensured that no mechanical damage was introduced at the notch root. The specimens were polished as for optical microscopy and heat treated to the same two conditions described earlier for the tensile tests. This geometry, though not perfect, was found to give reproducible results. There was sufficient overall area to give firm support at the butt end without a large cross sectional area in the region of the notch which may cause the stage to be overloaded and the thread to be stripped. The geometry did, however, cause limited out-of-plane shearing at the crack tip due to the reduced stiffness in the central region.

The specimens were held lightly in place by the wedge, and the displacement at zero strain recorded. The wedge was advanced incrementally, the displacement noted and the specimen examined. Due to the nature of the crack growth, only qualitative measures of the toughness could be obtained by this method. The test was, therefore, not strictly dynamic, but a series of "snap shots" of a dynamic test.

5.2.2 Results and Discussion

In common with the sections through cracks discussed in Chapter 4, some features of the *in situ* tests are common and generic to the fracture processes and others show the effects of the microstructural parameters on the mode of failure. One representative *in situ* study of the 20/10/Qu/1070 composite will be reproduced in detail to show these generic features and, where appropriate, micrographs from other composite systems will be given which show them more clearly or highlight differences.

An advantage of this technique over some others is that the accumulation of microstructural damage prior to fracture nucleation can be studied. On straining, the surface of the specimen, which was initially planar, became rippled, lifting the silicon carbide proud of the surface. As seen in Figures 5.4a-b, this extensive deformation occurred along well-defined directions, which were persistent. The particles localise and intensify the applied strain. Under the approximately plane stress conditions studied here, the particles can relieve this strain by displacement out of the plane of the surface. This was seen most clearly in the studies on the composites with 5% volume fraction of reinforcing phase. Figure 5.5 shows the pronounced matrix deformation. In Figures 5.6a-b, the effect of the particles on this flow pattern is clearly seen. Evidence for the onset of failure by shearing at the interface, contrary to the fractographic results for this system, and particle fracture may also be seen. Of additional interest in Figure 5.6a are the voids which have nucleated about splinters of silicon carbide. First note that voids have nucleated around the smaller particles before the larger ones, which indicates that they are more efficient at localising strain, and, secondly, that the voids have grown

laterally. Later figures will show that void growth from fractured particles is highly constrained.

As the strain was increased, nucleation events were seen before the formation of a macroscopic crack. Figures 5.7a-c show the representative study at zero strain and two subsequent strains. The onset of particle cracking was more easily seen in the composites containing 30μm particles as shown in Figures 5.8a-b. Thus, void nucleation by particle cracking can be seen to occur before matrix failure, contrary to the model of You *et al.* [71], confirming the proposal made in Chapter 4. Similarly, the wedge was advanced further before nucleation in the 10μm particles than in the 30μm particles, implying an increase in stress to nucleation, in accordance with a critical stress criterion for brittle failure of the ceramic particles. For composite systems where fractography has shown the fracture mode to be by interfacial decohesion, there was little sign of particle cracking. In the composites containing 3μm particles, there was some evidence of matrix failure before the onset of macrocracking as can be seen in Figure 5.9, although this was not as common as the particle cracking in other systems.

Figures 5.7a-c also show the effect of increased straining. The voids in the cracked particles have grown while the stress levels in new particles reach the fracture nucleation condition. This process of increasing the damage zone around the notch root continued until a macroscopic crack was formed, as can be seen in the standard test in Figure 5.10. Note also the large damage region. These cracks were discontinuous on the surface and, in general, followed one of the directions of intense matrix deformation described earlier. The discontinuous nature of the crack is perhaps better seen in Figures 5.11a-b of the 20/3/An/1070 material. As other *in situ* studies have reported [76,130-132], crack propagation was by failure of matrix ligaments between microcracked regions, containing either fractured particles or failed matrix, ahead of the crack tip and the main crack (Figures 5.12a-f). As the joining matrix failed, additional microcracked regions opened up ahead of the "new" crack tip. This is shown more clearly in Figures 5.13a-f and 5.14a-e. As in the analogous fracture of iron carbides during cleavage fracture in steels [209], the particle cracking may be considered to be stress controlled and, therefore, triggered at sites ahead of the crack tip where the tensile stresses are highest due to crack-tip blunting of the crack tip. Here, the maximum tensile stresses peak at some two crack-tip opening displacements directly ahead of the crack tip. This is based upon the asymptotic crack-tip solutions for a power-hardening solid by Hutchinson [210] and Rice and Rosengren [211] which were modified by the blunting solutions of Rice and Johnson [199] and McMeeking [212]. Quantitative toughness data could not be obtained because of this disjointed propagation mechanism which made the crack extension impossible to measure. This self-similar propagation was seen in the sections through the cracks described in Chapter 4. It should be noted that the extent of damage ahead of the crack tip in the *in*

situ tests was greater than that in the crack sections.

Figures 5.12a-f also show a number of features of the propagation sequence. First, the random distribution of crack orientations and positions within the particles in the microcracked regions is more consistent with a dislocation pile-up model than a continuum shear loading model. Similarly, Figure 5.15 shows a matrix slip band of localised deformation causing interfacial failure in the 20/10/An/5050 material. This may be a function of particle size as tests on composites containing 30μm particles showed the cracks in the particles aligned with the macrocrack, as shown in Figures 5.16a-b. Indeed, in the study of the 20/30/An/1070 material, not only were the cracks within the particles aligned with the main crack, but another feature can be seen. On the opposite side of the notch to the crack, in a kind of mirror locus, were cracked particles, as shown in Figure 5.17a-b. These correspond to the expected directions of maximum shear in the matrix, and, hence greatest matrix flow. This supports the hypothesis that the large particles are loaded by shear forces at the particle/matrix interface due to matrix flow.

Secondly, the propagating crack rarely passed through a silicon carbide particle even when the particle was already fractured, preferring instead to pass the particle away from the interface. The microcracked particles remain in the wake of the main crack. This is shown in the 20/10/Qu/1070 material in Figures 5.18a-b and for other systems in Figures 5.19a-d. For the 20/3/An/1070 composite, the entire crack appeared to be through the matrix. This same result on a similar composite was obtained by Wu and Arsenault [132], and was taken in isolation to show that the fracture path did not pass through any particles uncracked after fabrication or through the interface of any particle. Thus, while the stress field associated with the crack can cause nucleation, the crack itself was not attracted to these regions of apparently easy growth. This is possibly due to the plane stress conditions on the free surface. The plastic zone associated with the crack in plane stress is larger than that in plane strain, which may lead to observations on the surface that are unrepresentative of the specimen in tension. Similar results were obtained by Shang and Ritchie [205-207]. As they increased ΔK in their fatigue tests, and so increased the size of the plastic zone associated with the crack tip, they found more fractured particles ahead of the crack tip and increased crack bridging and branching. Indeed, they postulate a threshold δK below which crack bridging would not be observed. This was attributed to an increased statistical sampling volume. This, in conjunction with other discrepancies over the extent of deformation described earlier, must strike a note of caution in interpreting too much from the *in situ* studies alone. They should only be used where there is corroborative support from plane strain experiments which are more representative of the material in tension.

The crack tip stress field was also unable to cause local rupture of the matrix in

these regions, implying that ductile matrix fracture is governed by a critical strain criterion. The rigidly-bonded interfaces impose plastic constraint on the matrix which then passes the stress directly to the ceramic without undergoing much strain. Away from the interface, where the constraint is reduced somewhat, the matrix can be strained and failure may occur. Thomson and Hancock [213] have shown that the greatest strain is found just outside the interface of a non-deforming sphere in an elastic-plastic matrix, supporting this supposition.

Finally, the voids associated with cracked particles were constrained. Figures 5.20a-c show the void growth restricted to the width of the particle with no lateral growth even after extensive straining. This form of growth will continue until the constraint between neighbouring voids is overcome. For a free void, this occurs when the height of the void is approximately equal to the intervoid spacing. Voids from decohered particles may be considered free as they are not bonded to any non-deforming interfaces. They are also as high as the particles on nucleation, thereby reducing any growth strain. For fractured particles, however, this is not true. These voids are further constrained by the well bonded interfaces. Additionally, in the case of the uniaxial tensile test, they are "short", as here the voids tend to form across the width of the particle in the plane perpendicular to the tensile axis. Hence, greater growth strain is required to overcome the constraint. This is contrary to the model of Evensen and Verk [204] for void growth and the results of Da Silva *et al.* [130,131] for their *in situ* experiments. Both of these studies state that the crack in the particle acts to concentrate stress in the matrix, thereby enhancing void growth and reducing strain to failure.

The extended void growth strain, due to the difficulty of void coalescence, reduces the significance of the nucleation process particularly in the composites of low-strength alloy matrices considered in this study. In these alloys, stress concentrations at any crack tip are easily relieved by the generation and motion of dislocations. This is apparent in low magnification micrographs of the crack propagation on wedge increment which often show significant opening of the crack at the root of the notch without much advancement of the crack tip. Occasionally, however, there is major crack advance for a small increment of the wedge. In composites of dispersion-strengthened alloys, this dislocation motion is impeded by interactions with the matrix precipitates. This reduces the capacity to relieve the stresses at the crack tip. The crack tip advance was, in general, far greater in the composites of the Al-5050 matrix than in those of Al-1070 for the same wedge increment, showing a reduced toughness due to this inability to relieve stresses. Additionally, voids may be nucleated at the second phase particles, lowering the local plastic constraint and reducing the void growth strain. This would increase the importance of the nucleation process in these materials.

5.3 Acoustic Emission

This section comprises a brief introduction to the theory and practice of acoustic emission (AE). More detailed information can be found in a number of review papers [214-218]. The important parameters governing the surface displacement as the result of a buried acoustic source will be discussed. These will be shown to be the incremental defect size and the rate of change of this defect size. A technique will be introduced which can determine the magnitude of the source corresponding to a given surface displacement. This is based on a calibration using thermally-generated elastic waves in a laser-irradiated metal.

AE is the term used to describe the spontaneous release of transient elastic waves within solids caused by sudden, localised changes in stress. Deformation and fracture processes in materials are accompanied by such changes, and thus radiate elastic waves to the external surfaces of the body. These may be used to indicate and study this defect nucleation and growth within a material if they are of sufficient amplitude to be detected by transducers attached to the surfaces of a sample. The measured displacement is governed by the geometry of the specimen, because of reflections at boundaries and surfaces, as well as by the strength and type of the acoustic source.

Consider a body which is subjected to a constant or slowly increasing external load, as in Figure 5.21a. There will be within the body an equilibrium stress distribution. If a small "penny-shaped" crack of area A suddenly appears at the centre of the body as in Figure 5.21b, the tensile stress can no longer be transmitted across the crack, so the material along each crack face is not in equilibrium and can, therefore, be considered to be subject to a net resultant force perpendicular to the crack plane. This is equivalent to a pair of equal and opposite forces, one on each crack face, whose magnitude is given by $F=\sigma_o A$. These forces cause the crack faces to move until equilibrium is attained. There must be a new equilibrium distribution of stress and strain within the body, as in Figure 5.21c. For instance, the stress in the remaining material (in the plane of the crack) must have increased due to the reduction in area. This local increase is proportional to the area, A, to the first order. The stress and strain are redistributed by elastic waves which propagate away from the crack source at the speed of sound.

This simple example highlights many of the features of acoustic emission. First, the source of emissions is internal to the sample, originating in the defect itself. Thus, there is no mechanism by which the elastic wave field can be intensified externally to improve sensitivity and avoid missing weak events. The technique is, therefore, limited by the fact that high-sensitivity transducers must be used in low ambient acoustic and electrical noise environments to achieve good results.

Secondly, acoustic emissions are, in general, generated only when a material is being loaded. It is an irreversible process as defect growth is itself irreversible. AE only monitors defects if they grow or change the stress field in some way and even then only the change in size of the defect is found. The emissions are in real time and can be used directly to monitor the macroscopic strain states at failure events.

In this example it is assumed that the defect appeared instantaneously. The AE source function for this will thus take the form of a step or Heaviside function, $H(t\text{-}t_o)$. Since there is no net force, this can be represented as a dipole of the form,

$$D_{ij}(t) = D_{ij}H(t).$$

In practice, however, the time-dependence of the source function will vary according to local material and microstructural properties. Suppose that this defect growth can be represented by some time function f(t). Then, assuming all the dipole moments have the same time dependence,

$$D_{ij}(t) = D_{ij}f(t)$$

This can also be written in the form of a time convolution

$$D_{ij}(t) = D_{ij}H(t)*\frac{df(t)}{dt} = D_{ij}H(t)*f'(t)$$

This enables different source time histories to be modelled by a convolution of a basic source representation with a time function, f'(t). The dependence on the derivative of the time function arises because the Heaviside function acts as an integrator on convolution.

From this simple analysis it can be seen that the source strength is a function of the **rate of change** of incremental defect size and not of absolute defect size. This leads to widely differing sensitivities to defects undergoing the same incremental advance but over different time scales. AE can be very sensitive to minute incremental crack lengths in brittle materials with high crack velocities, and insensitive to larger crack advances in very ductile materials with low crack velocities.

This is perhaps more clearly explained in terms of the physics of the detection process. Transducers are sensitive to the direct compression (P) wave arrival, which theoretically takes the form of a delta function [214]. The strength of the delta function pulse, S, is defined by its area, and it is the area under the pulse, not its height, which is proportional to the strength of the source, i.e. to the volume δV of the crack

increment. The width of the pulse is controlled by the lifetime of the source, so that, with constant area, the pulse height is inversely proportional to the source lifetime. The height of the compression wave, u, in an unbounded medium is given by $\frac{dS}{dt}$, which can be shown to be

$$u = \frac{1}{2\,\pi\,c\,r}\,\frac{dV}{dt}$$

for a microcrack source at depth r vertically below the transducer growing at a rate $\frac{dV}{dt}$ where c is the compression wave velocity [219].

Figures 5.22a-b show how this controls the detectability of AE sources. Here, two microcrack events of the same size, δV, but different lifetimes produce signals of different height. The short lifetime event generates a signal that is well above the background noise and is, therefore, detectable, while the slower does not. The acoustic source causing the surface displacement can be characterised by two parameters, namely the incremental volume change, δV, and the rate of change of this volume, $f'(t)$.

The technique is, therefore, well suited to the study of fracture processes in materials containing brittle second phases, such as PRMMCs, as its sensitivity is maximised. In addition, the information comes from within the body of the specimen, eliminating any potential confusion associated with the plane stress condition on a free surface in an *in situ* study, in real time, so that the macroscopic strain for each event may be known. The use of acoustic emission will provide direct, dynamic information on the fracture processes occurring within the bulk of the material including the relative speeds of decohesion and particle cracking events and the values of far-field strain at nucleation.

5.3.1 Fracture Experiments

Specimens were fabricated by turning and centreless grinding to the geometry in Figure 5.23, and a surface finish of 3μm was achieved. Grinding was performed to ensure reproducibility of specimen dimensions, since the number of acoustic emissions will be proportional to the volume sampled. After fabrication, the specimens were heat treated to the same conditions described earlier for the tensile tests. Tensile tests to failure were performed at a strain rate of 6.7 x 10^{-4} s^{-1} on an Instron 1195, while monitoring the acoustic emissions.

The experimental scheme is shown in Figure 5.24. This arrangement allows both analogue and digital emission data to be recorded simultaneously with the load and displacement. For more detail on the setting up and execution of AE experiments, see any of a number of papers [220-222].

A Meccasonics 2.5MHz damped broadband piezoelectric transducer was held onto the end of the specimen by a spring within a specially designed tensile grip as shown in Figure 5.25. High vacuum grease was used as a coupling agent between the transducer and specimen. The transducer can detect surface displacements $> 3x10^{-14}$m and is designed to have a flat response below its natural frequency. The split grip is designed to give the specimen electrical and acoustic isolation from the Instron, while the grip itself is earthed to the Instron. The BBC microcomputer is triggered to record the digital data and then reset via a handshake link with the A/D converter. The digital data consists of a bin number in the range 0-255, which is proportional to the surface displacement, and the time at which the event occurred. The triggering threshold can be set independently to the ambient noise level of the experimental rig. The initial 30kHz high pass filter is to remove any acoustic background such as noise in the building or the rumbling of the Instron motor which are low frequency. The emissions of interest are transient and, therefore, of high frequency.

5.3.2 Results and Discussion

The results provide information on the micromechanisms of fracture in PRMMCs and on the acoustics of two-phase systems. The essential experimental results are presented in Tables 5.1a-b.

No acoustic emissions were detected from the unreinforced matrix alloys or the composites containing 3μm particles. The emissions from the 3μm particles were on the detection limits of the transducer used in the experiment. A criterion for the smallest volume increment that can be detected has been developed [214]. This is based upon the sensitivity of the transducer and the velocity of the crack advance, and is expressed as a minimum acoustic power that must be released by the event. For a crack growing in silicon carbide, but embedded in aluminium, measured in the experimental arrangement described above, with the transducer about 35mm from the centre of the gauge length, the criterion can be expressed as

$$\sigma \mathrm{A} \mathrm{v} = 25\mathrm{W}$$

where σ is the stress at the event, A is the area of the event and v the velocity of the event. On sustituting sensible values for σ and v, taken as the speed of sound in silicon carbide, one finds that events from a 4μm diameter particle should be detected. Thus, the emission from the 3μm particles was below the detection limit in the experimental arrangement used. However, if the transducer could be placed nearer to the source, that is, have a specimen with shorter gauge length, then the detection threshold could be reduced.

Figures 5.26a-b show two schematic reproductions of experimental runs, one containing 30μm particles and the other 10μm particles. The most important feature of both figures is the onset of AE just after yield which then continues throughout the entire plastic region. This confirms the results reported earlier under plane stress conditions which indicated that void nucleation occurs early in the straining process and continues until final macroscopic failure. This also supports the supposition that void nucleation is highly sensitive to local values of reinforcement size and volume fraction. If the composite consisted of a periodic array of uniformly sized particles without a distribution of flaw sizes, one might postulate that nucleation would occur globally at a fixed far-field strain. The reduction in modulus as a function of strain, given in Chapter 3, can now be associated with fracture nucleation events which reduce the effective load-bearing capacity of the reinforcing phase. The second feature of note is that the average event size is greater in the composites of 30μm particles than in the composites containing 10μm particles.

Tables 5.1a-b show the results of statistical analysis of the quantitative data recorded on the BBC microcomputer. This supports the qualitative result from the chart recorder that the mean event size increases with particle size. The mean event size for a given particle size is independent of matrix alloy but appears to be affected by the heat treatment, with increased amplitude on annealing. The mean event size is, in general, larger for the composites of 5% volume fraction than for the composites of higher volume fraction. In addition, the mean event size was monitored as a function of strain. Figure 5.27 presents graphically the salient results. Note the dramatic increase in mean event size with strain for the 5% volume fraction, 30μm particle system. This effect decreases with increasing volume fraction for composites with 30μm particles and is not present in the composites containing 10μm particles. It is, therefore, reduced as the rate of work-hardening is increased. One possibility is that the internal stress and strain fields interact with the propagating wave, reducing its amplitude. This could also account for the increased mean event size observed in the annealed composites. It cannot in isolation, however, explain the experimental results. First, the effect is likely to be small below 1MHz. Secondly, it would not imply increased amplitude on straining, but rather a slower rate of decrease as work-hardening still takes place but at a reduced rate. Thus, other factors must be taken into consideration. As the strain is increased there is increased strain energy in a particle. The strongest particles will, therefore, fail at higher strains and release greater energy. This would imply a similar increase in event size with strain for all particle sizes and volume fractions. However, it may be reasoned that only the composites of the larger particle sizes contain a genuine flaw size distribution and an associated strength variation. The increased volume fraction may lead to areas of poor spatial distribution, increasing the local stress at low strains, resulting in premature failure of the stronger particles. On straining, the transfer of

energy from the particle to the matrix may also become more efficient as the tension in the interfacial bond changes. The local matrix stress is increased on straining. In addition, the lower volume fraction composites undergo significant local deformation which may increase the local stress, leading to larger acoustic events.

The larger event size associated with decohesion, seen in the 5/30/5050 and 5/10/5050 composites, may be a consequence of the reasons given above or may be the result of an increased equivalent δV for the decohesion process. Here the volume of the source may be considered to be generated from the entire surface area of the particles rather than from the projection of the cross sectional area in the direction of stress which is the case for a microcrack source. Alternatively, resonance effects due to the propagation of the elastic relaxation wave around the interface may cause an amplification. Microcrack advance of crack tips has also been observed to produce this effect, where the entire macrocrack relaxes at the same time, substantially increasing the effective source volume [214].

5.3.3 Laser Calibration

In order to quantify the experimental data, so that incremental defect size may be determined, the response of the system to a standard acoustic source must be measured. It is important that this calibration be made in the same mode in which the transducer was used, in approximately the same experimental configuration and with a source which is a good representation of the actual acoustic event. Several methods for acoustic calibration have been attempted, including a helium gas jet [223], the fracture of pencil leads [224] or glass capillaries [225]. These three methods are easy to use, but have several disadvantages [226]. A pulsed laser source has been shown to meet the requirements outlined above [226-228] and was used in the present study. When used at low energy densities, the pulsed laser produces a thermoelastic source which can, to a first approximation, be modelled as a point thermal expansion. Here the laser radiation is absorbed quickly, setting up temperature gradients within the material. These in turn produce a rapidly changing strain field which radiates energy as elastic waves. Thus, the laser acts as a dipole source generating waves of ultrasonic frequency. A representation of the thermoelastic source will now be given and a relationship between the thermoelastic and microcrack source derived. A more complete treatment can be found in Scruby *et al.* [226].

5.3.3.1 Representation of the Source

Suppose that the material absorbs energy δE, from an incident energy E, instantly and uniformly throughout a volume, V, of metal at the surface given by

$$V_{th} = \pi \, a^2 \, \epsilon$$

where a is the radius of the beam and ϵ is the skin depth. δE is related to the incident energy by

$$\delta E = (1\text{-}R) \, T_c \, E$$

where R is the reflection coefficient at the metal surface and T_c the transmission coefficient of any array of optical filters which may be used. Thus the instantaneous temperature rise is given by

$$\delta T = \frac{\delta E}{\rho V_{th} \sigma} \, H(t)$$

where ρ is the density of the metal, σ its specific heat capacity, and H(t) the Heaviside step function.

The bulk strain is given by

$$\frac{\delta V_{th}}{V_{th}} = 3 \, \alpha \, \delta T$$

where α is the coefficient of linear expansion. Therefore,

$$\delta V_{th} = \frac{3\alpha}{\rho\sigma} \, \delta E \, H(t)$$

The source dipole associated with a volume increment of this size is

$$D_{ii} = K \, \delta V_{th}$$

where K is the bulk modulus of the metal [214]. Thus, the size of this thermoelastic source is known as well as its equivalent displacement dipole.

Similar expressions may be derived for a circular microcrack source of size δV_{cr}, where the displacement dipoles are now given by

$$D_{33} = (\lambda + 2\mu)\ \delta V_{cr}$$
$$D_{11} = D_{22} = \lambda\ \delta V_{cr}$$

with λ and μ the Lamé constants for the microcracked material [214]. For a uniaxial stress state within a tensile test, only the D_{33} term contributes.

If the calibration is performed on a specimen of the test material of the same geometry under the same experimental conditions, then the surface displacements at the transducer are directly proportional to the magnitudes of the source displacement dipoles as the propagation of both sources is the same. That is

$$\frac{U_{th}}{U_{cr}} = \frac{K\ \delta V_{th}}{(\lambda + 2\mu)\ \delta V_{cr}}$$

The elastic constants refer to the materials in which the events occur. Thus, the bulk modulus, K, is of the parent material and the Lamé constants are of the microcracked material. For the case under study of the fracture of an inclusion within a parent phase, there is an additional correction term which is a measure of the efficiency of energy transfer from the inclusion to the matrix, which is unknown to the author at present. A theory has been developed for this term [229], and it has been used in a study of the fracture of boron particles in an aluminium matrix [230]. This relied on metallographic determination of the size of the cracked particles by sectioning after the test, and assumed the theory to be correct rather than testing the theory. The laser calibration so described here should provide a direct test of the theory as the equivalent "ideal" volume increment, where there is 100% transfer of the energy from inclusion to matrix, would be determined. This may be better visualised as the equivalent volume microcrack within a monolithic specimen of the same material as the inclusion.

5.3.3.2 Calibration Experiment

A Q-switched Nd:YAG laser was used which generates 1ns pulses of 13mJ energy. The beam was defocussed to provide an irradiated area of approximately 3mm diameter, avoiding surface ablation of the material, and fired onto a blackened test specimen of the 20/10/Qu/1070 composite in the experimental arrangement described earlier. The specimen was blackened to give a reflection coefficient of zero. Various neutral density optical filters of known transmission coefficients were inserted between the laser and the specimen to provide a series of incident energies which covered the experimental energy range. The average surface displacement of twenty pulses was taken and a calibration curve constructed. This curve was used to calculate the ideal

source size for a given composite system by using the corresponding average event size determined by experiment.

5.3.3.3 Results and Discussion

The mean event size for a 30μm particle, averaged over all systems, was found to have a bin-number of 33. This equates with an ideal source volume, δV_{cr}, of 110.6μm^3. The corresponding source volume of the 10μm particle is 13.8μm^3. This must now be related to the actual size of the reinforcing particle. There are at least two possible alternatives. The first assumes that cracking takes place entirely within the silicon carbide, transfering the stored energy to the matrix through the interface. This is equivalent to the self-similar advance of a crack in a monolithic material and uses the fracture stress of the silicon carbide to evaluate a crack tip opening. The second notes that the edge of the crack is in the matrix and evaluates the equivalent source volume as if it were aluminium, using the macroscopic value of stress in the matrix and not the fracture stress of the particle to evaluate a crack tip opening.

Let us assume that the crack is under mode I loading. If we make the first approximation and assume that the cracked particle can be modelled as a circular crack of radius a which will open up to have an elliptical cross section. The crack opening 2U at the centre is given by [231]

$$2U = \frac{4\,(1 - \nu)}{\pi E}\,\sigma\,a$$

Thus, the volume of the elliptical source

$$V = \frac{4}{3}\,\pi\,a^2\,U$$

$$= \frac{8\,(1 - \nu)\,\sigma\,a^3}{3\,E}$$

Taking K_{Ic}=4.5MPam$^{1/2}$, and assuming the intrinsic flaw size to be half the particle dimension, the fracture stress of a 30μm particle is 650MPa, and of a 10μm particle is 1.1GPa. This will provide a lower limit of the fracture stress. Using data for a β-silicon carbide whisker, where ν=0.17 and E=427GPa [186], one finds on substitution that the equivalent ideal source size for a nominal 30μm particle is 33μm, and for a nominal 10μm particle it is 13μm.

This agreement is far better than expected considering the approximations that have been made. The ideal source should be smaller than the real source since some energy would be lost on transfer from the cracked particle to the surrounding matrix. However, the value of fracture stress used was a lower limit which would give a larger ideal source volume for the same surface displacement. The values taken for the elastic constants of silicon carbide, which was for a single crystal, may also be inappropriate for

the particulate reinforcements. The results do show, however, the correct ratio of ideal event sizes, changing by a factor of three. They are also consistent with the non-detection of emissions from the 3μm particles as the laser energy corresponding to the emissions from 10μm particles was just above the ambient noise level.

5.4 Summary

The dynamic tests have provided important additional information on the fracture processes in PRMMCs. The *in situ* SEM crack propagation studies compliment the sections through stable cracks reported in Chapter 4. They allowed the accumulation of damage before void nucleation to be studied as well as the crack growth and coalescence processes. The acoustic emission studies enabled real-time investigation of the fracture processes in plane strain conditions to be performed. This confirmed results previously found in plane stress conditions. The results may be summarised as:

a) The monitoring of acoustic emission during a tensile test showed that void nucleation occurs at low levels of plastic strain and continues throughout the plastic region until total failure. This supports a critical stress criterion for nucleation dependent upon the local values of reinforcement size and volume fraction and far-field strain.

b) *In situ* fracture studies revealed substantial void nucleation before the appearance of a macrocrack.

c) Crack advance is by the failure of matrix ligaments between microcracked regions ahead of the crack tip with simultaneous nucleation of other microcracked regions.

d) Void coalescence is constrained by rigidly bonded interfaces leading to extra void growth.

e) A qualitative measurement of toughness showed the Al-5050 matrix composites to be less tough than the Al-1070 matrix composites.

f) The plane stress condition observed during *in situ* experiments may provide misleading results. These include crack branching, where the extended plastic zone may cause failure locally in regions away from the main crack path, and the avoidance of particles by the crack.

g) The acoustic emission laser calibration technique can be used to find an equivalent source size for a second-phase particle cracking within a parent phase.

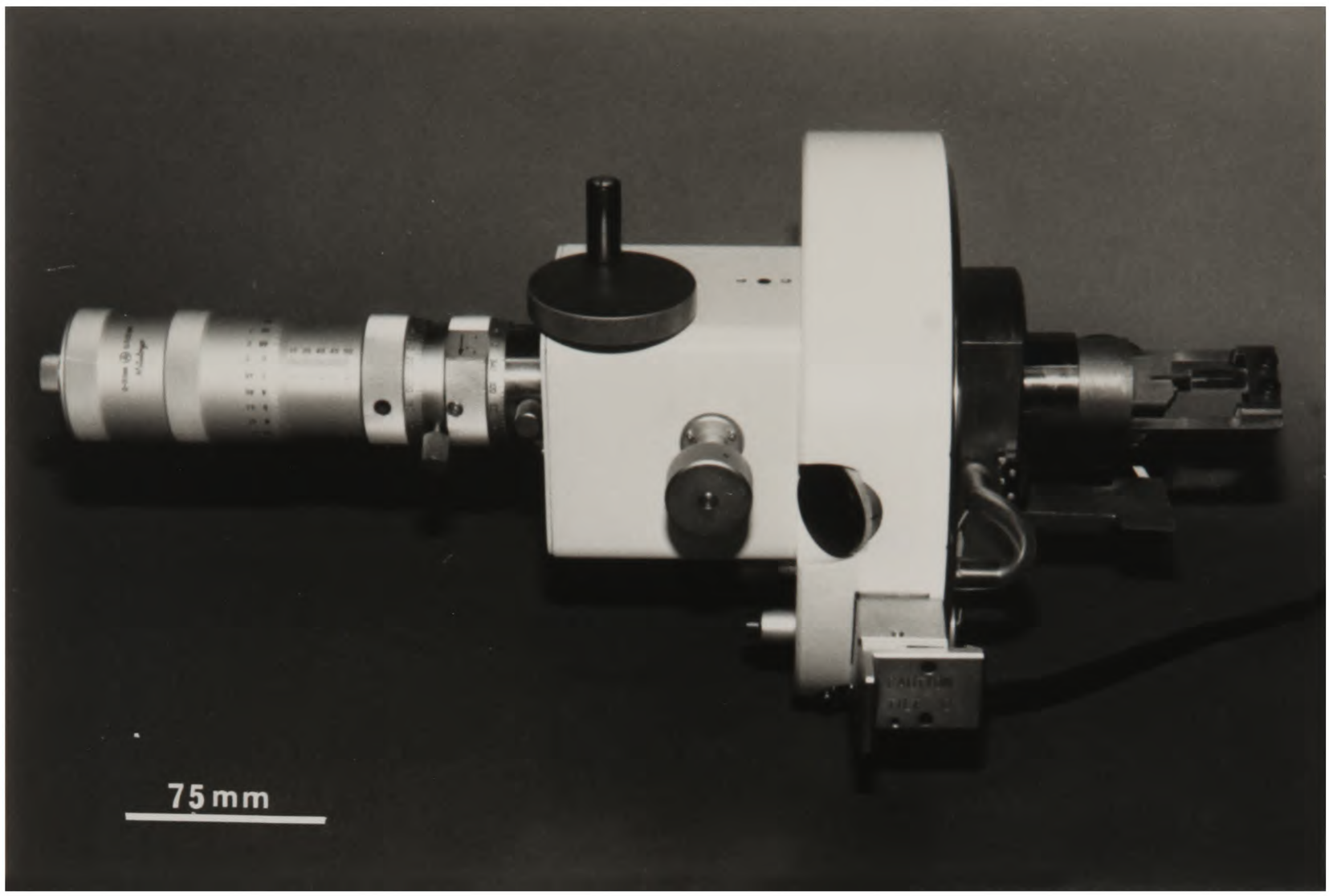

Figure 5.1: SEM straining stage.

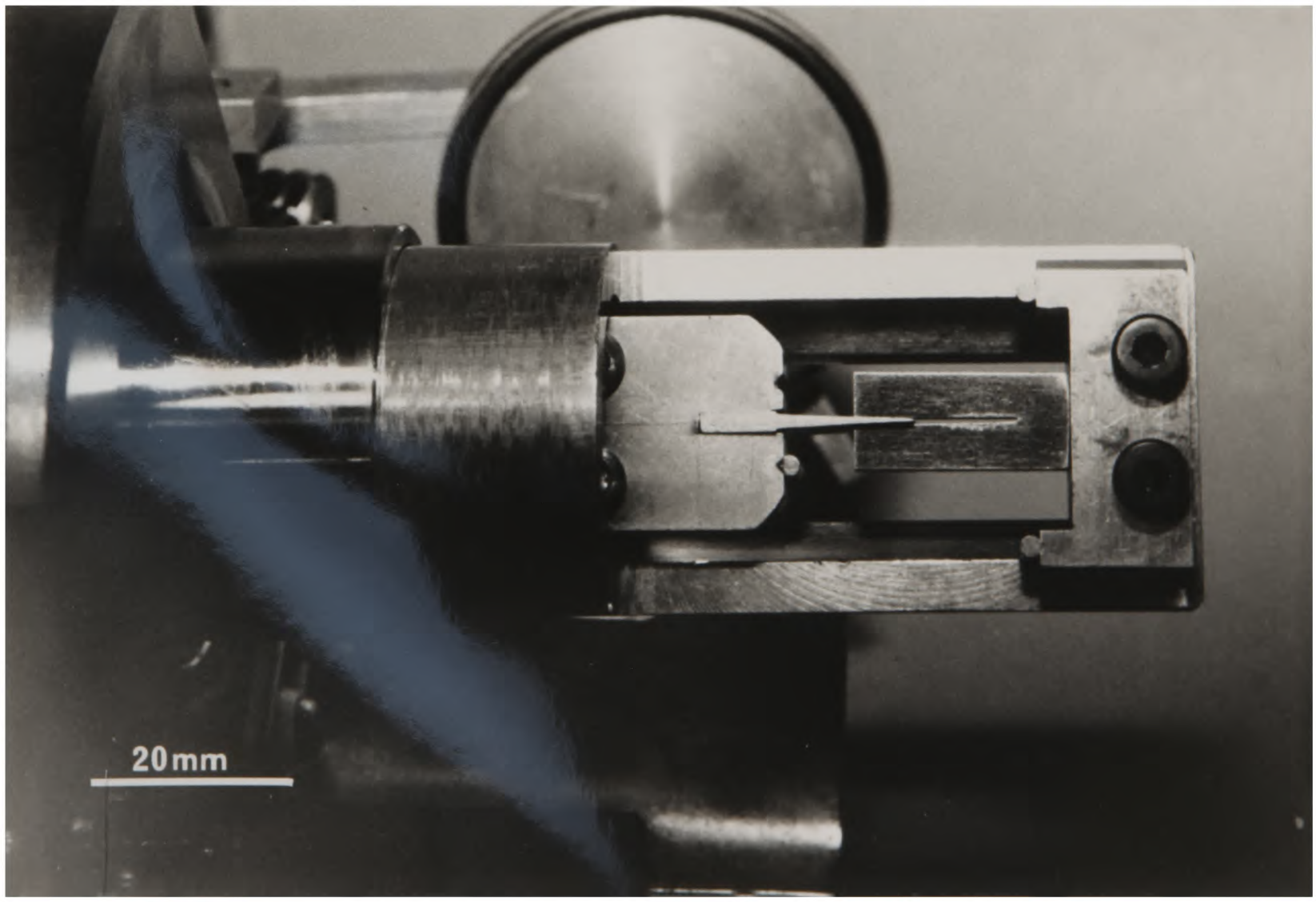

Figure 5.2: Constant displacement, double cantilever loading arrangement.

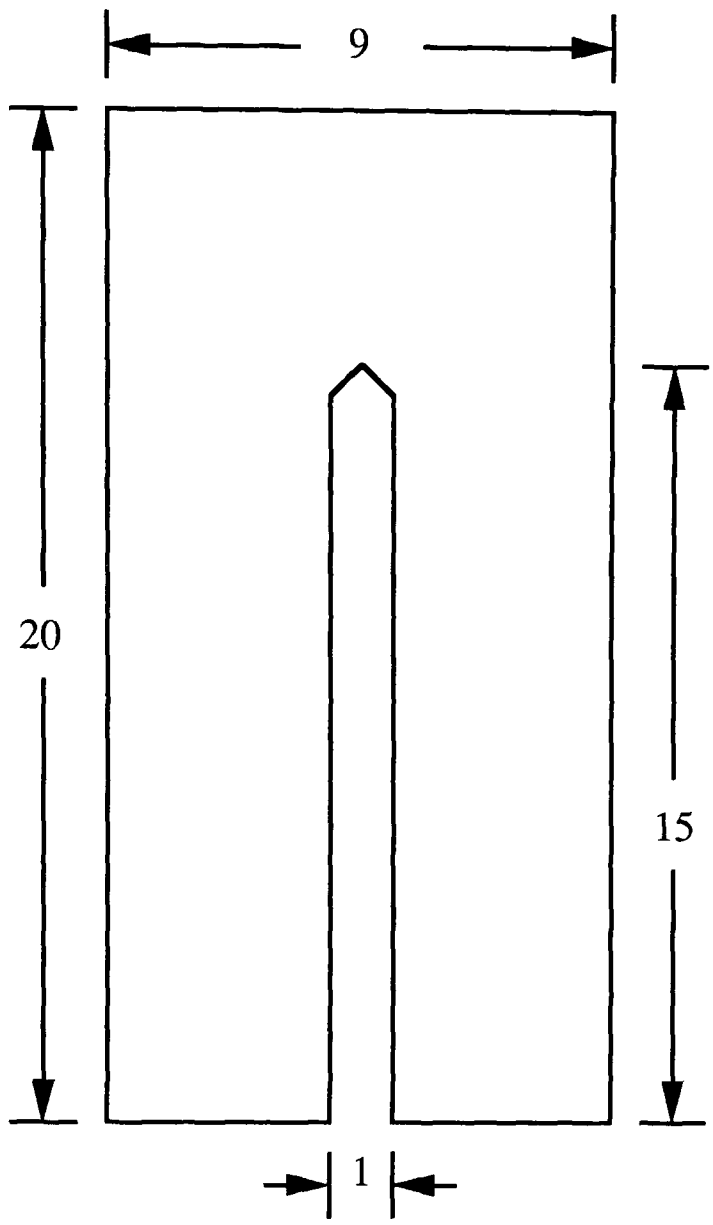

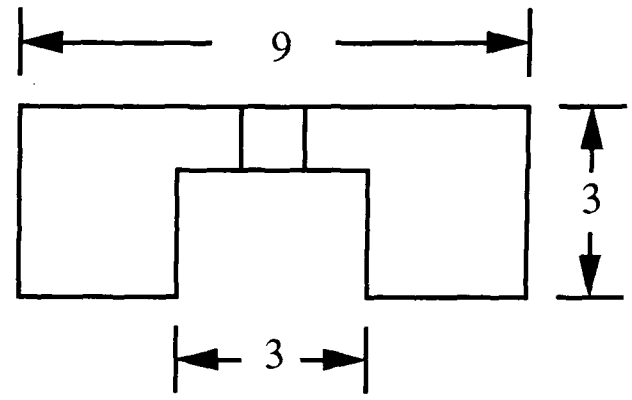

(a) (b)

Figures 5.3a-b: In situ test specimen geometry.

(a)

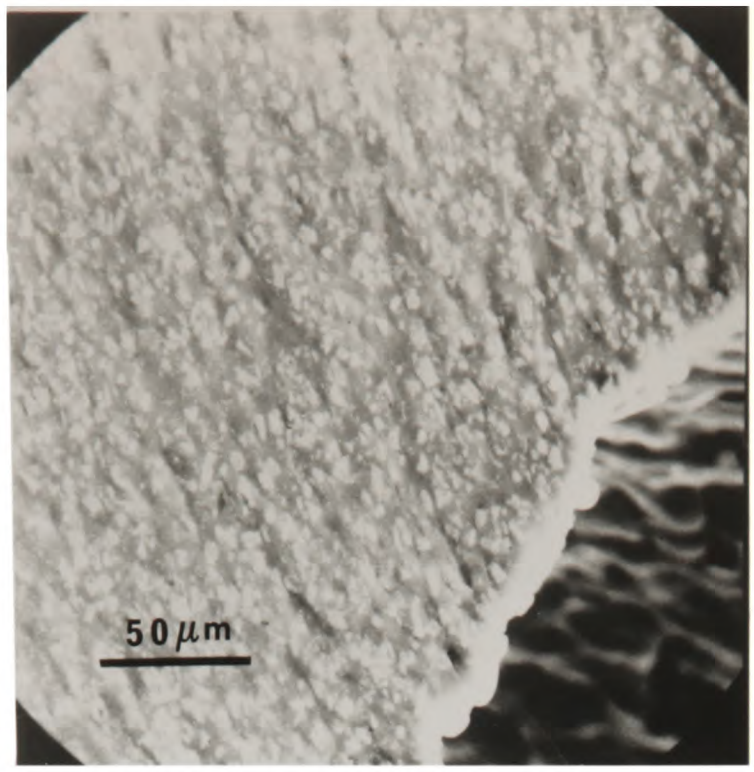

(b)

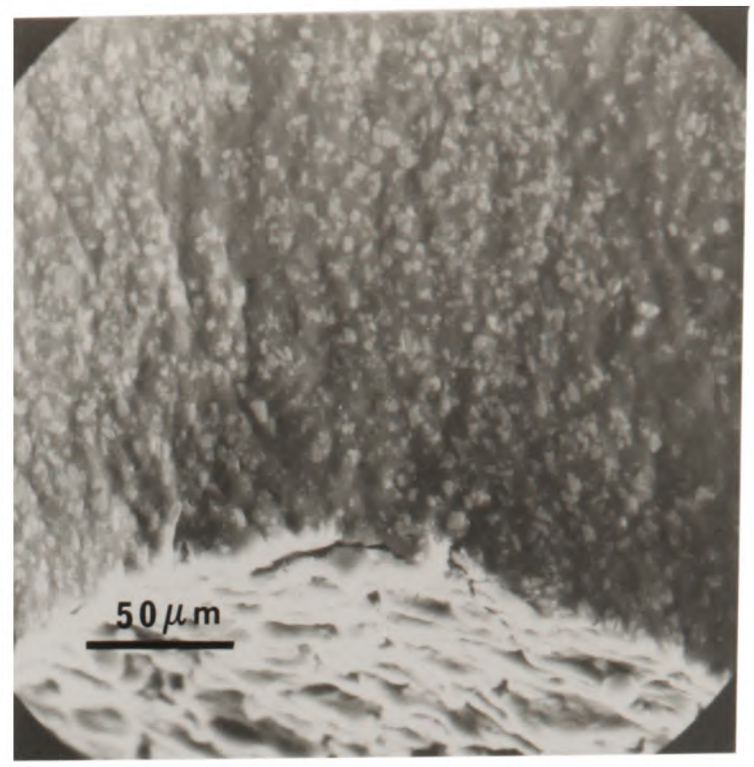

Figures 5.4 a+b: Extensive surface relief shown in the study of 20/3/An/1070.

Figure 5.5: Well-defined directions of deformation seen in 5/30/An/1070.

(a)

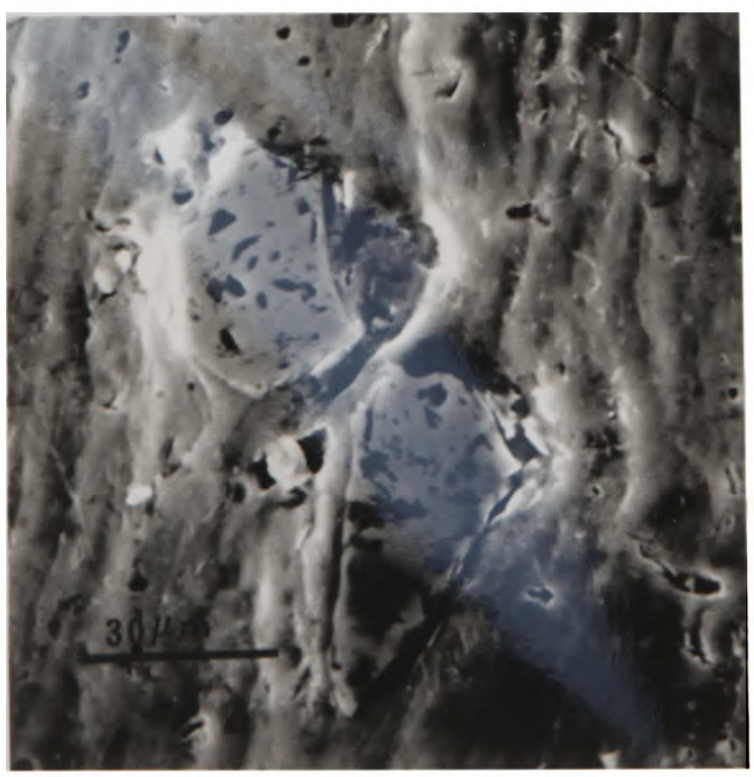

(b)

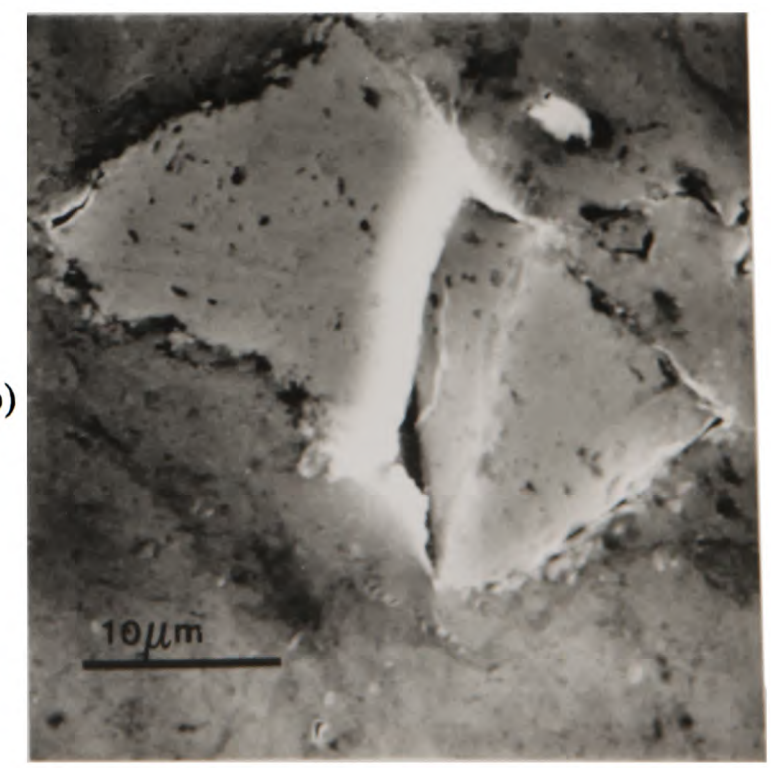

Figures 5.6 a+b: Effect of particles on matrix flow in 5/30/An/1070 showing (a) spall failure and (b) cracking.

(a)

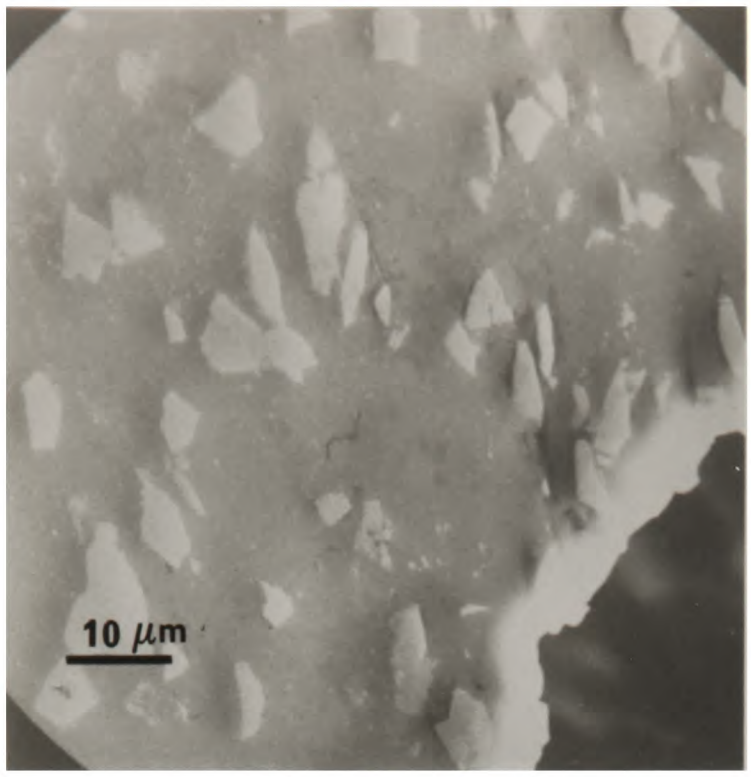

Zero strain

(b)

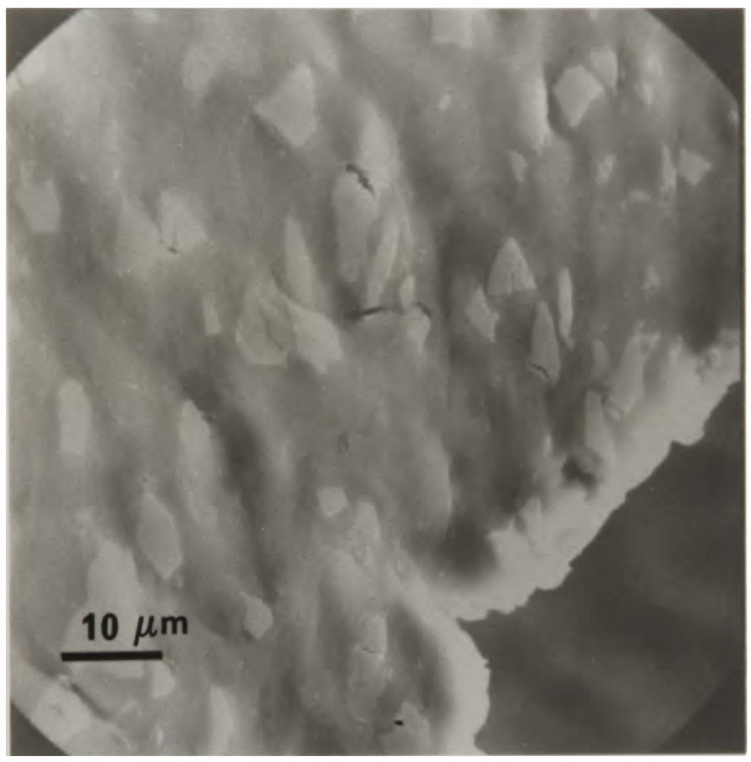

On straining

(c)

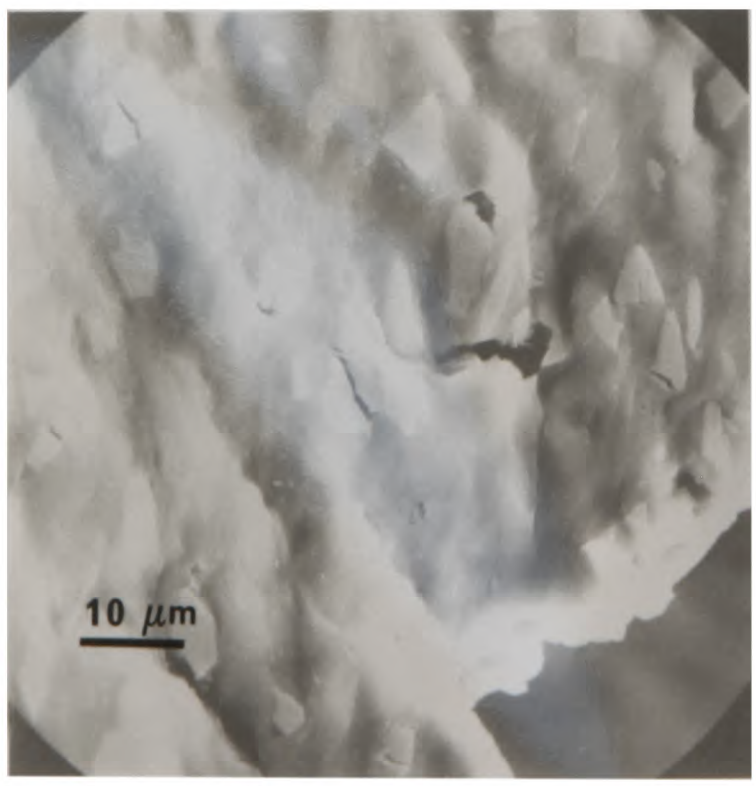

Figures 5.7 a-c: Evidence of nucleation events before macroscopic failure in 20/10/Qu/1070.

(a)

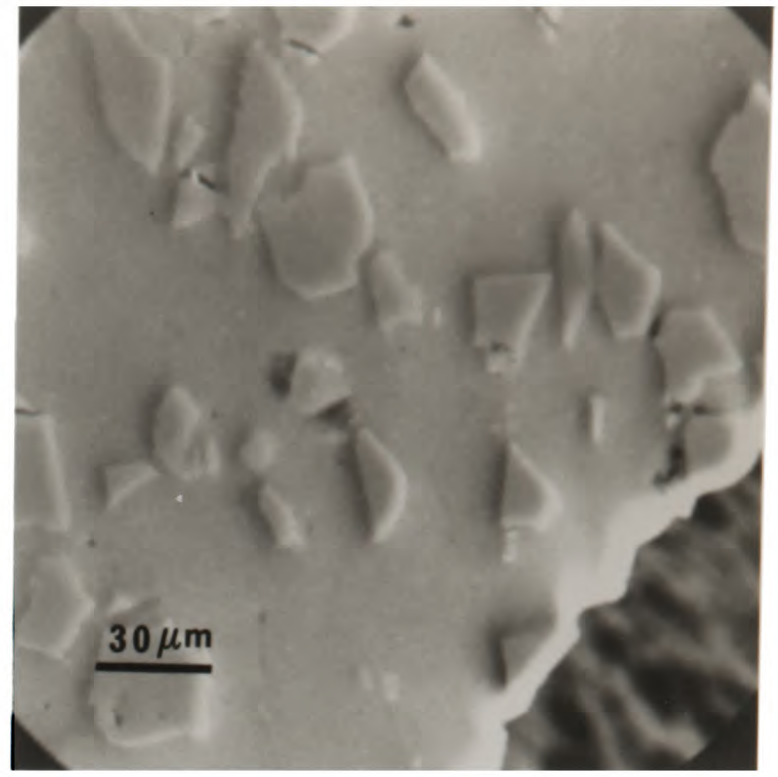

Zero strain

(b)

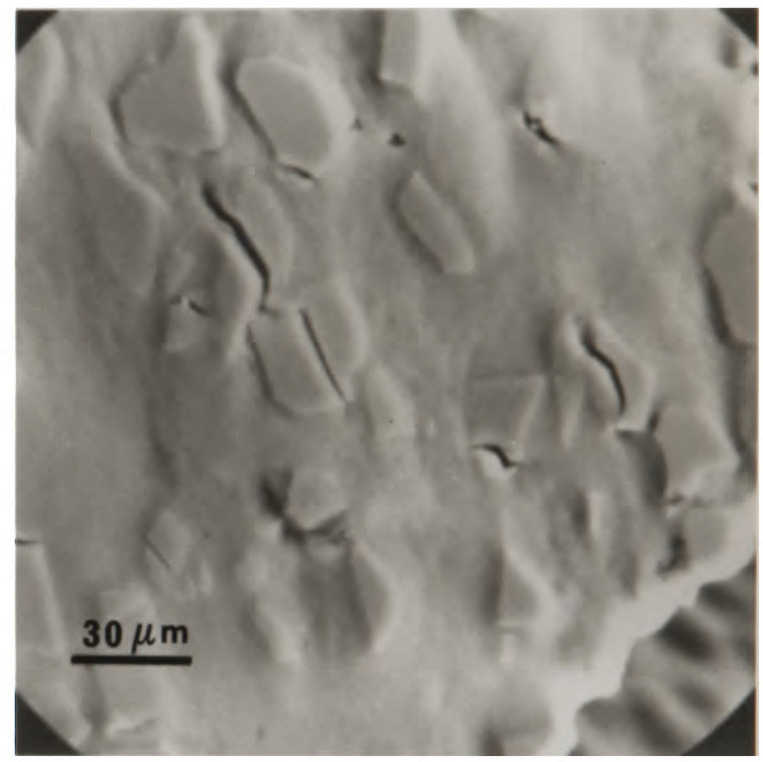

Figures 5.8 a+b: Nucleation events in 20/30/An/1070.

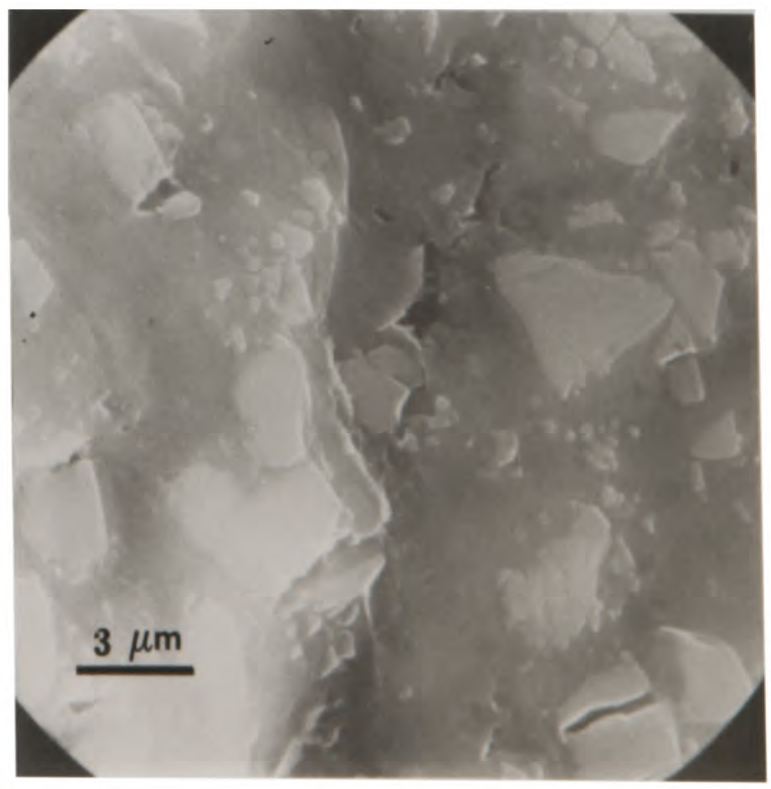

Figure 5.9: Local matrix failure in 20/3/An/1070.

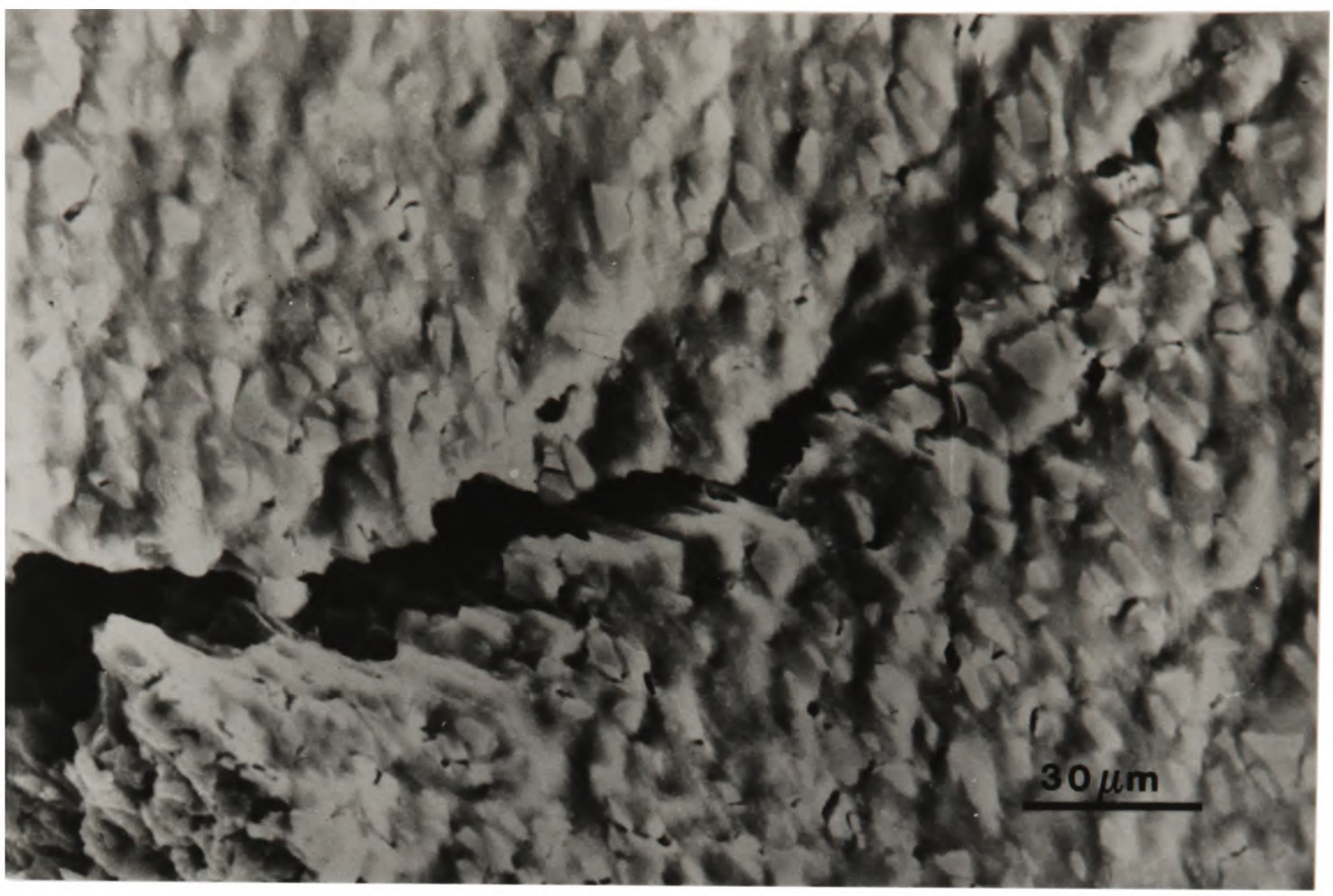

Figure 5.10: Macroscopic crack in 20/10/Qu/1070.

(a)

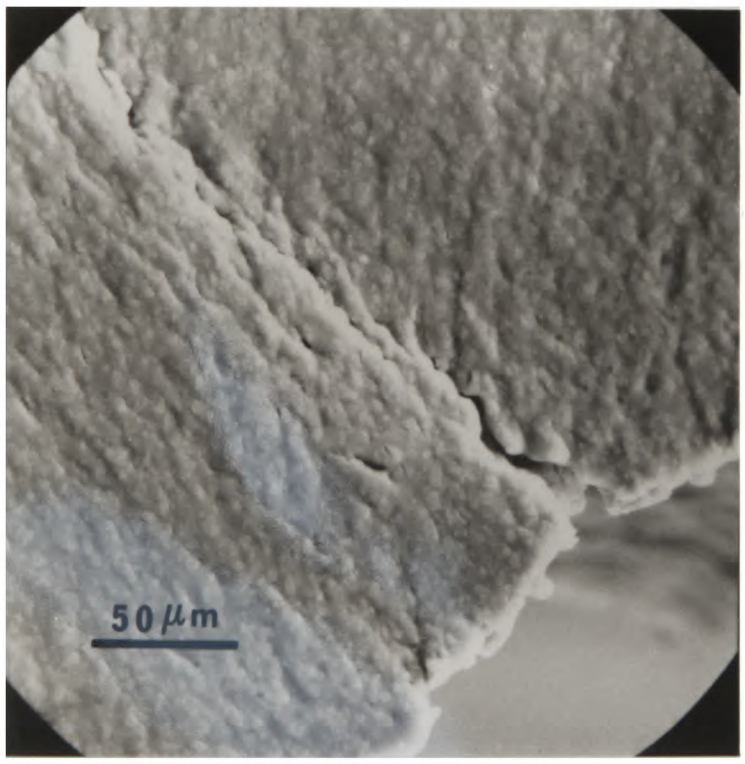

(b)

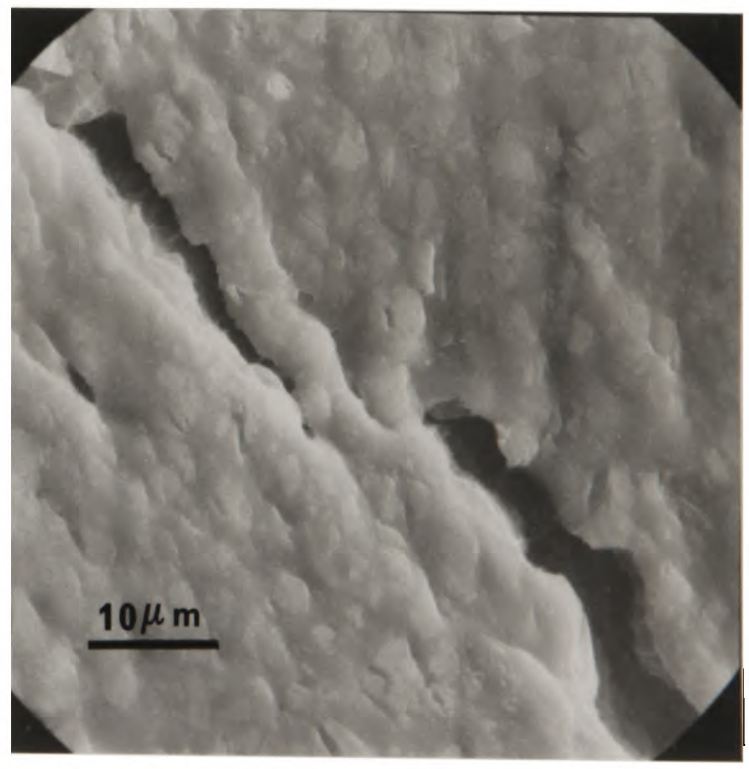

Figures 5.11 a+b: Discontinuous nature of cracks shown in 20/3/An/1070.

(a)

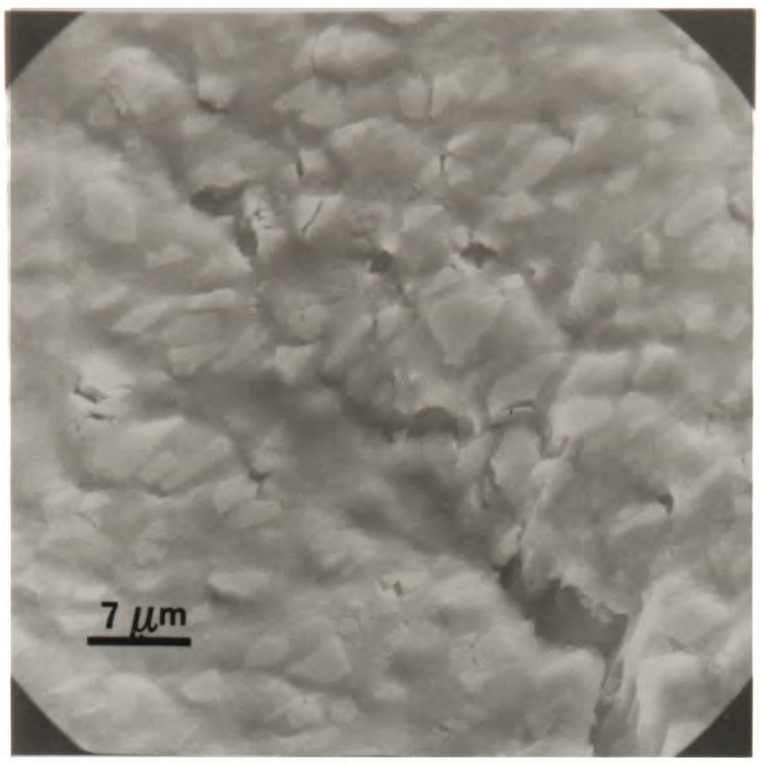

(d)

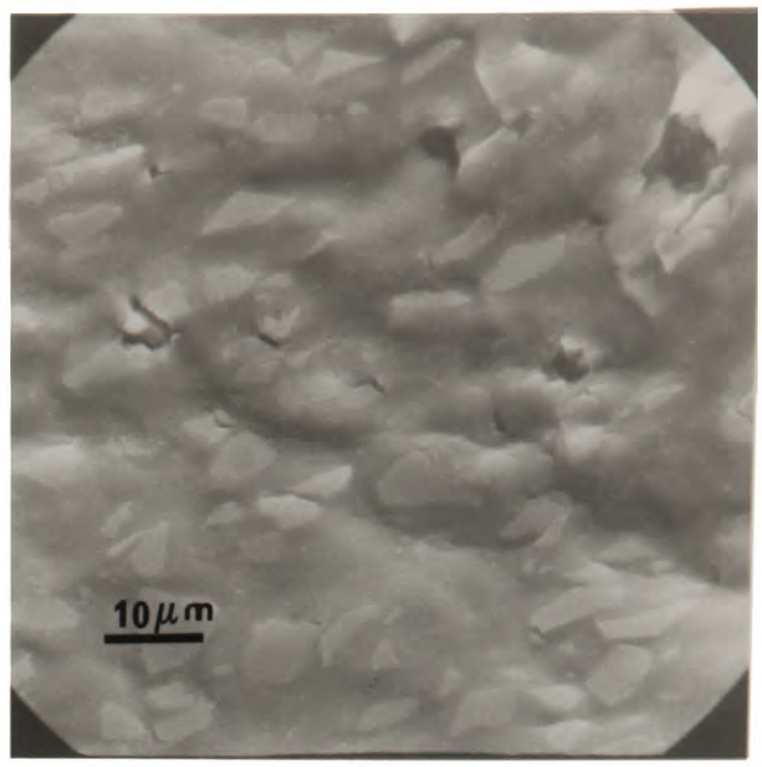

(b)

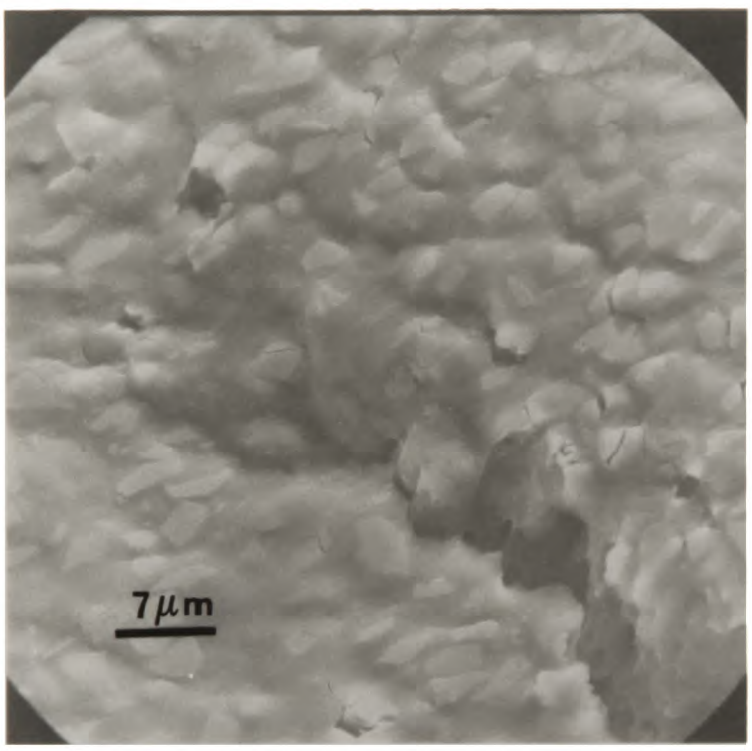

(e)

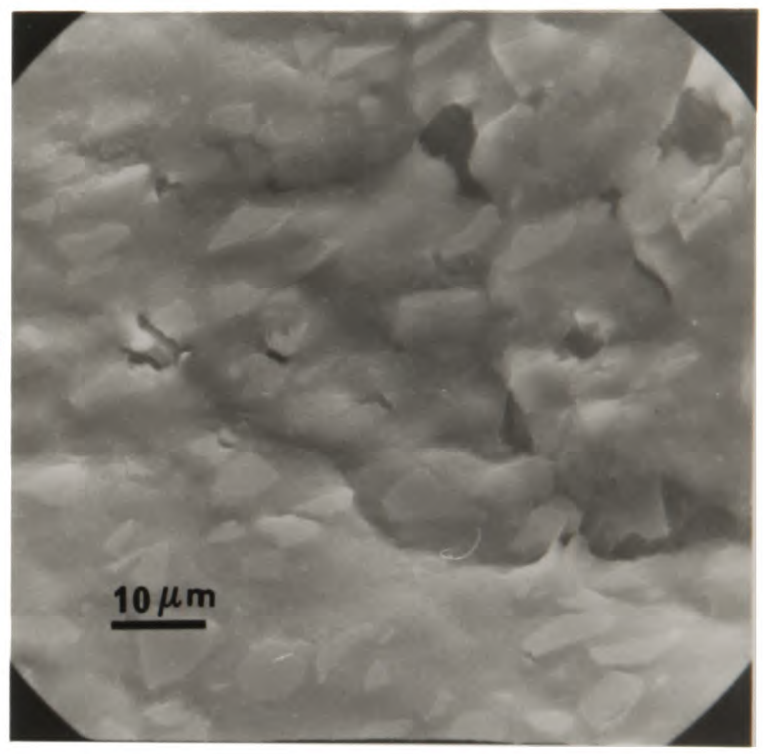

(c)

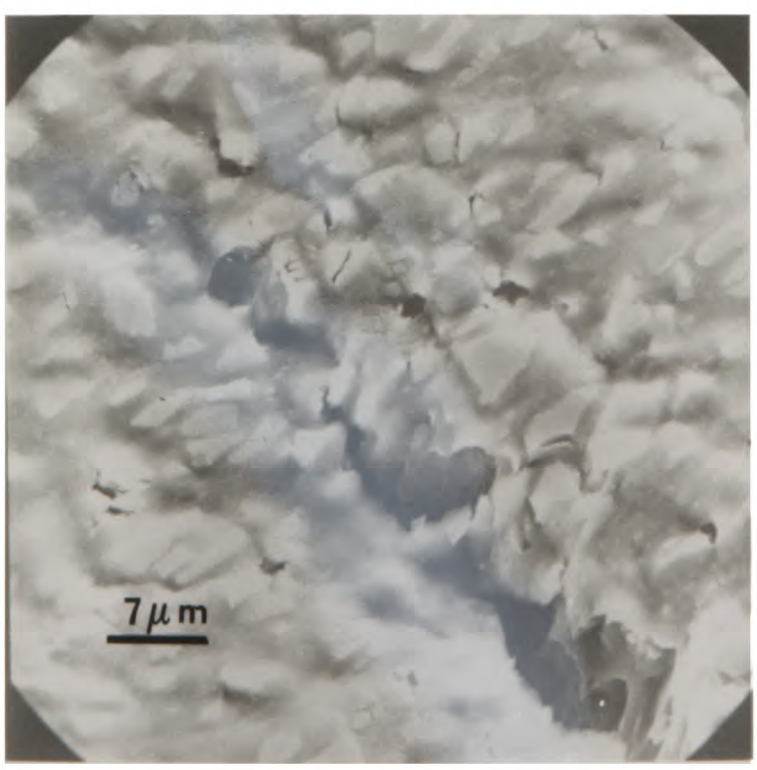

(f)

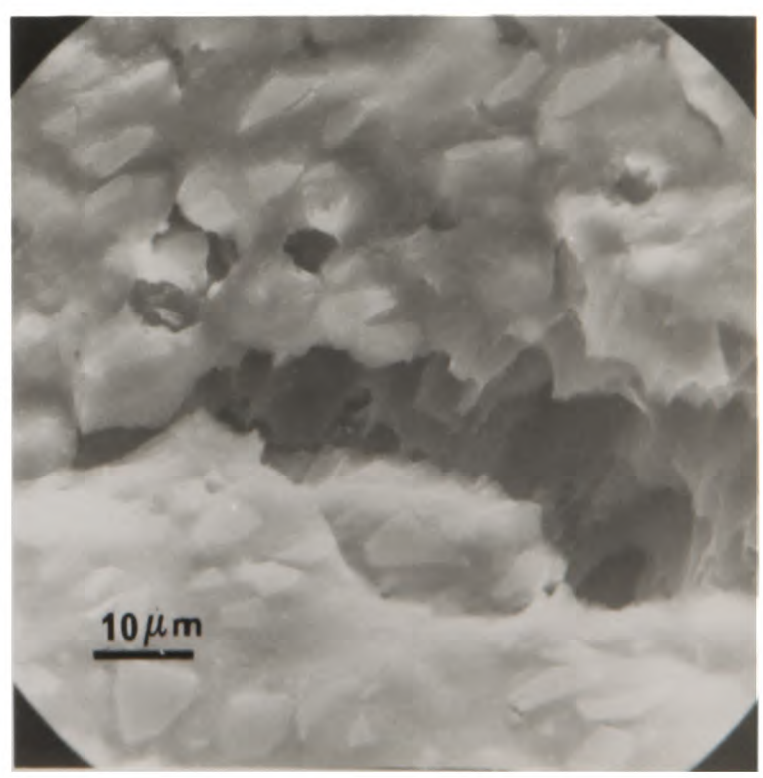

Figures 5.12 a-f: Crack propagation sequence at six strains in 20/10/Qu/1070.

(a)

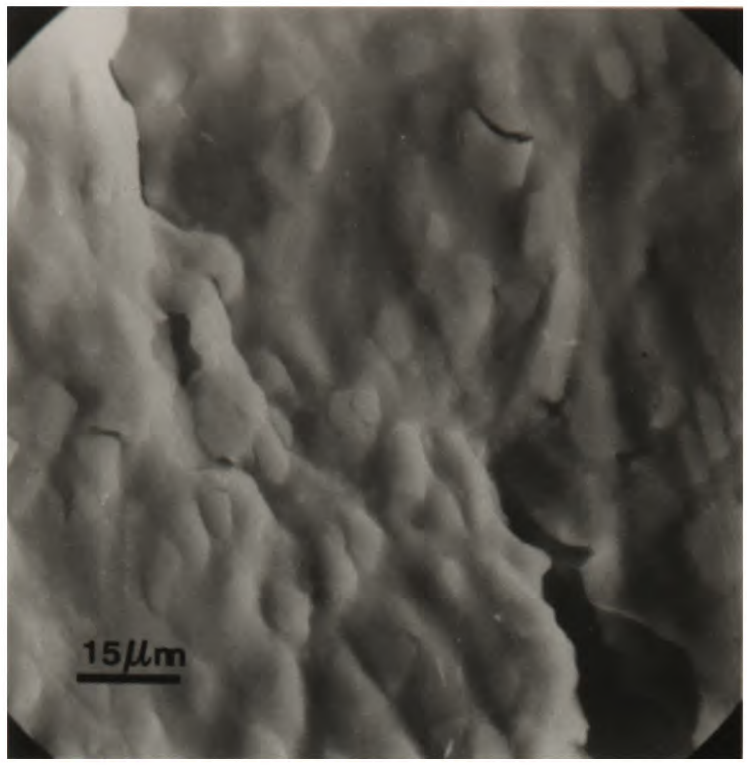

(b)

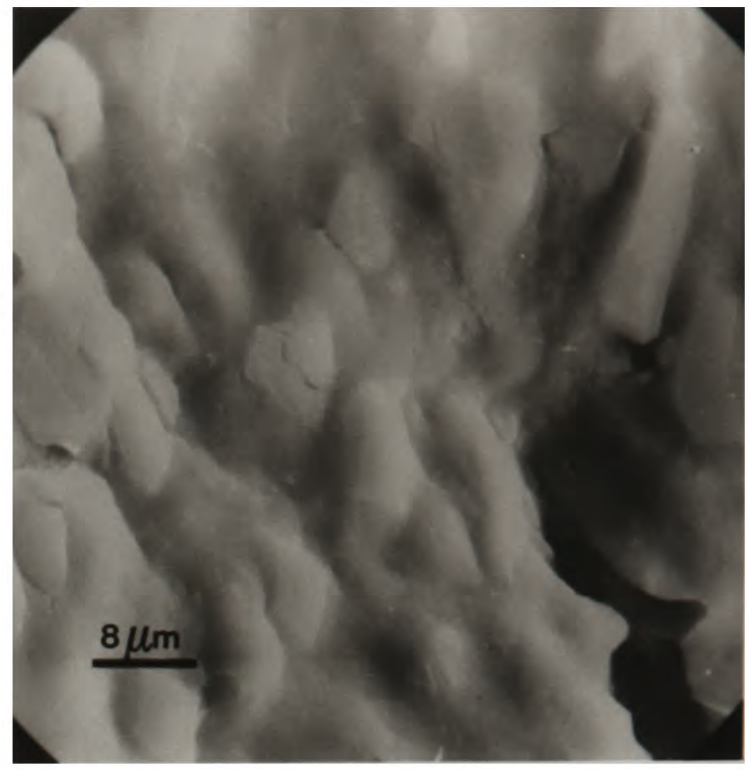

(c)

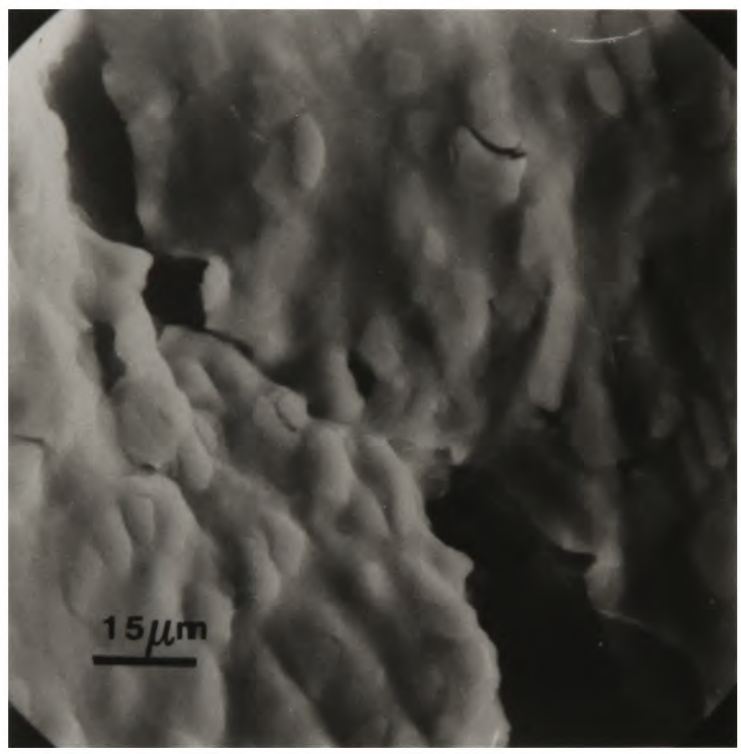

(d)

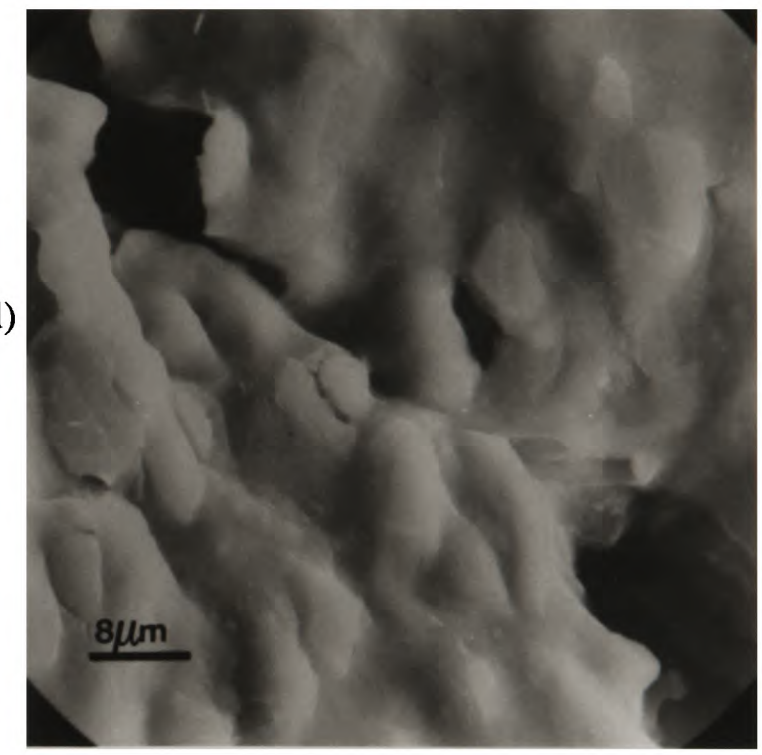

(e)

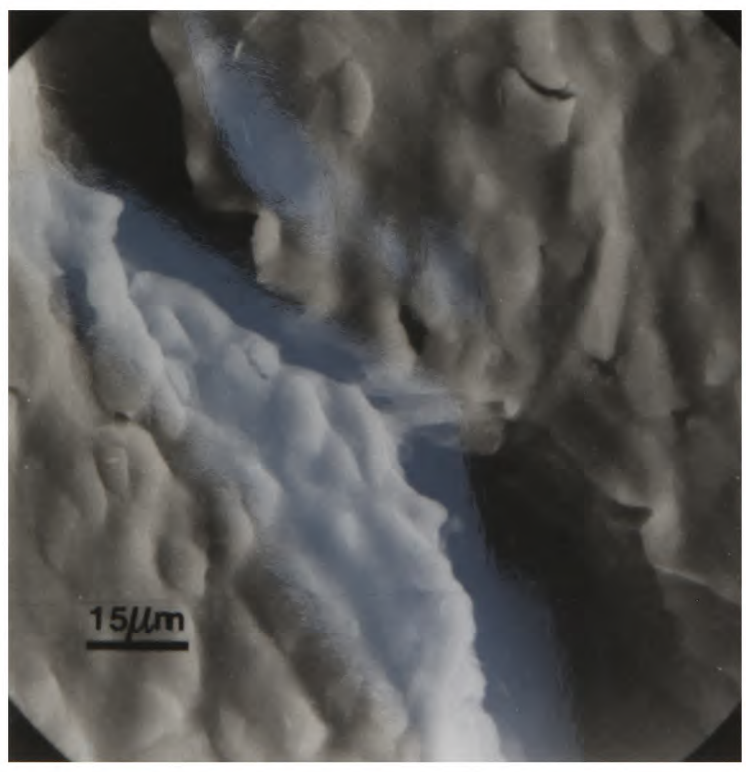

(f)

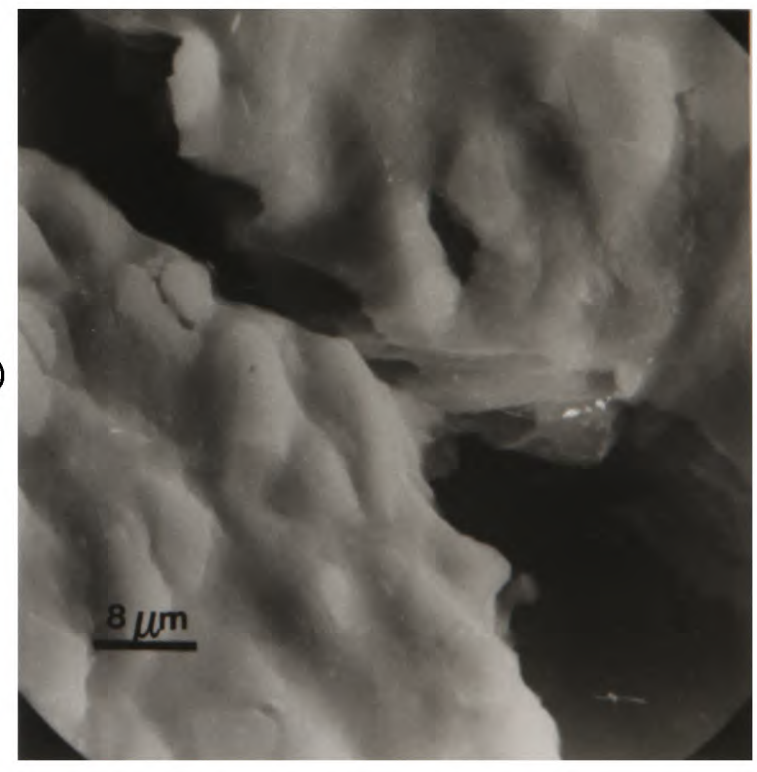

Figures 5.13 a-f: Crack propagation sequence in 20/10/An/1070 at three strains and two magnifications.

(a)

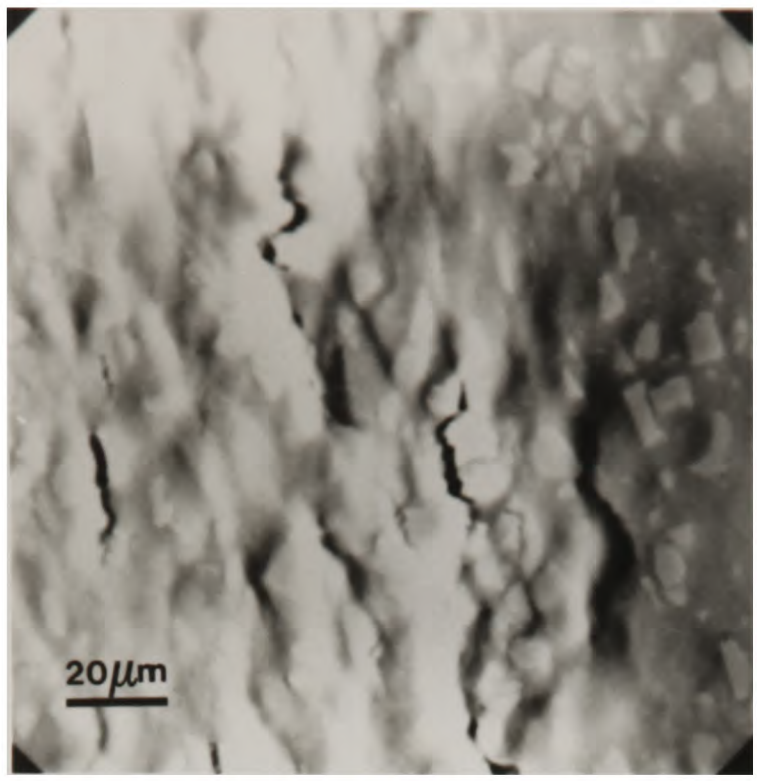

(b)

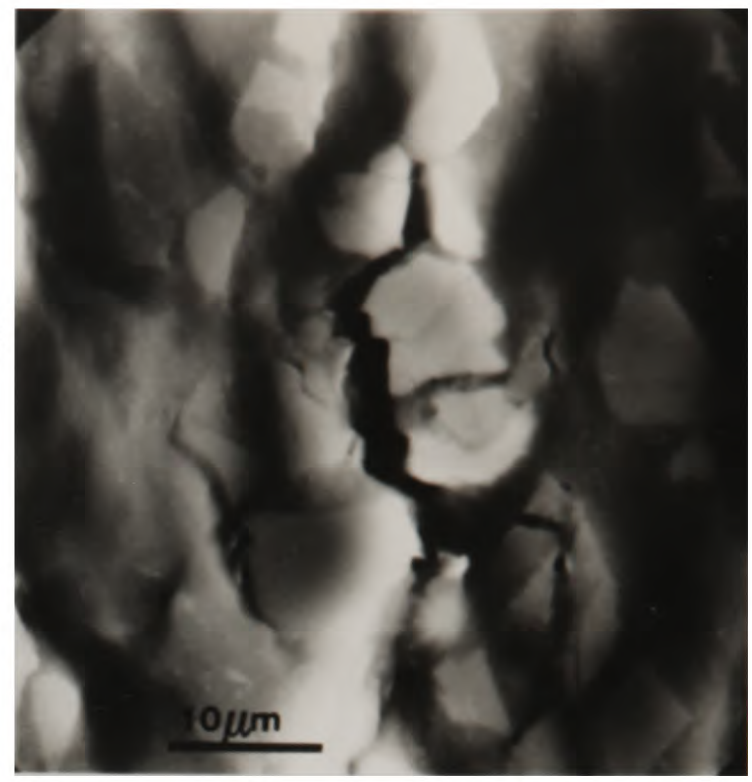

(c)

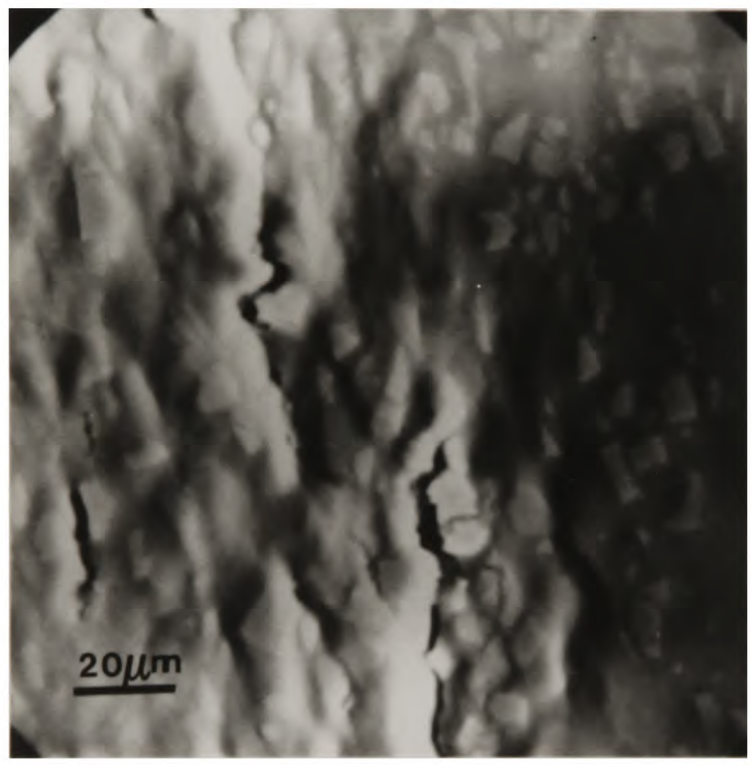

(d)

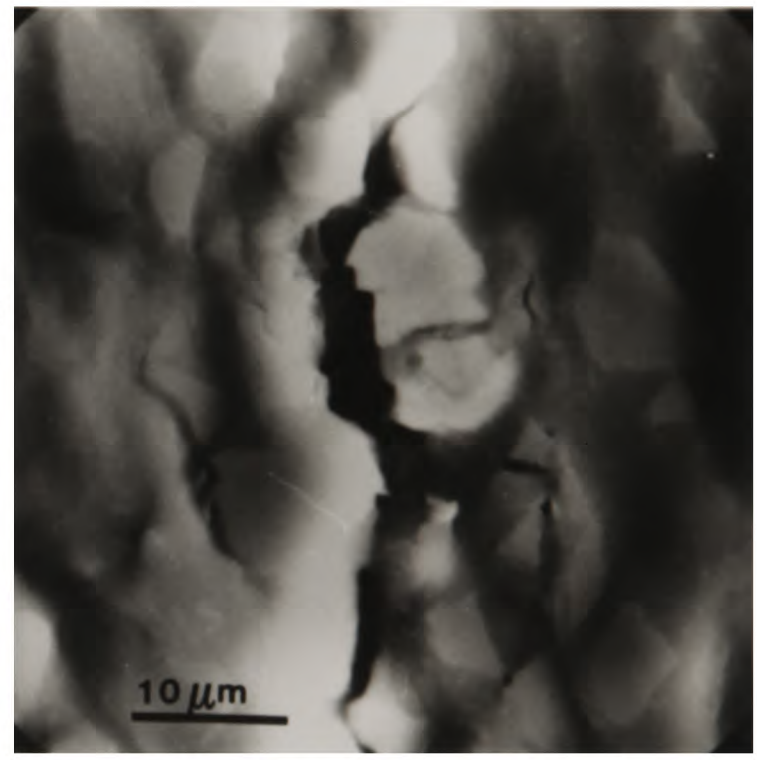

(e)

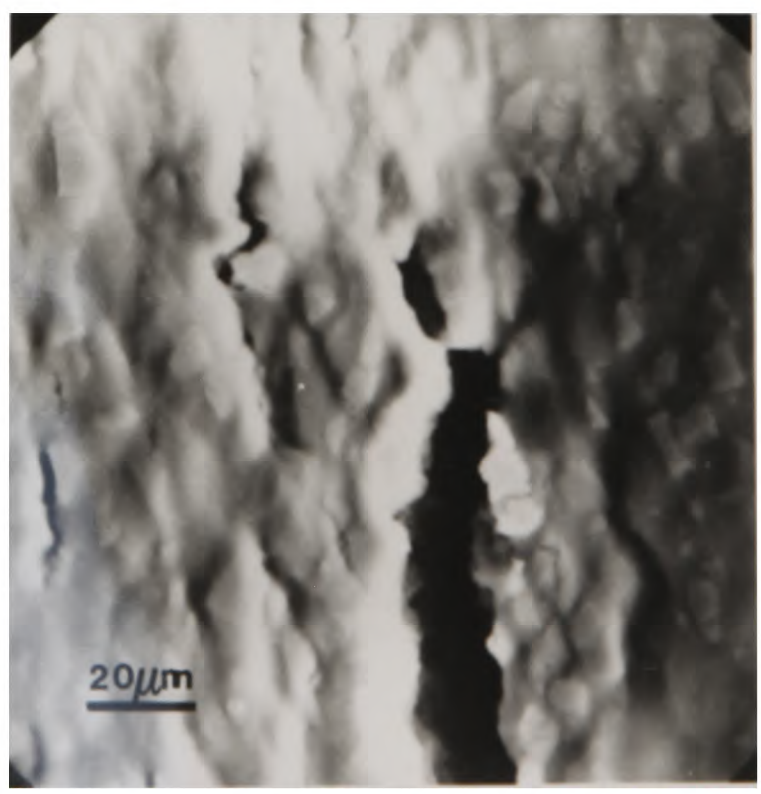

Figures 5.14 a-e: Crack propagation sequence in 20/10/Qu/5050 at three strains and two magnifications.

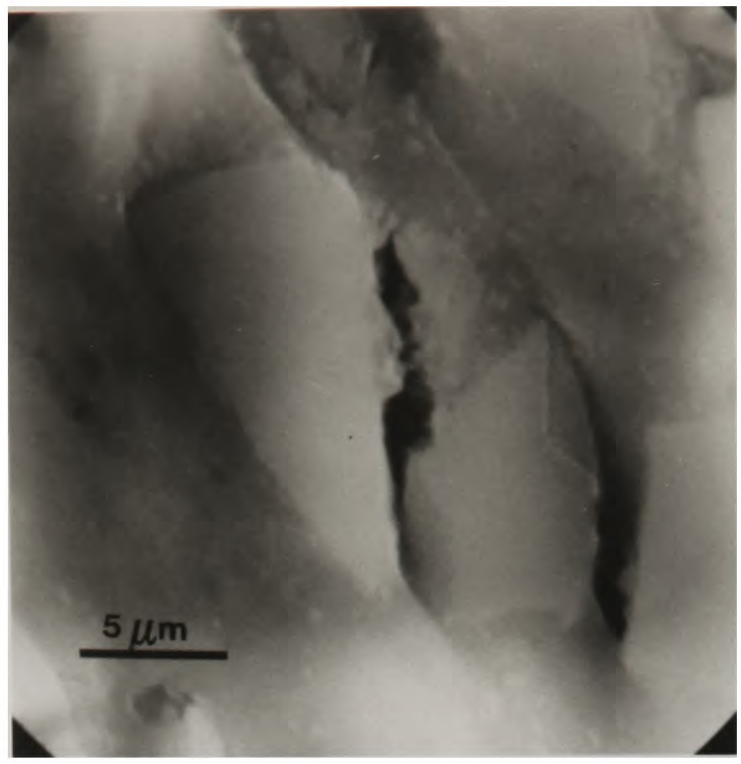

Figure 5.15: Localised deformation leading to interfacial decohesion in 20/10/An/5050.

(a)

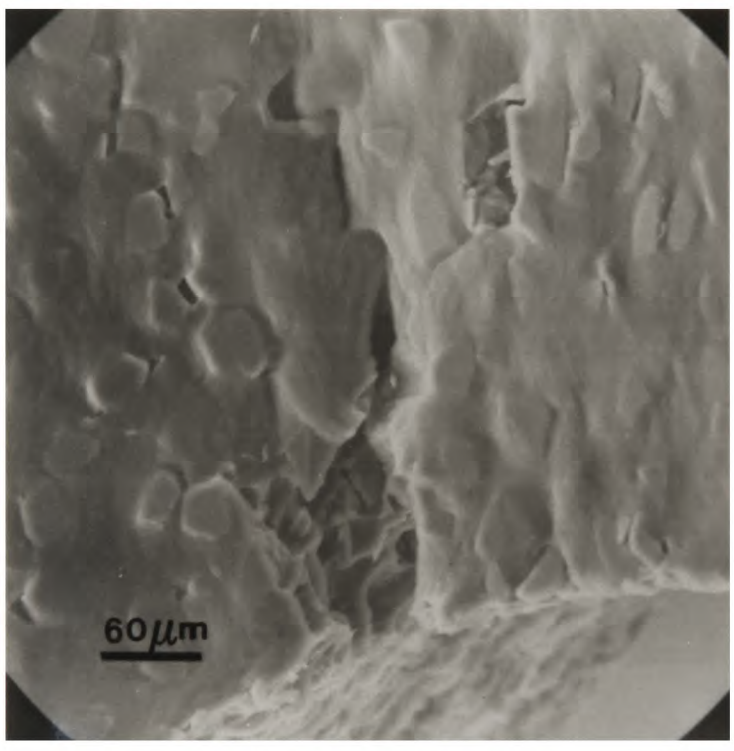

(b)

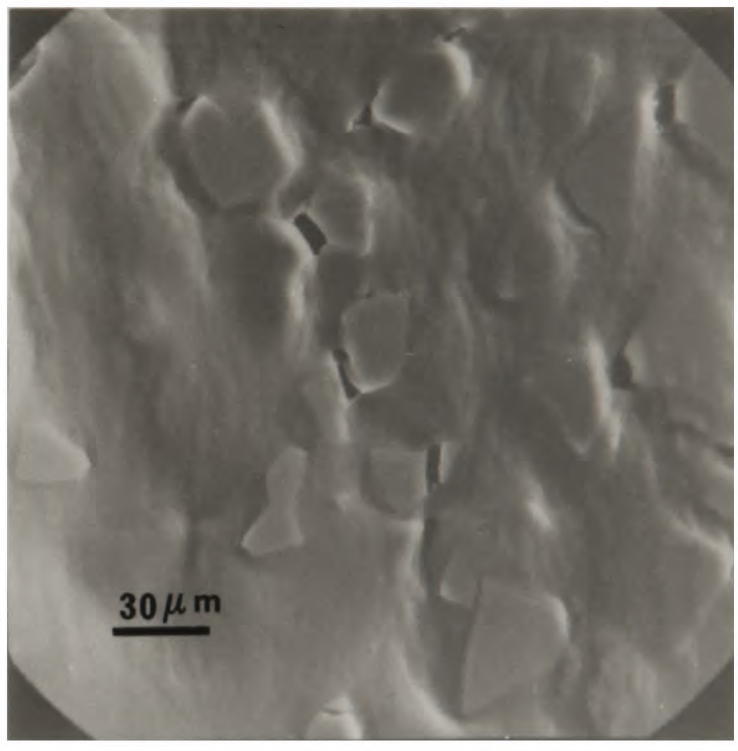

Figures 5.16 a+b: Alignment of microcracks with main crack in 20/30/Qu/1070.

(a)

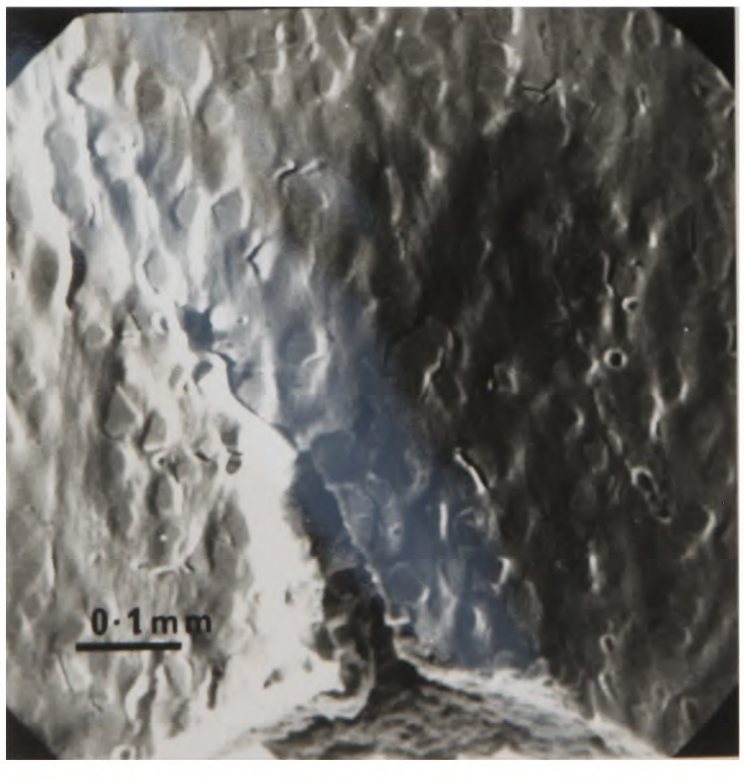

(b)

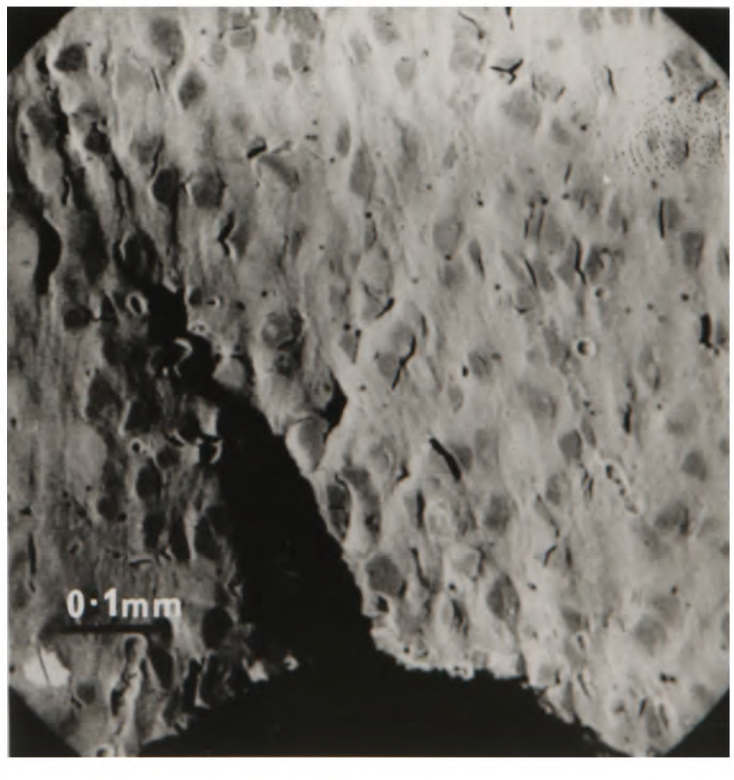

Figures 5.17 a+b: SEI (a) and BEI (b) of 20/30/An/1070 showing microcrack alignment with main crack.

(a)

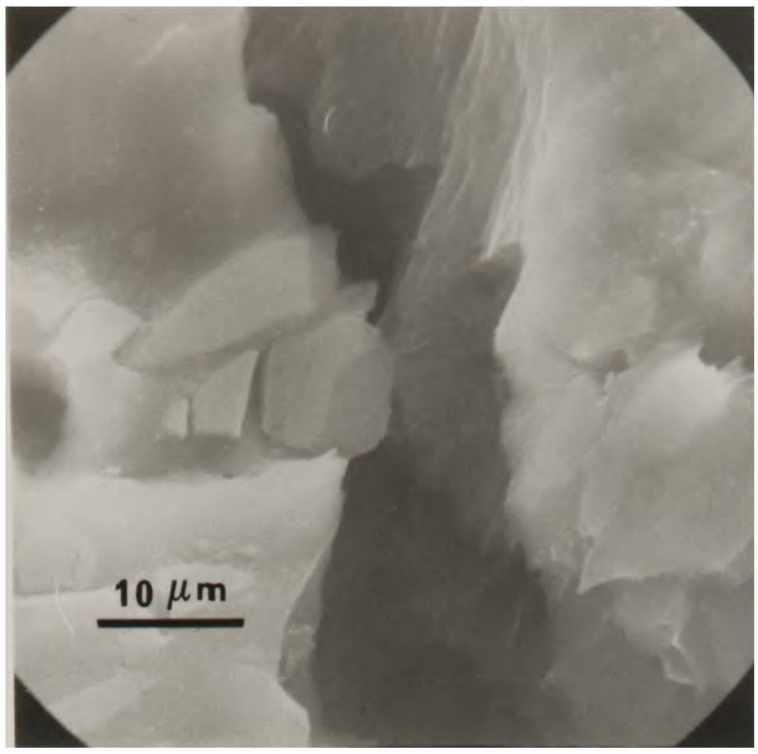

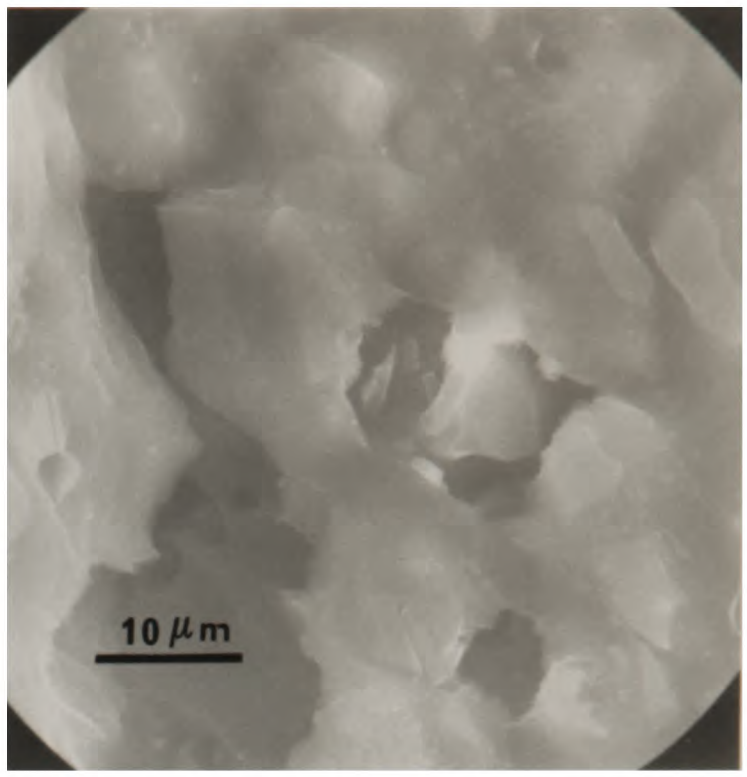

Figures 5.18 a+b: Cracked particles left in wake of main crack in 20/10/Qu/1070.

(a)

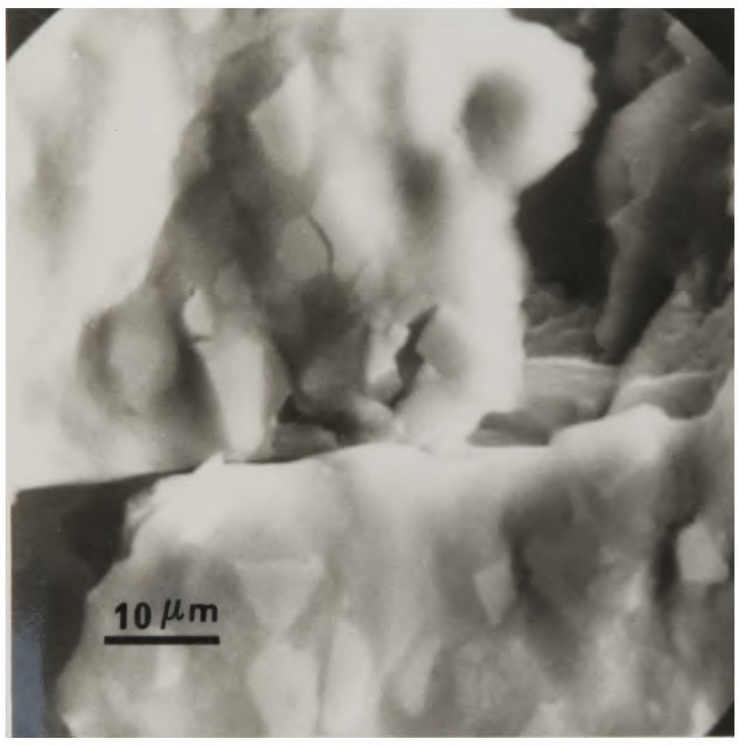

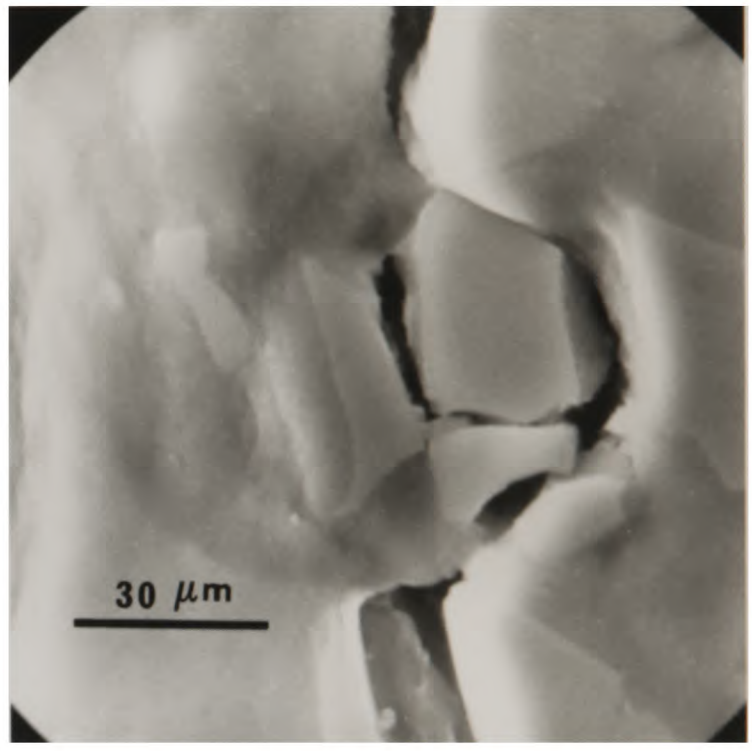

Figures 5.19 a+b: Main crack by-passing fractured particles in (a) 20/10/An/1070 and (b) 20/30/Qu/5050.

(c)

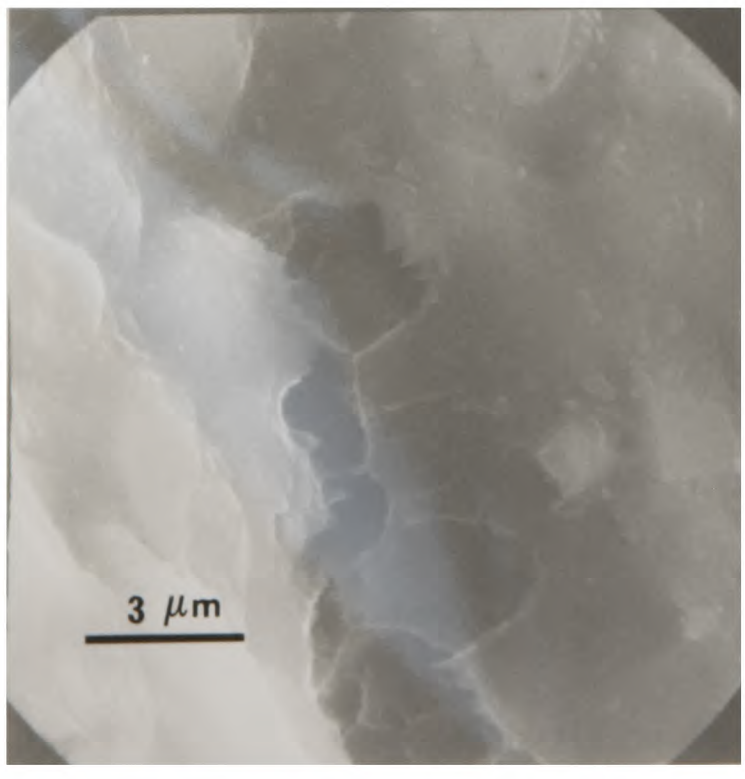

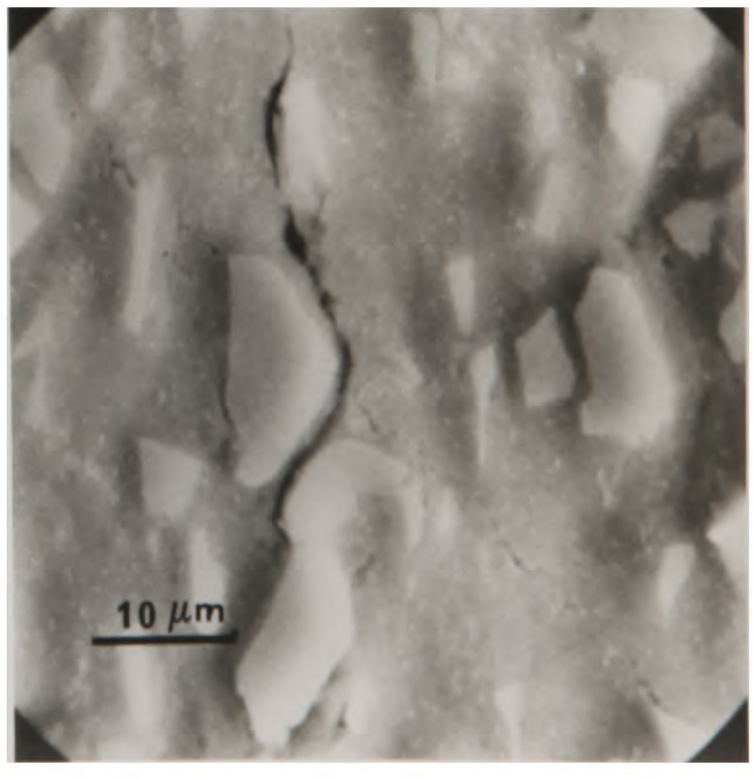

Figures 5.19 c+d: Crack propagating through matrix in (c) 20/3/An/1070 and by-passing particles in (d) 20/10/Qu/5050.

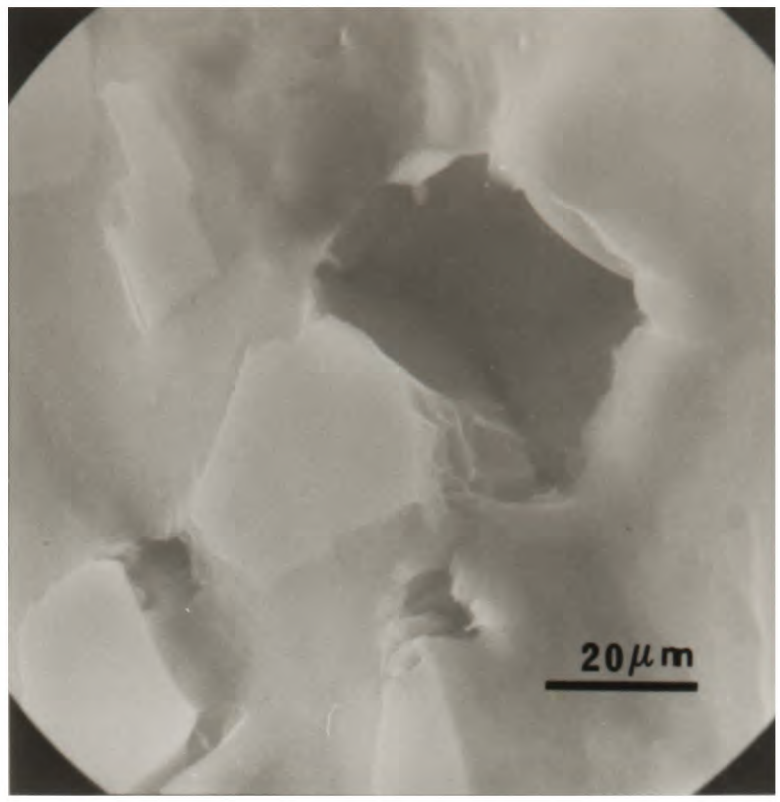

(a) 20/30/An/2070

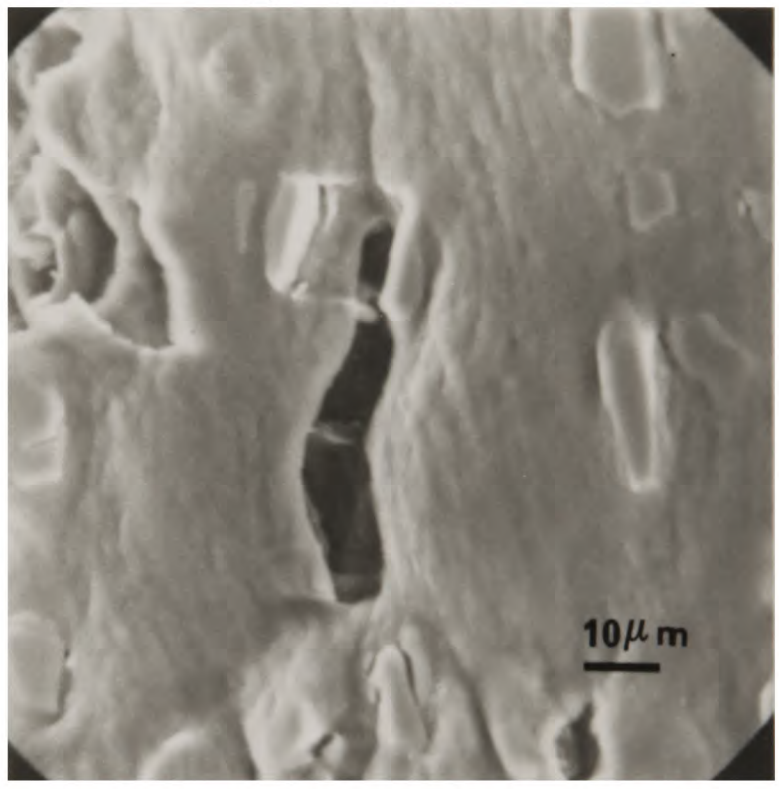

(b) 10/30/Qu/1070.

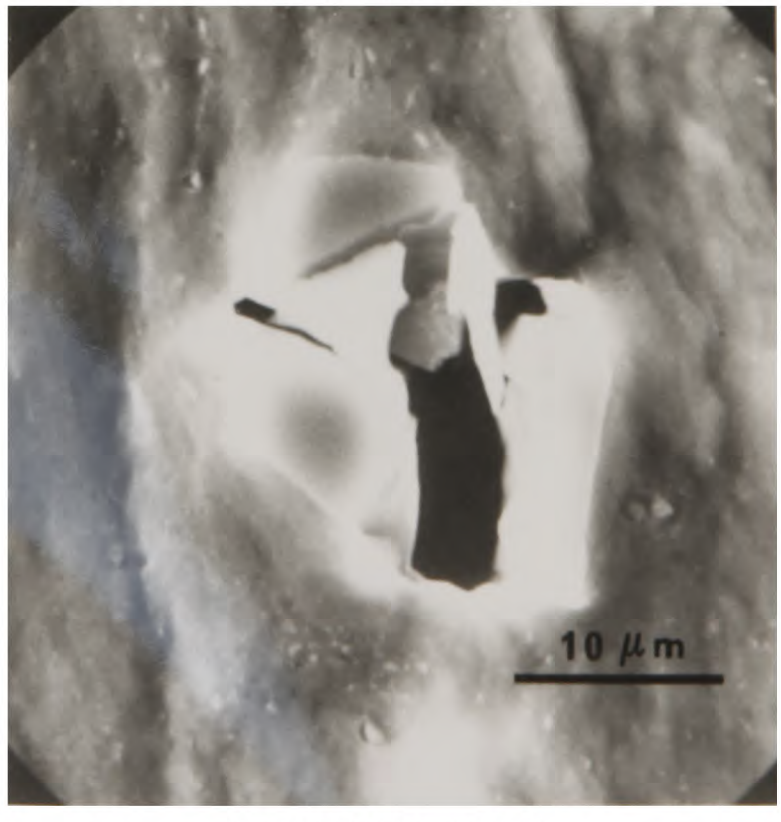

(c) 10/10/Qu/1070.

Figures 5.20 a-c: Restricted void growth in different systems.

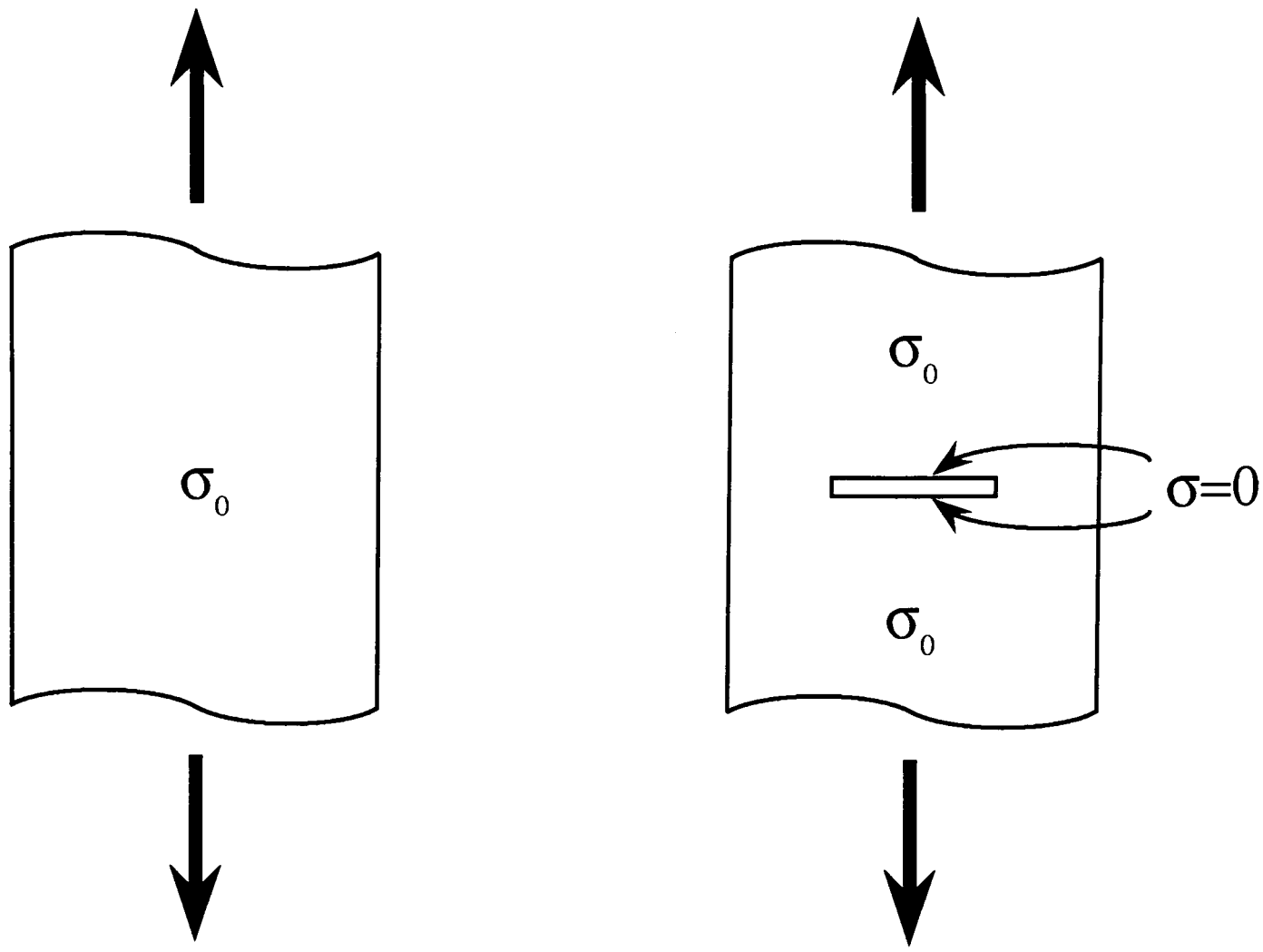

(a) (b) (c)

Figures 5.21a-c: Sudden growth of crack is accompanied by stress changes that disturb equilibrium. Stress is redistributed in sample by elastic waves that propagate away from crack.

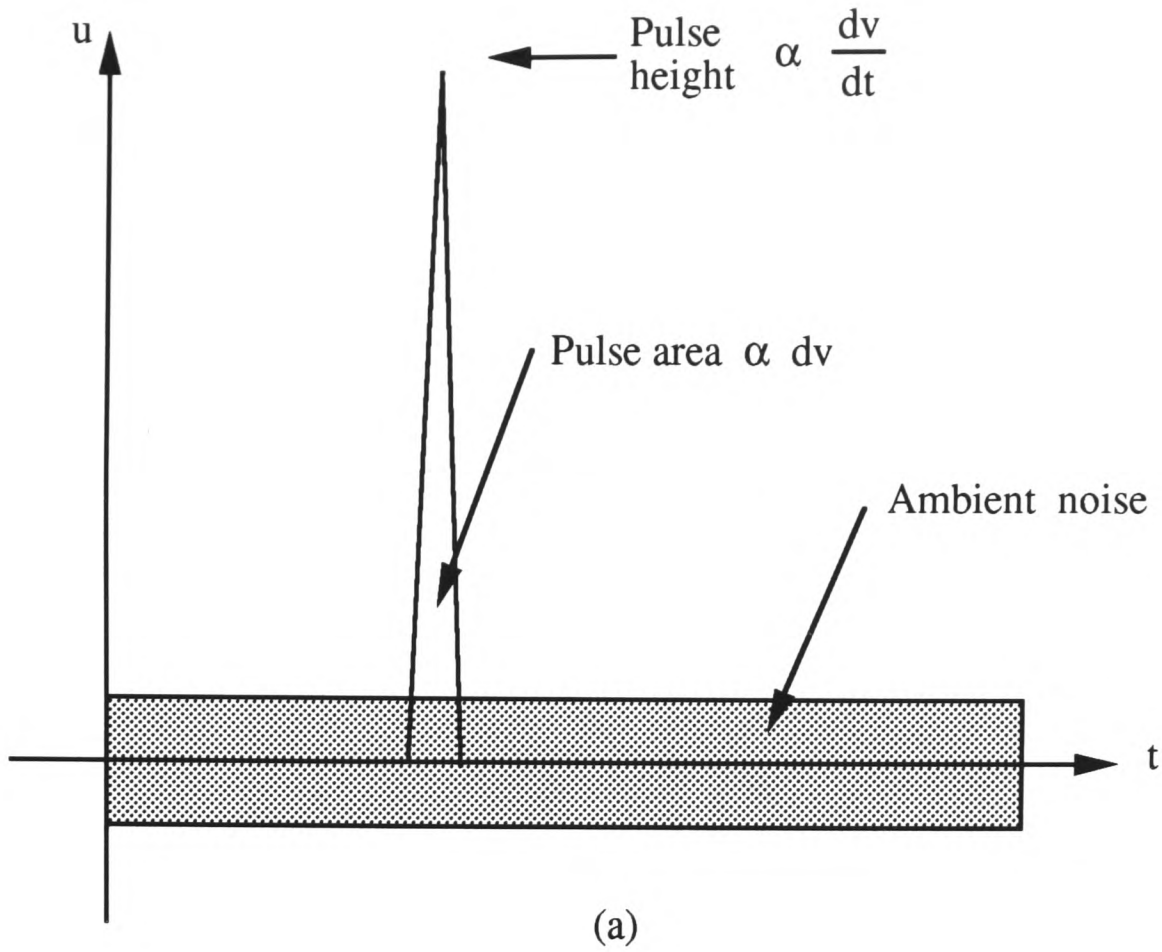

Figure 5.22a-b: Showing how defect source timescale affects detectability. (a) Rapid source, e.g. brittle crack, has dV/dt large enough to exceed ambient noise. (b) Slow source, e.g. very ductile crack, with small dV/dt is not detectable.

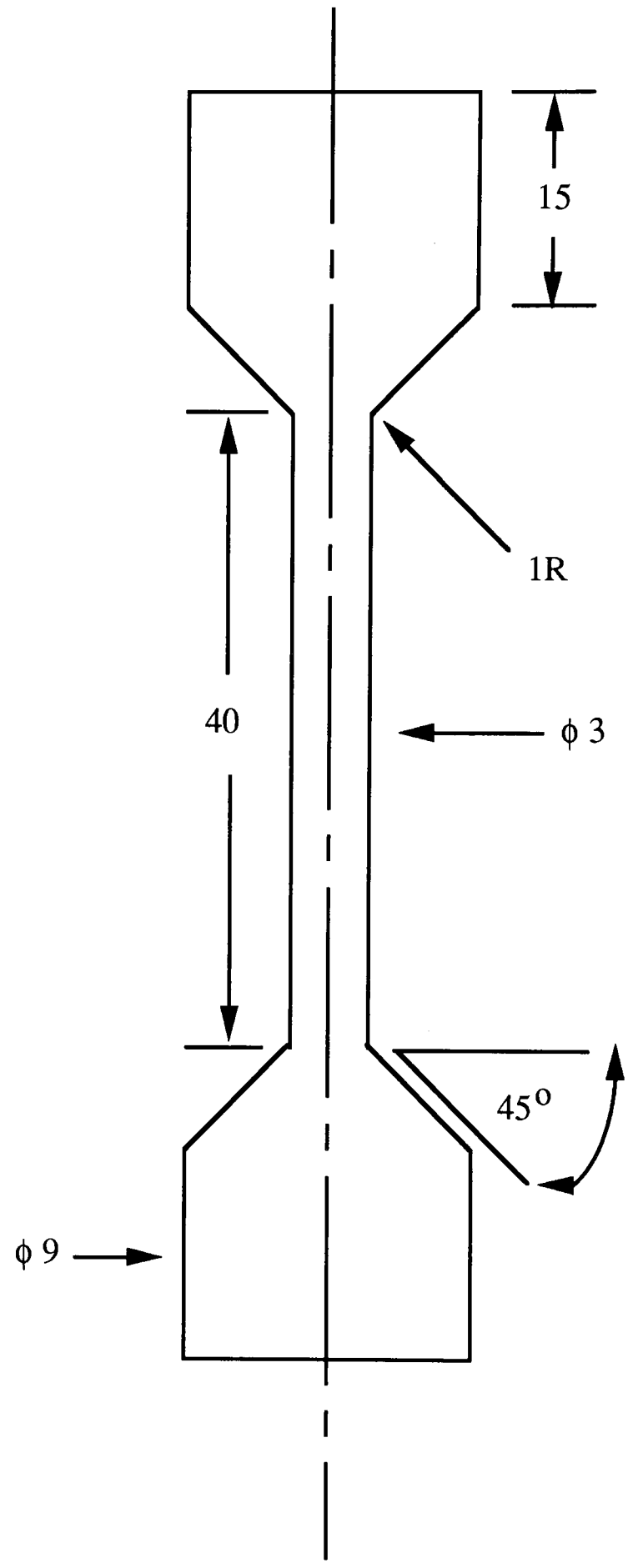

Figure 5.23: Acoustic Emission Specimen Geometry

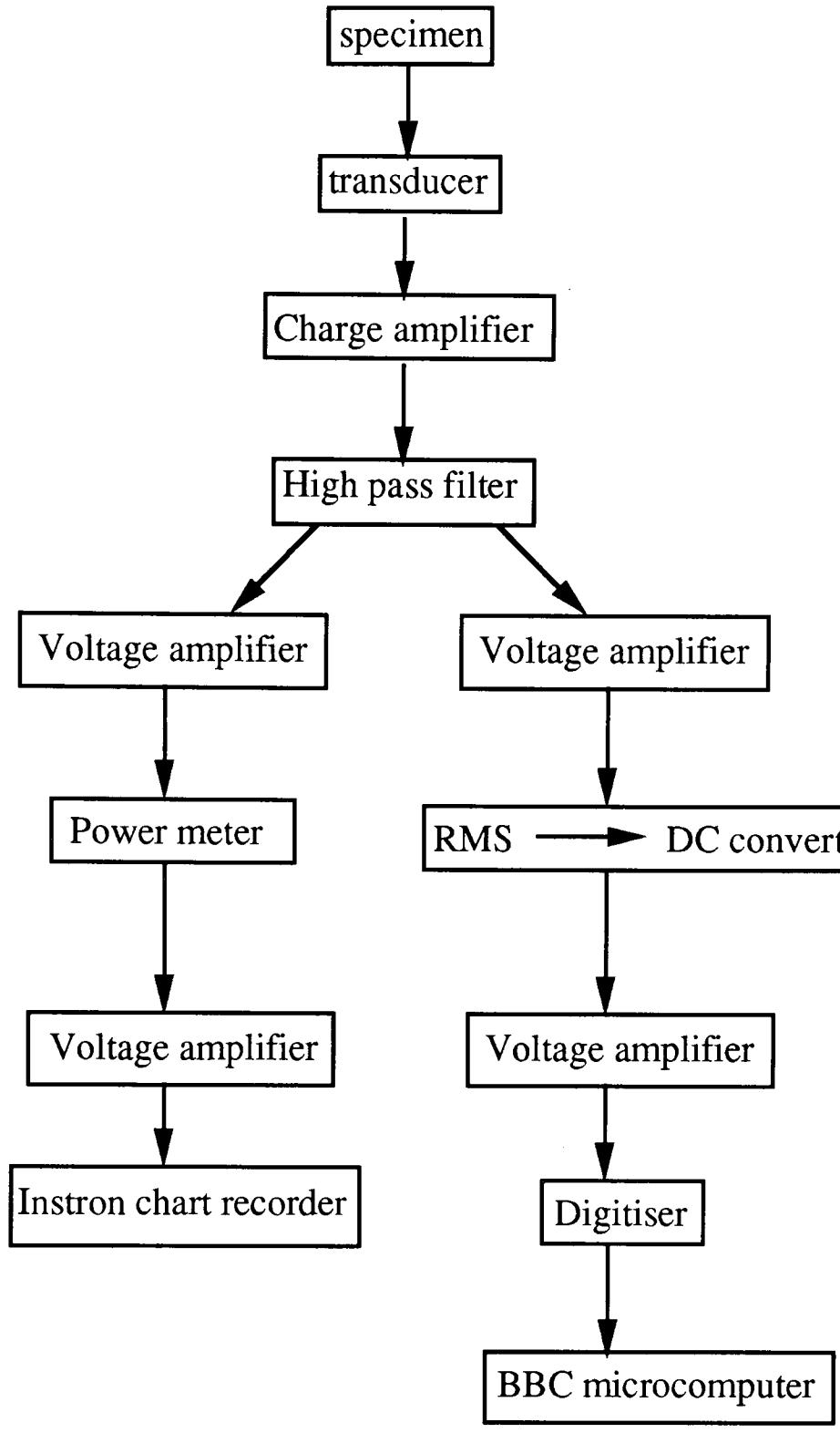

Figure 5.24: Acoustic Emission Signal Processing

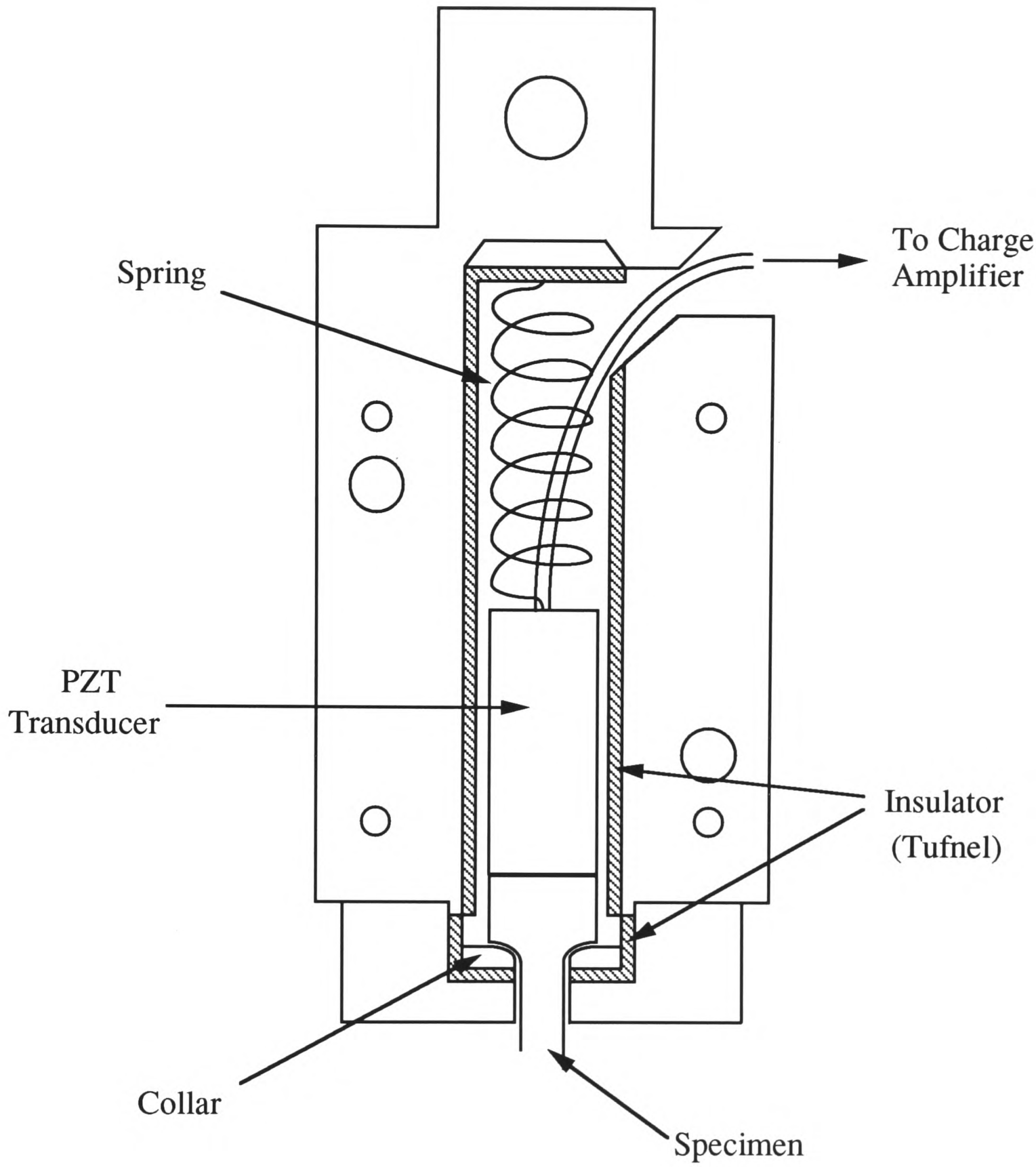

Figure 5.25: Section Through Split Grips for Instron

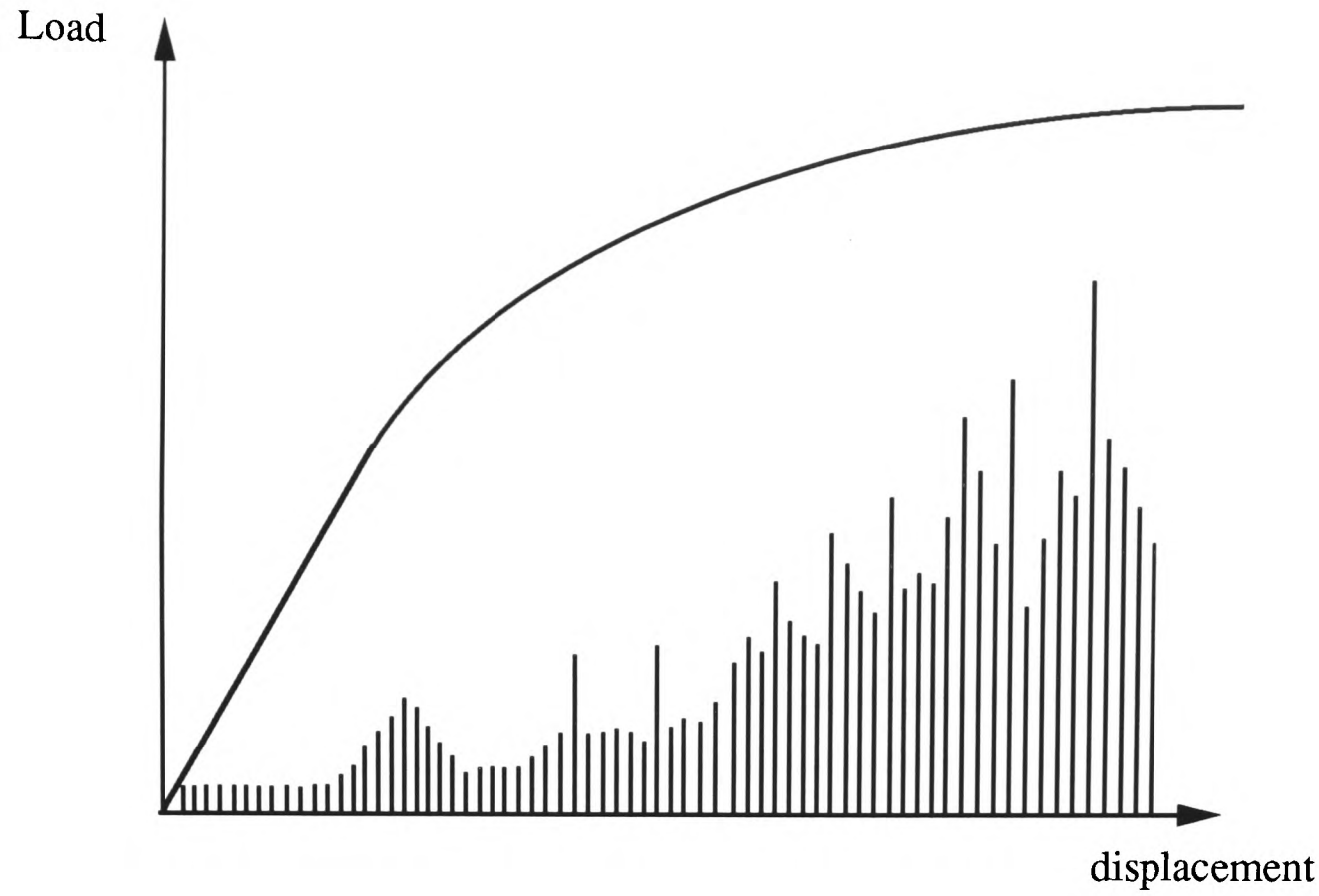

(a)

(b)

Figure 5.26a-b: Schematic reproductions of typical AE experiments containing in (a) 30 μm particles and in (b) 10 μm particles.

Figure 5.27: Mean Acoustic Event size as a function of time.

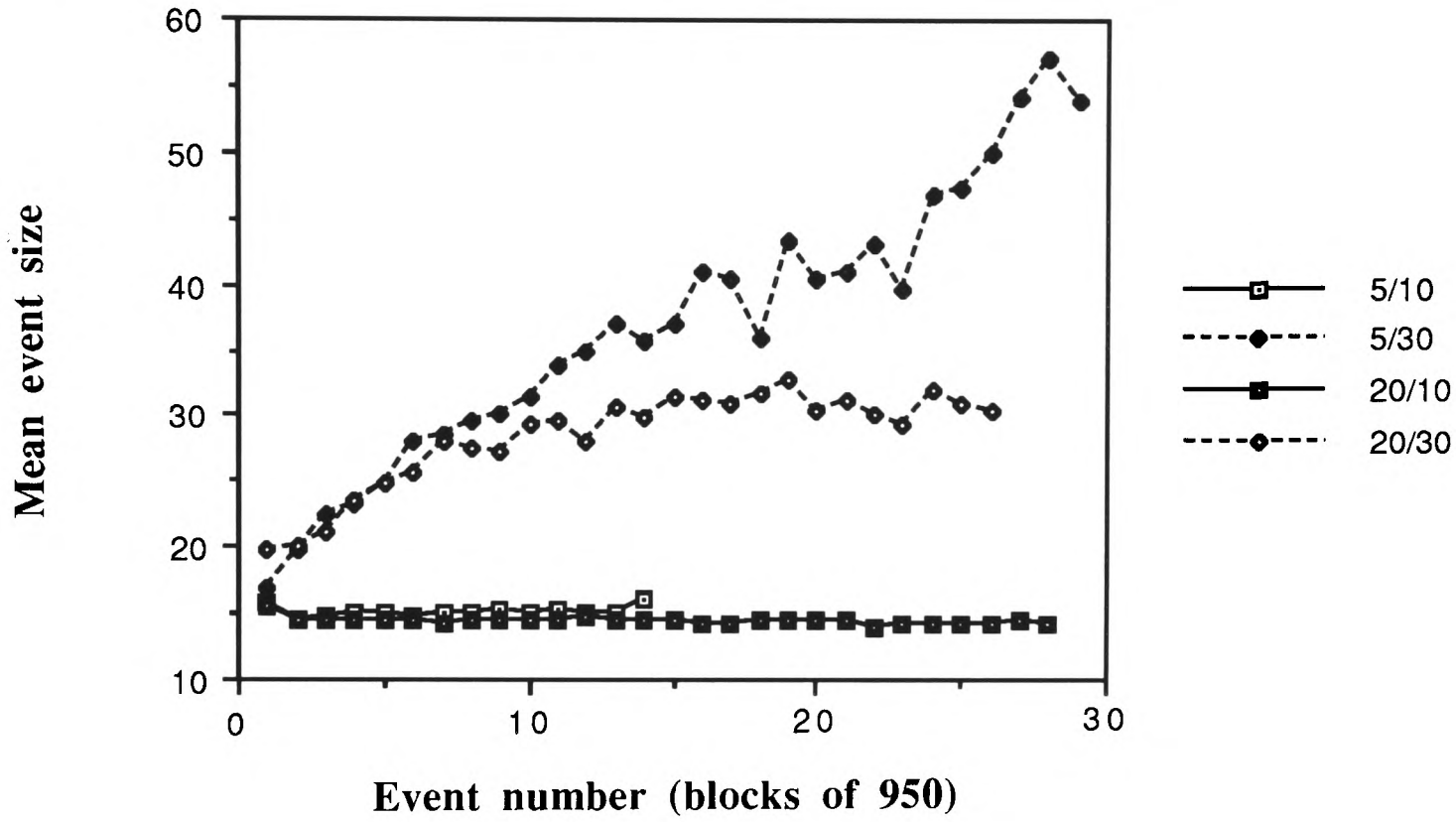

Specimen	No. of Events	Mean Event Size (Bin No)	2nd moment of Distribution	Integrated Signal
5/30/Qu	27690	33.65	2558.5	1544322
10/30/Qu	11142	18.75	680.71	299112
20/30/Qu	19080	21.90	961.42	938718
5/10/Qu	5388	11.02	183.49	62756
10/10/Qu	19398	9.98	151.83	293923
20/10/Qu	20424	10.69	137.36	421913
5/30/An	26070	36.64	2626.2	1590285
10/30/An	8550	22.48	835.42	289112
20/30/An	24228	28.29	1402.3	1444126
5/10/Qu	13098	15.05	259.40	233417
10/10/Qu	15894	14.94	270.93	306378
20/10/Qu	26178	14.52	227.93	628558

(a)

Table 5.1a-b: Quantitative Acoustic Emission data for (a) Al-5050 and (b) Al-1070 matrix composites.

Specimen	No. of Events	Mean Event Size (Bin No)	2nd moment of Distribution	Integrated Signal
5/30/Qu	2236	33.79	2711.77	994687
10/30/Qu	37524	22.57	981.99	125885
20/30/Qu	46548	32.40	2271.80	
5/10/Qu	10404	10.89	162.06	
10/10/Qu	12714	9.77	136.08	140490
20/10/Qu	11904	10.90	208.80	206336
5/30/An	19979	37.88	3060.30	1003269
10/30/An	37524	32.92	2180.60	1977425
20/30/An				
5/10/Qu	13308	15.23	255.20	239193
10/10/Qu	27996	15.17	274.57	550270
20/10/Qu	20424	14.79	251.94	463652

(b)

Chapter 6: Discussion and Suggestions for Further Work

6.1 Introduction

Chapter 1 showed that an enormous amount of effort has been expended by a large number of research groups on investigating the behaviour of PRMMCs, yet still many questions remained unanswered. In particular, the fracture properties and mechanisms are poorly understood. A study of the effects of systematic variations in reinforcement and matrix parameters on the fracture micromechanisms would at least address, if not solve, many of these problems. Such a study has been undertaken and the results presented in this thesis.

Commercial purity aluminium and a simple aluminium-magnesium solid solution alloy were chosen as model matrix materials to eliminate any possible complications from chemical or mechanical interactions which might obscure the effects of the reinforcing phase. Silicon carbide particles of size and volume fractions encompassing the current commercially favoured systems were chosen as reinforcements. The additional effect of residual dislocation density on mechanical and fracture properties was also considered by using simple quenching and annealing heat treatments.

The principal objective of the thesis was to elucidate the micromechanisms of fracture, and how they are affected by a variation in the microstructural parameters.

6.2 Experimental Results and their Implications for Fracture Mechanisms

Simple fractography was performed on matched fracture halves of the composites. This showed, in common with many previous studies, that fracture occurred by a ductile void nucleation, growth and coalescence mechanism. Transitions in the mode of failure from particle fracture to decohesion at the particle/matrix interface were seen on decreasing the particle size in composites of both alloy matrices. In addition, a similar transition from fracture to decohesion was observed on reducing the volume fraction of reinforcing phase from 20% to 5% for every particle size in the composites of the Al-5050 matrix material.

A simple critical stress criterion for void nucleation by particle fracture was proposed in the light of these results. Here nucleation proceeds by particle cracking when the local stress reaches the fracture stress of the particle. This follows the previous work on the fracture of brittle carbides in steels [200,209]. This explains the particle size dependence on mode of fracture adequately as there will be an increased probability of finding a critical sized flaw in the larger particles, thus reducing the average fracture stress. This simple stress criterion does not, however, explain the observed volume

fraction dependence on mode of failure. Work on dispersion-strengthened monolithic alloys has shown that the strain at which nucleation occurs is a strong function of the local volume fraction of second phase. This has been modelled by both continuum and dislocation mechanics approaches [25,141,232,233]. It is best described physically by the inability to relax stresses at the particle completely by the generation of secondary dislocations as their mobility is greatly reduced by the presence of dislocations generated about other particles. As the volume fraction of particles is increased, this impingement of one plastic zone upon another occurs at decreasing strains leading to the build-up of stresses at the interface at lower far-field strains. Thus, the reduction in volume fraction of reinforcing phase in the PRMMCs would only lead to the particle fracture stress being reached at greater far-field strains and, therefore, one would still expect the same mode of failure. This, however, assumes that the interfacial bond strength is independent of volume fraction of reinforcing phase. This will be held in systems where no interfacial reaction takes place, such as in the Al-1070 matrix composites, but may not be in systems where there is an interfacial reaction, such as the Al-5050 matrix composites. In the lower volume fraction composites there is a larger potential concentration of magnesium for a given surface area of silicon carbide, if segregation occurs, and so there may be an extended reaction or segregation process, reducing the interfacial bond strength. As discussed in Chapter 2, there is indeed evidence for magnesium segregation in the Al-5050 system. In this instance the stress criterion still holds for nucleation by decohesion. Alternatively, it may be argued that an additional strain criterion needs to be satisfied for nucleation by decohesion to occur. This has been proposed for nucleation by separation at the particle/matrix interface in a number of systems [141,232-234]. In materials containing a high volume fraction of second phase, the local stress is raised at the interface at lower far-field strains because relaxation processes are hindered. Thus, the critical stress for particle cracking may be attained before a secondary strain criterion for decohesion. In the composites of low volume fraction of reinforcing phase, such a strain criterion for decohesion may be met.

Void growth models developed for the ductile rupture process in monolithic alloys suggested that void nucleation would be the dominant event controlling ductility in materials containing a high volume fraction of second phase. Indeed, the model of Brown and Embury would have predicted zero growth strain for a material containing a volume fraction of 20% of second phase [139]. The void nucleation process in PRMMCs had not been isolated and determined. Models of failure in PRMMCs were also divided by the order in which fracture events occurred. Most workers, for example [28,40,73,91], assumed fracture followed the same sequence in PRMMCs as in monolithic alloys, namely nucleation at the second phase, with the subsequent failure of the matrix. You *et al.* [71] argued that the increased levels of stress and plastic constraint imposed by the reinforcing phase on the matrix led to void nucleation in the matrix first, with the final stage of fracture being the failure of the particles. Thus, it seemed important to

study the nucleation stage and preferably before any macroscopic crack had been formed. *In situ* SEM fracture studies were performed to this end.

By loading a notched specimen in a constant displacement, double cantilever arrangement, the accumulation of microstructural damage prior to nucleation as well as the nucleation process itself could be studied. This showed that nucleation was associated with the reinforcing phase, confirming the assumption of a similar order of fracture processes in PRMMCs and monolithic alloys, and that nucleation occurred before a macroscopic crack had formed. In addition, crack propagation was studied. Microcracked areas were found ahead of and near to the crack tip associated with a region of intense deformation there. These regions extended some tens of interparticle spacings from the crack tip. Crack propagation was shown to occur by a process whereby some of these microcracks join via matrix failure ahead of the original crack tip, concurrent with the initiation of additional microcracks ahead of the crack. This led to other experimental findings, such as crack branching and bridging. Similar results to these have also been reported in other *in situ* studies [76,130-132] and fatigue crack studies [205-207]. However, some further observations cast doubt on the validity of studying fracture processes in the plane stress conditions on a free surface. Before crack initiation, the surface became highly rippled, relieving the stress by deformation out of the plane. This stress relief mechanism would be unavailable in the bulk of the material. The crack path also appeared to avoid the particles, even if they were already fractured. Wu and Arsenault used results similar to this to suggest that the crack only passed through particles that had been broken during fabrication so that no new fracture events occurred on straining [132]. This is clearly untrue. The acoustic microscopic studies of extruded composite revealed negligible fabrication damage in this study, whereas the matched fracture halves clearly show particle fracture to occur with the large reinforcement sizes. A technique to study the crack propagation in the bulk of the material had to be developed to verify the results of the *in situ* experiments, a step that no-one else had taken. This was performed by sectioning stable cracks which had been loaded in a similar manner to the *in situ* tests.

Sectioning revealed characteristics of the crack propagation sequence similar to those found during *in situ* straining. Nucleation events were observed ahead of the crack tip, showing that the discontinuities in the crack on the surface do continue into the bulk of the material. However, the extent of deformation was greatly reduced, being restricted to one or two interparticle spacings. The features associated with the large deformation region on the surface, such as crack branching, were also not present. On moving into the body of the specimen, the condition ahead of the crack tip changes from plane stress to plane strain. The imposition of the plane strain condition reduces the size of the plastic zone ahead of the crack tip and, therefore, decreases the extent of the region of intense deformation. The particles are loaded by shear stresses due to

matrix flow at the particle/matrix interface and it may be reasoned, therefore, that the region of microcracking is reduced as the region of intense matrix flow is reduced. Shang and Ritchie, in their study of fatigue crack propagation in PRMMCs, showed that there was a threshold value of ΔK below which crack bridging by uncracked matrix ligaments did not occur [205-207]. This was associated with a reduction in plastic zone size and, therefore, volume of material containing brittle particles sampled by the crack. If a small volume is sampled by the crack, the opportunities for substantial microcracking leading to crack branching are lowered until they do not occur. The same crack propagation sequence was seen in the sections and the *in situ* tests, supporting the validity of these results obtained during *in situ* straining. However, the nucleation processes may be affected by the plane stress conditions. A technique for studying void nucleation in the bulk of the specimen in real time also needed to be developed. The monitoring of acoustic emissions during straining was chosen. This again was a new experiment capable of producing valuable data to enable an understanding of the fracture process.

The acoustic emission monitoring revealed that void nucleation occurred first at the onset of deviation from linearity and continued throughout the entire region of plastic deformation until final failure of the specimen. This emphasised the importance of the local values of reinforcing particle size and volume fraction in determining the far-field strain at which void nucleation occurs. Another manifestation of this early nucleation was seen in the results of the mechanical testing. It was found that the modulus of the PRMMCs varied with strain, falling by significant amounts on increased strain. This was associated with a reduction in the load-bearing capacity of the reinforcing phase on failure either by particle fracture or by decohesion. This has also been reported very recently by other workers [83,121]. In addition, these results indicate that the nucleation stage does not play such a dominant rôle determining the fracture strain. Verification of this finding has come from studying the deformation of PRMMCs under an applied hydrostatic pressure, where substantial increases in the elongation to failure have been reported [77,80,134,136,235,236]. The void nucleation mechanism was unaffected and the increases in ductility have been associated with the suppression of void growth processes. These results pose two questions; what are the local conditions at void nucleation and why is there substantial void growth?

Attempts to address these questions were made by sectioning along the gauge lengths and through the fracture surfaces of failed tensile specimens. As there was local deformation through necking, the sections show the strain history of the specimen. These sections revealed a number of interesting features which helped to clarify a few points. First, the extent of damage below the fracture surface was less in these sections than in the corresponding studies of the surface of the gauge length. This is again a feature of the increased plastic constraint associated with the plane strain conditions in

the body of the specimen. Secondly, fractured 30μm particles were observed further from the fracture surface, that is at lower far-field strains, than 10μm particles in the same matrix alloy. This is in accordance with the proposition of a critical stress criterion for void nucleation by particle cracking with a range of particle fracture stresses as the far-field strain is the same. This received additional support from the observation that there was greater damage at similar strains in composites of the higher yield strength matrix. Thirdly, void nucleation was found at lower far-field strains in regions of high local volume fraction. As discussed earlier in this chapter, the stress relaxation mechanisms at the particles are hindered in these areas by the presence of the surrounding particles and their own plastic zones. Additionally in PRMMCs, these regions are also likely to contain the highest residual dislocation densities, generated to maintain the displacement compatibility across the particle/matrix interface on cooling from the fabrication temperatures, increasing further the local stresses at lower strains [4,5,7]. Fourthly, the void growth from fractured particles was highly constrained to the width of the particle, with very little lateral growth at all. This seems to suggest that the void coalescence process is greatly inhibited by the presence of the still rigidly-bonded interfaces. Additional plastic flow must occur before this constraint is overcome and void coalescence by shear linkage becomes possible. It should also be noted that in the composite systems where void nucleation by decohesion occurred, the size of voids revealed on sectioning was much smaller than in those where nucleation was by cracking. This may just be a result of the reduced strain to failure of these composites or it may be that void coalescence occurs at lower strains and, therefore, there is smaller void growth. The third and fourth points are worthy of further discussion.

The spatial distribution of reinforcing phase has been shown to have a marked effect on the mechanical and fracture properties of PRMMCs [50-54,111,237]. Non-uniformities in void distributions have also been shown to affect the void nucleation and growth processes in dispersion-strengthened alloys, for example [22,25,238-245]. Both Fisher and Gurland [238] and Teirlinck *et al.* [239] have also considered the use of the particle size distribution to describe the progressive nucleation of voids, similar to the experimental results reported here. This can be considered systematically (Figure 6.1) as a reaction front passing through the particle size distribution at a rate dependent on both the level of plastic strain and the hydrostatic stress level. It should be noted that the hydrostatic stress level considered here is a strong function of local volume fraction as the plastic constraint is greatest. Thus, damage occurs due to the progression of the nucleation and the growth of voids. The spatial distribution of voids has been shown to affect void growth. Models for the flow in void-containing, elastic-plastic matrices show that flow localisation, and, therefore, ultimate ductility, is highly sensitive to the non-uniformity of the void distribution and also to the degree of stress triaxiality [240].

Thus, the experimental findings may be summarised. Fracture in PRMMCs has been shown to proceed by a void nucleation, growth and coalescence mechanism. Void nucleation appears to be controlled by a simple critical stress criterion, which has led to changes in the failure mode on reducing particle size. A change in failure mode on increasing volume fraction in the composites of an Al-5050 matrix may provide evidence for combined stress and strain criteria at decohesion or may be the result of an enhanced reaction at or segregation to the particle/matrix interface. *In situ* SEM fracture studies have revealed that the crack propagation mechanisms appear to be controlled by the extent of matrix deformation ahead of the crack tip. Propagation progressed by the simultaneous failure of matrix ligaments and formation of microcracked regions ahead of the crack tip. Acoustic emission studies have shown void nucleation occurring at low levels of plastic strain and continuing throughout the plastic regime. This, with support from micrographs of sections through failed tensile specimens and reductions in modulus on straining, suggests that damage occurs by progressive void nucleation continuing with matrix deformation and growth processes. The local values of volume fraction and particle size are seen to be critical in determining the far-field strain at which void nucleation occurs. Void coalescence between cracked particles is inhibited by the presence of rigidly-bonded interfaces. This extends void growth strain before final failure of the material.

6.3 Final Conclusions and Suggestions for Further Work

Fracture in PRMMCs shows similar characteristics to fracture in dispersion-strengthened alloys. However, the experimental observations suggest that specific modifications to existing models of ductile rupture processes must be made before they can adequately describe the fracture behaviour of PRMMCs. In particular, the process of continuous nucleation and growth during straining needs consideration. This makes the adoption of a fixed far-field strain at nucleation inappropriate. A description based upon the percolation of damage seems more appropriate.

The experimental observations have shown that the far-field strain at which void nucleation occurs is a strong function of the local values of reinforcing particle size and volume fraction. The nucleation process appears to be described by a simple critical stress criterion. Therefore, models of the stress state as a function of these local values of volume fraction and size of reinforcing phase need to be developed. Models based on any mean-field approximation, such as the Eshelby technique, are necessarily unable to model the local distributions. The understanding of dislocation mechanics at this high level of dislocation interaction is limited, and so it appears that continuum techniques such as the finite element method must be used. Argon *et al.* have developed a combined finite element and micromechanical model for such a situation [25]. Here, secondary dislocations are assumed to be punched from the interface of a non-deforming

particle in an elastic-perfectly plastic matrix. They account for interactions between the particles by assuming an opposing friction force through which the dislocations must move. This increases the local stress at the particle for a given applied strain. Christman *et al.* have considered simple cell arrangements in an attempt to model local inhomogeneities in the particle spatial distribution [111]. They see the local hydrostatic stress increasing in these clustered regions which will promote void nucleation at lower strains. However, much further work is needed here as the models proposed do not truly represent clustering but instead impose peroidic structures of repeat unit greater than the simplest unit of the matrix around one reinforcement. Much larger units of microstructure must be modelled to represent inhomogeneities. A major limitation of all continuum models was discussed in Chapter 3, namely that for accurate modelling of the bulk properties of PRMMCs, the constitutive relation of the metal must be known. It is not clear that there is sufficient understanding of matrix properties to be fully predictive.

The void coalescence mechanism appears to be inhibited in the composites where particle cracking has occurred. This manifested itself in the measurements of elongation to failure. In the composites containing a low volume fraction of reinforcing phase, where there is substantial void growth, an increase in ductility was seen as the nucleation mechanism changed from decohesion to particle fracture. This effect may only be seen in materials such as pure aluminium with very low yield stresses as the local stress concentration at the crack may be blunted by the motion of dislocations. To verify whether this is an effect of the specific system considered here or a more general result, the matrix flow about an inclusion containing a crack must be modelled. This should also be further extended to consider the effect of surrounding particles, some cracked, on the cracked particle. This is, again, best left to the realms of finite element modelling, but with the realisation that large units of the microstructure need to be considered to accurately reflect local constraints.

The spatial distribution of the reinforcing phase within the parent material determines the importance of each of the above results. The experiments have shown that void nucleation in itself is far from catastrophic, with additional strains of greater than 20% recorded before final fracture. Void coalescence has been shown to occur between particles which are close to one another but inhibited in other situations. These results suggest two approaches to describing the final failure in PRMMCs.

The continuous nucleation and simultaneous growth of voids implies steadily increasing microstructural damage. Thus, it may be appropriate to consider final fracture to occur at some critical value of a damage parameter. Such descriptions have been made of failure processes [246] and they may be invoked to describe failure in PRMMCs. The damage parameter could be identified with, perhaps, two measurable

quantities, namely the reduction in modulus on straining or the integrated acoustic emission.

The fracture process may also be considered as the percolation of damage through clustered regions with final failure occurring when these isolated regions coalesce. The regions of lowest interparticle spacing nucleate voids first. On increased straining these voids grow whilst nucleation occurs in regions of increased interparticle spacing. The critical factor determining total failure of the specimen would be the spatial relationship between these regions. If they were isolated then significant strain may be applied before any linkage between regions occurs. If, however, a path through the microstructure joining these regions could be found, then a smaller strain would occur before failure. This interpretation fits the experimental observations and reveals the importance of the spatial distribution of the particles. It also is the most physical representation of the fracture process. Such a description would necessarily combine the models of local stress and constrained void growth with a global parameter which characterises the spatial distribution of the particles. This model would have the benefit of giving a prediction of material performance without the need for performing destructive tests and may provide a means of on-line quality control at the fabrication stage. It is, however, fraught with theoretical problems. Apart fom the model development described earlier, a method for the quantitative description of the spatial distribution of a second phase within a parent material needs to be developed. This problem has eluded solution so far despite extensive analysis. In addition, a parameter, such as a critical density of locally high volume fraction regions, needs to be developed and identified with known material parameters.

Further experimental work is also required. Methods to check the predictions of the models of local stress state and plastic constraint need to be developed. These necessarily involve the sampling or observation of local properties. The local values of hardness and modulus on approaching a particle/matrix interface may be determined by the use of nanoindenting techniques, providing a measure of the matrix constraint. Here volumes $<1\mu m^3$ may be sampled. However, problems are associated with nanoindenting since the indentation is on the scale of the matrix sub-cell structure. Further *in situ* SEM experiments may be performed. The strain distribution around a particle could be determined by studying the deformation of a grid on the surface. Grids of $1\mu m$ spacing can quite easily be laid, providing information right up to the particle/matrix interface. Both techniques, however, sample the surface of the material which is in a plane stress condition. Care would need to be taken in interpreting the results from such experiments.

Any technique developed to describe quantitatively the spatial distribution of the reinforcing phase must be linked with a measurable property of the composite. Material

with varying degrees of inhomogeneity may be fabricated. This may be achieved by a number of routes. Mixing differing sizes of silicon carbide particles within a given matrix powder would produce an inhomogeneous distribution. The difference in sizes could be a measure of the inhomogeneity. Widely different matrix and reinforcement powder sizes could also be used. Here, the particles would be forced onto the periphery of the matrix grains in a sort of "necklacing" effect. In addition, differing extrusion ratios may be tried. The spatial distribution would be characterised and the mechanical properties of the composite measured.

An experiment to determine whether the decohesion observed on decreasing volume fraction in the Al-5050 matrix composites was an artefact of extended interfacial reaction needs to be performed. It was postulated that the increased volume fraction of reinforcing phase raised the local stress for lower far-field strains to such an extent that a critical strain criterion for decohesion could not be met. It may be possible to raise the local stress for a given far-field strain in the low volume fraction materials by using specimens of a constrained geometry, such as notched or waisted tensile specimens. If a transition to particle cracking was observed then it may be reasoned that an additional strain criterion needs to be satisfied for void nucleation by interfacial decohesion.

The acoustic emission technique has been shown to provide essential information on the fracture processes. Further applications of the technique may be to define a damage parameter, as described earlier, or in the study of the effects of hydrostatic pressure on deformation and fracture. The increased elongation to failure observed in these studies is, at present, associated with a suppression of void growth processes. However, void nucleation may be affected as well. Acoustic emission could be applied successfully to show if this is the case.

In conclusion, it can be seen that as many questions have been raised as have been answered by this study.

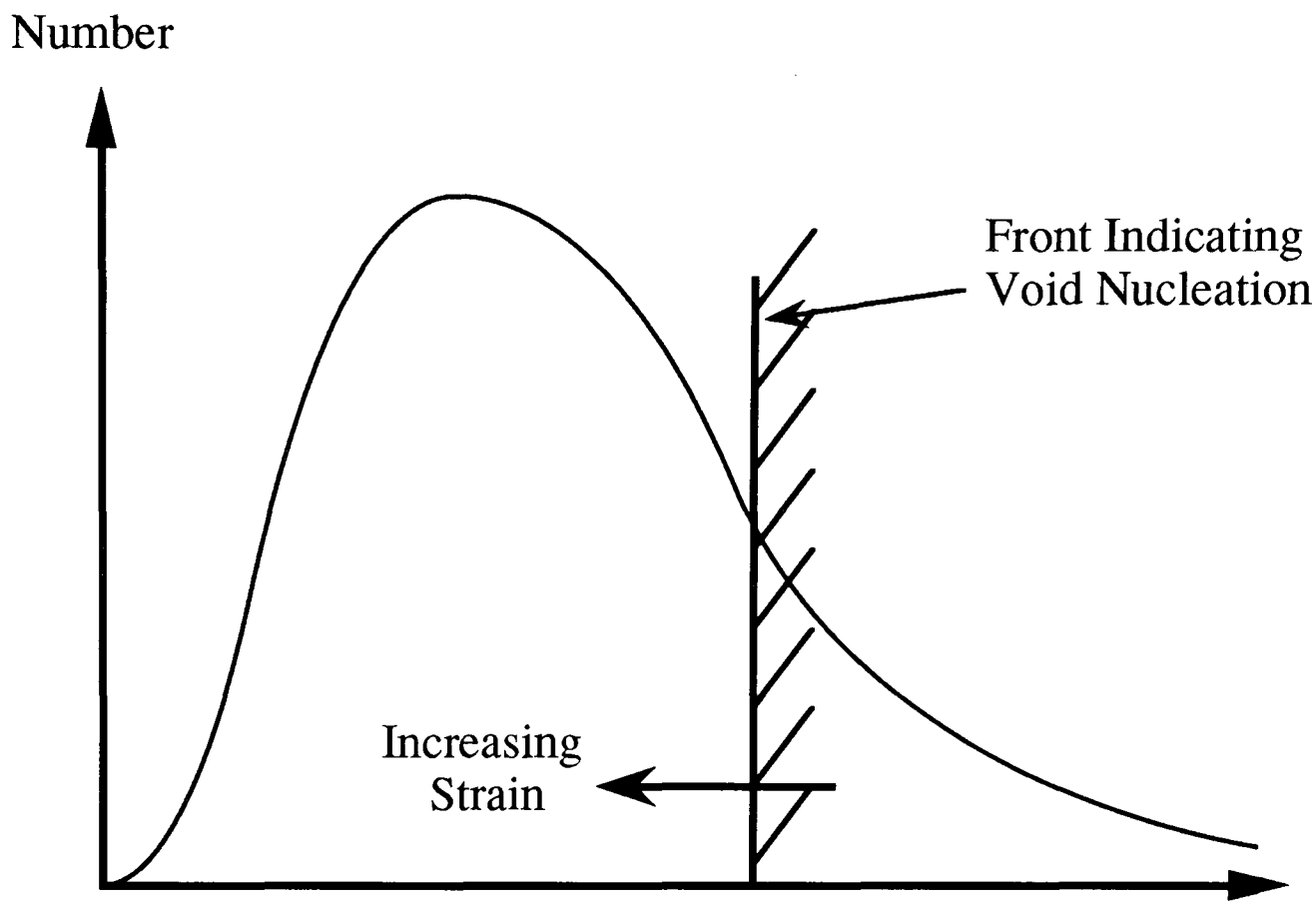

Figure 6.1: The Effect of the Particle Size Distribution on the Void Nucleation Size

Appendix B:

Mechanical Properties of Al-1070 and Al-5050 Composites

Table B.1. 0.05% and 0.2% proof stresses (in MPa) of Al-5050 matrix composites under annealed (A) and quenched (Q) conditions.

Particle size (μm)		Volume fraction (%)					
		5		10		20	
		Q	A	Q	A	Q	A
3	0.05	-	100	112	105	126	112
	0.2	-	142	148	135	174	142
10	0.05	114	-	109	113	117	112
	0.2	147	-	146	140	157	148
30	0.05	112	-	113	-	112	112
	0.2	146	-	140	-	152	146

Table B.2. 0.05% and 0.2% proof stresses (in MPa) of Al-1070 matrix composites under annealed (A) and quenched (Q) conditions.

Particle size (μm)		Volume fraction (%)					
		5		10		20	
		Q	A	Q	A	Q	A
3	0.05	94	54	98	76	101	85
	0.2	125	66	128	99	135	116
10	0.05	77	-	84	60	98	54
	0.2	113	-	125	75	126	79
30	0.05	73	42	77	48	79	58
	0.2	99	50	100	57	109	76

Table B.3. Modulus (GPa) of Al-5050 matrix composites, quenched, measured during unloading (U) and reloading (R).

Particle size (μm)	Volume fraction (%)					
	5		10		20	
	U	R	U	R	U	R
3	-	-	108	106	122	121
10	98	97	108	109	127	126
30	99	97	108	107	124	121

Table B.4. Modulus (GPa) of Al-5050 matrix composites, annealed, measured at given strains, during unloading (U) and reloading (R).

Particle size (μm)	Volume fraction (%)								
	5			10			20		
	U	R		U	R		U	R	
3	101	102	0.25%	111	108	0.25%	123	122	0.31%
	101	99	0.47%	109	107	0.57%	120	120	0.59%
	101	93	0.70%	107	102	0.89%	-	-	
10	-	-		107	107	0.28%	131	129	0.2%
				108	106	0.56%	129	124	0.39%
				104	106	0.84%	128	120	0.02%
							127	120	0.85%
30	-	-		-	-		126	123	0.23%
							125	117	0.47%
							121	114	0.79%

Table B.5. Modulus (GPa) of Al-1070 matrix composites under annealed (A) and quenched (Q) conditions.

Particle size (μm)	Volume fraction (%)			
	5		20	
	Q	A	Q	A
3	71	69	98	96
10	-	-	97	97
30	70	68	98	97

Table B.6 Primary work-hardening exponents (n^I) and coefficients (k, GPa) of Al-5050 matrix composites in the quenched (Q) and annealed (A) state.

Particle size (μm)		Volume fraction (%)					
		5		10		20	
		Q	A	Q	A	Q	A
3	n^I	0.84	0.77	0.88	0.90	0.96	0.94
	k (GPa)	24.8	20.0	-	47.8	136	83.2
10	n^I	0.81	-	0.85	0.97	0.87	0.86
	k (GPa)	26.5	-	42.0	64.7	59.1	47.1
30	n^I	0.80	-	0.84	-	0.85	0.82
	k (GPa)	24.7	-	34.5	-	38.3	36.2

Table B.7 Primary work-hardening exponents (n^I) and coefficients (k, GPa) of Al-1070 matrix composites in the quenched (Q) and annealed (A) state.

Particle size (μm)		Volume fraction (%)					
		5		10		20	
		Q	A	Q	A	Q	A
3	n^I	0.87	0.85	0.81	-	0.91	0.88
	k (GPa)	31.1	9.7	38.2	-	40.6	31.7
10	n^I	-	-	0.58	0.80	0.85	0.82
	k (GPa)	-	-	6.8	24	35.0	18.5
30	n^I	0.86	0.66	0.70	-	0.82	0.78
	k (GPa)	24.1	3.5	11.8	-	21.5	?

Table B.8 Secondary work-hardening exponents (n^S) and coefficients (k, GPa) of Al-5050 matrix composites in the quenched (Q) and annealed (A) state.

Particle size (μm)		Volume fraction (%)					
		5		10		20	
		Q	A	Q	A	Q	A
3	$n^{(S)}$	0.153	0.067	0.151	0.095	0.204	0.186
	k (GPa)	0.36	0.21	0.35	0.24	0.57	0.45
10	$n^{(S)}$	0.120	-	0.146	0.090	0.16	0.143
	k (GPa)	0.28	-	0.24	0.32	0.41	0.33
30	$n^{(S)}$	0.046	-	0.064	-	0.108	0.081
	k (GPa)	0.19	-	0.21	-	0.30	0.26

Table B.9 Secondary work-hardening exponents (n^S) and coefficients (k, GPa) of Al-1070 matrix composites in the quenched (Q) and annealed (A) state.

Particle size (μm)		Volume fraction (%)					
		5		10		20	
		Q	A	Q	A	Q	A
3	$n^{(S)}$	0.092	0.252	0.157	-	0.17	-
	k (GPa)	0.20	0.28	0.40	-	0.37	-
10	$n^{(S)}$	-	-	0.102	0.095	0.16	0.209
	k (GPa)	-	-	0.23	0.21	0.31	0.29
30	$n^{(S)}$	0.081	0.252	0.086	-	0.130	0.188
	k (GPa)	0.16	0.21	0.17	-	0.24	0.23

Table B.10. Elongation to failure (%) of Al-1070 matrix composites in the quenched (Q) and annealed (A) state.

Particle size (μm)	Volume fraction (%)					
	5		10		20	
	Q	A	Q	A	Q	A
3	23.5	26.4	20.1	21.3	17.0	18.5
10	-	-	20.1	20.8	66.8	18.3
30	25	28.2	19.1	19.7	16.5	18.1

Table B.11. Elongation to failure (%) of Al-5050 matrix composites in the quenched (Q) and annealed (A) state.

Particle size (μm)	Volume fraction (%)					
	5		10		20	
	Q	A	Q	A	Q	A
3	15.6	17.0	12.1	13.6	10.7	12.5
10	13.2	15.6	10.2	12.8	9.5	11.4
30	11.8	13.1	8.4	9.0	5.9	7.6

References

1 Chou, T. W., Kelly, A., and Okura, A., *Composites* **16**, 187 (1983).

2 Feast, E. A., *Metals and Materials*, p.273, May (1988).

3 Jarry, P., Loué, W., and Bouvaist, J., *Proc. ICCM-VI*, eds. F. L. Mathews *et al.*, 2, 2.350. Elsevier, Amsterdam (1987).

4 Arsenault, R. J. and Shi, N., *Mat. Sci. Eng.* **81**, 175 (1986).

5 Arsenault, R. J., *Mat. Sci. Eng.* **64**, 171 (1984).

6 Arsenault, R. J. and Fisher, R. M., *Scr. Metall.* **17**, 67 (1983).

7 Vogelsang, M., Arsenault, R. J., and Fisher, R. M., *Met. Trans* **17A**, 379 (1986).

8 Fu, L.-J., Schmerling, M., and Marcus, H. L., in "*Composite Materials, Fatigue and Fracture*", ed. H. T. Hahn, *ASTM STP* **907**, p. 51 (1986).

9 Arsenault, R. J. and Pande, G. S., *Scr. Metall.* **18**, 1131 (1984).

10 Nutt, S. R. and Carpenter, R. W., *Mat. Sci. Eng.* **75**, 169 (1985).

11 Withers, P. J., Stobbs, W. M., and Bourdillon, A. J., *J. Microscopy* **151**, 159 (1988).

12 Cao, L., Geng, L., Yao. C. K., and Lei, T. C., *Scr. Metall.* **23**, 227 (1989).

13 Mahon, G. J., Howe, J. M., and Vasudevan, A. K., *Acta Metall.* **38**, 1503 (1989).

14 Rack, H. J., *Proc. ICCM-VI*, eds. F. L. Mathews *et al.*, **2**. 2.382. Elsevier, Amsterdam (1987).

15 Christman, T. and Suresh. S., *Acta Metall.* **36**, 1691 (1988).

16 Rack, H. J., Mullins, J. W., in "*High Strength Powder Aluminium Metallurgy Alloys II*", eds. M. Koczak and G. Holdemann, TMS, Warrendale, PA, p. 155.

17 Dutta, I. and Bourell, D. L., *Mat. Sci. Eng.* **A112**, 67 (1989).

18 Dutta, I., Bourell, D. L., and Latiner, D., J. *Comp. Mater.* **27**, 827 (1988).

19 Friend, C. M. and Luxton, S. D., J. *Mat. Sci.* **23**, 3173 (1988).

20 Nieh, T. G. and Karlak, R. F., *Scr. Metall.* **18**, 25 (1984).

21 Flom, Y. and Arsenault, R. J., *Mat. Sci. Eng.* **77**, 191 (1986).

22 LeRoy, G., Embury, J. D., Edward, G., and Ashby, M. F., *Acta Metall.* **29**, 1509 (1989).

23 Argon, A. S., Im, J., and Needleman, A., *Met. Trans.* **6A**, 815 (1975).

24 Argon, A. S. and Im, J., *Met. Trans.* **6A**, 839 (1975).

25 Argon, A. S., Im, J., and Safoglu, R., *Met. Trans.* **6A**, 825 (1975).

26 Broutman, L. J. and Krock, H., *Compos. Mater.* **1**, 57 (1974).

27 McDanels, D. L., *Met. Trans.* **16A**, 1105 (1985).

28 Nair, S. V., Tien, J. K., and Bates, R. C., *Int. Met. Rev.* **30**, 275 (1985).

29 Girot, F. A., Quenisset, J. M., and Naslain, R., *Comp. Sci. Tech.* **30**, 155 (1987).

30 Majumdar, B. S., Yegneswaran, A. H., and Rohatgi, P. K., *Mat. Sci. Eng.* **68**, 85 (1984).

31 Ribes, H., Suery, M., L'Esperance, G., and Legoux, J. G., *Met. Trans.* **21A**, 2489 (1990).

32 Henriksen, B. R. and Johnsen, T. E., *Mat. Sci. Tech.* **6**, 857 (1990).

33 Peteves, S. D., Tambuyser, P., Helbach, P., Audier, M., Laurent, V., and Chatain, D., *J. Mat. Sci.* **25**, 3765 (1990).

34 L.-Cao, L.-Geng, Yao, C. K., and Lei, T. C., *Scr. Metall. Mater.* **23**, 227 (1989).

35 Shieu, F.-S., Raj, R., and Sass, S. L., *Acta Metall. Mater.* **38**, 2215 (1990).

36 Lloyd, D. J., *Comp. Sci. Tech.* **35**, 159 (1989).

37 Dutta, I., Tiedemann, C. F., and McNelley, T. R., *Scr. Metall. Mater.* **24**, 1233 (1990).

38 Nakagawa, A. H. and Gungor, M. N., in "*Fundamental Relations between Microstructures and Mechanical Properties in Metal Matrix Composites*", eds. M. N. Gungor and P. Liaw, TMS, Warrendale, PA, p.127 (1989).

39 Birt, M. J. and Johnson, W. S., in "*Fundamental Relations between Microstructures and Mechanical Properties in Metal Matrix Composites*", eds. M. N. Gungor and P. Liaw, TMS, Warrendale, PA, p.71 (1989).

40 Nieh, T. G., Rainen, R. A., and Chellman, D. J., *Proc. ICCM-V*, eds. W. C. Harrigan Jr. *et al.*, TMS, Warrendale, PA, p. 825 (1985).

41 Fujita, Y., Fukumoto, H., and, Kurita, Y., *Proc. ICCM-VI*, eds. F. L. Mathews *et al.*, **2**, 2.340. Elsevier, Amsterdam (1987).

42 Sun, J. and Greenfield, I. G., *Proc. ICCM-VI*, eds. F. L. Mathews *et al.*, **2**, 2.287. Elsevier, Amsterdam (1987).

43 Weaire, D. and Rivier, N., *Contemp. Phys.* **25**, 59 (1984).

44 Thomson, D. A. W., "*On Growth and Form*", Cambridge University Press (1942).

45 Smith, C. S., *Scientific American* **190**, 58 (1954).

46 Dormer, K. J., "*Fundamental Tissue Geometry for Biologists*", Cambridge University Press (1980).

47 Stevens, P. S., "*Patterns in Nature*", Atlantic-Little (1974).

48 Getis, A. and Books, B., "*Models of Spatial Processes*", Cambridge University Press (1979).

49 Rivier, N., in "*Thermodynamics and Pattern Formation in Biology*", Walter de Greyter, p. 447 (1988).

50 Wray, P. J., Richmond, O., and Morrison, H. L., *Metallography* **16**, 39 (1983).

51 Hunt Jr., W. H., Richmond, O., and Young, R. D., *Proc. ICCM-VI*, eds. F. L. Mathews *et al.*, **2**, 2.209. Elsevier, Amsterdam (1987).

52 Lewandowski, J. J., Liu, C., and Hunt Jr., W. H., in "*Processing and Properties for Powder Metallurgy Composites*", eds. M. Kumar *et al.*, TMS, Warrendale, PA, p. 117 (1988).

53 Spitzig, W. A., Kelly, J. F., and Richmond, O., *Metallography* **18**, 235 (1985).

54 Lewandowski, J. J., Liu, C., and Hunt Jr., W. H., *Mat. Sci. Eng.* **A107**, 241 (1989).

55 Ackermann, L., Charbonnier, J., Desplanches, G., and Koslowski, H., *Proc. ICCM-V*, eds. W. C. Harrigan Jr. *et al.*, TMS, Warrendale, PA, p. 687 (1985).

56 Divecha, A. P., Fishman, S. G., and Karmarkar, S. D., *J. Metals* **33**, 12 (1981).

57 Fukunaga, H., Goda, K., Kurita, Y., and Fujita, Y., *Proc. ICCM-VI*, eds. F. L. Mathews *et al.*, 2, 2.362. Elsevier, Amsterdam (1987).

58 Kuruvilla, A. K., Prasad, K. S., Bhanuprasad, V. V., and Mahajan, Y. R., *Scr. Metall. Mater* **24**, 873 (1990).

59 Nutt, S. R. and Duva, J. M., *Scr. Metall.* **20**, 1055 (1986).

60 Pandey, A. B., Mishra, R. S., and Mahajan, Y. R., *Scr. Metall. Mater.* **24**, 1565 (1990).

61 Pillai, U. T. S., Pandey, R. K., and Rohatgi, P. K., *Eng. Frac. Mech.* **28**, 461 (1987).

62 Pillai, U. T. S., Pandey, R. K., and Nigram, K. D. P., *Proc. ICCM-V*, eds. W. C. Harrigan Jr. *et al.*, TMS, Warrendale, PA, p. 895 (1985).

63 Ramichandran, K. S. and Dwarcikadasa, E. S., *J. Metals* **39**, 28 (1987).

64 Sakamoto, A., Hasegawa, H., and Minoda, Y., *Proc. ICCM-V*, eds. W. C. Harrigan Jr. *et al.*, TMS, Warrendale, PA, p. 699 (1985).

65 Froes, F. H., *J. Metals* **40** (11), 12 (1988).

66 Smith, P. R. and Froes, F. H., *J. Metals* **36** (3), 19 (1984).

67 Fleischer, R. L., *J. Mat. Sci.* **22**, 2281 (1987).

68 Taub, A. I. and Fleischer, R. L., *Science* **243**, 616 (1989).

69 Sauthoff, G., Z. *Metallk.* **77**, 654 (1986).

70 Lewis, M. A. K., Hill, M. A., Rollett, A. D., Dunn, P. S., and Mortensen, A., in "*Fundamental Relations between Microstructures and Mechanical Properties in Metal Matrix Composites*", eds. M. N. Gungor and P. Liaw, TMS, Warrendale, PA, p.761 (1989).

71 You, C. P., Thompson, A. W., and Bernstein, I. M., *Scr. Metall.* **21**, 181 (1987).

72 Davidson, D. L., *Met. Trans.* **18A**, 2115 (1987).

73 Crowe, C. R., Gray, R. A., and Hasson, D. F., *Proc. ICCM-V*, eds. W. C. Harrigan Jr. *et al.*, TMS, Warrendale, PA, p. 843 (1985).

74 Dixon, D. G., *Scr. Metall. Mater.* **24**, 577, (1990).

75 Kamat, S. V., Hirth, J. P., and Mehrabian, R., *Scr. Metall.* **23**, 523 (1989).

76 Manoharan, M. and Lewandowski, J. J., *Scr. Metall.* **23**, 1801 (1989).

77 Liu, D. S., Manoharian, M., and Lewandowski, J. J., *J. Mat. Sci. Lett.* **8**, 1447 (1989).

78 Doong, S. H., Lee, F. C., Robertson, I. M., and Birnbaum, H. K., *Scr. Metall.* **23**, 1413 (1989).

79 Roebuck, B., J. *Mat. Sci. Lett.* **6**, 1138 (1987).

80 Liu, D. S., Manoharian, M., and Lewandowski, J. J., *Scr. Metall.* **23**, 253 (1989).

81 Papazian, J. M. and Alder, P. N., *Met. Trans.* **21A**, 401 (1990).

82 Nieh, T. G. and Chellman, D. J., *Scr. Metall.* **18**, 925 (1984).

83 Lloyd, D. J., *Acta Metall. Mater.* **39**, 59 (1991).

84 Humphreys, F. J., in "*Mechanical and Physical Behaviour of Metallic and Ceramic Composites*" eds. S. I. Anderson *et al.* Risø National Laboratory, Denmark, p.25 (1988).

85 Miller, W. S. and Humphreys, F. J., in "*Fundamental Relations between Microstructures and Mechanical Properties in Metal Matrix Composites*", eds. M. N. Gungor and P. Liaw, TMS, Warrendale, PA, p.517 (1989).

86 Miller, W. S. and Humphreys, F. J., *Scr. Metall. Mater.* **25**, 33 (1991).

87 Mummery, P. M. and Derby, B., in "*Fundamental Relations between Microstructures and Mechanical Properties in Metal Matrix Composites*", eds. M. N. Gungor and P. Liaw, TMS, Warrendale, PA, p.161 (1989).

88 England, J. and Hall, I. N., *Scr. Metall.* **20**, 697 (1986).

89 Hasson, D. F., Hoover, S. M., and Crowe, C. R., *J. Mat. Sci.* **20**, 4147 (1985).

90 Derby, B. and Walker, J. R., *Scr. Metall.* **22**, 529 (1988).

91 Flom, Y. and Arsenault, R. J., *Proc. ICCM-VI*, eds. F. L. Mathews *et al.*, **2**, 2.189, Elsevier, Amsterdam (1987).

92 Flom, Y. and Arsenault, R. J. *Acta Metall.* **37**, 2413 (1989).

93 Kamat, S. V., Hirth, J. P., and Mehrabian, R., *Acta Metall.* **37**, 2395 (1989).

94 Arsenault, R. J., Wang, L., and Feng, C. R., *Acta Metall. Mater.* **39**, 47 (1991).

95 Taya, M., Lulay, K. E., and Lloyd, D. J., *Acta Metall. Mater.* **39**, 73 (1991).

96 Klipfel. Y. L., He, M. Y., McMeeking, R. H., Evans, A. G., and Mehrabian, R., *Acta Metall. Mater.* **38**, 1063 (1990).

97 Yang, J., Cady, C., Hu, M. S., Zok, F., Mehrabian, R., and Evans, A. G., *Acta Metall. Mater.* **38**, 2613 (1990).

98 Stephens, J. J., Lucas, J. P., and Hosking, F. M., *Scr. Metall.* **22**, 1307 (1988).

99 Manoharan, M. and Lewandowski, J. J., *Acta Metall.* **38**, 489 (1990).

100 Pedersen, O. B. and Brown, L. M., *Proc. 7th Int. Risø Symp.*, p.83 (1986).

101 Cox, H. L., Br. *J. Appl. Phys.* **3**, 72 (1952).

102 Nardone, V. C. and Prewo, K. M., *Scr. Metall.* **20**, 43 (1986).

103 Eshelby, J. D., *Proc. Roy. Soc.* **A241**, 376 (1957).

104 Eshelby, J. D., *Proc. Roy. Soc.* **A242**, 561 (1959).

105 Warner, F. J. and Stobbs, W. M., *Acta Metall.* **37**, 2873 (1989).

106 Withers, P. J., Stobbs, W. M., and Pedersen, O. B., *Acta Metall.* **37**, 3061 (1989).

107 Withers, P. J., *Phil. Mag.* **A59**, 759 (1989).

108 Pedersen, O. B., *Acta Metall.* **31**, 1795 (1983).

109 Arsenault, R. J. and Taya, M. *Acta Metall.* **35**, 651 (1987).

110 Christman, T., Needleman, A., Nutt, S., and Suresh, S., *Mat. Sci. Eng.* **107A**, 49 (1989).

111 Christman, T., Needleman, A., and Suresh, S., *Acta Metall.* **37**, 3029 (1989).

112 Levy, A. and Papazian, J. M., *Met. Trans.* **21A**, 411 (1990).

113 Tvergaard, V., *Acta Metall. Mater.* **38**, 185 (1990).

114 Dragone, T. L. and Nix, W. D., *Acta Metall. Mater.* **38**, 1941 (1990).

115 Kim, C. T., Lee J. K., and Plichta, M. R., *Met. Trans.* **21A**, 673 (1990).

116 Clegg, W. J., Horsfall, I., Mason, J. F., and Edwards, L., *Acta Metall.* **36**, 2151 (1988).

117 Clegg, W. J., *Acta Metall.* **36**, 2141 (1988).

118 Arsenault, R. J. and Taya, M., *Proc. ICCM-V*, eds. W. C. Harrigan Jr., *et al.*, TMS, Warrendale, PA (1985).

119 Fukuda, H. and Chou, T. W., *J. Mat. Sci.* **17**, 1003 (1982).

120 Ohori, K., Wanatabe, H., and Takeuchi, Y., in "*Aluminium Technology '86*", Inst. of Metals, London, p.57 (1986).

121 Hunt, W. H. Jr., Brockenbrough, J. R., and Magnusen, P. E., *Scr. Metall. Mater.* **25**, 15 (1991).

122 Kamat, S. V., Rollett, A. D., and Hirth, J. P., *Scr. Metall. Mater.* **25**, 27 (1991).

123 Taya, M. and Arsenault, R. J., *Scr. Metall.* **21**, 349 (1987).

124 Lederick, R. J. and Sastry, S. M. L., *Mat. Sci. Eng.* **55**, 143 (1982).

125 Lloyd, D. J., Legace, H., McLeod, A., and Morris, P. L., *Mat. Sci. Eng.* **A107**, 73 (1989).

126 Manoharan, M. and Lewandowski, J. J., *Scr. Metall.* **23**, 301 (1989).

127 Pickard, S. M., Derby, B., Harding, J., and Taya, M., *Scr. Metall.* **22**, 601 (1986).

128 Bauer, R. W., Lyles, R. L. Jr., and Wilsdorf, H. G. F., *Z. Metallk.* **63**, 525 (1972).

129 Balluffi, R. W. and Seigle, L. L., *Acta Metall.* **3**, 170 (1955).

130 DaSilva, R., Caldemaison, D., and Brethau, T., in "*Mechanical and Physical Behaviour of Metallic and Ceramic Composites*" eds. S. I. Anderson *et al.*, Risø National Laboratory, Denmark, p.333 (1988).

131 Ribes, H., DaSilva, R., Suery, M., and Bretheau, T., *Mat. Sci. Tech.* (in print).

132 Wu, S. B. and Arsenault, R. J., in "*Fundamental Relations between Microstructures and Mechanical Properties in Metal Matrix Composites*", eds. M. N. Gungor and P. Liaw, TMS, Warrendale, PA, p.241 (1989).

133 Davidson, D. L., *Met. Trans.* **18A**, 2115 (1987).

134 Vasudevan, A. K., Richmond, O., Zok, F., and Embury, J. D., *Mat. Sci. Eng.* **A107**, 63 (1989).

135 Edelson, B. I. and Baldwin, W. M. Jr., *Trans. Am. Soc. Metals* **55**, 230 (1962).

136 Liu, D. S., Rickett, B. I., and Lewandowski, J. J., in "*Fundamental Relations between Microstructures and Mechanical Properties in Metal Matrix Composites*", eds. M. N. Gungor and P. Liaw, TMS, Warrendale, PA, p. 145 (1989).

137 Davidson, D. L., *J. Mat. Sci.* **24**, 681 (1989).

138 Jones, R. H., Lavender, C. A., and Smith, M. T., *Scr. Metall.* **21**, 1505 (1987).

139 Brown, L. M. and Embury, J. D., *Proc. 3rd Int. Conf. on Strength of Metals and Alloys*, Inst. of Metals, London, p. 164 (1973).

140 Martin, J. W. in "*Micromechanisms in Particle-Hardened Alloys*", Cambridge University Press, p.112 (1980).

141 Goods, S. H. and Brown, L. M., *Acta Metall.* **27**, 1 (1979).

142 Tanaka, K., Mori, T., and Nakamura, T., *Phil. Mag.* **20**, 267 (1970).

143 Strangwood, M., Hippsley, C. A., and Lenandowski, J. J., *Scr. Metall. Mater.* **24**, 1483 (1990).

144 Ashby, M. F., *Phil. Mag.* **14**, 1157 (1966).

145 Embury, J. D., *Met. Trans.* **16A**, 2191 (1985).

146 Thomson, R. D. and Hancock, J. W., *Int. J. Frac.* **24**, 209 (1984).

147 Quigley, B. F., Abbaschian, G. J., Wunderlin, R., and Mehrabain, R., *Met. Trans.* **13A**, 93 (1982).

148 Westfall, J., "*Arc Spray Fabrication of Metal Matrix Composite Monotape*", US Patent Appl. SN 560035 (1987).

149 European Patent *EP-295-008-A* (1989).

150 Clyne, T. W., *Proc. ICCM-VI*, eds. F. L. Mathews *et al.*, **2**, 2.275, Elsevier, Amsterdam (1987).

151 Clyne, T. W. and Bader, M. G., *Proc. ICCM-V*, eds. W. C. Harrigan Jr. *et al.*, TMS, Warrendale, PA, p. 755 (1985).

152 Cornie, J. A., Mortensen, A., Gungor, M. N., and Flemings, M. C., *Proc. ICCM-V*, eds. W. C. Harrigan Jr. *et al.*, TMS, Warrendale, PA, p. 809 (1985).

153 Young, R. M. K. and Clyne, T. W., *Powder Metall.* **29**, 195 (1986).

154 Erich, D. L., *Int. J. Powder Metall.* **23**, 45 (1987).

155 Tweed, J. H., to be published in *Mat. Sci. Eng. (1991).*

156 Cappleman, G. R., Watts, J. F., and Clyne, T. W., *J. Mat. Sci.* **20**, 2159 (1985).

157 Iseki, T., Kameda, T., and Maruyama, T., *J. Mat. Sci.* **19**, 1692 (1984).

158 Kannikeswaren, K. and Lin, R. Y., *J. Met.* p. 17, Sept. 1987.

159 Lloyd, D. J. and Chamberlain, B., *Proc. Int. Symp. on Advances and Cast Reinforced Metal Composites*, eds. S. G. Fishman and A. K. Dhingra, ASM, Metals Park, OH, p. 263 (1988).

160 Kohyama, A. and Igata, N., *Proc. ICCM-V*, eds. W. C. Harrigan Jr. *et al.*, TMS, Warrendale, PA, p. 609 (1985).

161 Collier, J. R. and Gunasekera, J. S., *ASTM Standardisation News*, p. 45, Feb. 1986.

162 Petts, S., Private Communication, 1991.

163 Briggs, G. A. D., "*An Introduction to Scanning Acoustic Microscopy*", RMS Microscopy Handbook 12, Oxford University Press (1985).

164 Briggs, G. A. D., Jenkins, P. J., and Hoppe, M., *J. Micro.* ?? (1990).

165 Man, C.-F., Private Communication, 1991.

166 Man, C.-F., Private Communication, 1991.

167 Roebuck, B., Gorley, T. A. E., and McCartney, L. N., *Mat. Sci. Tech.* **35**, 105 (1989).

168 Johnsen, T. E. and Selnæs, T. D., in "*Fundamental Relations between Microstructures and Mechanical Properties in Metal Matrix Composites*", eds. M. N. Gungor and P. Liaw, TMS, Warrendale, PA, p. 557 (1989).

169 Kelly, A., in "*Strong Solids*", Clarendon Press, Oxford, p. 123 (1966).

170 Kelly, A. and Street, K. N., *Proc. Roy. Soc.* **A328**, 283 (1972).

171 Hedgepeth, J. M. and van Dyke, P., *J. Comp. Mater.* **1**, 294 (1967).

172 Kelly, A. and Davies, G. J., *Metall. Rev.* **10**, 1 (1965).

173 Cho, K. and Gurland, J., *Met. Trans.* **19A**, 2027 (1988).

174 Gerbase, J., Embury, J. D., and Hobbs, R. M., in "*Structure and Properties of Dual Phase Steels*", eds. R. A. Kot and J. W. Morris, TMS-AIME, New York, p. 118 (1979).

175 Tomota, Y., Kuroki, K., Mori, T., and Tamura, I., *Mat. Sci. Eng.* **24**, 85 (1976).

176 Gurland, J. and Cho, K., in "*Fundamental Relations between Microstructures and Mechanical Properties in Metal Matrix Composites*", eds. M. N. Gungor and P. Liaw, TMS, Warrendale, PA, p. 173 (1989).

177 Chang, Y. W. and Asaro, R. J., *Met. Sci.* **12**, 277 (1978).

178 Embury, J. D. and Duncan, J. L., *J. Met.* **34**, 24 (1982).

179 Tanaka, K. and Mori, T., *Acta Metall.* **18**, 831 (1970).

180 Brown, L. M. and Stobbs, W. M., *Phil. Mag.* **23**, 1185 (1971).

181 Mori, T. and Tanaka, K., *Acta Metall.* **21**, 571 (1973).

182 Pedersen, O. B. and Brown, L. M., *Acta Metall.* **25**, 1303 (1977).

183 Pedersen, O. B., *Z. Ang. Math. Mech.* **58**, 227 (1978).

184 McElroy, R. J. and Szopiak, Z. C., *Int. Met. Rev.* **17**, 175 (1972).

185 Lloyd, D. J., *Metal Sci.* **14**, 193 (1980).

186 Taya, M. and Mori, T., *Acta Metall.* **35**, 155 (1987).

187 Wakashima, K., Kurihara, S., and Umekana, S., *J. Japan Soc. Comp. Mater.* **2**, 1 (1976).

188 Lilholt, H., *Proc. 4th Int. Risø Symp.* p. 381 (1983).

189 Humphreys, F. J., in *"Dislocations and Properties of Real Materials"*, ed. M. H. Loretto, Inst. Metals, London, p. 175 (1985).

190 Foreman, A. J. E. and Makin, M. J., *Canad. J. Phys.* **45**, 511 (1967).

191 Gurland, J. and Plateau, J., *Trans. ASM* **56**, 442 (1963).

192 Rosenfield, A. R., *Metall. Rev.* **13**, 29 (1968).

193 Wilsdorf, H. G. F., *Mat. Sci. Eng.* **59**, 1 (1983).

194 van Stone, R. H., Cox, T. B., Low, J. R. Jr., and Psioda, J. A., *Int. Met. Rev.* **30**, 157 (1985).

195 Leslie, W. C., *Trans. Iron Steel Soc.* **2**, 1 (1983).

196 Plateau, J., Henry, G., and Crussard, C., *Rev. Métall.* **54**, 200 (1957).

197 Klimowitz, T. F. and Vecchio, K. S., in *"Fundamental Relations between Microstructures and Mechanical Properties in Metal Matrix Composites"*, eds. M. N. Gungor and P. Liaw, TMS, Warrendale, PA, p. 255 (1989).

198 Argon, A. S., *J. Engng. Mater. Tech., Trans. AIME* **98**, 60 (1976).

199 Rice, J. R. and Johnson, M. A., in *"Inelastic Behaviour of Solids"*, eds. M. F. Kanninen *et al.*, McGraw-Hill, New York, p. 641 (1969).

200 Park, I.-G. and Thompson, A. W., *Acta Metall.* **36**, 1653 (1988).

201 Hahn, G. T. and Rosenfield, A. R., *Met. Trans.* **6A**, 653 (1975).

202 Gurland, J., *Acta Metall.* **20**, 735 (1972).

203 Ashby, M. F., *Phil. Mag.* **20**, 399 (1970).

204 Evensen, J. D. and Verk, A. S., *Scr. Metall.* **15**, 1131 (1981).

205 Shang, J. K., Yu, W., and Ritchie, R. O., *Mat. Sci. Eng.* **A102**, 181 (1988).

206 Shang, J. K. and Ritchie, R. O., *Acta Metall.* **37**, 2267 (1989).

207 Shang, J. K. and Ritchie, R. O., *Met. Trans.* **20A**, 897 (1989).

208 Lawn, B. R. and Wilshaw, A. R., *"Fracture of Brittle Solids"*, Cambridge University Press, p. 61 (1975).

209 Ritchie, R. O., Knott, J. F., and Rice, J. R., *J. Mech. Phys. Sol.* **21**, 395 (1973).

210 Hutchinson, J. W., *J. Mech. Phys. Sol.* **16**, 13 (1968).

211 Rice, J. R. and Rosengren, G. R., *J. Mech. Phys. Sol.* **16**, 1 (1968).

212 McMeeking, R. M., *J. Mech. Phys. Sol.* **24**, 357, (1977).

213 Thomson, R. D. and Hancock, J. W., *Int. J. Frac.* **24**, 209 (1984).

214 Scruby, C. B., in *"Research Techniques in Nondestructive Testing"*, Vol. 8, ed. R. S. Sharp, Academic Press, London, p. 141 (1985).

215 Wadley, H. N. G., Scruby, C. B., and Speake, J. H., *Int. Met. Rev.* **3**, 41 (1980).

216 Wadley, H. N. G., Scruby, C. B., and Shrimpton, G., *Acta Metall.* **29**, 399 (1981).

217 Achenbach, J. D., *"Wave Propagation in Elastic Solids"*, Elsevier, New York (1973).

218 Scruby, C. B., *J. Phys. E: Sci. Instrum.* **20**, 946 (1987).

219 Scruby, C. B., Jones, C., Titchmarsh, J. M., and Wadley, H. N. G., *Met. Sci.* **15**, 241 (1981).

220 Sachse, W. and Kim, K. Y., *Ultrasonics* **25**, 195 (1987).

221 Heiple, C. R., Carpenter, S. H., and Carr, M. J., *Metal Sci.* **15**, 587 (1981).

222 Wadley, H. N. G. and Mehrabian, R., *Mat. Sci. Eng.* **65**, 245 (1984).

223 McBride, S. L. and Hutchison, T. S., *Can. J. Phys.* **54**, 1824 (1976).

224 Hsu, N. N., Simmons, J. A., and Hardy, S. C., *Mat. Eval.* **35**, 100 (1977).

225 Breckenridge, F. R., Tschiegg, C. E., and Greenspan, M., *J. A. S. A.* **57**, 626 (1975).

226 Scruby, C. B., Dewhurst, R. J., Hutchins, D. A., and Palmer, S. B., *J. Appl. Phys.* **51**, 6210 (1980).

227 Scruby, C. B., Wadley, H. N. G., Dewhurst, R. J., Hutchins, D. A., and Palmer, S. B., *Mat. Eval.* **39**, 1250 (1981).

228 Dewhurst, R. J., Hutchins, D. A., Palmer, S. B., and Scruby, C. B., *J. Appl. Phys.* **53**, 4064 (1982).

229 Kant, R., *"The Elastostatic Axisymmetric Problem of a Cracked Sphere Embedded in a Dissimilar Matrix"*, Doctoral thesis, Univ. of California, Berkley, CA (1979).

230 Heiple, C. R., Carpenter, S. H., and Christiansen, S. S., *Acta Metall. Mater.* 58, 611 (1990).

231 Green, A. T. and Zerna, W., *"Theoretical Elasticity"*, Clarendon Press, Oxford (1954).

232 Fisher, J. R. and Gurland, J., *Met. Sci.* **15**, 193 (1981).

233 Brown, L. M. and Stobbs, W. M., *Phil. Mag.* **34**, 351 (1976).

234 McClintock, F. A., *J. Appl. Mech.* **35**, 363 (1968).

235 Yuan, J., Hiltner, A., Baer, E., and Rahrig, D., *Polymer Eng. Sci.* **24**, 844 (1984).

236 Zok, F., Embury, J. D., Ashby, M. F., and Richmond, O., in "*Mechanical and Physical Behaviour of Metallic and Ceramic Composites*" eds. S. I. Anderson *et al.*, Risø National Laboratory, Denmark, (1988).

237 Lloyd, D. J., Private Communication, 1990.

238 Fisher, J. R. and Gurland, J., *Met. Sci.* **15**, 185 (1981).

239 Teirlinck, D., Ashby, M. F., and Embury, J. D., *Proc. 6^{th} Int. Conf. Fracture,* Bangalore, Pergamon, Vol. 1, p. 105, (1985).

240 Ohno, N. and Hutchinson, J. W., *J. Mech. Phys. Sol.* **32**, 63 (1984).

241 Magnusen, P. E., Dubensky, E. M., and Koss, D. A., *Acta Metall.* **36**, 1503 (1988).

242 Dubensky, E. M. and Koss, D. A., *Met. Trans.* **18A**, 1887 (1987).

243 Melander, A., *Mat. Sci. Eng.* **39**, 57 (1979).

244 Melander, A. and Stahlberg, U., *Int. J. Frac.* **16**, 431 (1980).

245 Melander, A., *Acta Metall.* **28**, 1799 (1980).

246 Lemaitre, J., *J. Eng. Mat. Tech.* **107**, 83 (1985).